CORRELATION MEASUREMENTS OF SIGNALS AND NOISE

A thesis submitted for the
degree of Doctor of
Philosophy at the University
of Aston in Birmingham.

Fenwick Arthur B.Sc., M.Sc.,

Birmingham, October 1968.

SUMMARY

It has recently been shown that the characteristic of an electronic device fluctuates, and that this may possibly account for the increase in noise level obtained when a.c. signals are applied to semiconductor devices. The aim of the present research is to investigate further the effect of these fluctuations in characteristic on the noise of electronic devices, and to determine how they will affect any signals being transmitted.

The investigation was carried out in two parts. In the first part a theoretical and experimental investigation of the shot noise of thermionic valves was made. As a result of this investigation it was concluded that a theory of space charge smoothing based on the hypothesis of a fluctuating characteristic gives a better estimate of the space charge smoothing factor than do other, more widely accepted, theories.

The second part is concerned with the transmission of signals through amplifiers. Both autocorrelation and crosscorrelation techniques were used to determine how these signals are affected by the fluctuations in characteristic. The results so obtained are shown to conflict with the results of an earlier experimentor, Hathaway, but not to conflict with those of another, Bozic, and indicate that signals are almost unaffected by fluctuations in the characteristic of the amplifier through which they are transmitted.

CONTENTS

PART III CORRELATION MEASUREMENTS OF SIGNALS AND NOISE

PART I

INTRODUCTORY SECTIONS

1. INTRODUCTION

In recent years experimental evidence has been obtained which indicates that the characteristic of an electronic device fluctuates. One recent example of this may be seen in the experiments of Bozic in which he found that the application of signals to an electronic device produced an increase in noise and that this increase was of a form which supported the idea of a fluctuating characteristic. Earlier examples may be found in the experiments of Richards, and Ince, both of whom obtained results indicating that the shot noise of a thermionic valve is a manifestation of a fluctuating characteristic.

With the view of obtaining further information on fluctuating characteristics, and on the validity of applying the idea of such to fluctuation theory, the present investigation was carried out.

The investigation may be roughly divided into two main sections. The first of these deals, both theoretically and experimentally, with the shot noise of thermionic diodes. The second, which utilises cross-correlation and autocorrelation techniques, is concerned with an investigation of the excess noise, i.e. noise due to signal, in amplifiers and with its effect on the signal being transmitted.

2. CORRELATION AND STATISTICAL METHODS

In the following chapters the terms autocorrelation function, crosscorrelation function and probability generating function will be frequently used. It is useful, therefore, to consider further these terms and to show how they are related to the processes with which they are associated.

2.1 Autocorrelation Function

To define the autocorrelation function consider an ensemble, $y(t)$, of real voltages (or any other real variable) in which $y^j(t)$ represents the j^{th} member of the ensemble. The autocorrelation function $R_y^j(\tau)$ of $y^j(t)$ is defined as (Refs. 4, 6, 19, 30, 37, 42)

$$R_y^j(\tau) = \lim_{T \to \infty} \frac{1}{T} \int_{-\frac{T}{2}}^{\frac{T}{2}} y^j(t)\, y^j(t+\tau)\,dt \tag{2.1}$$

In order to simplify the analytic work it will be assumed that the process is stationary so that $R_y^j(\tau)$ depends only on the time displacement τ and not on the particular time t. It will further be assumed that the process is ergodic so that the time and ensemble averages are equal and that the ensemble contains no d.c. terms. The ensemble average corresponding to Eq. (2.1) is

$$R_y^j(\tau) = \int_{-\infty}^{\infty}\!\!\int y_1 y_2 W_2(y_1, y_2; \tau) dy_1 dy_2 \qquad (2.2)$$

where $W_2(y_1, y_2; \tau)$ represents the probability of y having values between y_1 and $y_1 + dy_1$ at time t, and y_2 and $y_2 + dy_2$ at time τ later.

These equations are illustrative of the usefulness of the autocorrelation function. In many types of process involving random phenomena the relevant information is contained within the ensemble average (2.2) so that measurement of $R_y^j(\tau)$ enables this information to be recovered. In particular for those processes which are defined by their variances, e.g. shot noise, then $R_y^j(0)$ is the function to be measured. From Eq. (2.1) it can be seen that $R_y^j(0)$ represents the mean power of the wave and this relationship will be found useful in designing the experimental equipment.

2.2 Wiener-Khintchine Theorem [37,39,42]

Let $y^j(t)$ represent a member of an ensemble of current, or voltage, waves which vanishes everywhere outside some finite interval T $(-\frac{T}{2} < t < \frac{T}{2})$. The average power of the wave may be defined as

$$P_y^j = \lim_{T \to \infty} P_y^j(T) = \lim_{T \to \infty} \frac{1}{T} \int_{-\frac{T}{2}}^{\frac{T}{2}} y_T^j(t)^2 \, dt \qquad (2.3)$$

where $y_T^j(t)$ means the function exists within a finite interval ,T, and where the limit is assumed to exist (such an assumption is in no way restrictive, however, since processes dissipating infinite power are anti-physical).

Using Plancherel's theorem Eq. (2.3) can be written in the frequency domain as

$$P_y^j = \int_{-\infty}^{\infty} W_y(f)df$$

where $W_y(f)$, the power spectrum, is given by:

$$W_y(f) = \begin{cases} \left(\lim\limits_{T \to \infty} \dfrac{\overline{2(|S_y^j(mf_o)|^2)}}{T^2}\right) \delta(f - mf_o) & (m=0,1,2\ldots) \text{ for periodic processes} \\ \left(\lim\limits_{T \to \infty} \dfrac{\overline{2(|S_y^j(f)_T|^2)}}{T}\right) & \text{for random processes} \end{cases}$$

Where $\delta(f - mf_o)$ is the unit impulse function (Appendix 1) and

$$S_y^j(f)_T = \int_{-\infty}^{\infty} y_T^j \, e^{-iwt} \, dt \ , \ w = 2\pi f$$

When the ensemble is ergodic a simple relationship exists between the power density spectrum and the auto-correlation function. This relationship may be written as

$$R_y^j(\tau) = \int_0^{\infty} W_y(f) \cos 2\pi f\tau \, df \qquad (2.4a)$$

$$W_y(f) = 4 \int_0^\infty R_y^j(\tau) \cos 2\pi f\tau \, d\tau \qquad (2.4b)$$

and is known as the Wiener-Khintchine theorem.

2.3 Autocorrelation and the Spectrum of Linear Filtered Waves [19,42]

In analysing random phenomena it is often the case that a measuring system is used in which the frequency characteristic is quite different from that of the source. Such a system is shown in schematic form in Fig. 2.1 in which x(t) represents the input ensemble, y(t) the output ensemble and A the linear

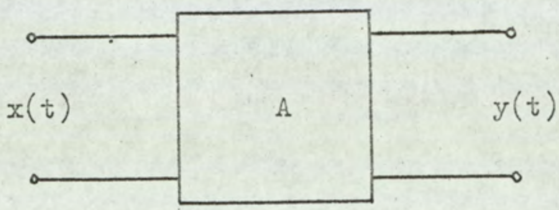

Fig. 2.1

, constant parameter, measuring network. The output, y(t), is given by the convolution integral

$$y(t) = \int_{-\infty}^{\infty} x(\sigma)\, h(t - \sigma)\, d\sigma$$

where $x(\sigma)$ represents the amplitude of the input at time σ, and $h(t - \sigma)$, the weighting function, is the response of the network A at time $(t - \sigma)$ after it has been excited by a unit impulse. Using this equation in conjunction with Eqs. (2.1) and (2.4) above, and with steady state network theory it can be shown:

(i) The input, $R_x^j(\tau)$, and output $R_y^j(\tau)$, autocorrelation functions are related by

$$R_y^j(\tau) = \int_{-\infty}^{\infty} h(\nu)d\nu \int_{-\infty}^{\infty} h(\sigma)d\sigma R_x^j(\mu) \tag{2.5}$$

where $\mu = \tau + \nu - \sigma$

(ii) The system function, Y(iw), which represents the ratio of the complex amplitudes of y(t) and x(t), and the weighting function, h(t), are a Fourier transform pair, i.e.,

$$Y(iw) = \int_{-\infty}^{\infty} h(t)e^{-iwt}dt \tag{2.6a}$$

$$h(t) = \int_{-\infty}^{\infty} Y(iw)e^{iwt}df \tag{2.6b}$$

(iii) The output power spectrum, Wy(f), is related to that of the input by

$$W_y(f) = |Y(iw)|^2 W_x(f) \tag{2.7}$$

2.4 Crosscorrelation Function[6,19,42]

Corresponding to the autocorrelation function of a single ensemble a similar relationship exists between a pair of ensembles x(t) and y(t). This relationship, known as the crosscorrelation, is defined in the time domain as

$$R^{j}_{xy}(\tau) = \lim_{T \to \infty} \int_{-\frac{T}{2}}^{\frac{T}{2}} x^{j}(t)y^{j}(t + \tau)dt \tag{2.8}$$

where τ is the time delay between the waves. When the processes are ergodic the crosscorrelation function may also be determined by averaging over the ensembles. Equation (2.8) then becomes

$$R_{xy}(\tau) = \iint_{-\infty}^{\infty} x_1 y_1 W_2(x_1, y_1, \tau)dx_1 dy_1 \tag{2.9}$$

where $W_2(x_1, y_1, \tau)$ is the probability that $x(t)$ will lie between x_1 and $x_1 + dx_1$ at some time t, and that $y(t)$ will lie between y_1 and $y_1 + dy_1$ at time τ later.

Under the condition that the sources are statistically indpendent Eq. (2.9) simplifies to

$$R^{j}_{xy} = \overline{x}_1 \; \overline{y}_1 = \text{constant} \tag{2.10}$$

where the bars signify an ensemble average. This case is common but there are conditions in which the sources are interdependent, though not identical, so that the crosscorrelation may be used as a measure of their coherence.

2.5 Probability Generating Functions [15,24,34]

In the study of random processes it is sometimes the case that the random variable can take only discrete values. When this occurs a useful aid in analysing such processes is the probability generating function (p.g.f.).

A p.g.f. of a random variable n is defined by the polynomial

$$N(x) \quad = \quad \sum_n a_n x^n \tag{2.11}$$

where n takes only integral values and a_n represents the probability of a particular value of n occuring.

Consider now the result of differentiating this equation with respect to x. Then

$$N^1(x) \quad = \quad \Sigma\, n a_n x^{n-1}$$

$$N^{11}(x) \quad = \quad \Sigma(n)(n - 1)x^{n-2} a_n$$

which on making the substitutions $x = 1$, $\sigma_n^2 = \overline{n^2} - \bar{n}^2$ give

$$\bar{n} = N^1(1) \tag{2.12a}$$

and $$\sigma_n^2 = N^{11}(1) - [N^1(1)]^2 + N^1(1) \tag{2.12b}$$

Hence, once a p.g.f. of a random variable has been obtained it is a simple matter to derive its mean value and variance. There are difficulties, however, the main one being in the construction of the p.g.f. since this has to be done in a manner which takes into account all the events taking place in the system.

If the events taking place are very simple such as the addition or subtraction of two sets of elementary particles - represented by the numbers n and m - then the p.g.f. for the sum, n + m is

$$(N + M)\ (x) = N(x)M(x) \tag{2.13}$$

and for the subtraction, n - m, is

$$(N - M)\ (x) = N(x)M(x^{-1}) \tag{2.14}$$

and the corresponding mean values and variances - from Eqs. (2.12a), (2.12b) - are

$$\overline{n + m} = \bar{n} + \bar{m} \tag{2.15a}$$

$$\sigma^2_{n+m} = \sigma^2_n + \sigma^2_m \tag{2.15b}$$

$$\overline{n - m} = \bar{n} - \bar{m} \tag{2.16a}$$

$$\sigma^2_{n-m} = \sigma^2_n + \sigma^2_m \tag{2.16b}$$

If, on the other hand, the events taking place are multiplicative such that the occurrence of one event, represented by the number m, is dependent on the occurrence of another , say n, then the construction of the p.g.f. for the consequent event nm is less straightforward than those above. For this reason Table 2.1 has been included.

If now reference is made to Table 2.1 it can be seen

Table 2.1

Initiating Event	Consequent Event
n = 0	0
n = 1	$M(x)$
n = 2	$(M(x))^2$
n = 3	$(M(x))^3$
etc.	

that the p.g.f. for a multiplicative process is given by

$$(NM)(x) = \sum_n a_n (M(x))^n = N(M(x)) \tag{2.17}$$

which, in turn, gives (Appendix 2)

$$\overline{n\,m} = \overline{n}\;\overline{m} \tag{2.18a}$$

$$\sigma^2_{nm} = \overline{m}^2\,\sigma^2_n + \overline{n}\,\sigma^2_m$$

Consider now the application of some of the above ideas to the binomial and Poisson probability distributions.

2.5.1 Probability Generating Function of a Binomial Distribution[24]

A binomial distribution describes the probabilities of the various outcomes of an experiment which is conducted under the conditions that :

(i) There is a fixed number of trials.

(ii) Each trial must result in a success or a failure.

(iii) All trials must have identical probabilities of success.

(iv) The trials must be independent of each other. Assuming the number of trials to be represented by f, and p and q to represent the probability of a success and failure respectively the probability for n successes and (f-n) failures in any given order is the product of n p's and (f-n) q's, i.e. $p^n q^{f-n}$. However, there are $\frac{f!}{n!(f-n)!}$ points with n successes each having the probability $p^n q^{f-n}$ assigned to it. Hence the binomial distribution may be written

$$P(n,f) = \frac{f!}{n!(f-n)!} p^n q^{f-n} \tag{2.19}$$

where P(n,f) represents the probability of n successes and (f-n) failures.

It follows, therefore, that the p.g.f. associated with a binomial distribution (Feller) takes the form

$$N(x) = \sum_{n=o}^{f} \frac{f!}{n!(f-n)!} (px)^n q^{f-n} = (q + px)^f \tag{2.20}$$

From which it follows that

$$N'(x) = fp(q + px)^{f-1}$$

$$N''(x) = (f)(f-1)p^2(q + px)^{f-2}$$

which, in turn, give (Eq. 2.12)

$$\bar{n} = fp \tag{2.21a}$$

$$\sigma_n^2 = fp(1-p) = fpq \tag{2.21b}$$

2.5.2 Probability Generating Function of a Poisson Distribution[24]

If p is very small and the number of trials large, Eq. 2.19 approximates to

$$P(n,f) = \frac{\bar{n}^n}{n!} e^{-\bar{n}} \tag{2.22}$$

which is referred to as the Poisson distribution.

It, therefore, follows from this equation and Eq. (2.11) that the p.g.f. for a Poisson distribution takes the form

$$N(x) = \sum_{n=0}^{\infty} e^{-\bar{n}} \frac{(\bar{n}x)^n}{n!} = e^{\bar{n}(x-1)} \tag{2.23}$$

Hence from Eq. (2.12) it follows that the mean and variance of a Poisson distribution are equal.

It can be seen, therefore, that the method of p.g.f.s. is an exceedingly useful one and it will be used extensively in the succeeding chapters.

PART II

SHOT NOISE OF THERMIONIC VALVES

3. THEORY OF SPACE CHARGE SMOOTHING FACTOR

3.1 Introduction

In a thermionic diode the emitted electrons have a velocity distribution which, on the average, is Maxwell Boltzmann.[1,20,58] Because of this distribution the anode voltage - anode current characteristic can be separated into three regions (Fig. 3.1), viz:

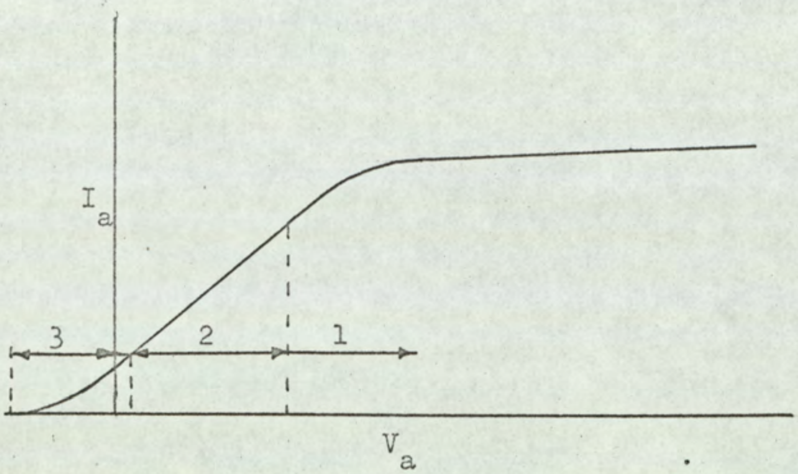

Fig. 3.1

(1) Temperature limited region in which all the emitted electrons reach the anode and the distribution of emission energies is, at least to a very good first approximation, unimportant.

(2) Space charge limited region in which the anode voltage is insufficient to collect all the emitted electrons so that a cloud of electrons forms around the cathode producing a potential barrier containing a negative potential minimum, V_m, which limits the current flow.

(3) Retarding field region in which the lowest potential is that of the anode, the junction between this region and region 2 occurring at that anode potential at which the minimum in the barrier has moved out to the anode.

Experimental investigations (Refs. 29, 32, 43, 50, 54, 59) of the noise in each of these three regions have established that the mean square fluctuating current ,$\bar{i}^2$, is given by

$$\bar{i}^2 = 2e\bar{I}df\Gamma^2 \qquad (3.1)$$

where $\bar{I}$ is the mean anode current, e the electronic charge, df an elemental bandwidth and Γ^2, the space charge smoothing factor, has the value unity in the temperature limited and retarding regions of the diode and is much less than unity under space charge limited conditions.

The explanation of Eq. (3.1) has initiated much theoretical work. As yet, however, no theory has been proposed which is consistent throughout all three regions of the valve. With this in mind the present investiation was carried out; the intentions were:

(i) To determine - using fluctuating characteristic theory - a more adequate theory for the space charge smoothing factor.

(ii) To compare this new theory with experimental measurements of shot noise in thermionic diodes.

3.2 Historical Survey of Space Charge Smoothing Theory

Probably the most widely accepted theory for the calculation of the space charge smoothing factor is that due to D. O. North.[43] North took the view that the diode fluctuates through a series of stationary states in which the number of electrons of a particular velocity class remained constant at a level above, or below, the mean. From this North moves to the view that the effect of the fluctuations is to modulate the height of the potential barrier and produce a compensatory flow of charge, which in one case - where the fluctuation is below the mean - is towards the anode and in the other towards the cathode. Thus the fluctuations in emission are smoothed.

By finding the smoothing effect of each of the velocity classes and integrating over all classes North derived an expression for Γ^2 which for $\frac{\bar{I}}{I_s} \ll 1$ (I_s = saturation current) may be written

$$\Gamma^2 = 1.29 g \frac{kT_c}{e\bar{I}} \tag{3.2}$$

where g = anode conductance $= \overline{(\partial I/\partial V_a)}_{I_s}$, k = Boltzmann's constant

T_c = cathode temperature and V_a = anode voltage.

The derivation of this equation is very long, so long in fact that it has never been given in full. It may be criticised, however, on several physical grounds, viz:

(i) It is difficult to imagine small intervals of time in which the emission remains constant at a certain value and in which the valve is in a stationary state. The latter can surely only be established over periods which are not short.

(ii) North uses entirely deterministic methods, assuming at all times that he knows which electrons will overcome the barrier and which will not.

(iii) The smoothing effect of electrons with energy just sufficient to reach the potential minimum $, V_m,$ is infinite and this produced infinite discontinuities in North's equations when low anode voltages were being considered. For this reason North was unable to determine Γ^2 for low values of $\frac{eV_a}{kT}$, although he knew it was unity in the retarding region.

In an endeavour to simplify North's derivation Fürth utilised the theories of thermodynamics and showed that for space charge limited valves Γ^2 is given by:

$$\Gamma^2 = \frac{gkT_c}{e\bar{I}} \tag{3.3}$$

which is very similar to that obtained by North.

To obtain this result, however, Fürth used the hypothesis that the valve was in thermodynamic equilibrium. It seems to the writer, however, that this is not a permissible assumption and that the only time the valve can be considered in equilibrium is when every part of it is at the same temperature as its surroundings, no supply voltage is used and the mean anode current is exactly zero. From this point of view, therefore, it would seem that Eq. (3.3) is invalid.

More recently, Bull[14], using a completely different approach has obtained an expression for the smoothing factor which in North's nomenclature may be written

$$\Gamma^2 = \frac{gkT_c}{e\bar{I}} \overline{\left(\frac{\partial V_a}{\partial V_m}\right)_I} \tag{3.4}$$

Bull's approach was based on the hypothesis that the valve characteristic $(\partial I/\partial I_s)$ could fluctuate between the values of zero and unity according to a binomial distribution. It is a property of this distribution that it has the p.g.f. (Eq. (2.20))

$$N(x) = (q + px)^f$$

where the $(n + 1)^{th}$ term represents the probability of n successes and (f - n) failures in f trials. Bull, however, was only able at the time to use a binomial distribution with a fractional index and this makes the validity of his method questionable. Nonetheless, Richards has shown that Eq. (3.4) gives a better estimate of the space charge smoothing than does North's (Eq.(3.2)) or Fürth's (Eq. (3.3)).

3.3 Theory of the Fluctuating Characteristic

In a series of papers on fluctuation theory [12 - 14] Bull put forward the view that since electrons are atomic in nature they cannot be subjected to precise and detailed control. Accordingly, when small signals are applied to an electronic device then although it is usually possible to be very specific about the input signal the actual corresponding change of current, or voltage, which occurs during particular small intervals of time is unpredictable. This unpredictability may be taken into account by allowing the characteristic of the device to fluctuate about its long term mean.

Bull then applied his ideas to the characteristics of thermionic diodes. He showed[11] that the characteristic curves of such devices may be represented by a set of 30 partial differential coefficients which are interrelated. Hence, if it is assumed that one of these differential coefficients fluctuates, they all must.

With this in mind Breeze made a number of experiments on thermionic valves in which he verified that the impedance of a valve fluctuates. Later, Bozic[8] showed that when a.c. signals are applied to semiconductor devices there is an increase in noise level and that the fluctuating characteristic theory goes some way towards explaining it.

It is apparent, therefore, that the case for making the hypothesis of a fluctuating characteristic is sound. However, before using the hypothesis to determine the space charge smoothing factor it is necessary to remove the deficiency of Bull's approach by avoiding the use of a binomial distribution with a fractional index. It will be shown below that this may be effected by using as a basis the hypothesis that the electric field is discontinuous to an extent determined by the electron charge.

3.4 The Discontinuous Electric Field.

In the study of electricity it has long been known that electric charges exist only in integral multiples of the electronic charge e. Nonetheless, in developing noise theory theoriticians have sometimes found it necessary to postulate the existence of charges which are not integral multiples of the electronic charge e.

One of the first to recognise and to attempt to remove the anomalies of such a proposal was E. N.Rowland. Confining his attention to the shot noise of temperature limited valves Rowland first tried the effect of assuming that each electron at the anode spent some time there - during which time it induced a voltage - e/C - and then disappeared abruptly. By regarding the individual lifetimes of the electrons to be distributed at random and the fluctuations about the mean to represent the shot noise then by using Campbell's theorem (Appendix 3) he was able to calculate the magnitude of the fluctuations. As a result he predicted that the mean square value of the fluctuations should be twice as large as the observed value. He then proved, however, that this discrepancy could be completely removed by assuming that each single electron decayed from the anode according to the same exponential law applicable to macroscopic charges. He was obliged to conclude that the electron behaves as a discontinuous charge in the vacuum and as continuous charge in the circuit.

It appeared at the time as if this conclusion was inevitable and it has hardly been questioned since. For example, Bell[2] is at pains to explain why this view is tenable.

In his use of Rowland's work Bell proposed that as an electron crossed from anode to cathode there was a gradual transference of charge. Thus he proposes that when an electron is distance x from the cathode the charge on the anode is given by

$$q = e \left[1 - \frac{x}{d} \right]$$

(d being the anode-cathode spacing). Consequently fractional electron charges would be observed to flow in the anode circuit during the motion of the electron in the space between electrodes.

To explain the transference of fractions of electronic charge Bell suggested that the behaviour of the conduction electrons in the conductingpart of the circuit was similar to the behaviour of electrons in a polarised dielectric; the mean position of the conduction electrons shifting slightly with respect to the fixed positive charges, so that the average effective charges at the cathode and anode surfaces are changed by appropriate amounts.

In view of the basic difference in behaviour between polarised dielectrics and conductors then Bell's attempt to utilise an analogy between the two is questionable. Furthermore, in view of Rowland's failure with conventional means to get appropriate results using an electron as an indivisible particle, and that the adoption of continuous methods, by both him and Bell, while accepted by force of circumstances is not in accordance with modern methods of statistics, e.g. Fermi-Dirac, it is apparent that a new model of the interaction between fields and particles is required if the deficiencies of Rowland's, and all other work, are to be removed. Such a model has been put forward by Dirac and, independently, by Bull.[15] It has been adapted by the latter to fluctuation theory.

The new model is based on the hypothesis that the electric field is a discontinuous assembly of field lines each of which terminates on a charge equal to that of the electron, and at the other on a positive charge of equal magnitude. The picture of an electric field presented, is, therefore, very similar to that described by Faraday;

the difference being that the Faraday lines of force which were taken by Maxwell and all later theoreticians merely to be mapping lines of a field are now quantised.

In the new picture of the electric field the fundamental unit, the field line, has the properties that it has direction, it may be cut laterally thus forming an electron charge at one end of the cut and a positron charge at the other and it may be stretched longitudinally.

3.5 A New Theory of the Space Charge Smoothing Factor

Aware of the basic deficiency of his theory of the space charge smoothing factor, i.e. the use of a binomial distribution with a fractional index, Bull[15] later attempted to improve it by utilising the discontinuous field theory discussed above. This new approach, however, although it removed the earlier deficiency predicted that the shot noise in the temperature limited and retarding regions would be twice the observed value. Nonetheless, it was an improvement on some of the earlier work in that it was obtained without the necessity of:

(i) being deterministic about the behaviour ofelectrons; and

(ii) postulating the existence of fractional electrons.

From this point of view, therefore, it appeared to be worthy of further consideration.Accordingly, the theory discussed below was formulated.

To simplify the discussion it is expedient to begin by considering a valve operating under temperature limited conditions. Under such conditions field lines, as defined at the end of the last section, will be leaving the battery and upon arrival at the anode-cathode space will disappear on account of electron emission. The disappearance will occur in one of two ways, viz:

(i) The negative charge will detach itself from the surface of the cathode, when the field line shortens and collapses on the anode.

(ii) An electron will emerge from the cathode and set up a field line between it and the cathode. This line is in the opposite direction to the lines from the battery and after it has moved a little way from the cathode it may collide with one of the latter. In Fig. 3.2 below is shown how this may lead to the collapse of a field line on the cathode and an emitted electron taken over to the anode.

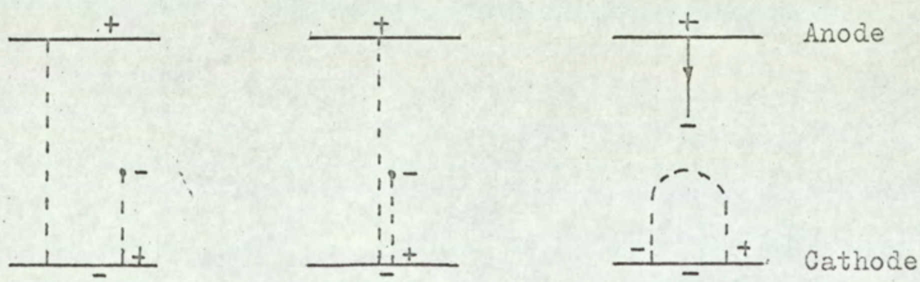

Fig. 3.2

Consider now the circuit shown in Fig. 3.3. where the valve is operating under temperature limited conditions. Here, v field lines arrive from the battery on the circuit

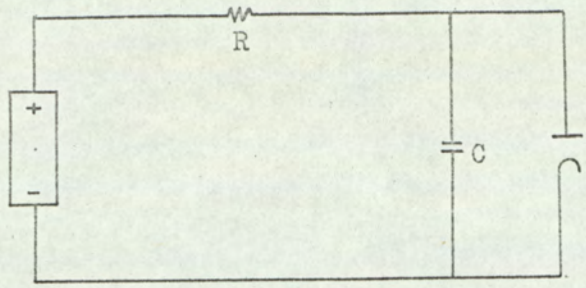

Fig. 3.3

capacitance, including space between electrons in a time interval δt - where δt depends on the shortest time interval over which an effective observation of the voltage across the valve can be made. Let vk be the number of field lines neutralised by cathode emission; then since, on the average, the number of field lines arriving is equal to the average number being neutralised by the cathode emission then $\bar{k} = 1$. In time δt, therefore, the number of field lines on the anode will change by a number r where

$$r = v(1 - k) \tag{3.5}$$

The p.g.f. for r may be written (Sec. 2.5)

$$R(x) = V(x(K(x^{-1})))$$

where V(x) and K (x) are respectively the p.g.f.s for v and k respectively. It follows from this equation that

$$\bar{r} = 0 \text{ and } \sigma_r^2 = \bar{v}\sigma_k^2$$

The effect of a change in the number of field lines on the anode is to change the energy of the condenser by ΔE, where

$$\Delta E = \frac{(p + r)^2 e^2}{2C} - \frac{p^2 e^2}{2C} = \frac{r^2 e^2}{2C} + \frac{pre^2}{2C}$$

and p is the number of field lines on the capacitor C at the beginning of the interval. The mean change in energy, $\overline{\Delta E}$, will therefore be, since $\bar{r} = 0$,

$$\overline{\Delta E} = \frac{\overline{r^2 e^2}}{2C} = \frac{\sigma_r^2 e^2}{2C} = \frac{\bar{v}\sigma_k^2 e^2}{2C} \tag{3.6a}$$

This average change in energy is always positive and Bull assumes that it cannot be allowed to collect in the circuit but must be dissipated in the circuit resistance R. Hence, if $\overline{V^2}$ represents the mean square noise voltage across R, then

$$\frac{\overline{V^2}}{R}\,\delta t = \frac{\bar{v}\sigma_k^2 e^2}{2C}$$

and

$$\overline{V^2} = \frac{\bar{v}\sigma_k^2 e^2}{2C\delta t} = \frac{\bar{I}\sigma_k^2 eR}{2C}$$

Assuming a Poisson distribution (Sec. 2.5.2) for k so that $\sigma_k^2 = \bar{k}$, this simplifies to

$$\overline{V^2} = \frac{\bar{I}eR}{2C} \tag{3.6b}$$

This equation was originally given by Schottky using methods similar to Rowland's and Campbell's and is very well supported by experiment. It has here been developed, however, without using continuous variations of charges at any point. Also, it will be seen that it is the neutralisation rate, k, not the battery supply rate v which, in the main, determines the fluctuations.

Neutral Field

A region where the density of the anode field lines is equal to the density of the cathode field lines.

Under the space charge limited conditions the rate of arrival of field lines from the battery is much less than the rate of emission of electrons from the cathode and the electric field configuration within the valve will be of the form shown in Fig. 3.4. Hence when a field

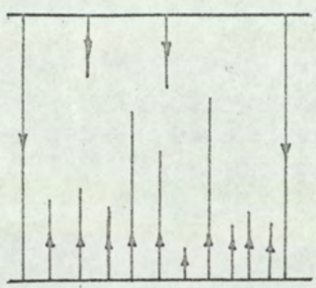

Fig. 3.4

line arrives from the battery it is almost certain to collide with one of the reverse field lines in the space charge area. Accordingly, the factor k of Eq. (3.5) will be unity for almost every field line arriving giving $r \doteqdot 0$ and $\sigma_r^2 \doteqdot 0$. At the same time, however, the cathode emission rate will be fluctuating and it is these fluctuations which contribute to the shot noise of a space charge limited valve.

According to Llewellyn[40] the fluctuations in emission current produce a corresponding fluctuation in anode current given by

$$\delta I = \delta I_s \left(\frac{\partial I}{\partial I_s}\right)_{V_a} \qquad (3.7)$$

In terms of discontinuous noise theory this may be written

$$\delta v = \delta u . \left(\frac{\partial v}{\partial u}\right) \tag{3.8}$$

where δv and δu are small changes in successive intervals of time, of :

(i) the number of electrons arriving at the anode; and

(ii) the number of electrons emitted.

By considering further the constituent terms of the right hand side of this equation it is possible to derive an expression for the mean and variance in terms of the characteristics of the valve.

Consider first the quantity δu. This term has already been defined as the change in emission between successive time intervals δt. The problem now arises of defining this change in terms of physically occurring events, i.e. as a function of the electrons emerging from the cathode. The solution of this problem is rather complicated and may be best explained with the aid of a diagram.

This diagram is shown below and represents two successive

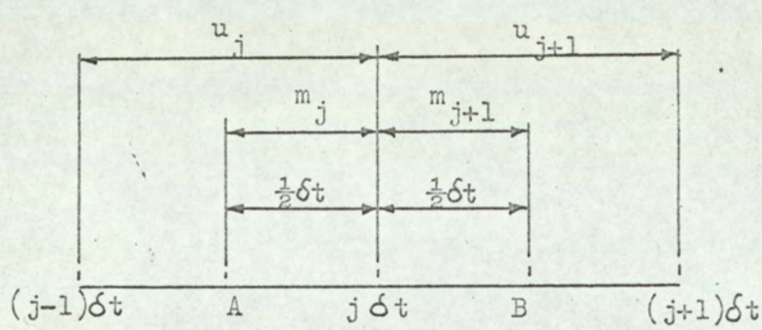

Fig. 3.5

intervals of time in which u_j and u_{j+1} are the electrons emitted in these intervals. Between points A and B of Fig. 3.5 the change in emission will be $(m_{j+1} - m_j)$ where:

(i) m_{j+1} is the contribution from the u_{j+1} electrons in time $\frac{1}{2}\delta t$; and

(ii) m_j is the contribution from the u_j electrons in time $\frac{1}{2}\delta t$.

Since m_j and m_{j+1} are fractions of the u_j and u_{j+1} electrons then

$$m_{j+1} - m_j = u_{j+1}f_{j+1} - u_jf_j$$

where f has the properties:

(i) It fluctuates from one interval to the next.

(ii) $0<f<1$

(iii) Since the distribution of the u electrons within the interval δt follow the laws of chance then it may be represented by a probability distribution. Furthermore, in order to enable the method of p.g.f.s to be used it will be assumed that the distribution is discontinuous, e.g. binomial.

(iv) The distribution describing f must be such that $\bar{f} = \frac{1}{2}$

Now returning to Eq. (3.8) and in particular the term $(\partial v/\partial u)$. Since this quantity depends on both the number and the velocity of the electrons emitted and since it is impossible to be precise about the distribution of either it will be evident that the quantity $\frac{\partial v}{\partial u}$ will fluctuate from one interval to the next. To enable this fluctuation to be incorporated in the theory of the space charge smoothing factor it will, for the moment, be postulated that $\frac{\partial v}{\partial u}$ is representable by a p.g.f.

It therefore follows from the above that Eq. (3.8) may be rewritten as

$$\delta v_j = (u_{j+1} f_{j+1} - u_j f_j) \frac{\partial v}{\partial u}$$

$$= u_{j+1} f_{j+1} \frac{\partial v}{\partial u} + u_j f_j \cdot \left(-\frac{\partial v}{\partial u}\right) \tag{3.9}$$

Since the quantities u and f are positive numbers the second form of this equation is more representative of the physical events occurring than is the first. From this latter equation the p.g.f. for δv_j, say $\Delta V(x)$, is given by

$$\Delta V(x) = U(F(W(x))). \ U(F(W(x^{-1}))) \tag{3.10}$$

where $U(x)$, $F(x)$, $W(x)$ are respectively the p.g.f.s for u, f and $\frac{\partial v}{\partial u}$.

It will be observed from this equation that no suffices are used. This arises because the suffices, j and (j+1), were used only to identify particular processes, and time intervals for the development of an equation between successive random events in terms of integral numbers. Once this equation has been established the numbers such as u_j, u_{j+1}, can take any values allowed by the physics, and are fully represented by the p.g.f.s without further reference to suffices.

It now follows from Eq. (3.10) (Appendix 4) that:

$$\overline{\delta v} = \bar{u}\,\bar{f}\,\bar{w} - \bar{u}\,\bar{f}\,\bar{w} = 0 \tag{3.11}$$

and

$$\sigma^2_{\delta v} = 2[\bar{f}^2\,\bar{w}^2\,\sigma^2_u + \bar{u}\,\bar{f}\,\sigma^2_w + \bar{u}\,\bar{w}^2\,\sigma^2_f] \tag{3.12}$$

Simplification of this second equation necessitates the assignation of suitable distributions to u, f and w. Regarding the latter there are two possible states for each emitted electron, i.e. it may or may not reach the anode. Accordingly, w may be represented by a binomial of mean value $\bar{w}$, i.e.

$$W(x) = \bar{s} + \bar{w}x \;;\quad \bar{s} = 1 - \bar{w}\,,\ \bar{w} = \overline{\left(\frac{\partial v}{\partial u}\right)}$$

Similarly, U(x) may be represented by a binomial distribution. In this case, however, since the number of electrons emitted is very small compared with the number impinging on the surface barrier from the inside of the emitter then this binomial will be of a very high order, and may be approximated to a Poisson distribution (Sec. 2.5.2).

Substituting for σ^2_f, σ^2_u and $\bar{f}$ in Eq. (3.12) gives

$$\sigma^2_{\delta v} = [\bar{f}\,\bar{w}^2\,\bar{u} + \bar{u}\,\bar{w}\,(1 - \bar{w}) + 2\,\bar{u}\,\bar{w}^2\,\sigma^2_f]$$

$$= \frac{\bar{u}}{2}\overline{\left(\frac{\partial v}{\partial u}\right)}^2 + 2\,\bar{u}\,\sigma^2_f\overline{\left(\frac{\partial v}{\partial u}\right)}^2 + \bar{u}\,\overline{\left(\frac{\partial v}{\partial u}\right)}\;\overline{\left(1-\frac{\partial v}{\partial u}\right)}$$

Suffices have been omitted from partial differentials see Bull (Ref.15) p.178 Table 11.1.

By further substituting

$$\overline{\left(\frac{\partial v}{\partial u}\right)} = \overline{\left(\frac{\partial I}{\partial I_s}\right)} \text{ and } \frac{\bar{I}}{\bar{I}_s} = \frac{\bar{v}}{\bar{u}}$$

this simplifies to

$$\sigma^2_{\delta v} = \frac{\bar{v}}{2} \cdot \left(\frac{\bar{I}s}{\bar{I}}\right) \overline{\left(\frac{\partial I}{\partial I_s}\right)}^2 + 2 \bar{v} \sigma^2_f \left(\frac{\bar{I}s}{\bar{I}}\right) \overline{\left(\frac{\partial I}{\partial I_s}\right)}^2$$

$$+ \bar{v} \left(\frac{\bar{I}s}{\bar{I}}\right) \left(1 - \frac{\partial \bar{I}}{\partial I_s}\right)$$

It has been shown by Bull, however, that

$$\overline{\left(\frac{\partial I}{\partial I_s}\right)} = \frac{\bar{I}}{\bar{I}_s} \cdot g \frac{kTc}{e\bar{I}} \cdot \overline{\left(\frac{\partial Va}{\partial V_m}\right)} = \frac{\bar{I}}{\bar{I}_s} (1 + \xi)$$

hence Eq. (3.13) may be rewritten in the form

$$\sigma^2_{\delta v} = \frac{v}{2} \cdot \frac{\bar{I}}{\bar{I}_s} \cdot (1 + \xi)^2 + 2\sigma^2_f \bar{v} \left(\frac{\bar{I}}{\bar{I}_s}\right)(1 + \xi)^2$$

$$+ \bar{v} (1 + \xi) \left(1 - \frac{\bar{I}}{\bar{I}_s} (1 + \xi)\right)$$

Substituting this expression in Eq. (3.6) for $\overline{\Gamma^2}$ gives

$$\Gamma^2 = \frac{\bar{I}}{2\bar{I}_s} (1 + \xi)^2 + 2\sigma^2_f \left(\frac{\bar{I}}{\bar{I}_s}\right) (1 + \xi)^2$$

$$+ (1 + \xi) \left(1 - \frac{\bar{I}}{\bar{I}_s} (1 + \xi)\right) \tag{3.14}$$

For space charge limited valves where $\frac{\bar{I}}{\bar{I}_s} << 1$ and

$(1 + \xi) < 1$, (Richards) this equation gives

$$\Gamma^2 = (1 + \xi) = \frac{gkT_c}{e\bar{I}} \cdot \overline{\left(\frac{\partial V_a}{\partial V_m}\right)} \tag{3.15}$$

for space charge limited diodes under conditions of interest for noise.

Even when the diode is operated in the retarding field region of its characteristic and there is little or no space charge, all the quantities required to utilise equation (3.14) can be identified, i.e.:

(i) there is a potential barrier opposing current flow, Figs. 3.6 and 3.7; and

(ii) the anode current I is much less than the emission current I_s.

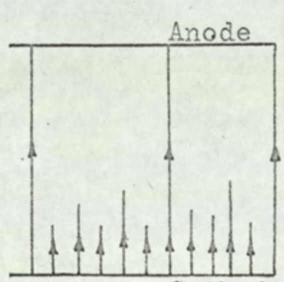

Fig. 3.6

Field Line Configuration in Retarding Field Diode

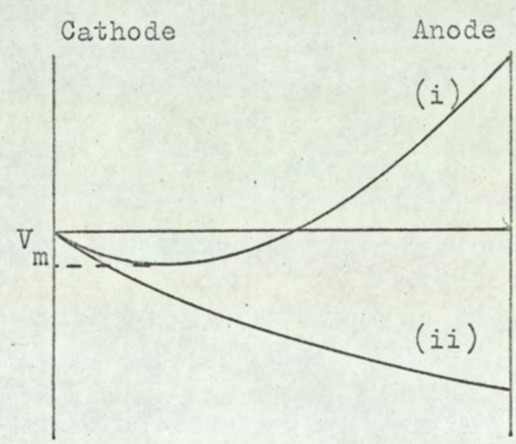

Fig. 3.7

Electric Field of Diode

(i) Space charge limited diode

(ii) Retarding field diode

It might be expected, therefore, that Eqs. (3.14) and (3.15) would predict the magnitude of the fluctuations in a retarding field diode. This may be tested by substituting the appropriate values of $\frac{\bar{I}}{\bar{I}_s}$ and $(1 + \xi)$ in Eq. (3.14) - $\frac{\bar{I}}{\bar{I}_s} \ll 1$, $(1 + \xi) = 1$. Using these substituions then all terms in the right hand side of the equation, with the exception of the third are small enough to be disregarded giving

$$\Gamma^2 = 1$$

which agrees with the experimental data.

When the valve is temperature limited, however, Eq. (3.14) can no longer be used to describe the fluctuations since all the emitted electrons are absorbed in neutralising the field lines from the battery. The random nature of the emission current is then taken into account by the factor k of Eq. (3.5) and Eq. (3.6b) gives a quantitative description of the fluctuations.

4. NOISE MEASUREMENTS

In noise measurements the powers involved are very small so that in order to obtain a perceptible reading amplification of the source of noise is required. The measuring system, therefore, takes the form shown in Fig. 4.1 where S is the source, A a linear amplifier and M.S.V. for reasons which will become apparent later, a mean square voltmeter.

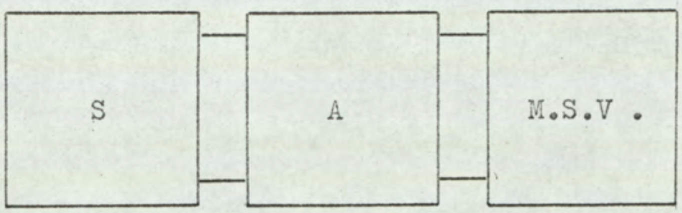

Fig. 4.1

Applying Eqs. (2.4) and (2.7) to this system gives the meter defelction, θ, in terms of the system parameters. Thus

$$\theta = \int_0^\infty |Y(w)|^2 |A(w)|^2 W_x(f) \frac{dw}{2\pi} \tag{4.1}$$

where $W_x(f)$ is the power frequency spectrum of the source, and $A(w)$ and $Y(w)$ are the system functions of the amplifier and source respectively.

For the arrangement used in the experimental work in which the source has a white noise spectrum and the amplifier a frequency characteristic which is directly proportional to the mid-band gain G, Eq. (4.1) simpifies to

$$\theta = G^2 W_x \int_0^\infty |Y(w)|^2 |F(w)|^2 \frac{dw}{2\pi} \tag{4.2}$$

where GF(w) represents the amplifier frequency response (Fig. 4.2).

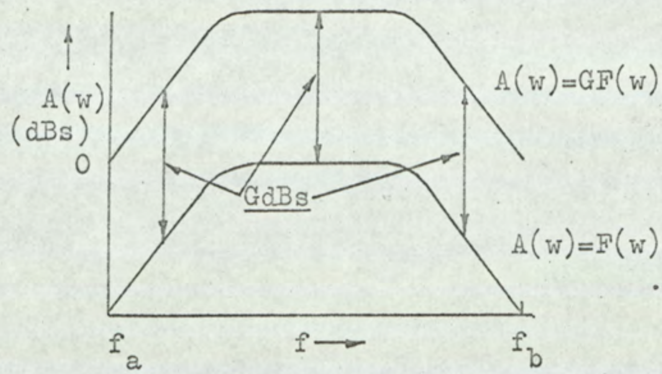

Fig. 4.2

It follows, therefore, that the meter deflection is proportional to the power and hence to the variance of the source. Accordingly, this system may be used for the measurement of sources for which the variance provides an accurate and calculable description of the processes occurring.

It is obvious from the above that if the amplifier gain drifts then the meter deflection will drift also. However, since it is difficult to construct an amplifier with sufficient constancy of gain to allow the measuring equipment in which it is incorporated to be permanently calibrated it is necessary to use a comparison method, i.e. the source noise is compared with some standard of source of noise at the input to the amplifier. In the present measurements two such standards are used, these are:

(i) Thermal noise[33,45] in a resistor R in equilibrium with its surroundings.

(ii) Shot noise [29,32] in a temperature limited diode.

These noise sources together with their equivalent circuits are shown below (Fig. 4.3) where:

$\overline{i^2}$ = equivalent mean square noise current generator.

$\overline{v^2}$ = equivalent mean square noise voltage generator.

k = Boltzmann's constant.

df = elemental bandwidth.

$\bar{I}$ = mean current in diode.

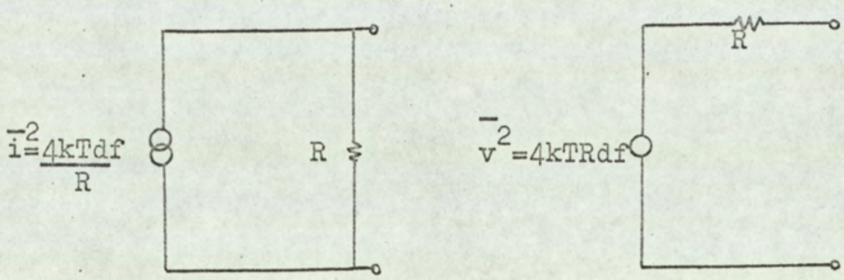

a) Current source b) Voltage source

Thermal Noise Sources

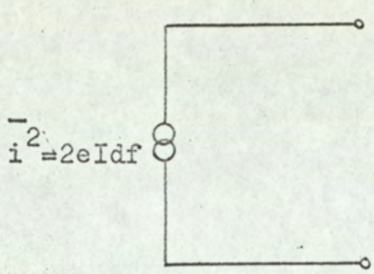

c) Shot Noise Source

Fig. 4.3

It will now be shown how these two sources may be used for the calibration of noise measuring equipment and the determination of the noise level of space charge limited diodes.

4.1 Amplifier Noise[47,48]

The basic difficulty with noise measurement is that before the source noise can be determined it is necessary to take account of the background noise of the amplifier. Probably the simplest method of calibrating the amplifier noise is to use the Johnson noise from a resistive input. Thus, if the amplifier is represented by an equivalent noise resistance R_n in series with the input grid lead the system appears as in Fig. 4.4.

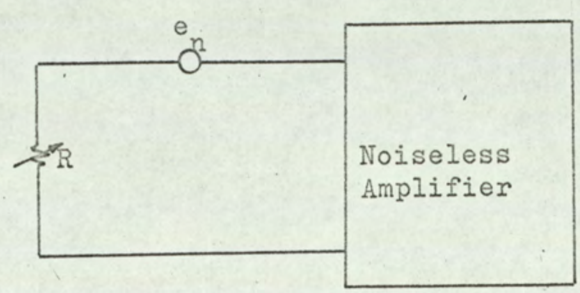

Fig. 4.4

Assuming the conditions of Eq. (4.2) apply the meter deflections will be :

For R = 0

$$\theta_0 = 4kTR_nG^2 \int_0^\infty |F(w)|^2 df \qquad (4.3)$$

For $R \neq 0$

$$\theta_1 = \theta_o + 4kTRG^2 \int_0^\infty |F(w)|^2 df \tag{4.4}$$

and $\theta_1 = 2\theta_o$ when $R = R_n$

If the amplifier has no extraneous feedback, so that $F(w)$ is entirely independent of the gain, and the indicator gives an accurate mean square value then the varying of R should give a linear plot (Fig. 4.5), thus providing a useful method of checking the equipment.

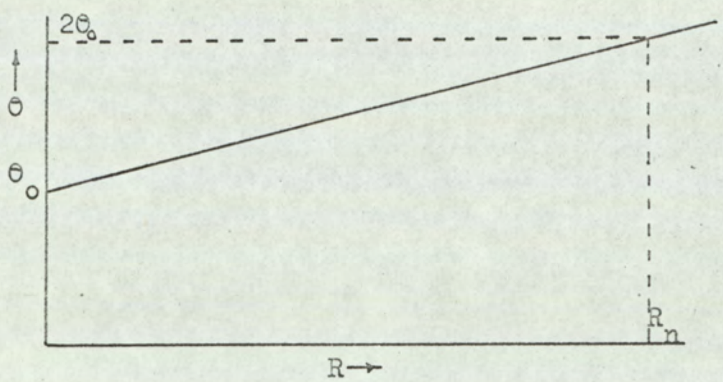

Fig. 4.5

4.2 Comparison of Shot and Thermal Noise Sources

Consider the schematic diagram shown in Fig. 4.6 where i_c and i_r represent respectively the shot noise of a temperature limited diode and the thermal noise of a resistor R. If the power density spectra of these source are represented by W_c and W_r respectively then from Eq. (4.2) the meter deflections will be :

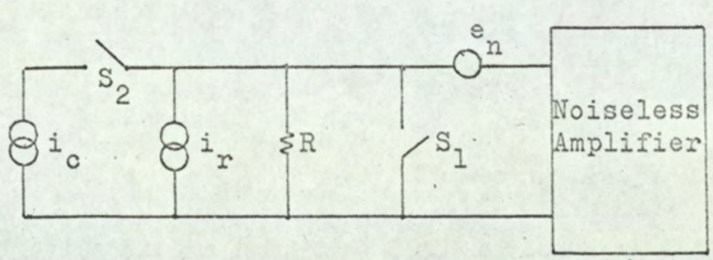

$$\theta_0 = 4kTR_n G^2 \int_0^\infty |F(w)|^2 df \qquad S_1 \text{ closed}$$

$$\theta_1 = \theta_0 + W_r R^2 G^2 \int_0^\infty |F(w)|^2 df \qquad S_1 \text{ and } S_2 \text{ open} \qquad (4.5)$$

$$\theta_2 = \theta_1 + W_c R^2 G^2 \int_0^\infty |F(w)|^2 df \qquad S_1 \text{ open, } S_2 \text{ closed} \qquad (4.6)$$

and $$W_c = W_r \frac{\theta_2 - \theta_1}{\theta_1 - \theta_0} \qquad (4.7)$$

If the substitutions $W_c = 2eI_c$ (Fig. 4.3c), $W_r = \frac{4kT}{R}$ (Fig. 4.3a) are made in the above then it follows:

(i) the plot of $\theta_2 - I_c$ is a straight line law, (Fig. 4.7)

and(ii) $\theta_2 - \theta_1 = \theta_1 - \theta_0$ when $I_c = I_{cr} = \frac{2kT}{eR}$ (4.8)

and these two conditions may be used as further criteria for checking the equipment.

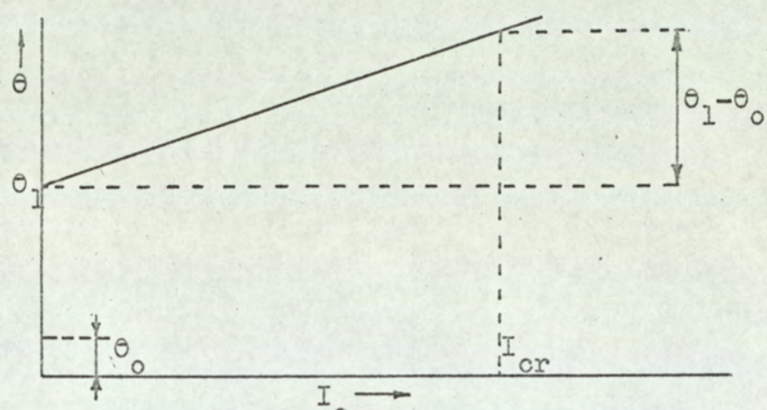

Fig. 4.7

4.3 Measurement of Noise of Space Charge Limited Diodes

Here two methods for measuring the noise of space charge limited diodes are described; the standard of comparison for both methods being a temperature limited diode.

4.3.1 Method 1

The sources and their equivalent generators are shown below. R represents a resistor which may be switched to either the source under test, i_d, or to the standard source, i_c, and R_a represents the impedance of the test diode. Substituting W_d, W_c and W_r for the power spectra of the test diode, standard diode and thermal noise sources respectively the meter deflections will be given by :

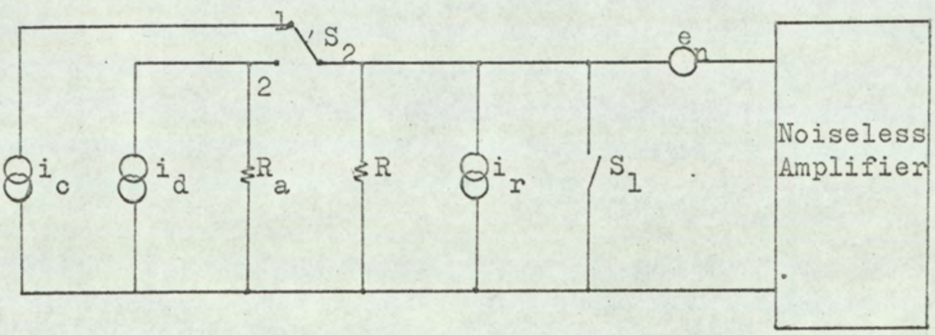

Fig. 4.8

$$\theta_0 = 4kTR_n G^2 \int_0^\infty |F(w)|^2 df \qquad S_1 \text{ closed}$$

$$\theta_1 = \theta_0 + W_r R^2 G^2 \int_0^\infty |F(w)|^2 df \qquad S_1 \text{ and } S_2 \text{ open}$$

$$\theta_2 = \theta_0 + (R^2 G^2)(W_r + W_c) \int_0^\infty |F(w)|^2 df \qquad S_1 \text{ open, } S_2 \text{ in position 1} \qquad (4.9)$$

$$\theta_3 = \theta_0 + (GRR_a/R+R_a)^2 (W_r + W_d) \int_0^\infty |F(w)|^2 df$$

S_1 open

S_2 in position 2 (4.10)

$$\therefore \quad \frac{\theta_3 - \theta_0}{\theta_2 - \theta_0} = \frac{W_r + W_d}{W_r + W_c} \quad \frac{R_a^2}{(R_a + R)^2}$$

and since

$W_r = 2eI_{cr}$ Eq. (4.8)

$W_d = 2eI_d\Gamma^2$; I_d = mean current in diode

$W_c = 2eI_c$

then

$$\frac{\theta_3 - \theta_0}{\theta_2 - \theta_0} = \frac{(\Gamma^2 I_d + I_{cr})}{(I_c + I_{cr})} \quad \frac{(R_a)^2}{(R + R_a)^2} \tag{4.11}$$

$$\text{and } \Gamma^2 = \frac{\theta_3 - \theta_0}{\theta_2 - \theta_0} \quad (R + R_a/R_a)^2 \quad \frac{(I_c + I_{cr})}{I_d} - \frac{I_{cr}}{I_d} \tag{4.12}$$

Since all the factors in this equation are measurable the smoothing factor Γ^2 may be determined.

The derivation of this equation has been made assuming that Y(w) of Eq. (4.2) is resistive over the entire frequency range of the amplifier. In practice, however, it has been found that the input capacitance of the amplifier makes Y(w) reactive and this affects the accuracy of the measurement.

Let C represent the input capacitance of the amplifer. This capacitance will be distributed across the resistance R. From Eq. (4.2) the meter deflections will be :

$$\theta_o = 4kTR_n G^2 \int_{f_a}^{f_b} |F(w)|^2 df \qquad S_1 \text{ closed}$$

$$\theta_1 = \theta_o + G^2 W_r \int_{f_a}^{f_b} \frac{|F(w)|^2 R^2 df}{(1 + w^2C^2R^2)} \qquad S_1 \text{ and } S_2 \text{ open}$$

$$\theta_2 = \theta_o + G^2 R^2 (W_r + W_c) \int_{f_a}^{f_b} \frac{|F(w)|^2 df}{1 + w^2C^2R^2} \qquad S_1 \text{ open, } S_2 \text{ in position 1} \tag{4.13}$$

$$\theta_3 = \theta_o + G^2 r^2 \int_{f_a}^{f_b} \frac{(|F(w)|^2 df)}{1 + w^2C^2r^2} (W_r + W_d) \qquad S_1 \text{ open, } S_2 \text{ in position 2} \tag{4.14}$$

where

$$r = \frac{RRa}{R + R_a}$$

and f_a, f_b are the frequencies at which the amplifier gain has fallen to a negligibly small value, i.e. where $|F(w)| << 1$.

Hence

$$\frac{\theta_3 - \theta_o}{\theta_2 - \theta_o} = \frac{\int_{f_a}^{f_b} \frac{(|F(w)|^2 r^2 df)}{1 + w^2C^2r^2} (W_r + W_d)}{\int_{f_a}^{f_b} \frac{(|F(w)|^2 R^2 df)}{1 + w^2C^2R^2} (W_r + W_c)} \tag{4.15}$$

which for $(2\pi Cf_b R)^2 << 1$, the condition under which most of the experiments are made, is identical to Eq. (4.11).

4.3.2 Method 2[31,54]

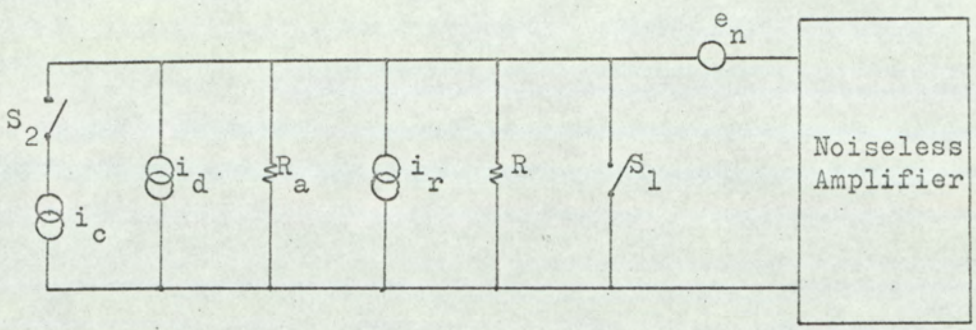

Fig. 4.9

Consider Fig. 4.9 which represents in schematic form the experimental arrangement. Using Eq. (4.2) and the same nomenclature as in method 1 above the meter deflections will be:

$$\theta_o = 4kTR_n G^2 \int_{f_a}^{f_b} |F(w)|^2 df \qquad S_1 \text{ closed}$$

$$\theta_1 = \theta_o + G^2 r^2 \int_{f_a}^{f_b} \frac{|F(w)|^2 df}{1 + w^2 C^2 r^2} (W_r + W_d) \quad S_1 \text{ and } S_2 \text{ open} \tag{4.16}$$

$$\theta_2 = \theta_o + G^2 r^2 \int_{f_a}^{f_b} \frac{(|F(w)|^2) df}{1 + w^2 C^2 r^2} (W_r + W_c + W_d) \quad S_1 \text{ open, } S_2 \text{ closed}$$

$$= \theta_1 + G^2 r^2 \int_{f_a}^{f_b} \frac{(|F(w)|^2 df)}{1 + w^2 C^2 r^2} (2eI_c) \tag{4.17}$$

A plot of $\theta_2 - I_c$ will, therefore, follow the form shown in Fig. 4.10.

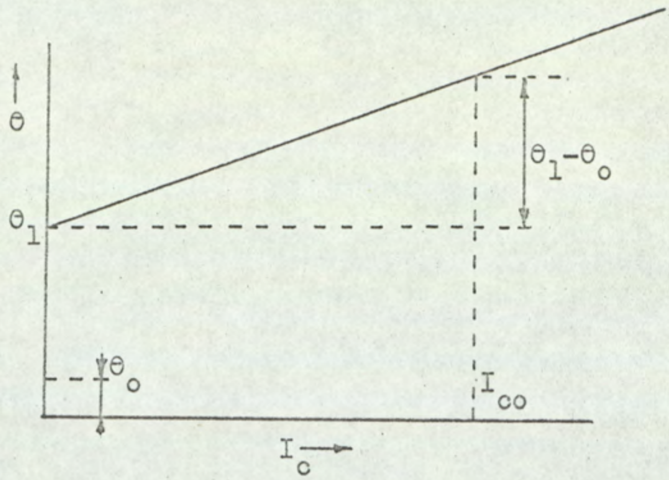

Fig. 4.10

From Eqs. (4.16) and (4.17)

$$\frac{\theta_2 - \theta_o}{\theta_1 - \theta_o} = \frac{(W_r + W_c + W_d}{W_r + W_d)}$$

so that when $\theta_2 - \theta_o = 2\theta_1 - 2\theta_o$, then

$$W_c = W_r + W_d$$

$$I_{co} = I_{cr} + \Gamma^2 I_d$$

and $$\Gamma^2 = \frac{I_{co}}{I_d} - \frac{I_{cr}}{I_d} \qquad (4.18)$$

-I_{co} being the current at which $\theta_2 - \theta_o = 2\theta_1 - 2\theta_o$ (Fig.4.10).

An important feature of this method is that - unlike that of method 1 - its accuracy is not influenced by the amplifier input capacitance. This is due to the fact that the source load , Y(w), is constant throughout the measurement.

It should be noted that the preceding analyses have been confined to linear circuits where the parameters are invariant. It has been postulated, however, in Chapter 3 that the valve impedance fluctuates and this has been confirmed experimentally by Breeze and others (Chapter 3). It is apparent, therefore, that Eqs. (4.12) and (4.18) may need to be modified to include the possibility of an impedance fluctuation. Unfortunately, however, it is not yet apparent how this may achieved.

5. EXPERIMENTAL WORK

5.1 Purpose of the Investigation

In Chapter 3 a theoretical examination of space charge smoothing has been made using the model of a discontinuous electric field. As a result it was concluded that the space charge smoothing factor of a planar diode may be represented by an equation of the form

$$\Gamma^2 = (1 + \xi) = \frac{g.kT_c}{e\bar{I}} \overline{\left(\frac{\partial V_a}{\partial V_m}\right)} \qquad (5.1)$$

Bull[11] has shown that all the factors of this equation may be derived from anode current - anode voltage curves. Richards has carried out the experiment of drawing the curves and from them calculating the smoothing factor. His results when compared with experimental measurements by Bell on a similar type of valve have indicated that Eq.(5.1) gives a better estimate of the space charge smoothing factor than North's equation (Eq. 3.2).

The fact that Richards was obliged to compare his measurements of $(1 + \xi)$ with measurements of noise made by Bell on a different valve of the same type must, however, detract greatly from the value of the comparison. It is apparent, therefore, that before any generalisations concerning the validity of Eq. (5.1) can be made further experimental evidence is required. The aim of the present investigation is to obtain this evidence.

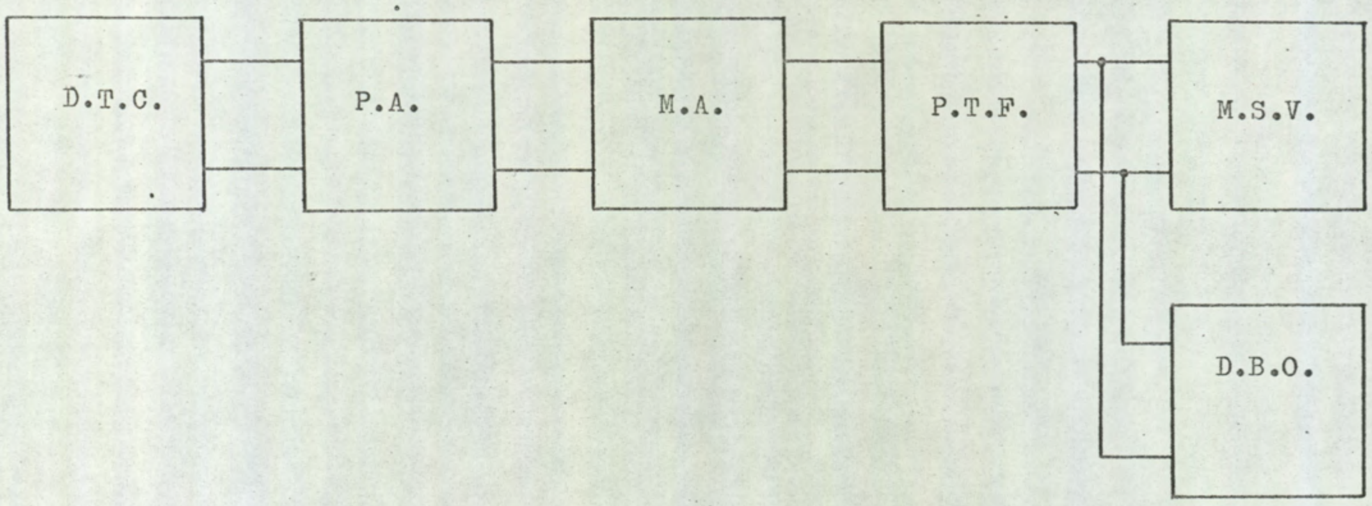

Fig. 5.1 Block Schematic

5.2 Experimental Equipment

The experimental arrangement is shown in schematic form in Fig. 5.1, it comprises: a diode test circuit (D.T.C.), a preamplifier (P.A.), a main amplifier (M.A.), a 50 Hz parallel-tee-filter (P.T.F.), a mean square voltmeter (M.S.V.) and a double beam oscilloscope (D.B.O).

The oscilloscope was used to monitor continuously the input signal to the measuring device. In this way it was possible to observe any unwanted electrical, or microphonic, disturbances and hence eliminate the errors due to these causes. Of the unwanted disturbances those due to stray fields were reduced, as far as was possible, by suitable shielding; e.g. most of the components were encased in earthed metal boxes and all interconnectors were made of coaxial cable.

5.2.1 Diode Test Circuit.

During the course of the investigation the two diode circuits shown in Figs. 5.2 and 5.3 were used. As can be seen from the diagrams the two circuits are very much alike with resistors and capacitors for removing l.f. pick up from the connecting leads to the h.t. units and meters, and with a temperature limited diode as a reference source.

The main difference between the circuits is in the inclusion of a signal generator, S.G. and two switches

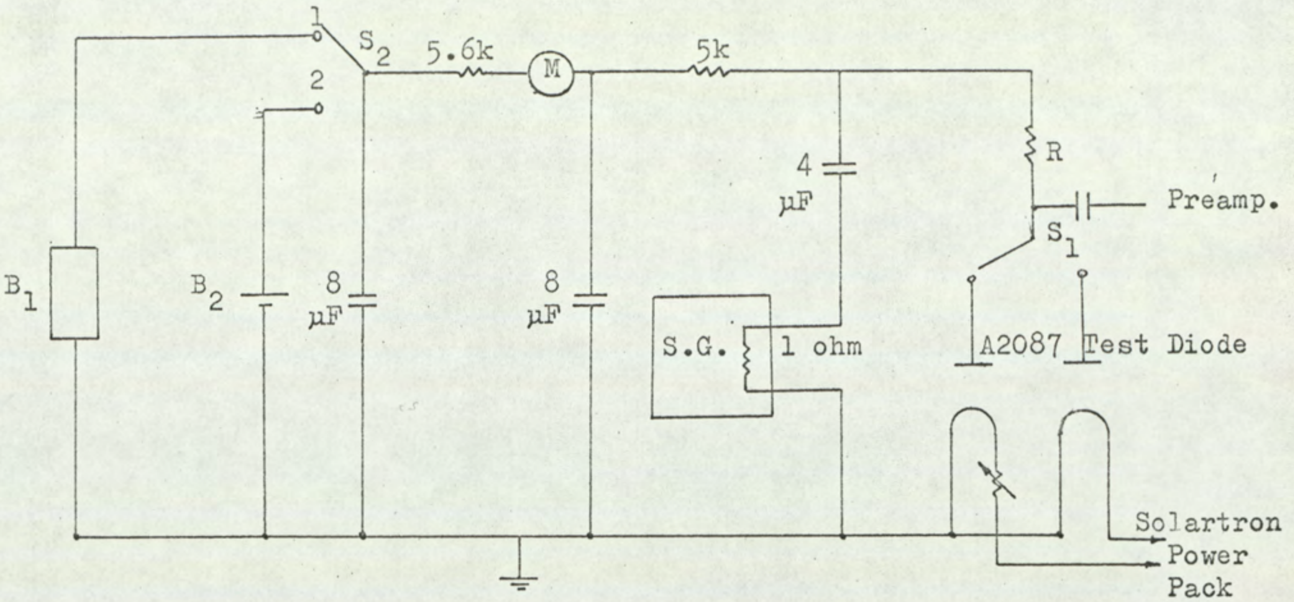

B_1 Solartron Power Supply B_2 120V Battery S.G. Signal Generator
M Cambridge Microammeter

Fig. 5.2

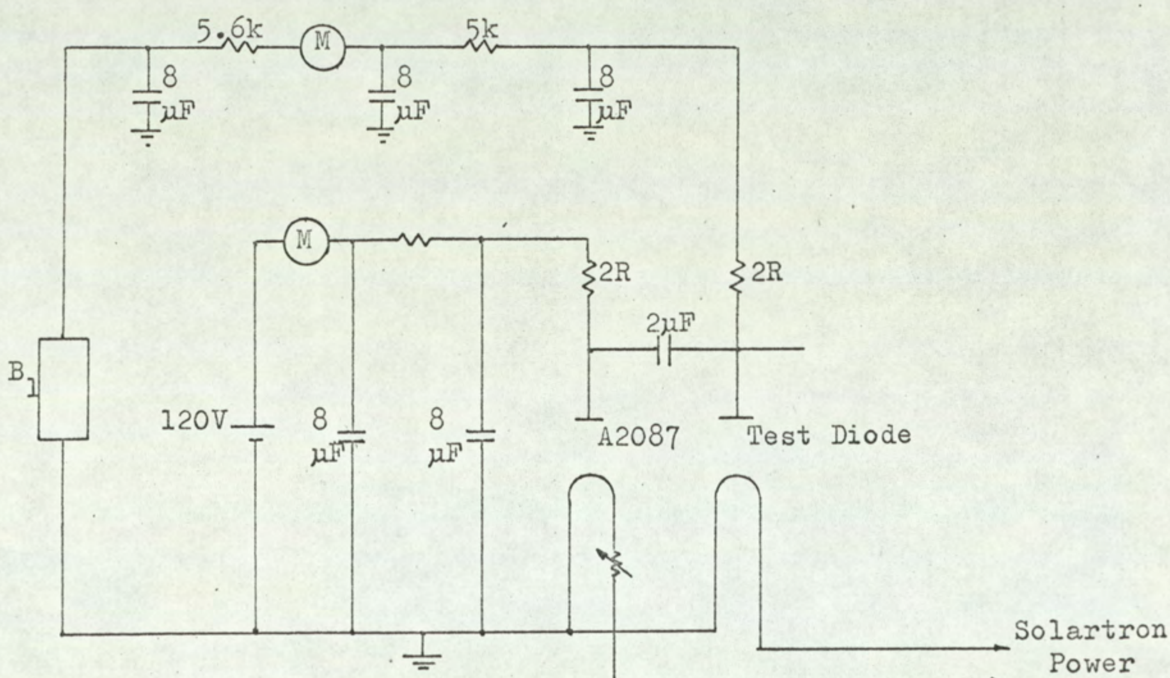

B_1, M as above

Fig. 5.3

S_1 and S_2 in test circuit 1 (Fig. 5.2). The inclusion of the signal generator enabled measurements of the valve impedance to be made (Sec. 5.4). The switches, on the other hand, were used to isolate each of the valves in turn and so enabled the noise of each valve to be measured separately.

Thus with switch S_1 the amplifier may be connected to the anode of either the test diode or the reference (A2087) diode. Furthermore, since the test diode was operated from a variable supply voltage - thus enabling it to be operated under a variety of operating conditions - whereas the reference diode was operated with a high anode voltage - so eliminating space charge effects - then when making the switch from one valve to the other it was also necessary to switch the supply units. This was the function of the switch S_2 which was used to switch between a 120V battery and a $\pm$ 30V (variable in o.1 V steps) Solartron power pack; the first of these being the h.t. supply for the reference diode and the second that for the test diode.

5.2.2 Preamplifier

The circuit arrangement (Fig.5.4) of the preamplifier is of the type developed by Bozic. Its gain is constant over the frequency range 1-400 kHz (Fig. 5.5), and its equivalent noise resistance when measured - using the method described in Sec. 4.1 - over the bandwidth of the amplifier is 380 ohms. (Fig. 5.6).

Fig. 5.4 Preamplifier

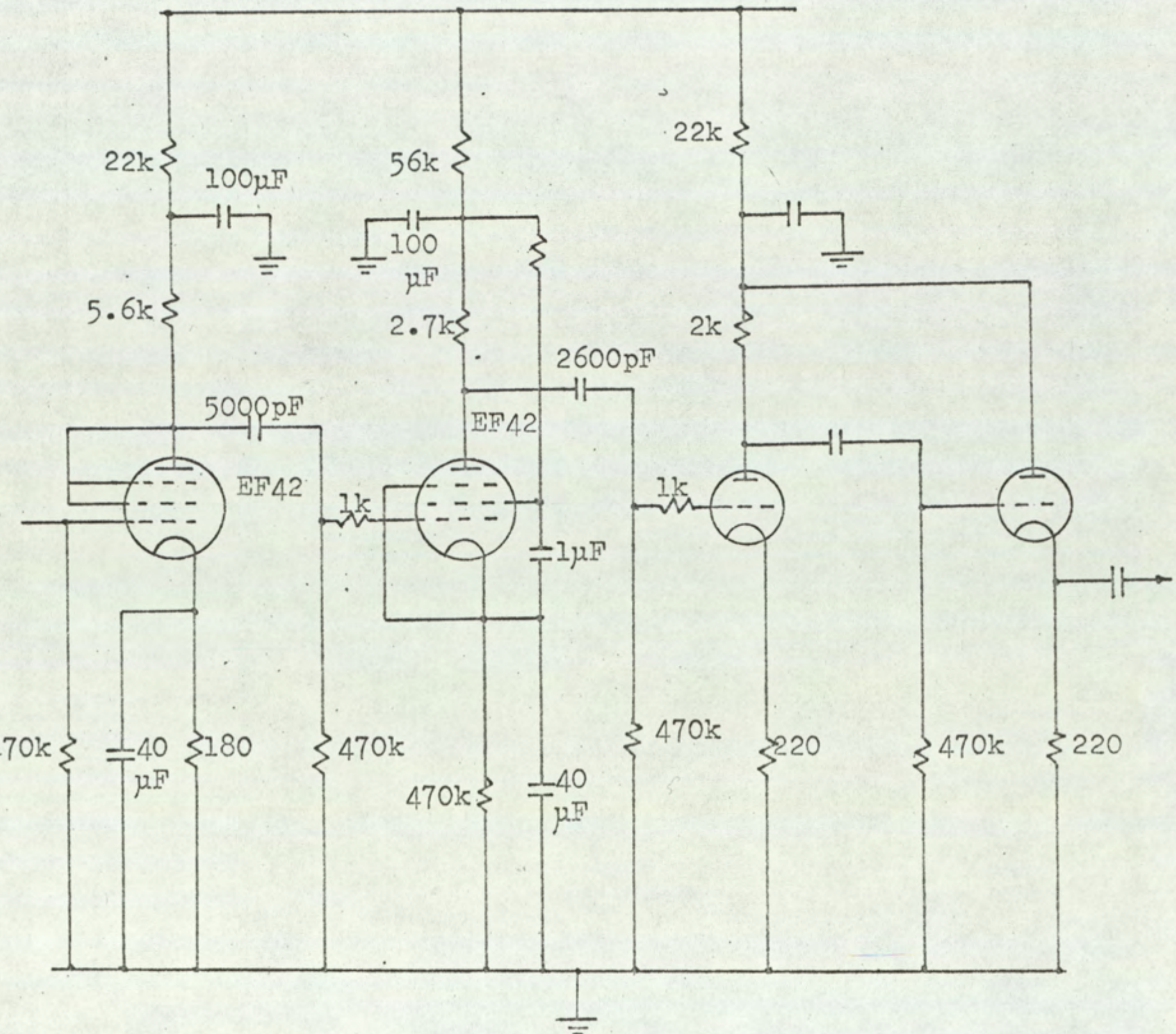

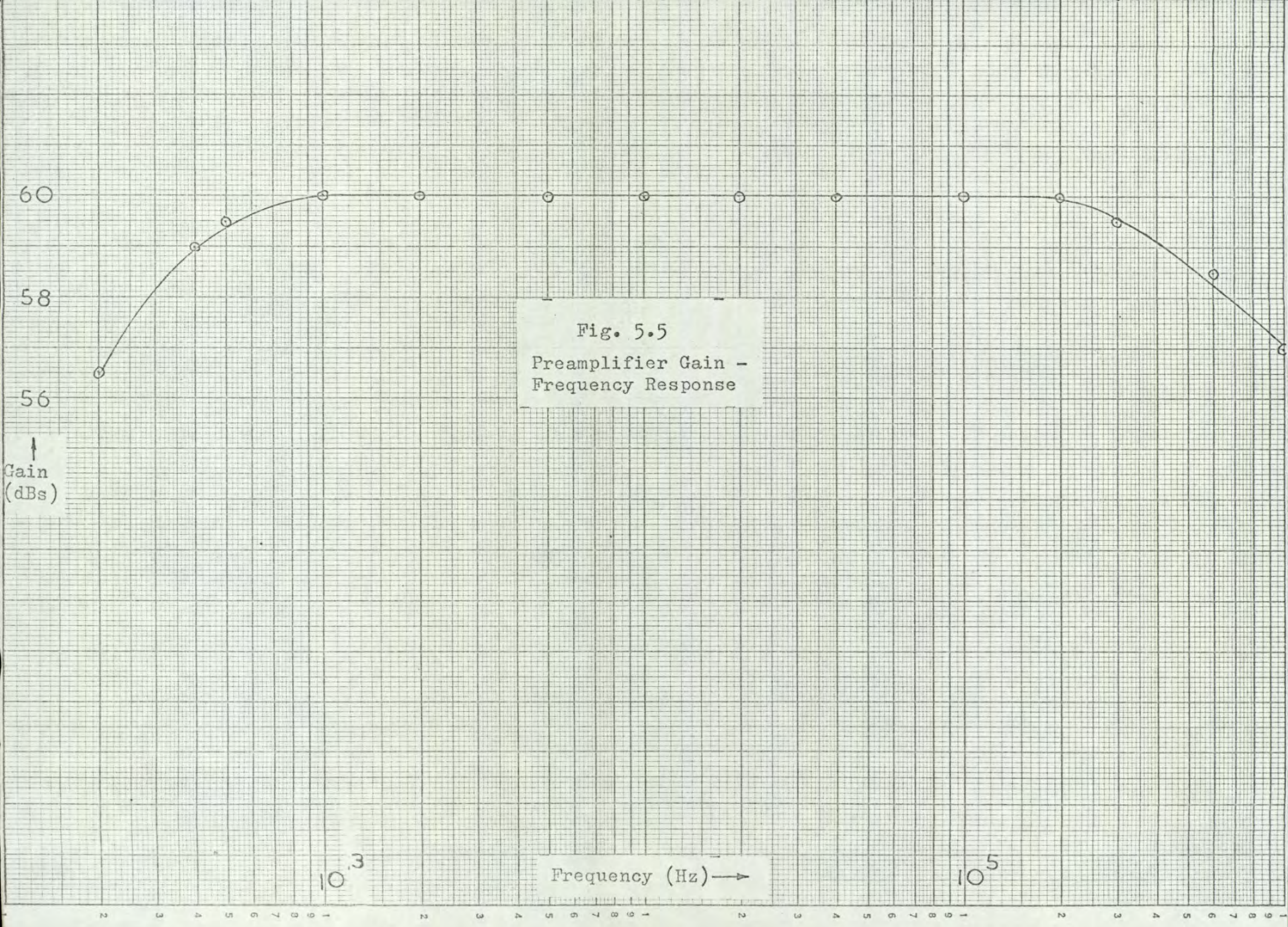

Fig. 5.5

Preamplifier Gain - Frequency Response

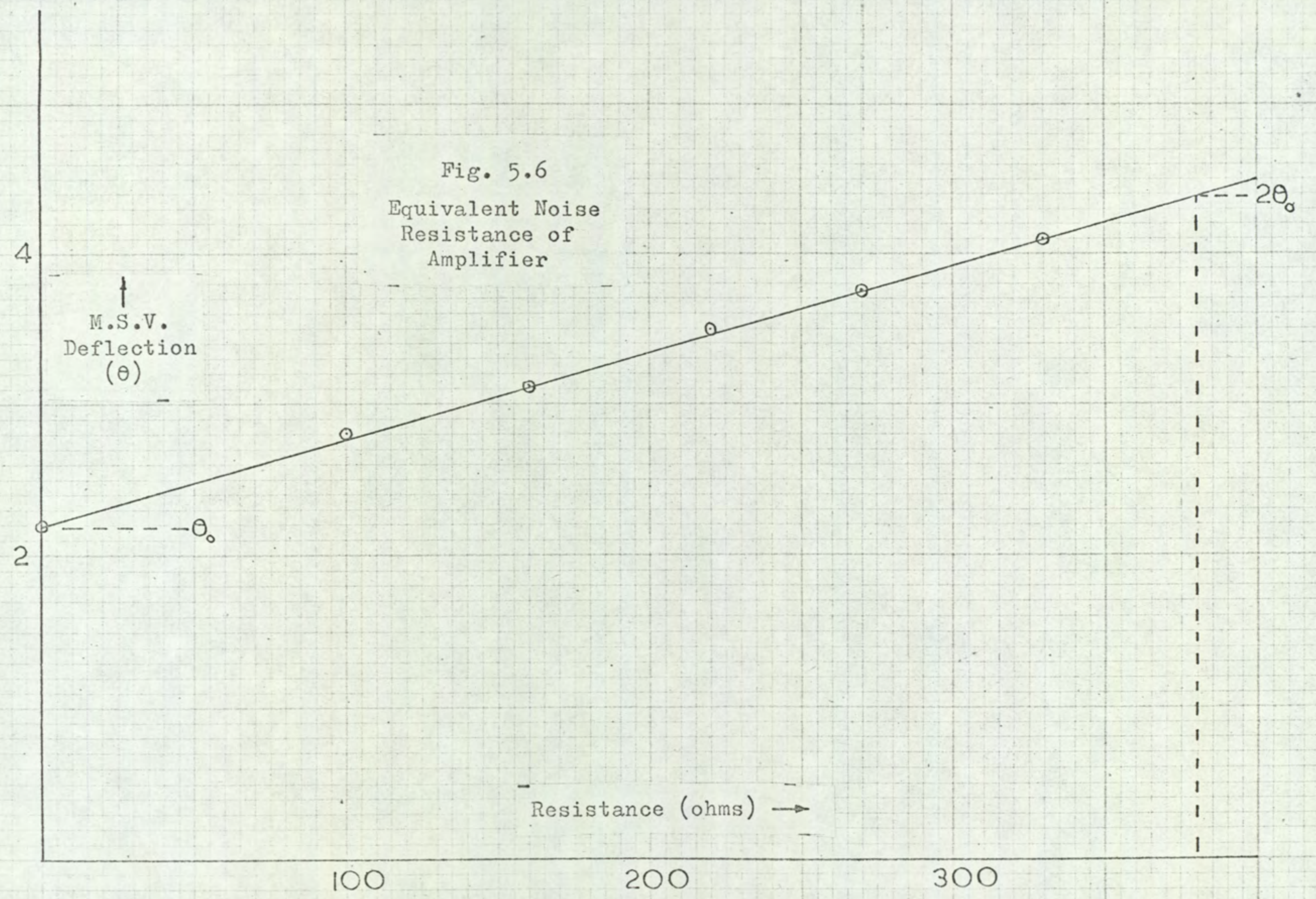

Fig. 5.6
Equivalent Noise
Resistance of
Amplifier
M.S.V.
Deflection
(θ)
4
2
θ_0
$2\theta_0$
Resistance (ohms)
100
200
300

5.2.3 Main Amplifier

The main amplifier is a variable gain device, this device being varied according to the sensitivity of the detector and the noise level of the source under test. Because of the high gain of the preamplifier stage the signal level at the input to the main amplifier is sufficiently high for the noise of the latter to be neglected.

The amplifier used in the tests was a commercially available Solartron AWS51A. This amplifier has a maximum gain of approximately 80 dBs (Fig. 5.7) and incorporates an attenuator for varying the gain. Checks on this attenuation system indicated that within the bandwidth of the device the errors were negligible.

5.2.4 Parallel-Tee-Filter[22,51]

In much of the equipment described above the supply units - largely as a matter of convenience - were mains-operated devices. Unfortunately, however, the use of this mains-operated equipment increased the susceptibility of the system to unwanted 50 Hz pick up. Accordingly, a filter was inserted into the system to remove this pick up.

The filter used was a parallel-tee-network of the form shown in Fig. 5.8. The insertion loss of this filter - that is the attenuation that is introduced when the filter is inserted - shows a maximum of 23dBs at 50 hz decreasing to 3dBs for frequencies greater than 1kHz

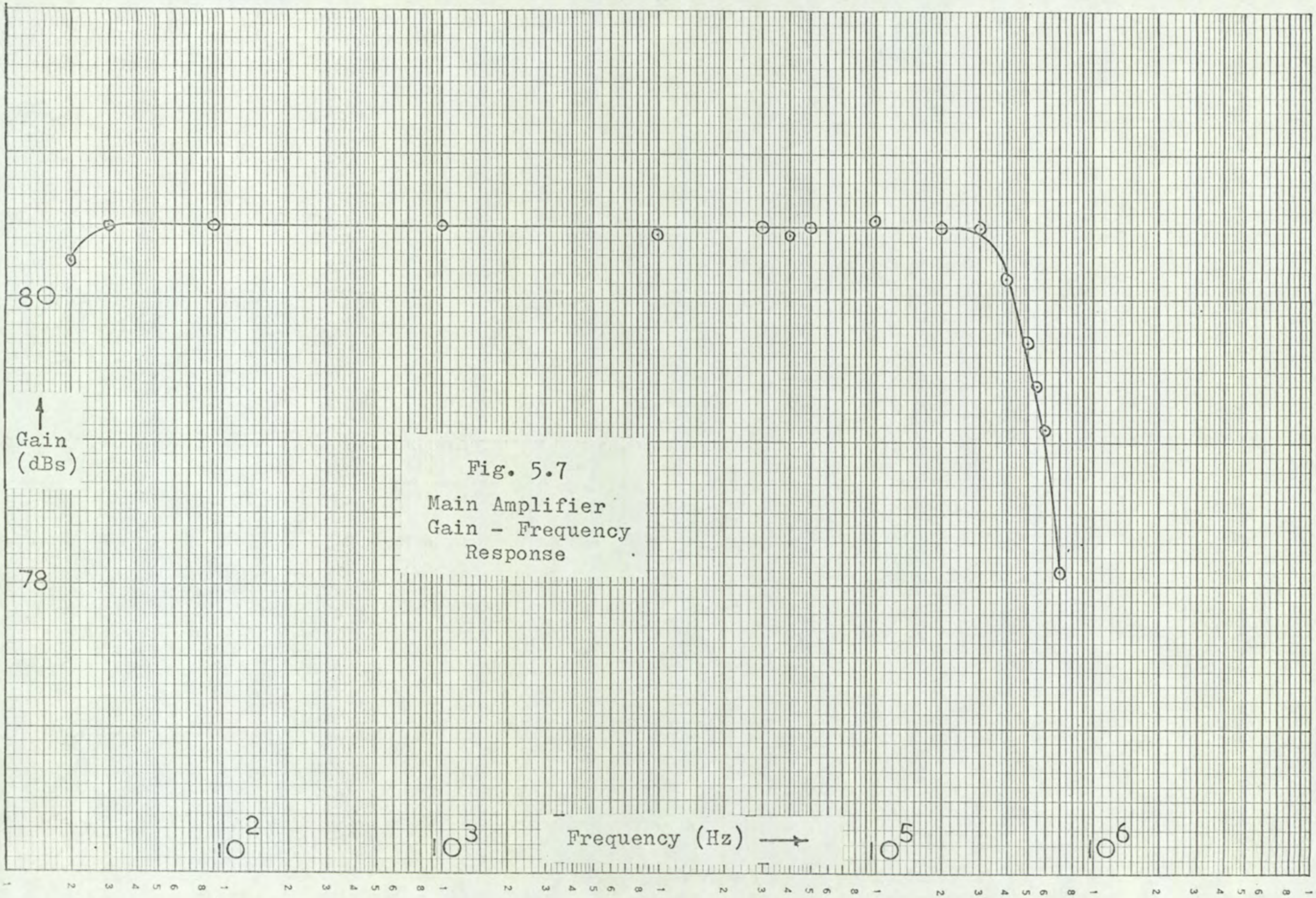
80
78
Gain
(dBs)
Fig. 5.7
Main Amplifier
Gain - Frequency
Response
10^2
10^3
10^5
10^6
Frequency (Hz)

(Fig. 5.9).

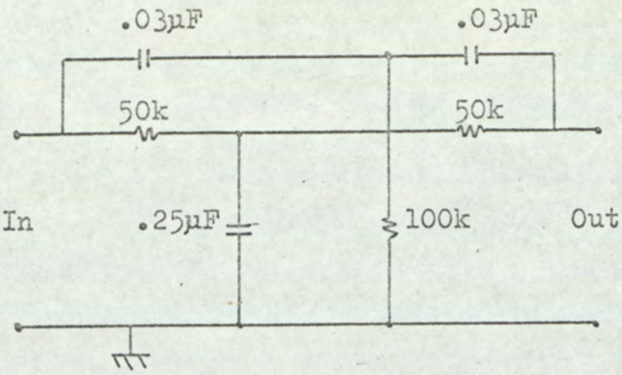

Fig. 5.8

5.2.5 Mean Square Voltmeter

The mean square voltmeter was of the type used by Bozic and will be dealt with more fully in Chapter 8.

5.3 Determination of Space Charge Smoothing Factor from Characteristic Curves[11,50]

To show how the characteristic curves of a valve may be used to determine the smoothing factor consider Fig. 5.10 which represents the $l_n\bar{I} - V_a$ plot for constant heater voltage.

In the retarding and space charge limited regions the curve of Fig. 5.10 behaves according to the law.

$$\bar{I} = \bar{I}_s \exp \frac{eV_m}{kT_c} \tag{5.2}$$

where $\bar{I}_s$ and T_c are determined by the heater voltage. Since in the retarding region the potential barrier opposing the current flow, that is V_m, is equal to the anode voltage V_a then for large negative voltages this equation becomes

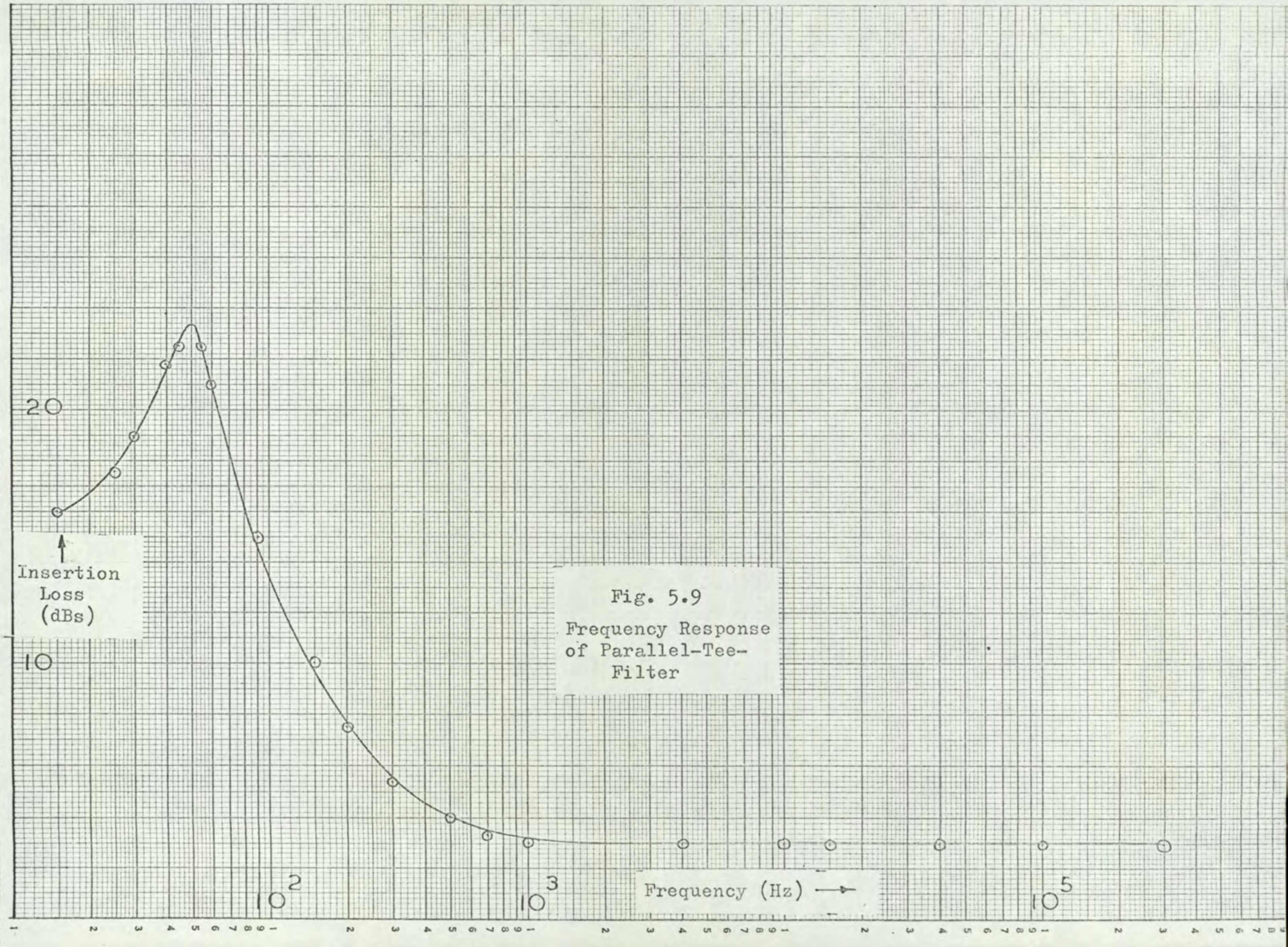

20
10
Insertion
Loss
(dBs)
Fig. 5.9
Frequency Response
of Parallel-Tee-
Filter
Frequency (Hz)
10^2
10^3
10^5

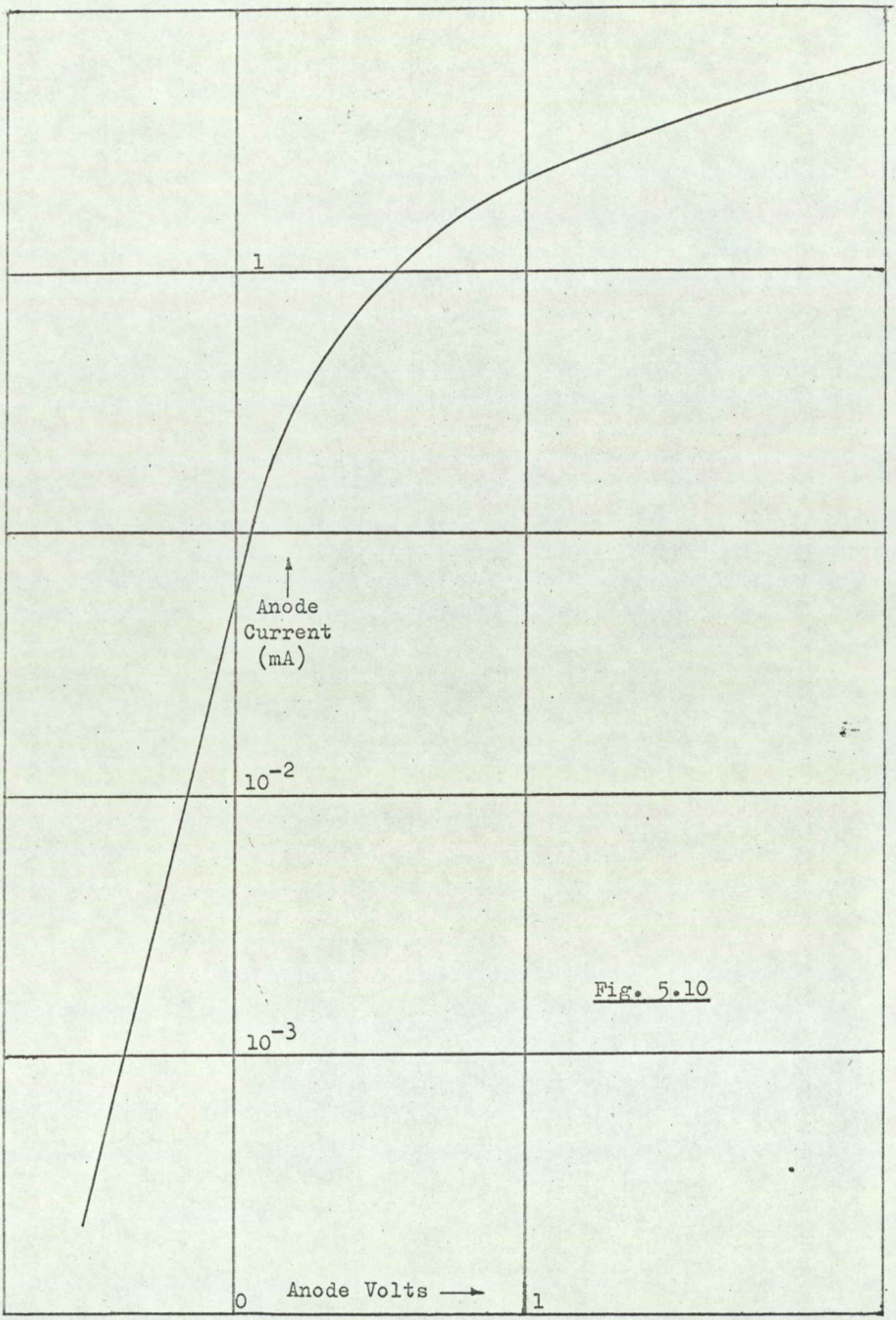

Fig. 5.10

$$\bar{I} = \bar{I}_s \exp \frac{eV_a}{kT_c} \tag{5.3}$$

By expressing Eq. (5.2) in its logarithmic form and using the results of reference (11) it can be shown that

$$\frac{\partial \ln \bar{I}}{\partial V_m} = \frac{g}{\bar{I}}$$

Similarly from Eq. (5.3) it follows

$$\frac{\partial \ln \bar{I}}{\partial V_a} = \frac{e}{kT_c}$$

i.e. the slope of the characteristic curve (Fig. 5.10) in the retarding region is $\frac{e}{kT_c}$

Thus the determination of the slope of the valve characteristic in the retarding and space charge limited regions gives the information necessary for the determination of North's smoothing factor $\left(\Gamma^2 = 1.29\ g.\frac{kT_c}{e\bar{I}}\right)$

If now reference is made to Eq. (5.1) which represents the smoothing factor obtained using the discontinuous approach it can be seen that in order to determine this smoothing factor and so compare it with North's it is necessary to find $\overline{(\partial V_a/\partial V_m)}$. For any value of anode current I_o the method is as follows:

(i) Draw a characteristic curve at a temperature slightly different from the operating temperature of the valve (Fig. 5.11).

(ii) Through the point A representing the current I_o a line ADB is drawn parallel to the voltage axis and the points at which this line intersect the characteristic curves represent V_a and $V_a + \delta V_a$ respectively.

(iii) Extrapolate the linear portion of the characteristics to intersect the line AD at C and C' respectively. Those intersections represent the potential barrier at the different cathode temperatures namely V_m and $V_m + \delta V_m$.

(iv) Measure CC' and AB and since all points on the line AD represent a constant value of $\bar{I}$ then.

$$\frac{AB}{CC'} = \overline{\left(\frac{\partial V_a}{\partial V_m}\right)}$$

It was by computations of this type that Richards obtained his results. He found, however, that the determination of points such as A and B becomes very difficult at the higher currents. The method is, therefore, best used with linear plots of $\bar{I} - V_a$ instead of log $\bar{I} - V_a$ plots since in this case the lines of constant current intersect the curves at high angles, and the points of intersection are consequently well defined.

In the present work the method of Richards has been slightly modified. Instead of trying to determine the conductance g graphically it is found by applying small

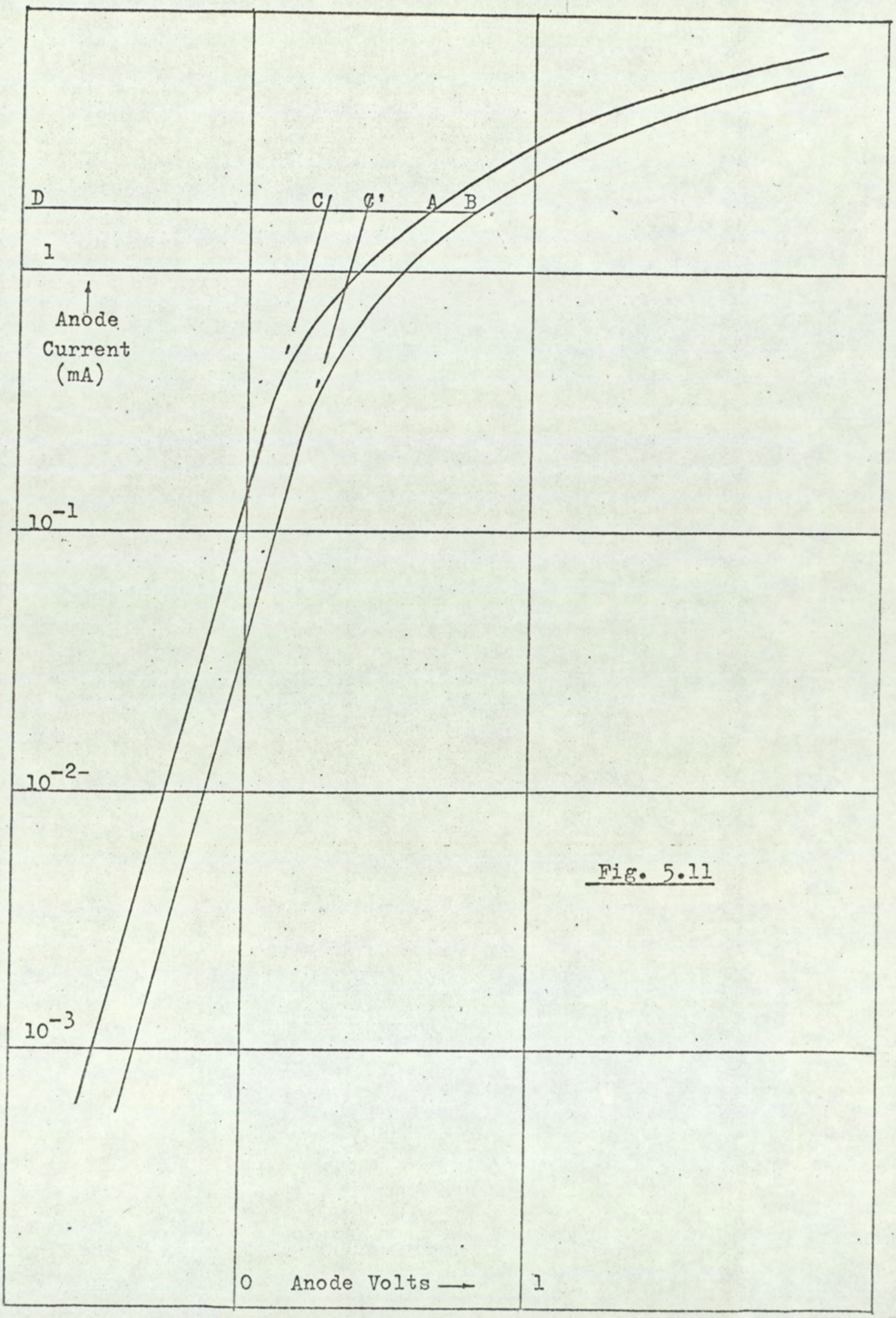

Fig. 5.11

signals to the valve. This has two advantages over Richards' method:

(i) It eliminates the necessity of having to judge the tangential slope of a graph, always a difficult operation.

(ii) The increments in voltage considered are very much smaller so that the direct measurements gives a value for the impedance which is probably much nearer the true incremental slope at a point on curve.

5.4 Direct Measurement of Valve Impedance

The valve impedance measurements were effected using the system of Fig. 5.1 in conjunction with the test diode circuit of Fig. 5.2.

Providing that the output of the signal generator, S.G., (Fig. 5.2) is greater than say 10 times the noise voltage of the system, the mean square voltmeter deflection with first the A2087 diode and then the test diode will be

$$\theta_1 = C_1 \overline{E^2}$$

$$\theta_2 = C_1 \overline{E^2} \quad \overline{\left(\frac{R_a}{R_a+R}\right)^2}$$

where C_1 is a constant, $\overline{E^2}$ the mean square voltage of the signal generator and $R_a = \frac{1}{g}$ = the mean incremental slope. Thus if R is accurately known - from a bridge measurement - θ_1 and θ_2 are noted then from

$$\left(\frac{\theta_1}{\theta_2}\right)^{\frac{1}{2}} = \frac{R_a}{R_a + R}$$

R_a may be calculated.

The small signal voltages required for the measurement were provided by the signal generator of Fig. 5.12. This generator was of the type described by Hathaway and was capable of providing 0.8μV - 1024μV in 1dB steps over a frequency range of 15Hz - 50kHz.

Before attempting any measurements on actual valves it was decided to check the accuracy of the experimental technique. To do this the test diode of Fig. 5.2 was replaced by a resistor and its resistance, R_t, measured by a method analogous to that described above. This measured value of resistance could then be compared with its known value - obtained using a bridge with an accuracy of better than 0.1%.

The results so obtained are shown below, from which it can be seen that there is a tendency for the method to become a little less accurate as the ratio $\frac{R}{R_t}$ increases. Nonetheless, it may be expected that the valve impedance measurements will be correct to within 3%.

Fig. 5.12 One Ohm Signal Generator

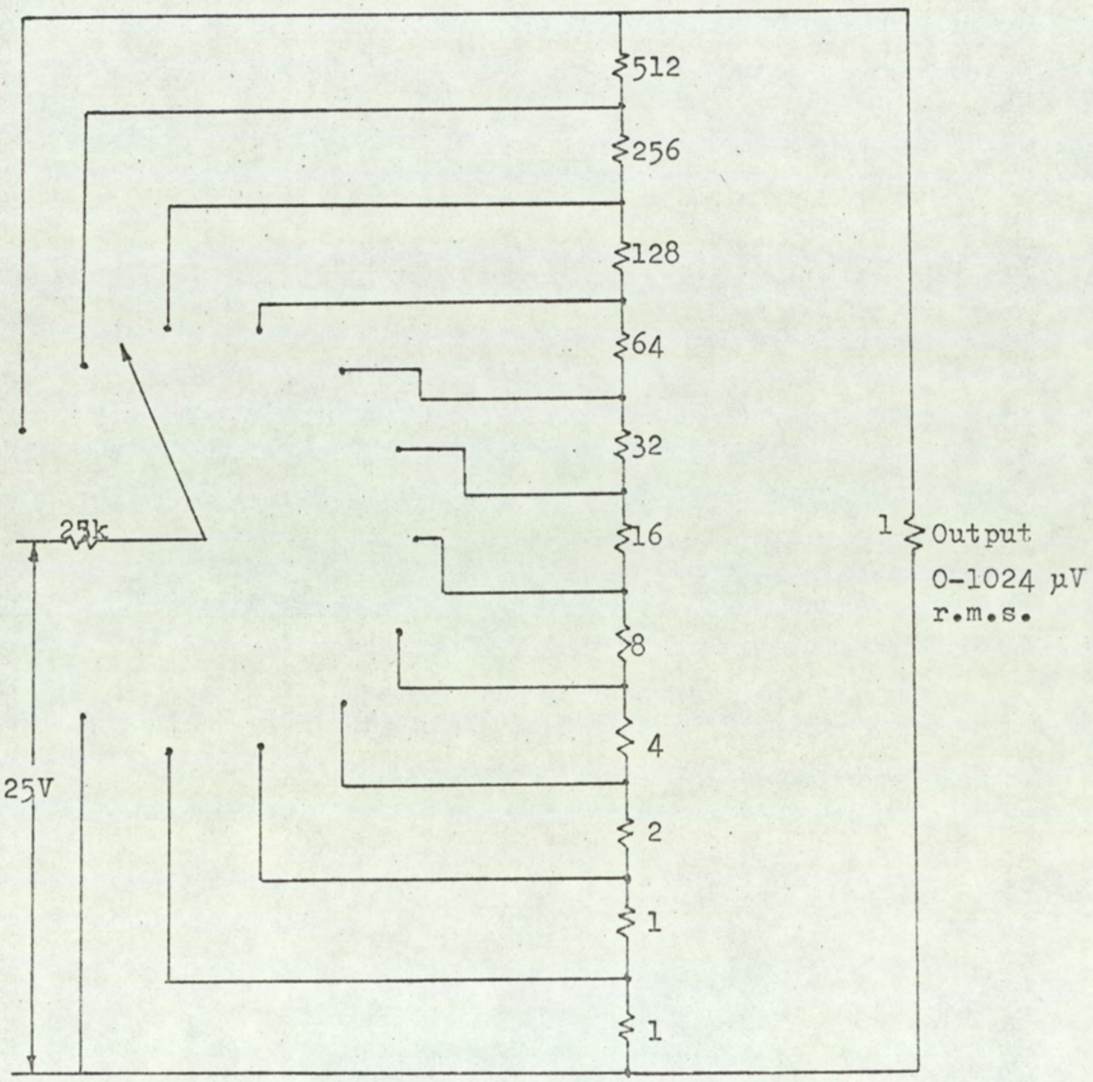

All resistors high stability
measured in ohms.

Anode load resistor R	Actual Value of test resistor	Measured Value of test resistor
10kΩ	6.18 kilohms	6.15 kilohms
10kΩ	1 kilohms	0.99 kilohms
10kΩ	500 ohms	492 ohms
10kΩ	110 ohms	107 ohms

5.5 Measurement of the Space Charge Smoothing Factor.

In Sections (4.3.1) and (4.3.2) two methods for finding space charge smoothing factors have been suggested. The first of these - which will be referred to as method 1 - enables the slope impedance to be found at the same time and this may be used in Eqs. (3.2) and (5.1) for making a theoretical determination of the space charge smoothing factor. The other method, method 2, on the other hand, provides information about the smoothing factor only. In the present investigation both methods have been used, thus serving as a cross check on their accuracy.

During the course of the investigation four valves, all of the EB91 type, were tested. These valves have a structure which is almost planar and measurements of the type described by Fitch (Appendix 5) have indicated that in the space charge region they may be expected to show complete space charge limitation. It follows, therefore, that for the experiments in the space charge region the conditions will be those for which Eqs. (3.2) and (5.1), i.e. the smoothing factor equations, are applicable.

Using Method 1 - test diode circuit of Fig. 5.2 - the smoothing factor of each of the four valves was measured. The measurements were effected in five stages:

(i) The preamplifier was short circuited and the mean square voltmeter deflection, θ_0, noted.

(ii) With the preamplifier connected to the reference diode the method described in Sec. (4.2) was used to find I_{cr} (the equivalent shot noise current of the anode load resistor).

(iii) The preamplifier was switched to the EB91 valve, the anode current, I_d, set to a suitable value and the mean square voltmeter reading noted.

(iv) S_1 and S_2 (Fig. 5.2) were switched so that the reference valve was again connected to the amplifier. By means of its heater supply voltage the anode current, I_c, was adjusted to a value equal to that of the test diode, i.e. $I_c = I_d$.

(v) With the method described in the preceding section the valve impedance was measured.

These measurements were then repeated with a different value of anode load resistance thus enabling a cross check of the impedance measurements to be made.

At the same time as these tests were being carried out, Shaw, using an experimental arrangements almost identical to that of Fig. 5.1 made - using Method 2 - experimental checks on two of the valves (designated as valves 2 and 3). Finally, to complete the smoothing factor measurements, the author - also using Method 2 - made, with the diode test circuit of Fig. 5.3, tests on valves 1 and 4.

Having completed the space charge smoothing factor tests an experimental arrangement was set up to enable the anode current - anode voltage characteristics to be found. From these characteristics a theoretical determination of the space charge smoothing factor (Sec. 5.3) was made.

The arrangement for determining the valve characteristics is shown in Fig. 5.13. The anode current was measured by means of either the d.c. microammeter or d.c. amplifier depending on whether the current was greater or less than one microamp. The anode voltage, on the other hand, was obtained by measuring the supply unit voltage and subtracting the voltages dropped across the circuit components.

5.6 Correction for Input Capacitance

In a previous section it has been shown that(Section 4.3.1) when the input capacitance of the amplifier is

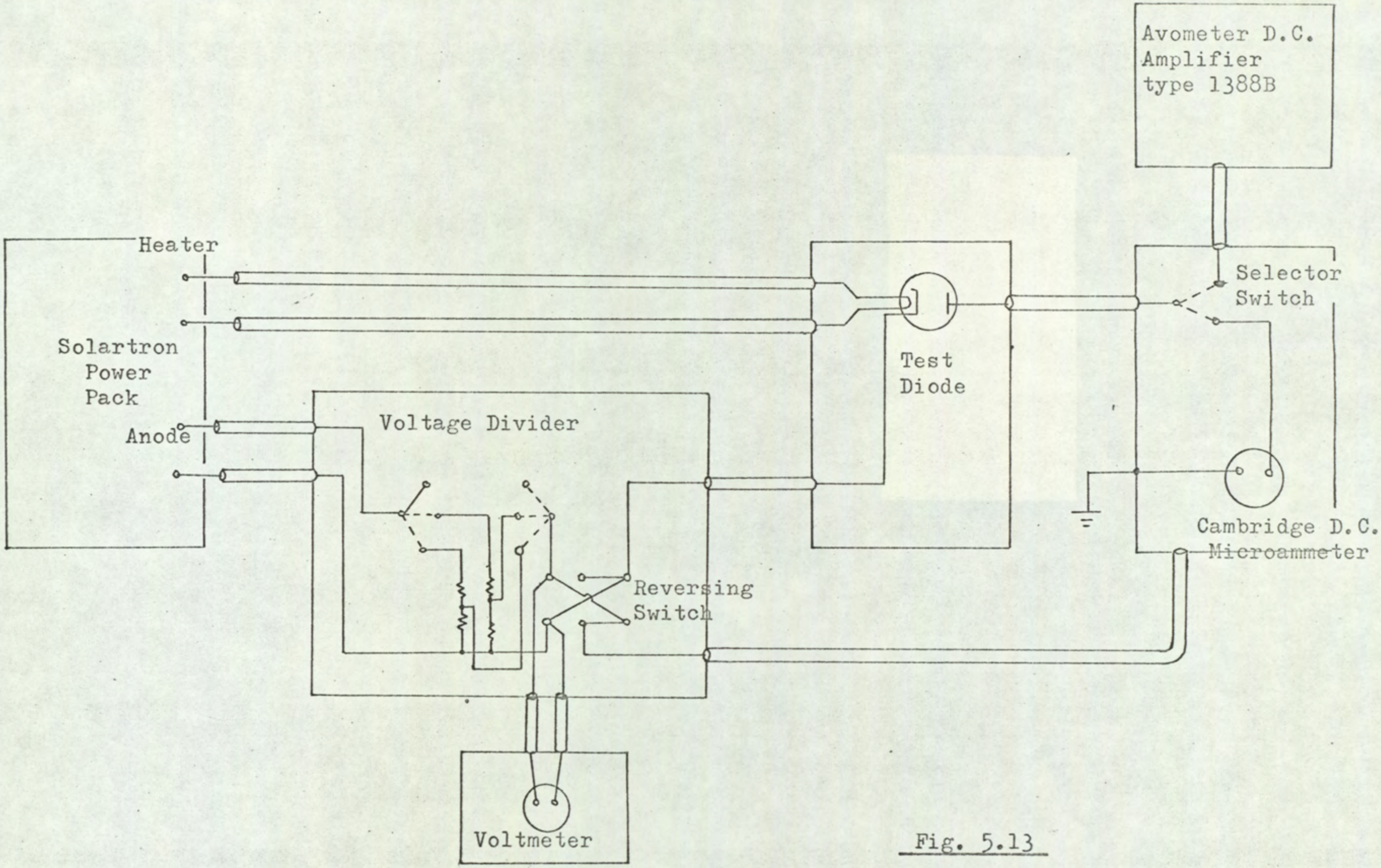
Avometer D.C.
Amplifier
type 1388B
Heater
Selector
Switch
Solartron
Power
Pack
Test
Diode
Voltage Divider
Anode
Reversing
Switch
Cambridge D.C.
Microammeter
Voltmeter

Fig. 5.13

$$\Phi = \frac{\int_{f_a}^{f_b} \frac{|F(w)|^2}{1+w^2C^2r^2}\,df}{\int_{f_a}^{f_b} \frac{|F(w)|^2}{1 + w^2C^2R^2}\,df}$$

finite then

$$\frac{\theta_3 - \theta_o}{\theta_2 - \theta_o} \left(\frac{R_a + R}{R_a}\right)^2 = \frac{\left(\int_{f_a}^{f_b} \frac{|F(w)|^2}{1+ w^2C^2r^2}\, df\right) [I_{cr} + I_d\Gamma^2]}{\left(\int_{f_a}^{f_b} \frac{|F(w)|^2}{1+ w^2C^2R^2}\, df\right)[I_{cr} + I_c]}$$

Assuming that $I_c = I_d$ and $(2\pi Crf_b)^2 << 1$ it follows that

$$\left(\frac{R_a + R}{R_a}\right)^2 \left(\frac{\theta_2 - \theta_o}{\theta_3 - \theta_o}\right) = \left(\frac{\Gamma^2 + \frac{I_{cr}}{I_d}}{1 + \frac{I_{cr}}{I_d}}\right)\Phi \tag{5.4}$$

where Φ is a constant for all values of current being equal to unity for small values of R and greater than unity for large values. Furthermore, it can be seen from this latter equation that if the valve is operated in the retarding region - where it is an experimental fact that $\Gamma^2 = 1$ - then

$$\left(\frac{\theta_3 - \theta_o}{\theta_2 - \theta_o}\right) \left(\frac{R_a + R}{R_a}\right)^2 = \Phi \tag{5.5}$$

Thus a useful method of measuring the space charge smoothing factor, taking into account the amplifier capacitance, is to first of all measure the quantities θ_3, θ_2, θ_o and R_a with the valve operating in the retarding region, use these quantities to calculate Φ, then substitute this value of Φ in Eq. (5.4) to find the space charge smoothing factor. In the present series of tests this was the procedure followed. It was found, however, that the capacitive effect only manifested itself - the smoothing factor being greater than unity in the retarding region - with high values of anode load. For this reason many of the results described below have been obtained using Eq. (4.12) (in addition bridge measurements have indicated that the capacitance C is such that for values of R below about 5 kilohms the effect is negligible).

5.7 Results

The results of the smoothing factor measurements using method 1 are shown on log Γ^2 - anode current axes in Figs. 5.14 - 5.17. The curves for the 1 and 3 kilohm resistors were computed using Eq. (4.12) - the results in the retarding region indicating that $\Phi = 1$ - and those for the 10 kilohm load from Eq. (5.4) (where Φ was approximately 1.1).

The results of method 1 are reproduced again in figs. 5.18 - 5.21 and Figs. 5.22 - 5.25. In the first set of curves they are compared with the results of method 2, and in the second set with the curves calculated from Eqs. (3.2), North's, and (5.1), the author's.

These calculated curves were obtained in the manner described earlier the relevant factors being derived from:

(i) The measured values of diode impedance.

(ii) Log anode current - anode voltage characteristics

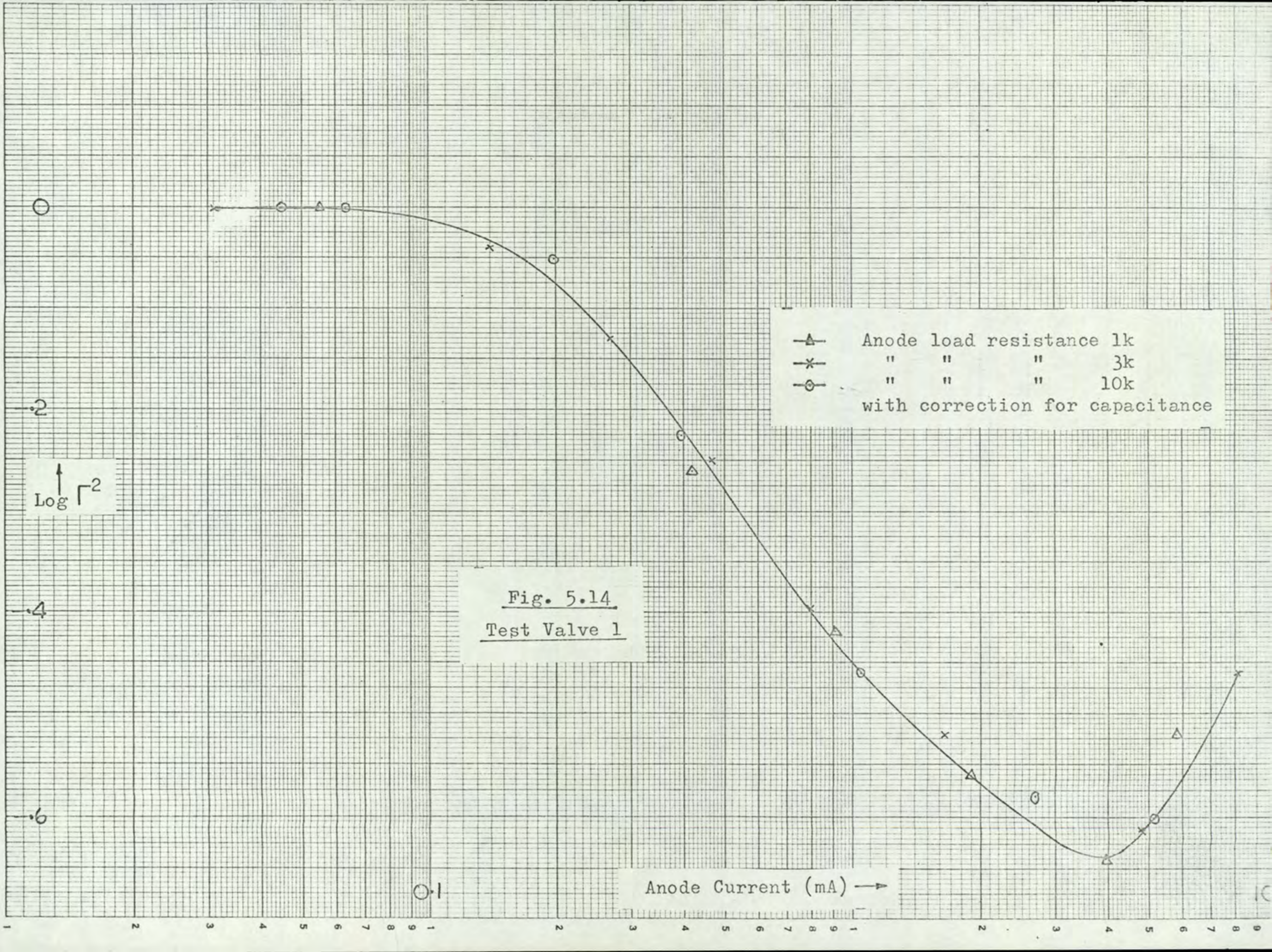

Fig. 5.14

Test Valve 1

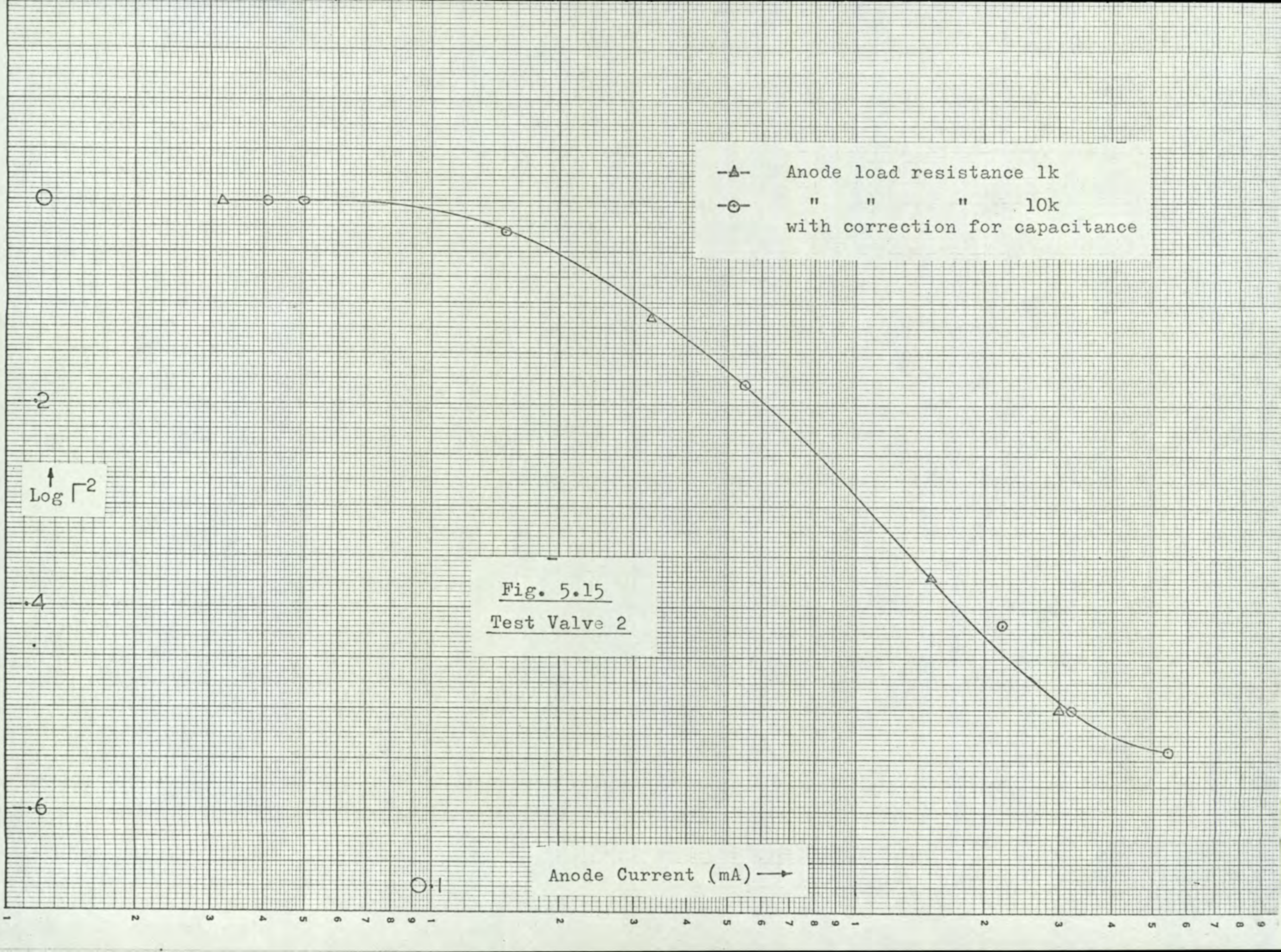

Fig. 5.15

Test Valve 2

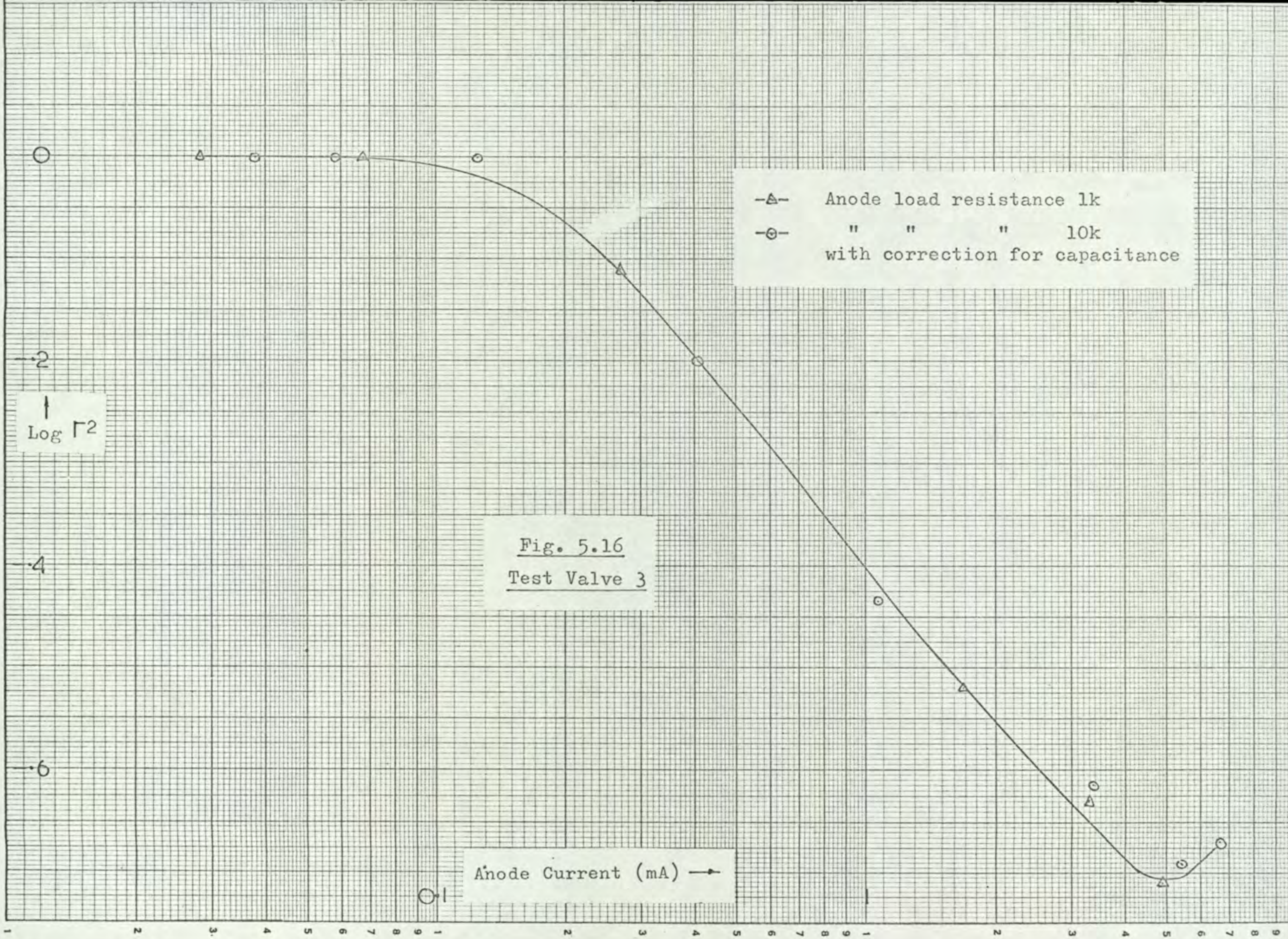

Fig. 5.16

Test Valve 3

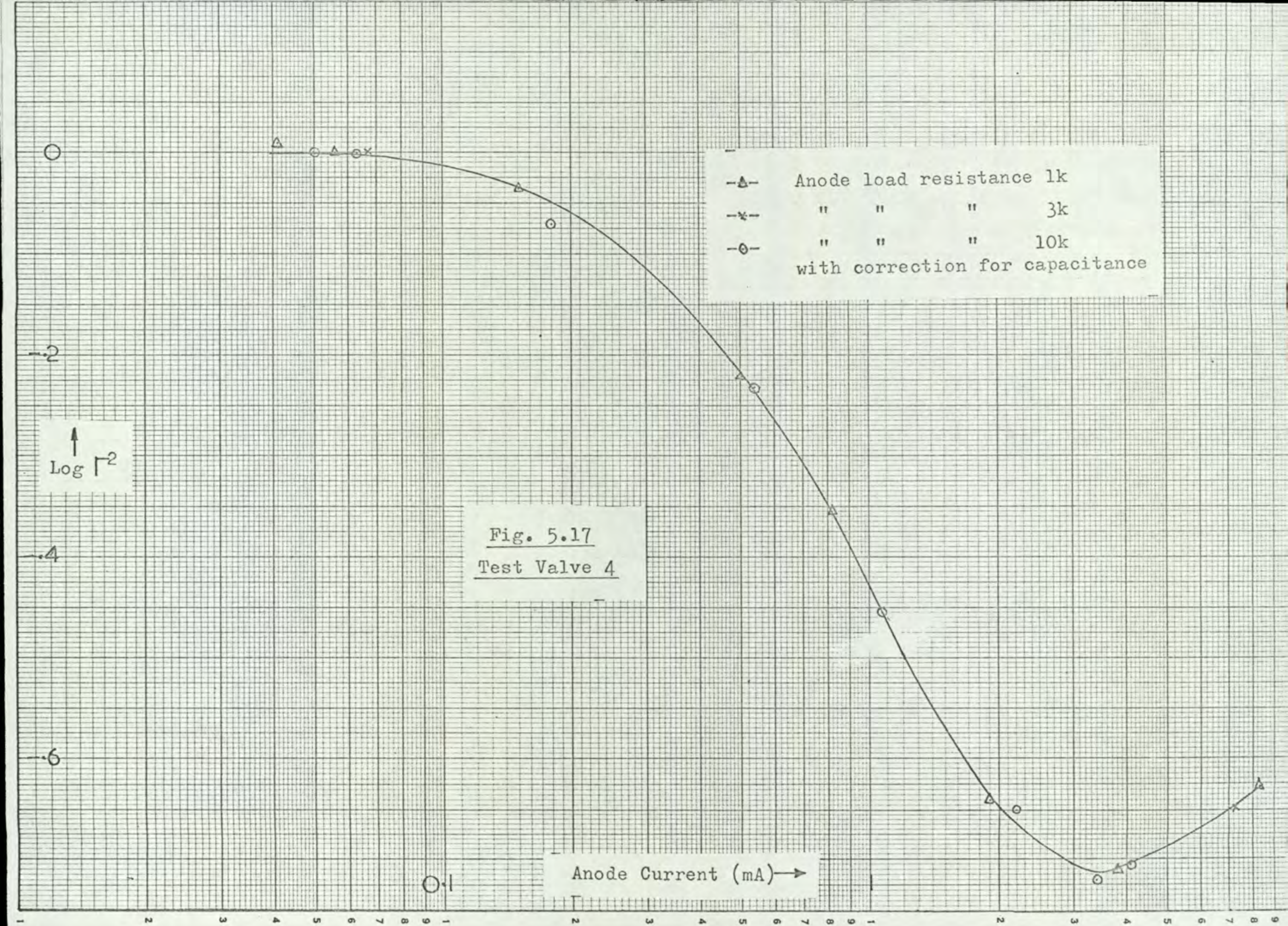

Anode load resistance 1k
" " " 3k
" " " 10k
with correction for capacitance
Fig. 5.17
Test Valve 4
Log Γ^2
0
-·2
-·4
-·6
0·1
1
Anode Current (mA)

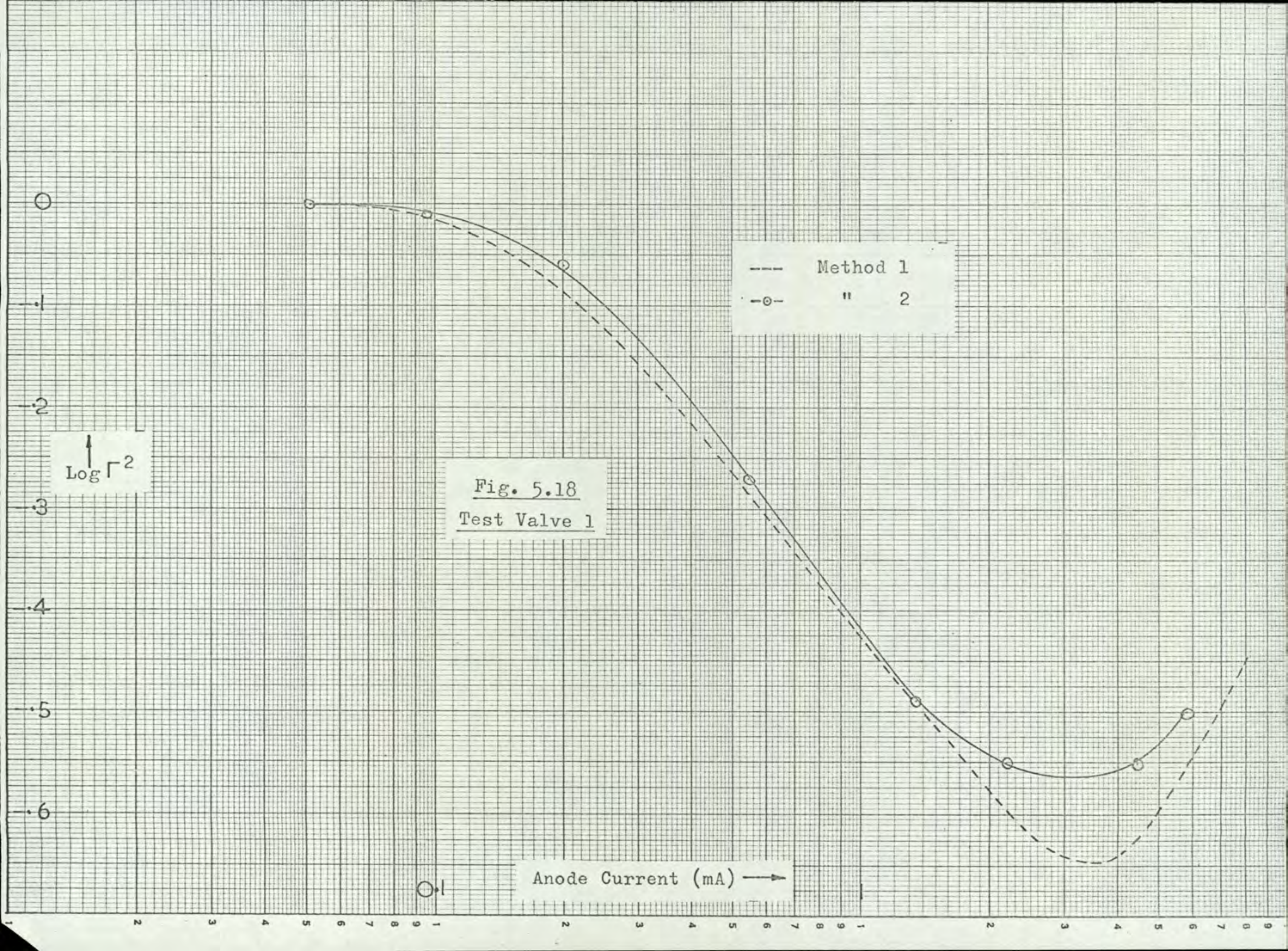

Fig. 5.18
Test Valve 1

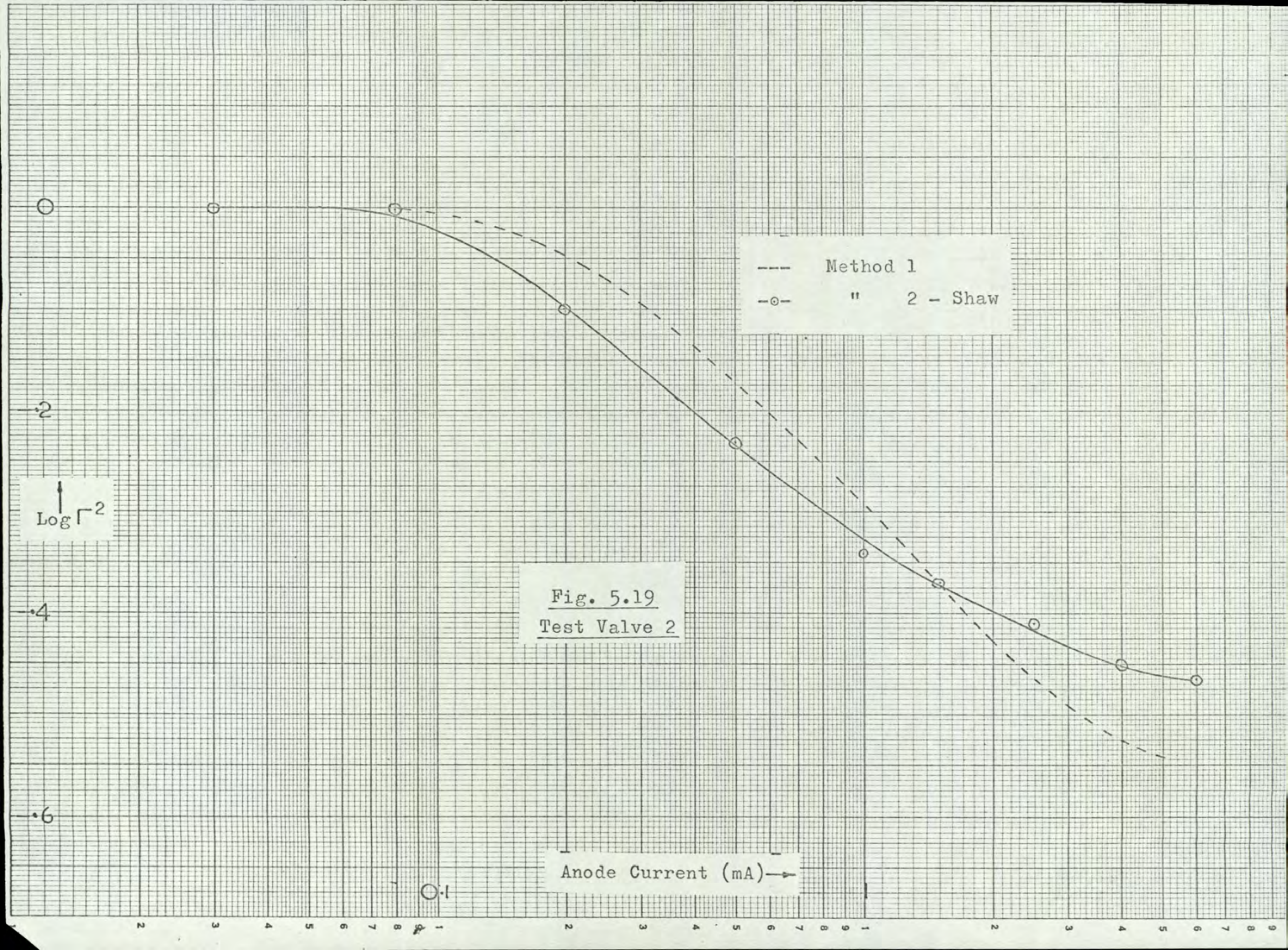

Fig. 5.19
Test Valve 2

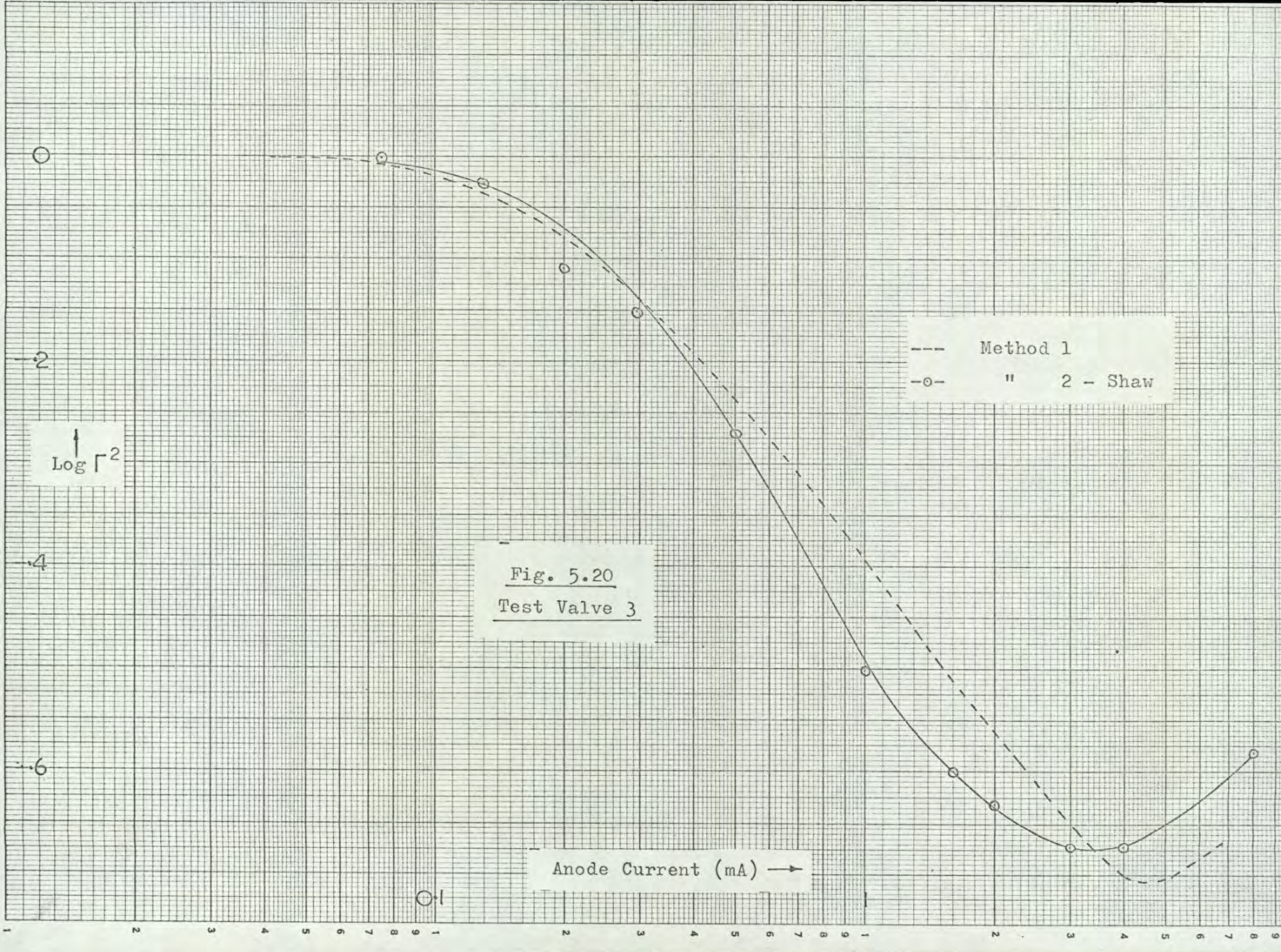

0
-2
-4
-6
Log Γ^2
--- Method 1
-o- " 2 - Shaw
Fig. 5.20
Test Valve 3
Anode Current (mA) ⟶
0·1
1

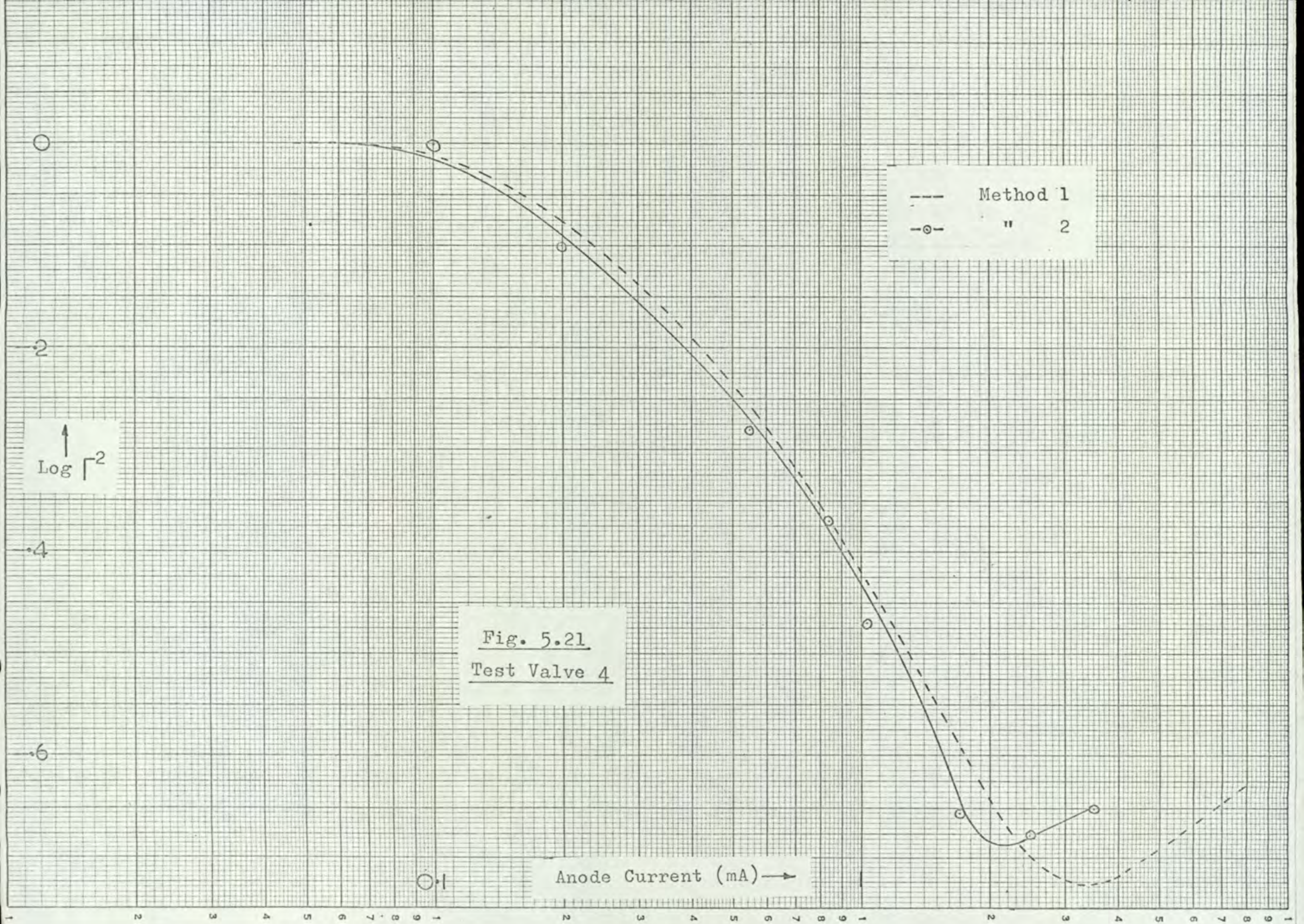

Fig. 5.21
Test Valve 4

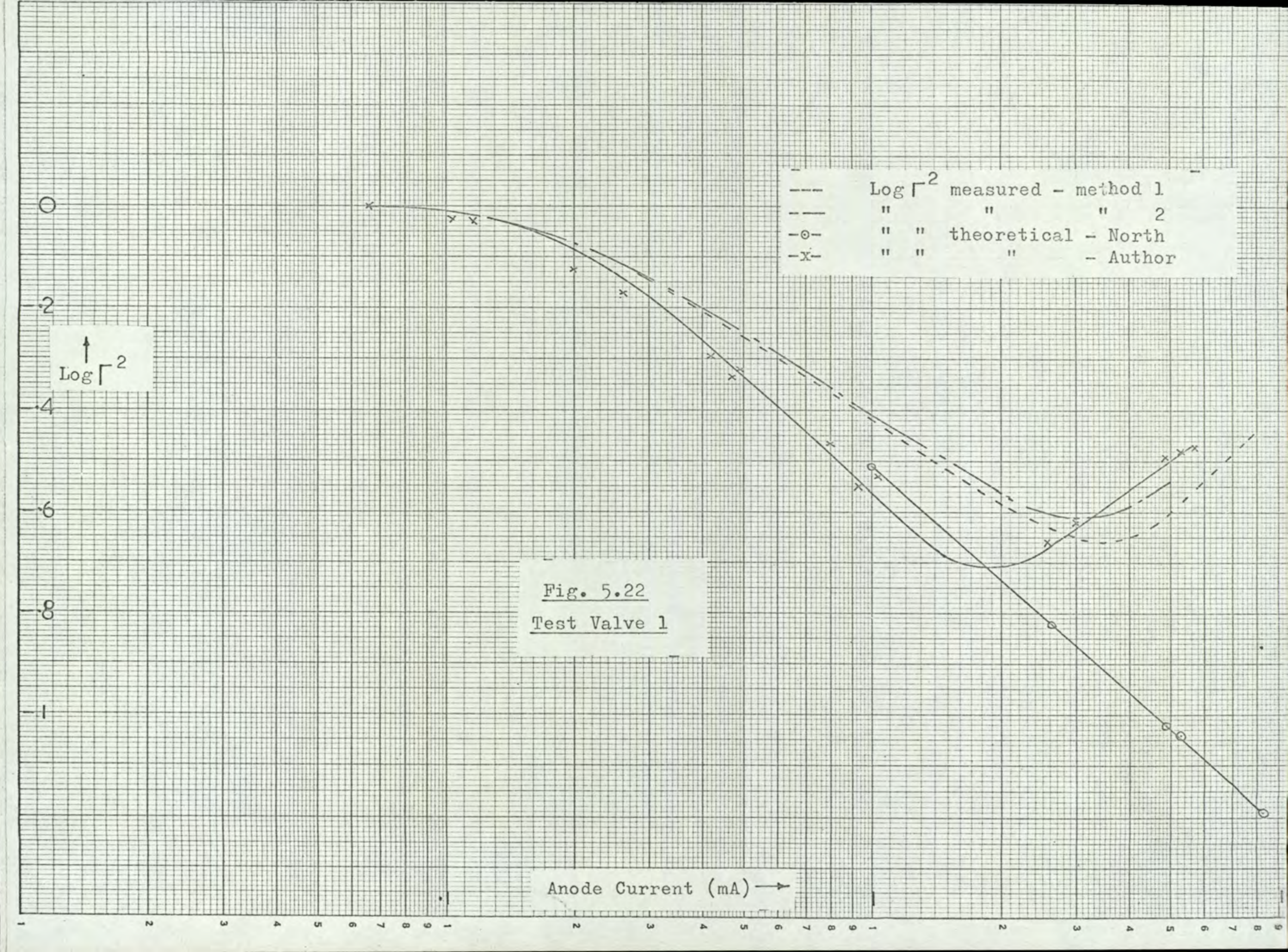

Log Γ^2 measured - method 1
" " " 2
" " theoretical - North
" " " - Author
0
-2
-4
-6
-8
-1
Log Γ^2
Fig. 5.22
Test Valve 1
Anode Current (mA)

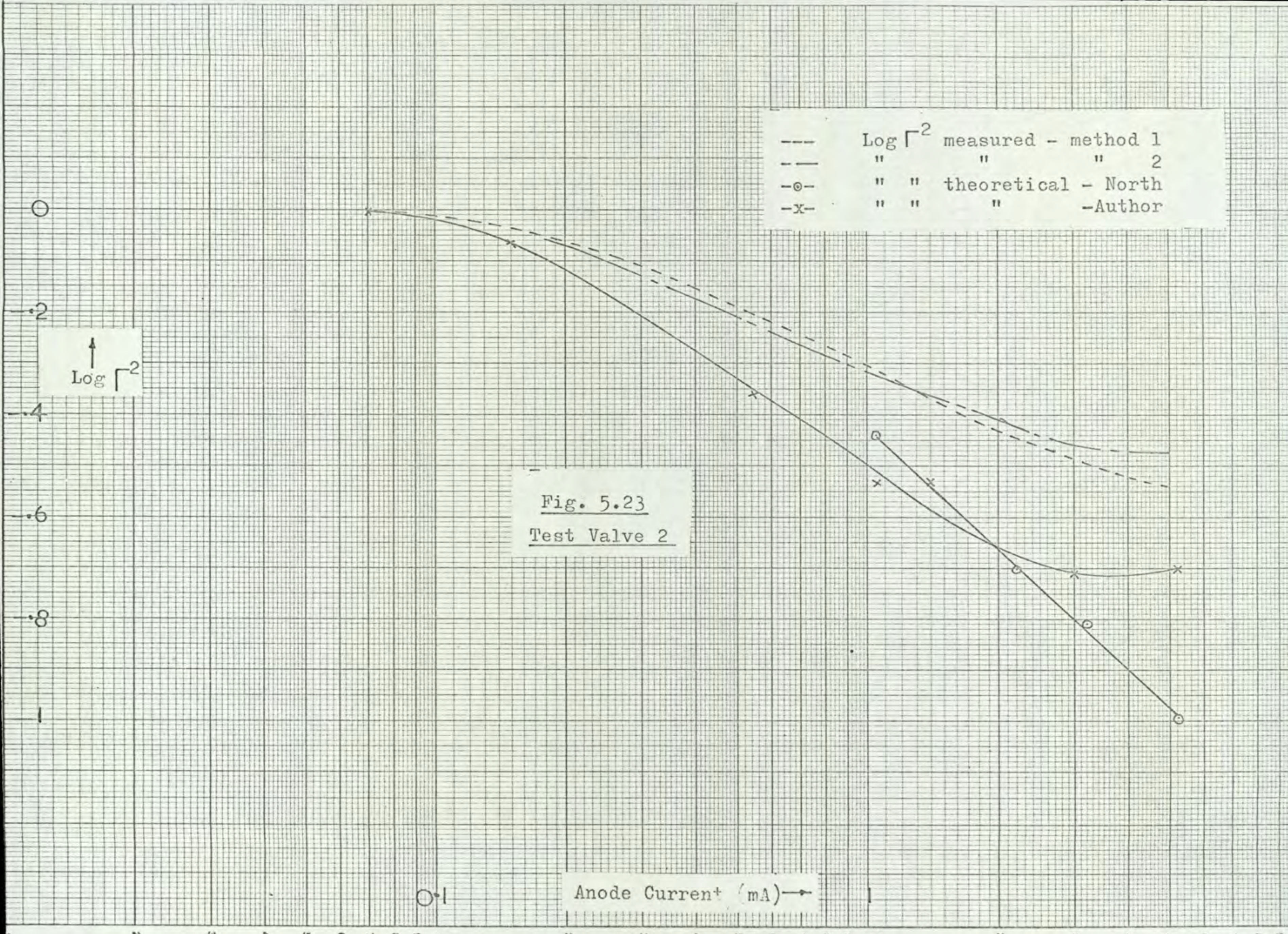

Fig. 5.23
Test Valve 2

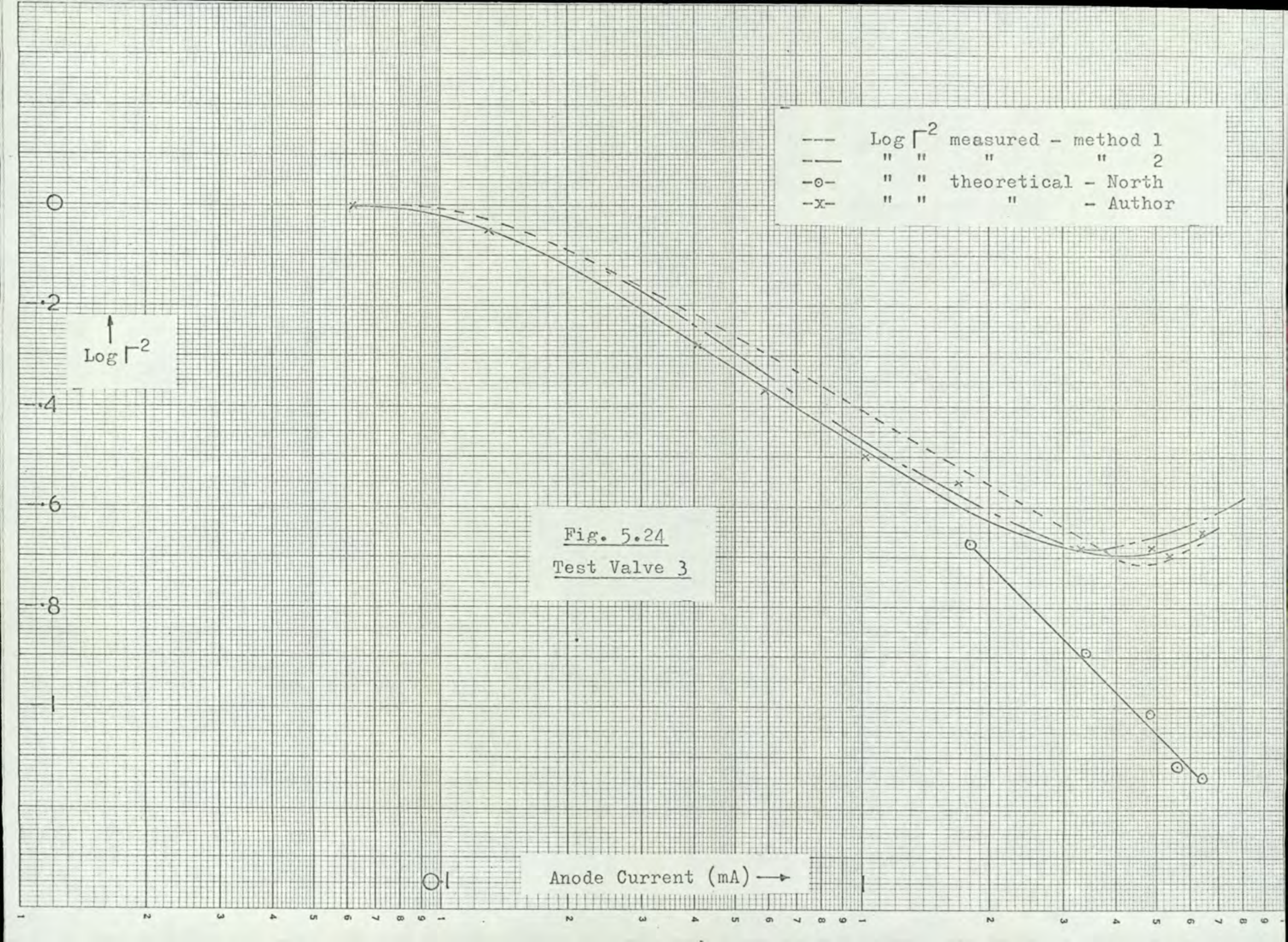

--- Log Γ^2 measured - method 1
-·— " " " " 2
-⊙- " " theoretical - North
-x- " " " - Author
0
·2
Log Γ^2
·4
·6
·8
1
Fig. 5.24
Test Valve 3
0·1
Anode Current (mA)
1

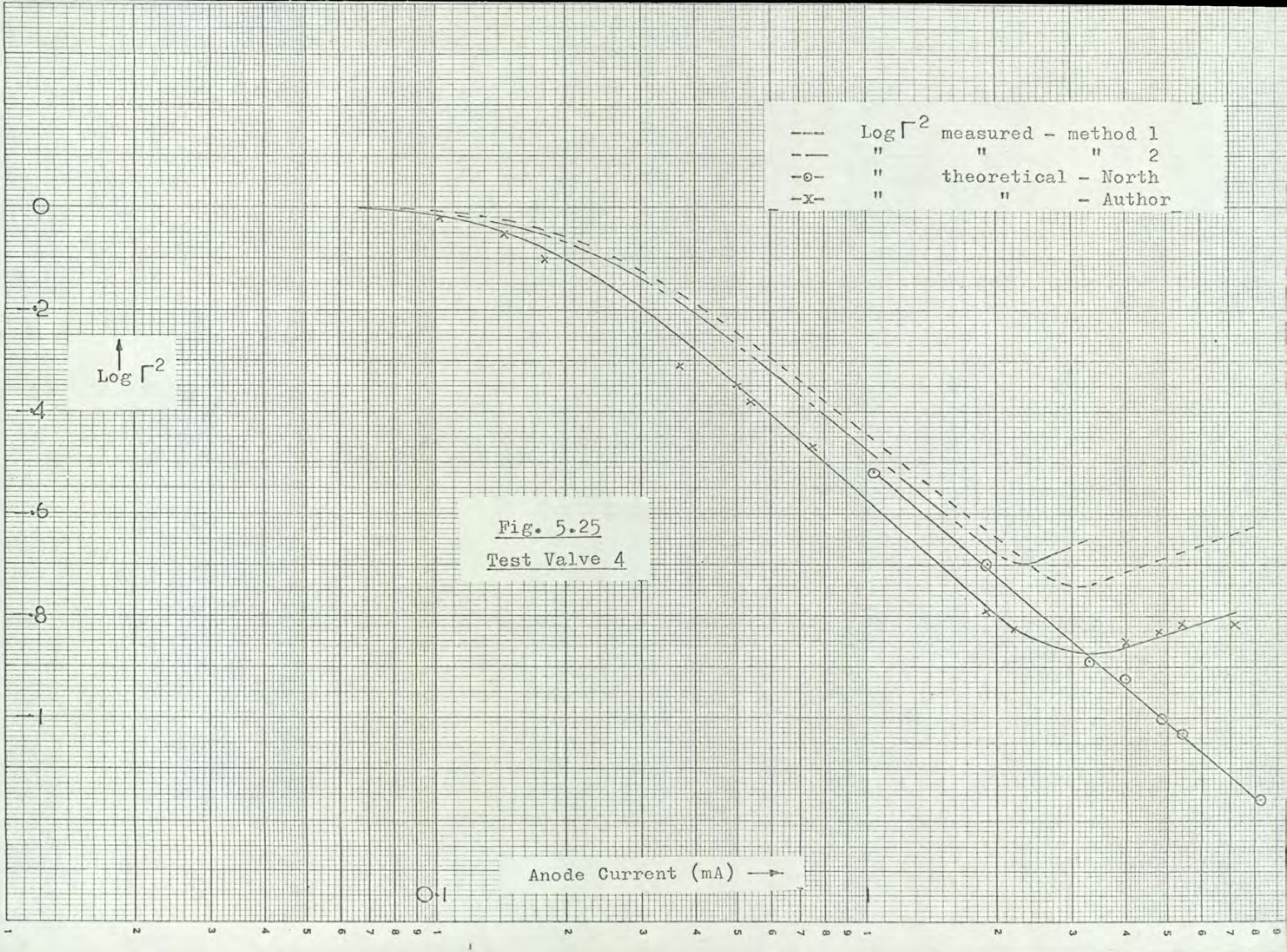

Fig. 5.25
Test Valve 4

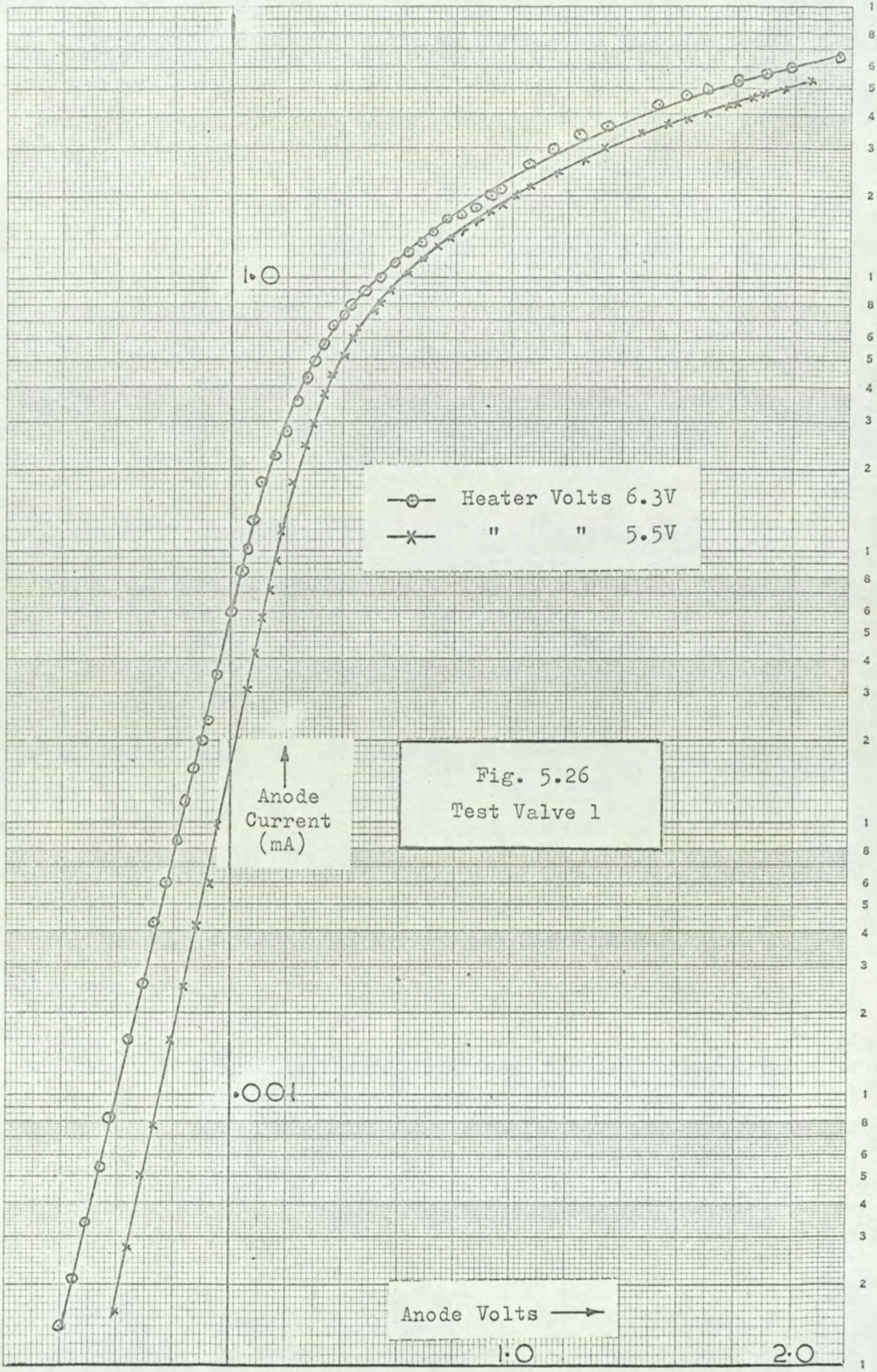
Heater Volts 6.3V
" " 5.5V
1.0
.001
Anode Current (mA)
Anode Volts
1.0
2.0
Fig. 5.26
Test Valve 1

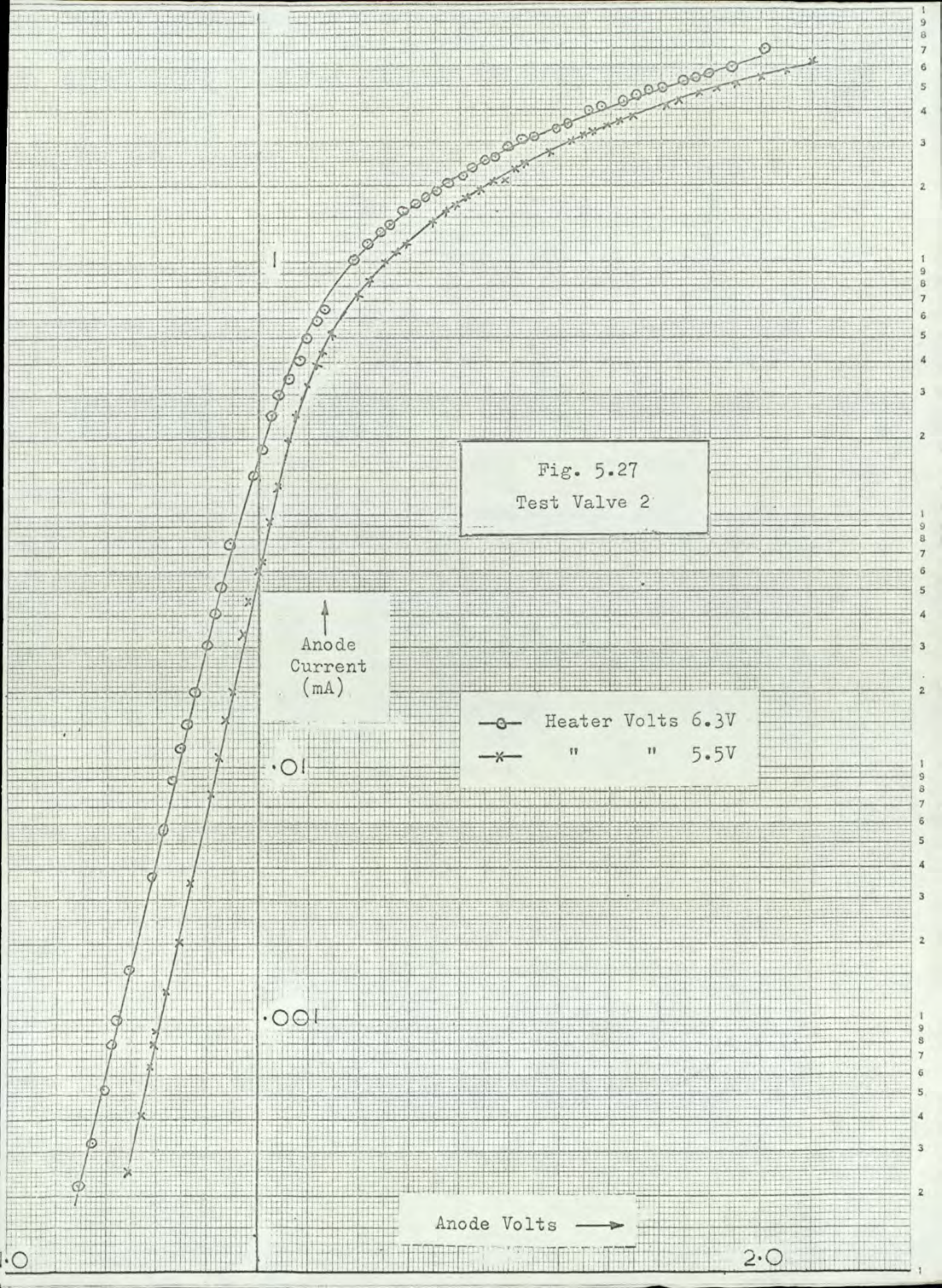
Fig. 5.27
Test Valve 2
Anode Current (mA)
Heater Volts 6.3V
" " 5.5V
1
·01
·001
Anode Volts
1·0
2·0

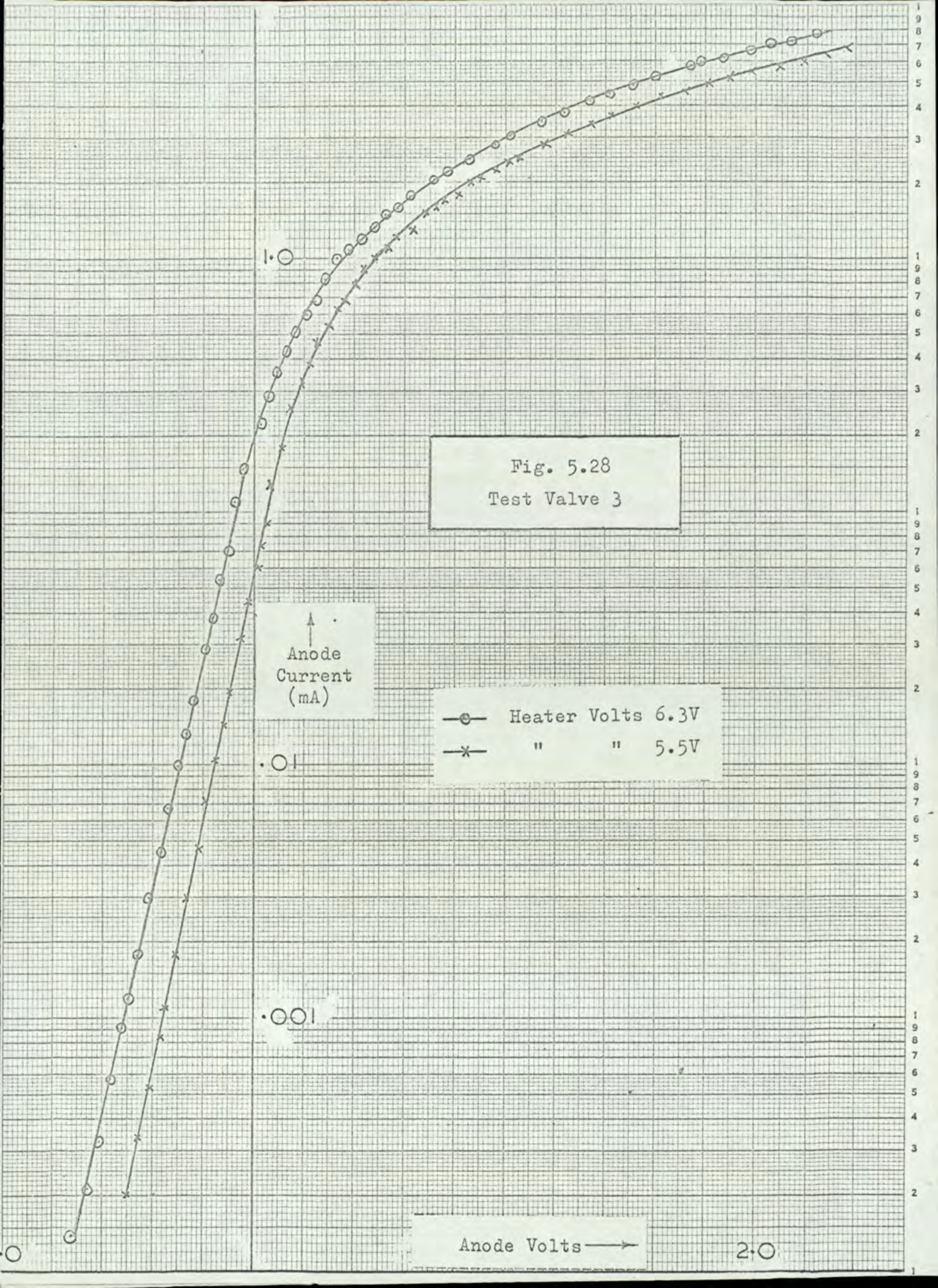
Fig. 5.28
Test Valve 3
Anode Current (mA)
Heater Volts 6.3V
" " 5.5V
1·0
·01
·001
·0
2·0
Anode Volts

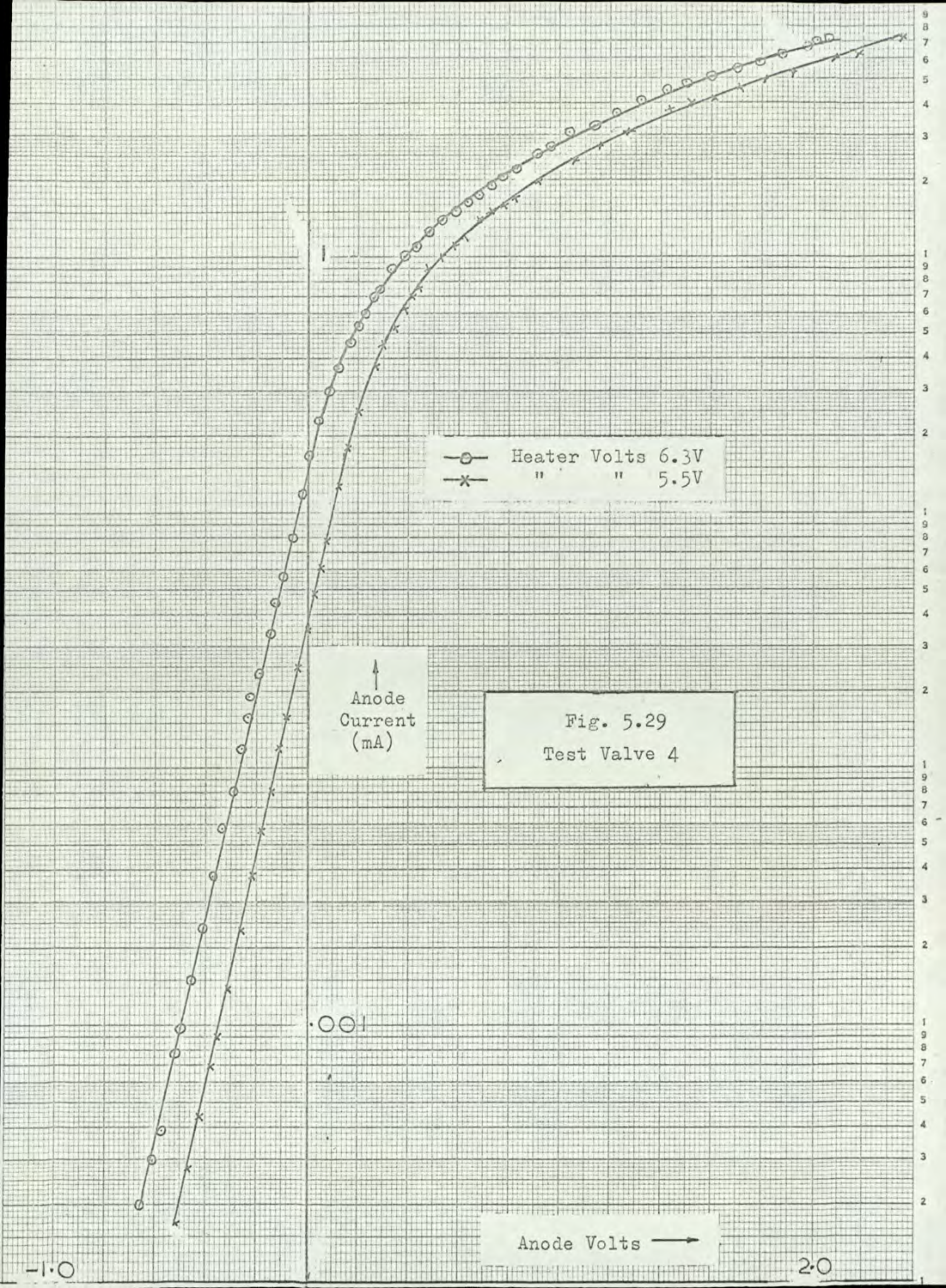

Fig. 5.29
Test Valve 4

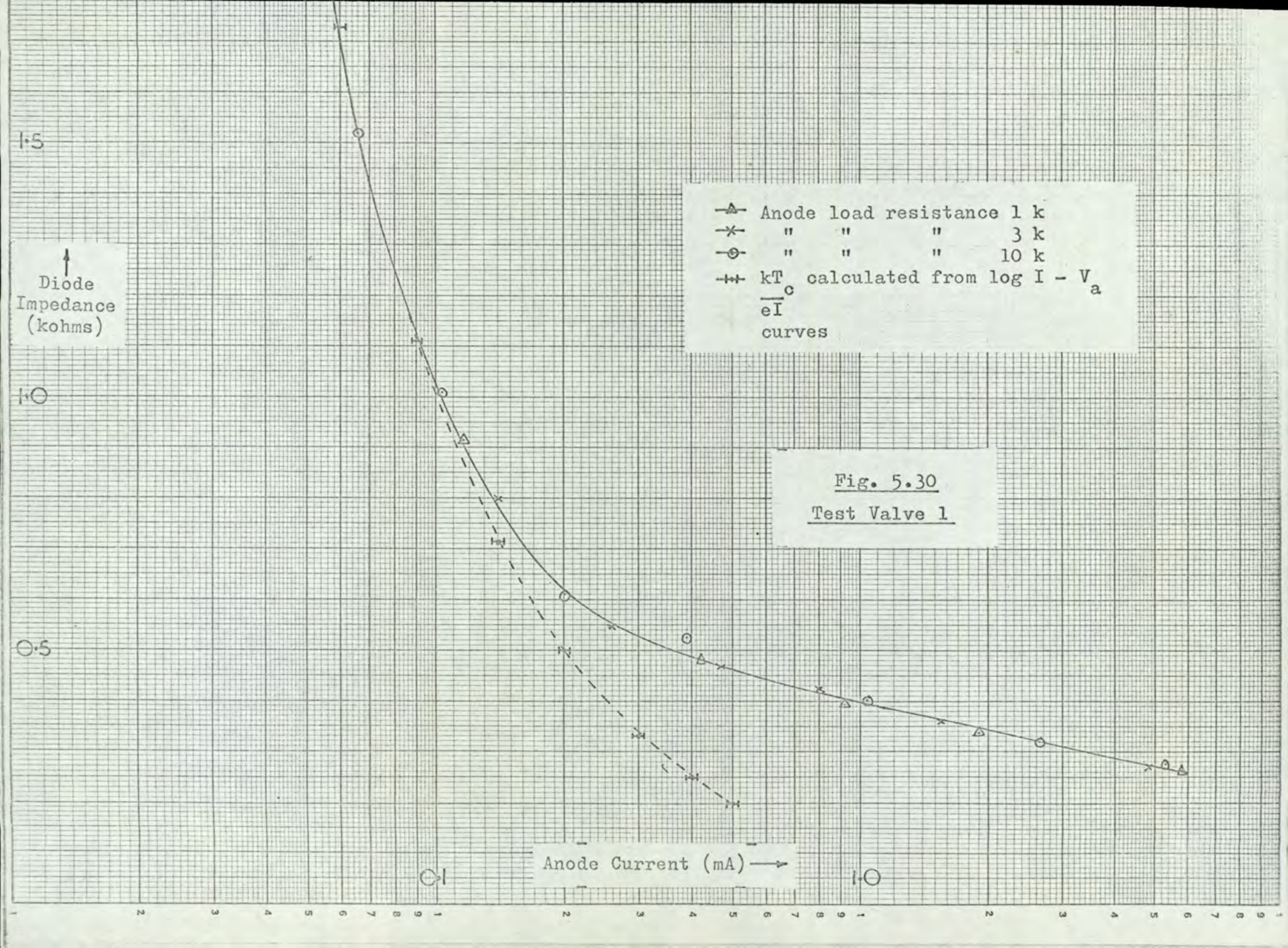

Fig. 5.30

Test Valve 1

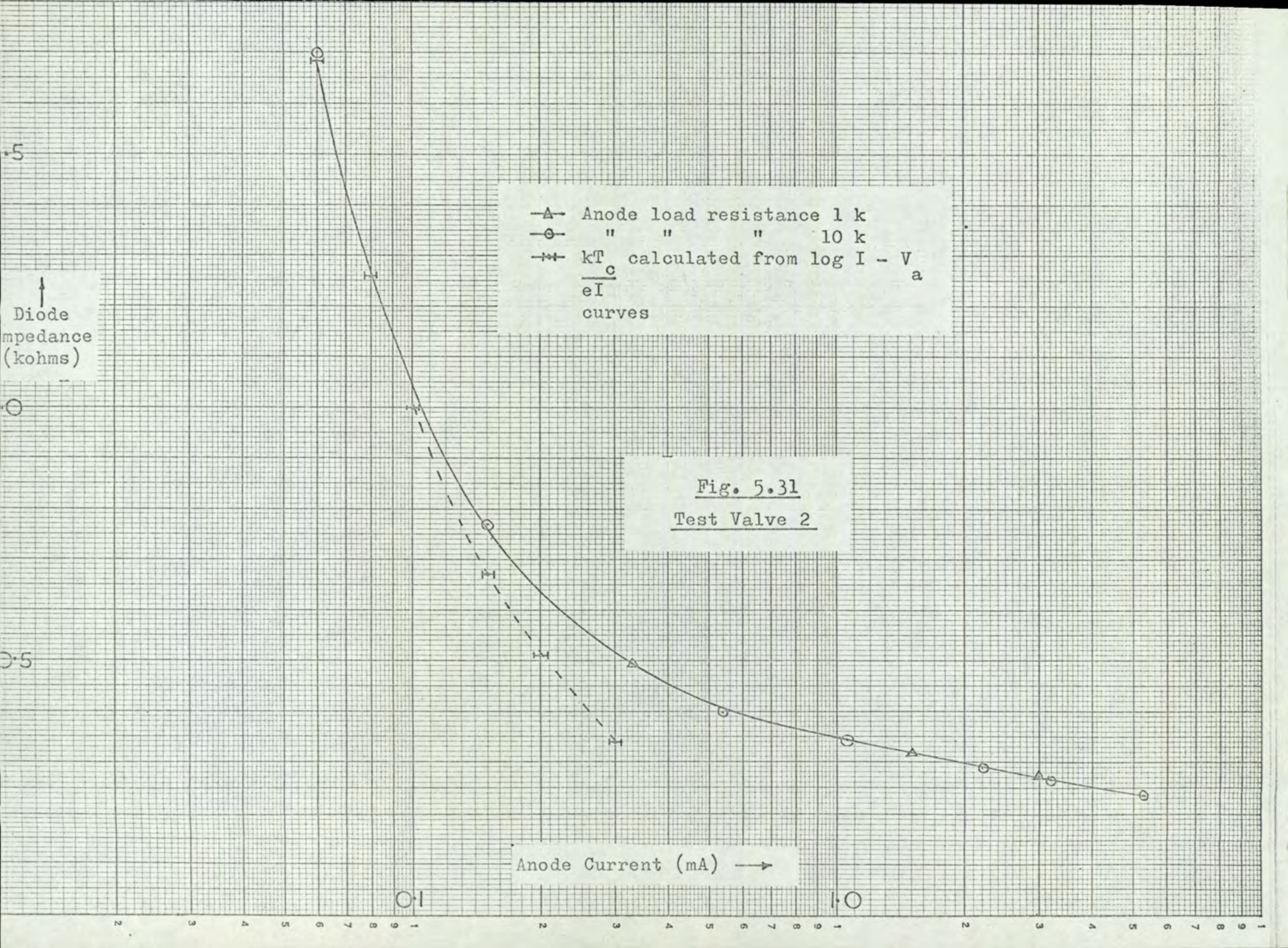

Anode load resistance 1 k
" " " 10 k
$\frac{kT_c}{eI}$ calculated from log $I - V_a$ curves
Diode impedance (kohms)
·5
·0
0·5
Anode Current (mA)
0·1
1·0
Fig. 5.31
Test Valve 2

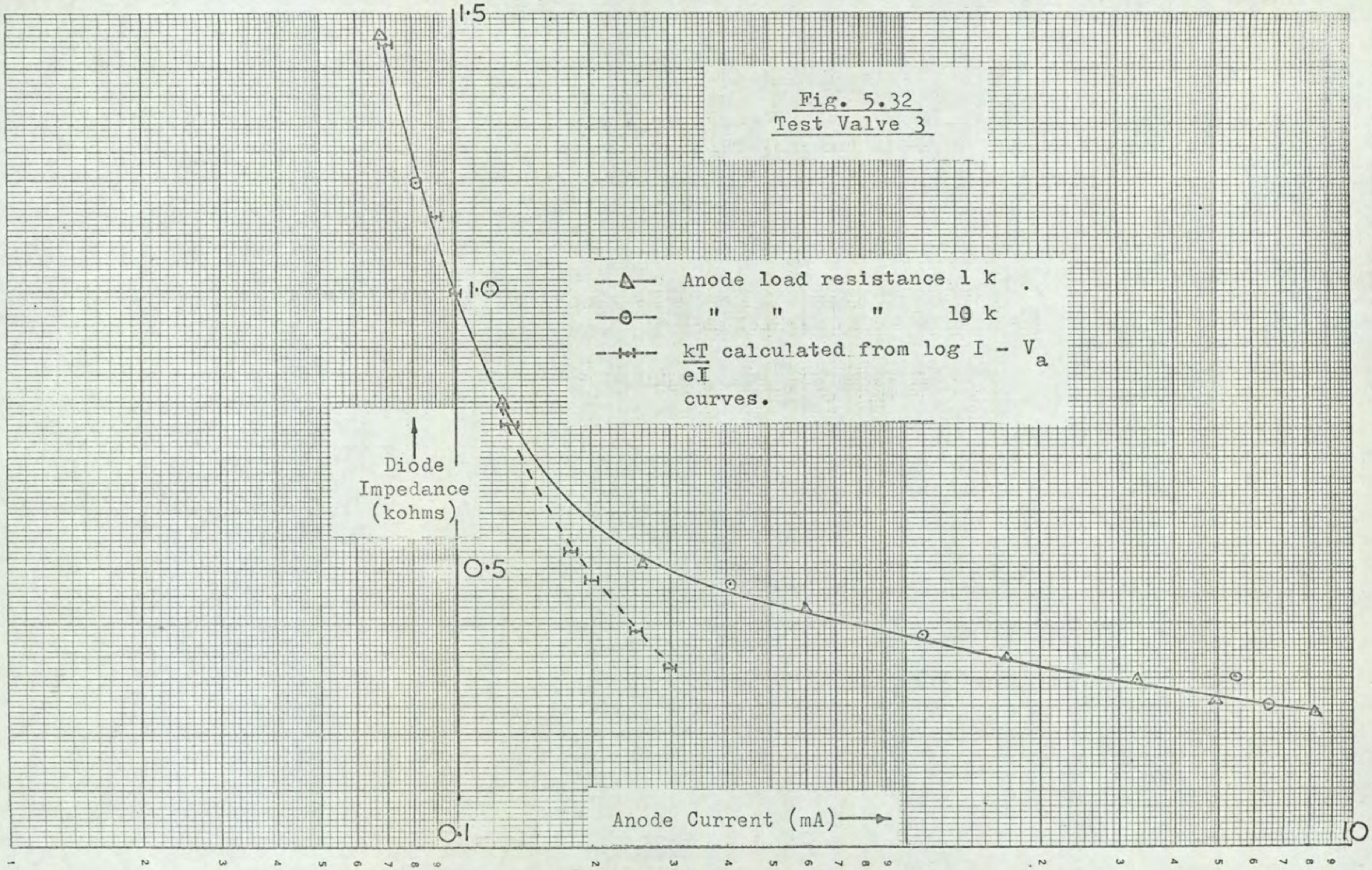

Fig. 5.32
Test Valve 3
Anode load resistance 1 k
" " " 10 k
kT/eI calculated from log I - V_a curves.
Diode Impedance (kohms)
1·5
1·0
0·5
0·1
10
Anode Current (mA)

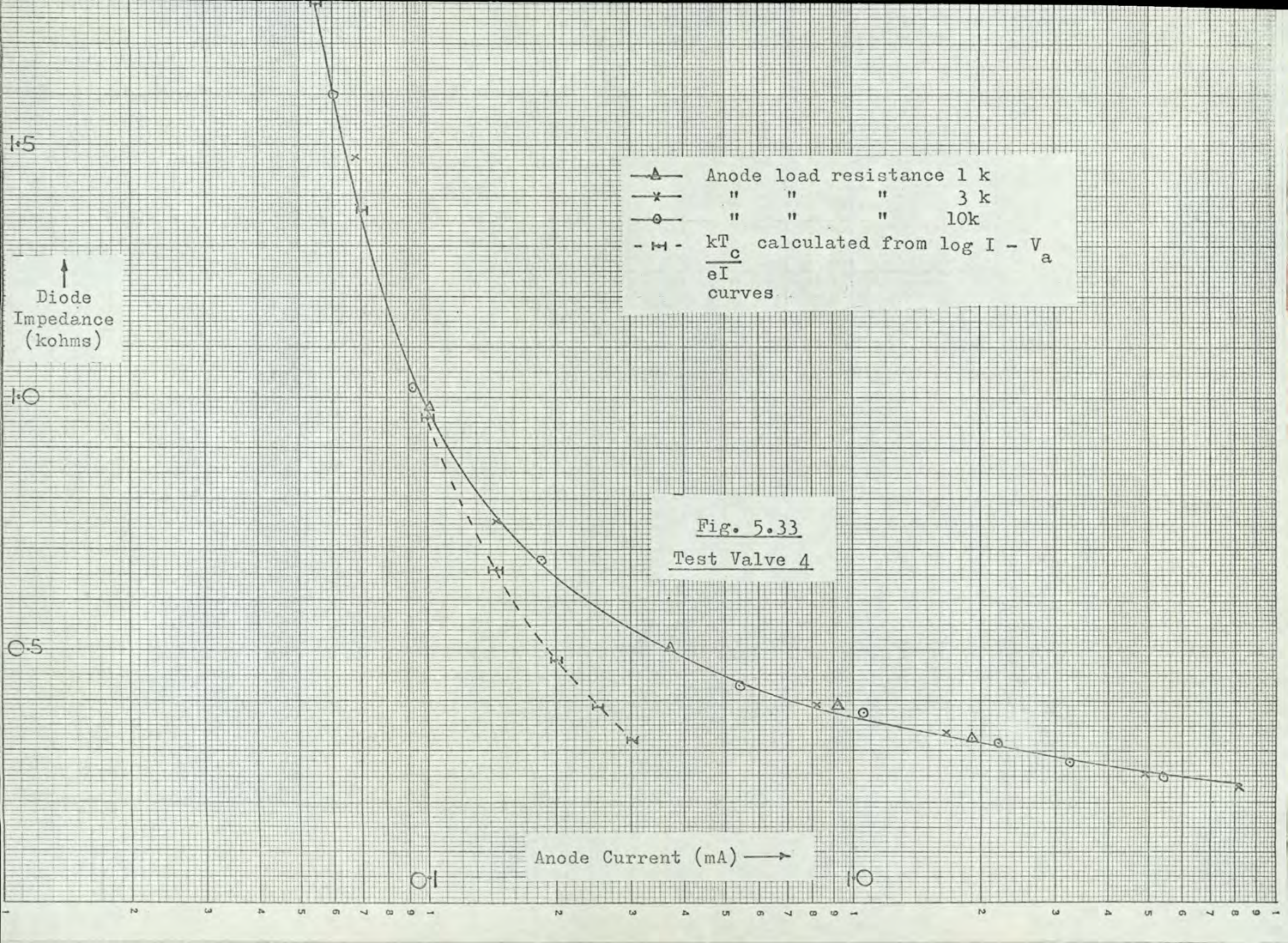

Anode load resistance 1 k
" " " 3 k
" " " 10k
kTc/eI calculated from log I - Va curves
Diode Impedance (kohms)
1·5
1·0
0·5
Anode Current (mA)
0·1
1·0
Fig. 5.33
Test Valve 4

(although on much larger scale) of the type shown in Figs. 5.26 - 5.29.

(iii) Linear plots of anode current - anode voltage and anode current - potential barrier (Appendix 6).

It should be noted that in the plots of North's equation the curves extend over only a limited range of current; corresponding to the region $(V_a - V_m \frac{e}{kT_c} > 5$; i.e. the region for which North's equation is applicable.

Finally, in Figs. 5.30 - 5.33 the measured values of diode impedance are shown plotted against anode current. These curves also contain the plot of $\frac{kT_c}{e\bar{I}}$ where $\frac{kT_c}{e}$ is derived from the log anode current - anode voltage curve.

5.8 Discussion of Results

From Figs. 5.30 - 5.33 it can be seen that in the retarding region the slope impedance is $\frac{kT_c}{e\bar{I}}$ and that the errors in the measurement - since the impedances measured regardless of the anode load lie on the same curve - are small.

Also from Figs. 5.18 - 5.21 it can be seen that the two methods of measuring the smoothing factors give results which are compatible. However, when a comparison is made between these measured values and the calculated values of smoothing factor (Figs. 5.22 - 5.25) the degree of compatibility is not nearly so good.

Consider first of all the results (Figs. 5.22 - 5.26) obtained using North's expression for the space charge smoothing factor. Here, it can be seen that the difference between the measured and the calculated values increases with current and in one case (valve 4) the ratio Γ^2 (measured)/Γ^2 (calculated) with an anode current of 7mA is 4:1. Errors of this order were not, however, unknown to North[44] and he endeavoured to explain them, in terms of secondary electron emission from the anode.

He supposed that those electrons that reach the anode and are elastically reflected return along their original paths towards the cathode. As they approach the potential minimum they are once more reflected and are returned to the anode. To illustrate this consider the case of a unit increase in the emission of electrons of a particular velocity class. Without space charge compensation there would follow a unit increase in anode current. In terms of North's theory, however, in the presence of space charge there flows a compensating current of $-(1-\gamma)$ so that there is a net increase in anode current of $1-(1-\gamma)=\gamma$ and it is this increase which North uses in deriving his expression for the space charge smoothing factor. Suppose, however, that all of the original electrons are reflected back along their path towards the cathode, the net increase in anode current will be given by an equation of the form:

$$1 - (1 - \gamma) - (1 - \gamma) - (1 - \gamma) = -2 + 3\gamma$$

On a mean square basis this means that the compensating effect of the emission electrons has increased from γ^2 to $(-2 + 3\gamma)^2$; e.g. if $\gamma = 0.25$ the noise has been increased twenty-five fold.

Now a brief calculation of the form shown above shows that if as little as 10% of the anode current is reflected as described the total mean square shot effect could be increased by a correction factor of three or more. Furthermore, if it is assumed that the coefficient of reflection varies little with anode voltage it follows that the correction factor will increase with current; a result - but only with respect to the values derived from North's equation (Eq. 3.2) - which is in agreement with the present experiments.

As a test of the validity of this theory of the effects of secondary emission, and hence of his smoothing factor equation, Eq. (3.2), North[44] made some measurements of the space charge smoothing factor of negative gr id triodes. Such valves, since:

(i) the electrons penetrate the anode further and so have fewer reflected; and

(ii) the reflected electrons have to pass the grid field barrier before reaching the cathode potential barrier;

may be expected to show much smaller secondary electron effects than diodes. From this point of view, therefore, the use of triodes instead of diodes is a better way of testing the validity of Eq. (3.2). Accordingly, when North found that Eq. (3.2) when applied to triodes - by replacing the triode by its hypothetical equivalent diode - gave an accurate estimate of the space charge smoothing factor he concluded that his theory of space charge smoothing had been verified.

There are, however, several reasons, apart from those (Sec. 3.2) mentioned earlier, for rejecting this conclusion. In the first place the results with triodes are open to doubt because:

(i) The method involved the use of a correction factor for the relative roles of grid-cathode and grid-anode spaces which may involve errors of the order of 50% (Bell[3]).

(ii) The hypothetical diode was derived from the work of Llewellyn[41] in which no account was taken of either the focussing properties of the grid or the emission velocities of the electrons (this latter omission is incompatible with the model, described earlier, on which North founded his theory).

Secondly, the probability of a considerable fraction of the anode current being elastically reflected so exactly along its original path seems very small, especially since the total fraction reflected will only be of the order of 5 - 10% (Farnsworth).

If now attention is turned to the curves of the space charge smoothing factor calculated with Eq. (5.1) it can be seen that here also there are differences between the experimental and theoretical results. It is possible that these may be due to differences between the actual valves and the theoretical model on which Eq. (5.1) was based, e.g. finite length of electrodes, non-planar structure, existence of secondary electrons. Furthermore, if this is the case the results with valve 2, would indicate that because of structural defects in the valve these differences may be sufficient to cause differences of the order of 40% (certainly the high noise level of this valve as compared to that of the others would seem to indicate that there are structural differences). Nonetheless, even though Eq. (5.1) does not give a perfect estimate of the space charge smoothing factor, the discrepancies are very much smaller than when North's equation is used.

5.9 Conclusions

In Chapter 3 it has been shown that there are theoretical reaons for supposing that a theory of the space charge smoothing factor in which the electron behaviour is described in terms of a probability distribution will give a better estimate of the smoothing factor than will North's theory. As a means of testing the validity of the reasoning an experimental comparison, using planar diodes, was then made between the two theories; the results of which tended to support the theoretical arguments concerning the relative merits of them.

PART III

CORRELATION MEASUREMENTS OF SIGNALS AND NOISE

6. CROSSCORRELATION MEASUREMENTS OF SIGNALS AND NOISE

6.1 Introduction

In the previous chapters reference has been made to the work of a number of experimentors in which evidence of a fluctuating characteristic has been found, and the work of the writer on the noise of diodes tends to support this evidence. Further, as a manifestation of the same phenomenon Hathaway, using a crosscorrelation technique, has observed that there is a conversion of signal power to noise power as a signal is transmitted through an amplifier.

Unfortunately, on account of the limited performance of the transistor circuits used in his correlating equipment, Hathaway was only able to make measurements over a limited frequency range of 1kHz - 50kHz and, possibly because he used such a limited range, was unable to specify a frequency dependence. In view, therefore, of these limitations of Hathaway's work it was decided to set up a new series of experiments in which:

(i) Hathaway's measurements could be extended to a higher frequency range; and

(ii) the frequency dependence of the effect, if any, could be investigated.

To enable these new measurements to be made it required that new equipment, capable of operating at higher frequencies, be designed. However, before discussing how this was achieved it is intended to begin by considering the theory of the method of measurement and to follow this, because of its relevance to the present work, by an examination of Hathaway's experiment.

6.2 Theory of the Experimental Method

In Sec. (2.4) the crosscorrelation between two signals $x(t)$, $y(t)$ in the time domain has been defined as:

$$R_{xy}(\tau) = \langle x(t)y(t+\tau)\rangle$$

where the brackets $\langle\ \rangle$ signify that the average is with respect to time. If $y(t)$ is deterministic, say $S_y(t)$, and $x(t)$ is an additive component of a deterministic, $S_x(t)$, and a random component, $N(t)$, i.e.

$$x(t) = S_x(t) + N(t)$$

then

$$R_{xy}(\tau) = \langle(S_x(t) + N(t))(S_y(t+\tau)\rangle \tag{6.1}$$

which for an ergodic process (Sec. (2.1)) may be rewritten as

$$R_{xy}(\tau) = R_{ss}(\tau) + \overline{N.S}_y$$

where the bar represents an ensemble average and $R_{ss}(\tau)$ the crosscorrelation of $S_x(t)$ and $S_y(t)$. Since S_y and N are statistically independent then for the case of a random noise process where $\langle N\rangle = 0$, Eq. (6.1) simplifies to

$$R_{xy}(\tau) = R_{ss}(\tau) \tag{6.2}$$

which for two coherent sine waves of the same angular frequency, w, may be written

$$R_{xy}(\tau) = R_{ss}(\tau) = V_x V_y \cos w\tau \qquad (6.3)$$

(V_x and V_y being r.m.s. values).

For the particular case of zero delay then

$$R_{ss}(\tau) = V_x V_y \qquad (6.4)$$

From these equations it appears, therefore, that the application of a corrcorrelation technique enables the signal to be recovered from the noise irrespective of the signal/noise ratio. In several respects this represents a better method of detection than a narrow band filter. Firstly, the correlator operates in the time domain to achieve a result that an extremely narrow band filter could only produce in the frequency domain. Furthermore, while the correlator separates a sinusoid from random noise irrespective of its frequency, as long as it is within the bandwidth for which the correlator is designed, a narrow band filter, as its name implies, does not have this advantage. For these reasons, therefore, the measurements described here will utilise the correlation method and in order that the correlator be utilised at its maximum sensitivity the measurement will - in the main - be made with zero time delay between the x and y waveforms.

6.3 Hathaway's Experiment

The basic measuring system used by Hathaway is shown in Fig. 6.1. The incoming noisy signal (x) to the cross-correlator (C.C.) is derived from an amplifier, A, via a

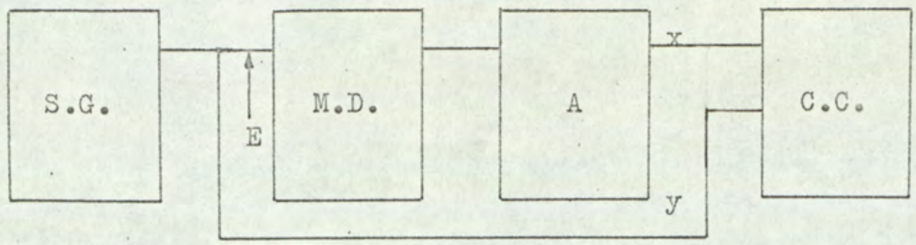

Fig. 6.1

microvolt divider (M.D.) and a signal generator (S.G.). This same generator provides the local (or reference) signal to the correlator so that variations in R_{xy} due to drifts in frequency will not occur, i.e. full coherence between x and y is maintained whatever drifts of frequency or waveform occur in S.G.

Starting with an input voltage to the amplifier of one millivolt this was decreased - whilst maintaining the signal generator (E) and hence the local signal (y) voltages constant - by means of the microvolt divider down to voltages of the order of one microvolt. At the same time the gain of the amplifier was increased so as to maintain the amplitude of the sinusoidal signal at the amplifier output (S_x) at a constant level; e.g. with an input of 1mV r.m.s. the amplifier gain might, for example, be 46 dBs and this would be increased to 106 dBs for an input of 1μVr.m.s. Each time the level of the input signal was changed the correlator reading was noted. The noise of the amplifier was then increased (by placing a resistor in series with the grid) and the measurements repeated.

A set of results which is fairly typical of those obtained by Hathaway is shown in Fig. 6.2, where the ordinate represents the crosscorrelation function - the value with large signals being termed 100%, i.e. all signal recoverable - and the abscissa the log of the input signal. This curve indicates:

(i) There is a loss of signal power in the amplifier and this may be as high as 50% when the input signal is 1μV.

(ii) The rate at which signal is lost increases as the system noise is increased.

In addition from power measurements which he made, and which were ancillary to those described above, Hathaway found that the signal which was lost was converted into an exactly equal amount of noise; i.e. total power varied as signal input power.

In terms of Eqs. (6.2) and (6.3) above which predict that R_{xy} for constant S_x and S_y, i.e. V_x and V_y, should remain constant, the curves of Fig. 6.2 are incomprehensible. It is apparent, therefore, that if these curves are valid then a new theory is required. Such a theory, based on discontinuous mathematical methods, has been developed, and is shown below.

6.4 Theory for the Loss of Correlation

In the theory to be discussed below the processes which occur will be described in terms of p.g.f.s, the formation

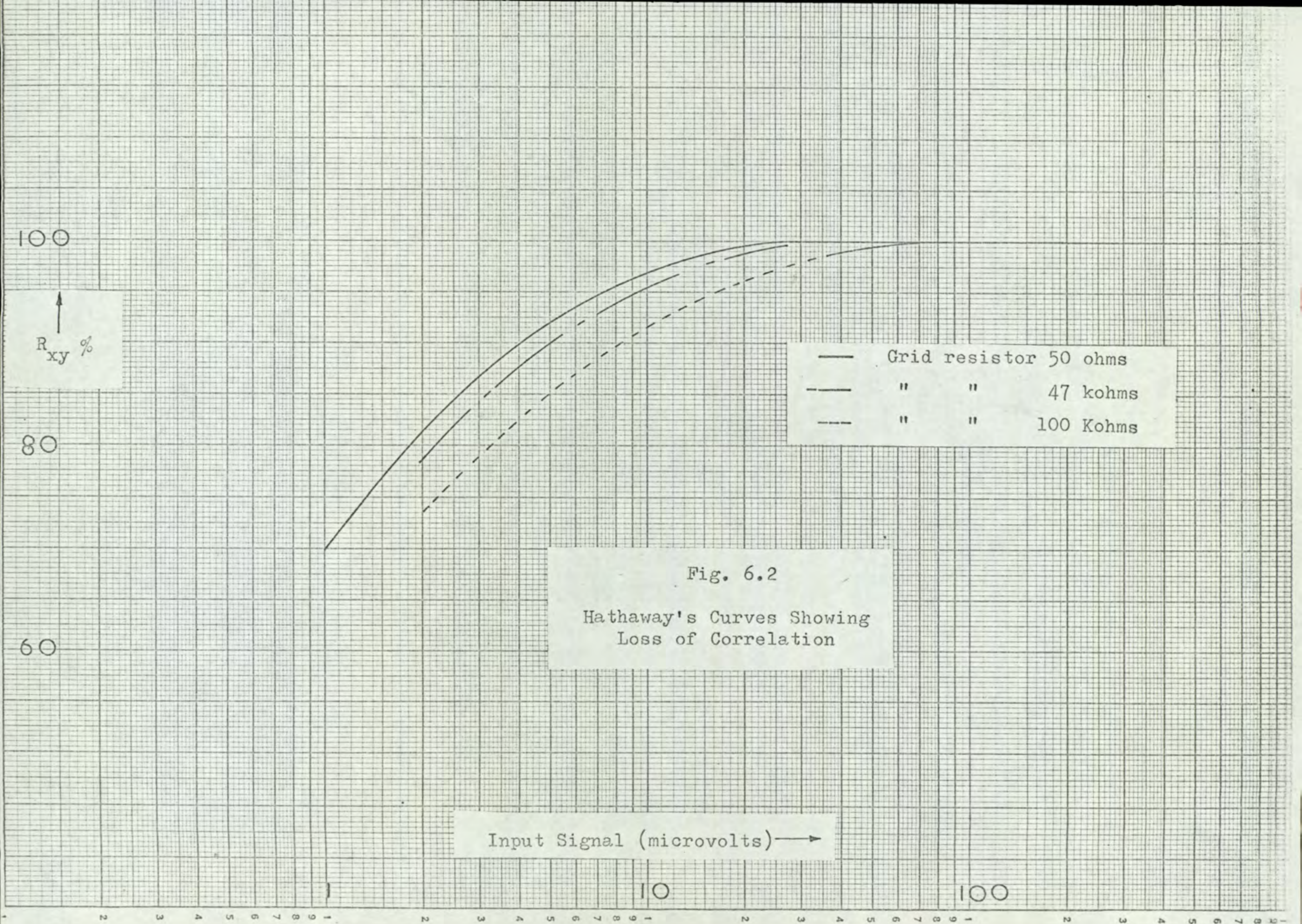

Fig. 6.2

Hathaway's Curves Showing Loss of Correlation of which are based on the work of Bull. From these p.g.fs an expression for determining the mean square value of the fluctuations occurring within the system is derived. This expression is the sum of a number of complicated terms which may be interpreted as predicting a fall in correlation. It is this interpretation, formulated by Hathaway, which forms the theoretical basis for much of the present work.

To understand the theory it is necessary to refer back to the work of Chap. 3. Here, a stationary state was maintained by ensuring that for each of the v charges arriving on the capacitance C, from the battery, on the average, one was neutralised by the action of the electronic device.

It is now proposed to make the system non-stationary by adding a further integral number of charges for each of the v arrivals which represent the outcome of an applied signal to the device and will be represented by a set of integral numbers s.

If the applied signal is periodic and is symmetrical about zero then by Fourier analysis it may be represented as the sum of separate sinusoidal harmonics. Accordingly, if one of these harmonics is analysed a similar analysis can be applied to them all.

Now if the characteristic of the active device is assumed to be a constant then the resultant of the sinusoidal input will be a sinusoidal output whose amplitude at all times is known (Figs. 6.3a and 6.3b). However, it is now well established, both theoretically and experimentally,

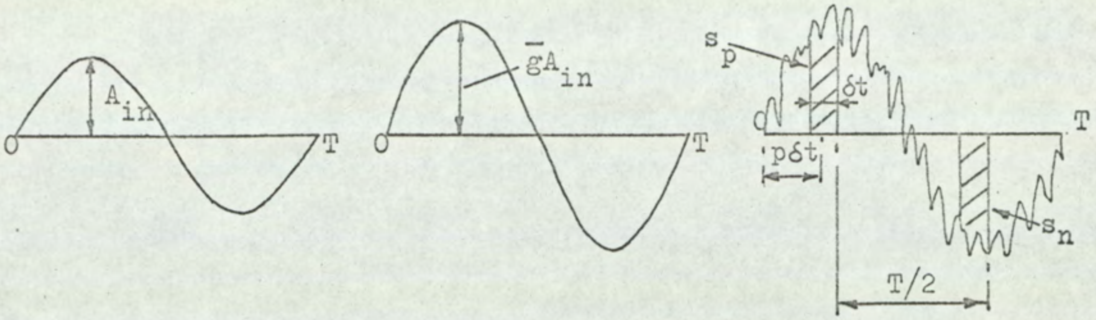

a) Input Wave

b) Output When Characteristic is Constant

c) Output When Characteristic Fluctuates

Fig. 6.3

that the characteristic of any device is not constant but fluctuates, one manifestation of this being shot noise. Accordingly, the output waveform will not be exactly defined and may take the form shown in Fig. (6.3c) in which the actual amplitude at any instant cannot be measured exactly.

Now let the input waveform be divided into a number of separate intervals each of width δt (Fig. 6.3c) and let s_p represent the manifestation of the signal at the output in the p^{th} interval δt. Thus, over the total period T of the wave the signal output s_o is given by

$$s_o = \sum_{o}^{\nu} (s_p) + \sum_{\nu}^{2\nu}(s_n)$$

where $n = (\nu + p)$ and s_p and s_n represent the amplitudes in the p^{th} and $(\nu + p)^{th}$ intervals δt.

Thus in the p^{th} interval the application of a signal to the system can be represented using the equation representing integral numbers:

$$r_p = v_p(1 + k_p + s_p) \tag{6.5}$$

where r_p is the excess number of field lines on the capacitance C, k_p is the number of field lines from the cathode and s_p the effect of the signal. If it is accepted that the characteristic of the device, since the electrons are not under precise control, for a particular value of signal fluctuates and that this fluctuation follows the rules of chance, then the signal may be represented by a probability distribution. Accordingly, Eq. (6.5) may be represented by a p.g.f. of the form

$$R_p(x) = V_p(x.K_p(x).S_p(x)) \tag{6.6}$$

Following the procedure described earlier the expression for $\bar{r}_p$, the mean value of r_p (Fig. 6.4) is given by

$$\bar{r}_p = R_p^1(1) = \bar{v}_p[1 + \bar{k}_p + \bar{s}_p] \tag{6.7a}$$

Similarly for negative excursions of signal

$$\bar{r}_n = R_n^1(1) = \bar{v}_n\,[1 + \bar{k}_n + \bar{s}_n] \tag{6.7b}$$

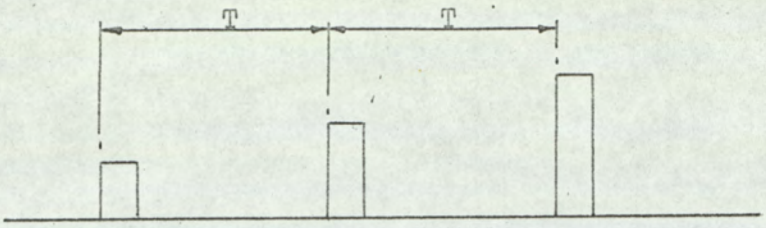

Fig. 6.4

Thus $\bar{\bar{r}}$, the mean of all r_p and r_n is given by

$$\bar{\bar{r}} = \frac{1}{2\nu}\,[\sum_{o}^{\nu} \bar{r}_p + \sum_{\nu}^{2\nu} \bar{r}_n] \tag{6.8}$$

where $\bar{\bar{r}} = 0$ otherwise the output stage will become overloaded in time.

Also

$$R_p^{11}(1) = \bar{v}_p^2\,\bar{s}_p^2 + \sigma_{vp}^2\,\bar{s}_p^2 - \bar{v}_p\,\bar{s}_p$$

$$+ \bar{v}_p\,\sigma_{sp}^2 + \bar{v}_p\,\sigma_{kp}^2$$

Therefore, from Eq. (2.12)

$$\sigma_{rp}^2 = R_p^{11}(1) - (R_p^1(1))^2 + (R_p)^1(1)$$

$$= \sigma_{vp}^2\,\bar{s}_p^2 + \bar{v}_p\sigma_{sp}^2 + \bar{v}_p\,\sigma_{kp}^2 \tag{6.9}$$

Hence the mean value σ_r^2 of σ_{rp}^2 and σ_{rn}^2 is given by

$$\sigma_r^2 = \frac{1}{2\nu}\left(\sum_0^{\nu} \sigma_{rp}^2 + \sum_{\nu}^{2\nu} \sigma_{rn}^2\right)$$

Assuming that the fluctuations about the mean of v and k are the same for all p and n so that $\sigma_{vp}^2 = \sigma_{vn}^2 = \sigma_v^2$ and $\sigma_{kp}^2 = \sigma_{kn}^2 = \sigma_k^2$ and that $\bar{v}_p = \bar{v}_n = \bar{v}$ then

$$\sigma_r^2 = \frac{1}{2\nu} \left[\sum_0^{\nu}(\sigma_v^2 \bar{s}_p^2 + \bar{v}.\sigma_{sp}^2 + \bar{v}.\sigma_k^2) + \sum_{\nu}^{2\nu}(\sigma_v^2 \bar{s}_n^2 + \bar{v}.\sigma_{sn}^2 + \bar{v}.\sigma_k^2)\right]$$

$$= \sigma_v^2.\bar{\bar{s}}^2 + \bar{v}.\overline{\sigma_s^2} + \bar{v}.\sigma_k^2 \tag{6.10}$$

It follows, therefore, that the mean square value of r, $\bar{\bar{r^2}} = \sigma_v^2.\bar{\bar{s}}^2 + \bar{v}.\overline{\sigma_s^2} + \bar{v}.\sigma_k^2 + \frac{1}{2\nu} \left[\sum_0^{\nu} \bar{r}_p^2 + \sum_{\nu}^{2\nu} \bar{r}_n^2\right]$

$$= \sigma_v^2.\bar{s}^2 + \bar{v}.\sigma_s^2 + \bar{v}.\sigma_k^2 + \bar{v}^2\,\bar{\bar{s}}^2 \tag{6.11}$$

since $(1 + \bar{k})$ represents the stationary state giving $\bar{k} = -1$.

Now at the end of the p^{th} interval the charge on the capacitor is $(p + r_p)$. Hence, the mean energy (Sec. 3.5) stored in the capacitor is given by

$$\bar{E}_c = \frac{1}{2\nu} \left[\sum_0^{\nu} \overline{(p + r_p)^2} + \sum_{\nu}^{2\nu} \overline{(p + r_n)^2}\right] \frac{e^2}{2C}$$

$$= \frac{1}{2\nu} \left[\sum_0^{2\nu} p^2 + \sum_n \sum_p 2p\,(\bar{r}_p + \bar{r}_n) + \sum_n \sum_p (\overline{r_p^2} + \overline{r_n^2})\right] \frac{e^2}{2C}$$

Since p is a constant and $2p\left[\sum_n \sum_p (r_p + r_n)\right] = 0$ then

$$\bar{\bar{r}}^2 = \frac{1}{2\nu} \left[\sum_n \sum_p (\overline{r_p^2} + \overline{r_n^2})\right]$$

is representative of the mean square output power.

From Eq. (6.11) $\overline{\overline{r^2}}$ is given by

$$\overline{\overline{r^2}} = \sigma_v^2\, \overline{\overline{s^2}} + \bar{v}\, \overline{\sigma_s^2} + \bar{v}\, \sigma_k^2 + \bar{v}^2\, \overline{\overline{s}}^2 \tag{6.11}$$

An expression identically equal to this was given by Bull[15] but the manner of derivation was inadequate. The more exhaustive calculations given above remove this inadequacy and allow the equation to be used without further doubts about its derivation.

If now reference is made to Eq. (6.11) it can be seen that $\overline{\overline{r^2}}$ has the following constituent terms:

1. $\bar{v}^2\, \overline{\overline{s}}^2$, which is a measure of the signal power at the output of the system, since $r = vs$ is the manifestation of the signal and was deliberately selected to represent the appearance of signal.
2. $\bar{v}.\sigma_k^2$, recognisable as the shot noise term of Sec. 3.5.
3. $\overline{\overline{s^2}}\, \sigma_v^2 + \bar{v}\, \overline{\sigma_s^2}$, a measure of the noise power in the device due to the application of signal.

It follows, therefore, that in a time δt the average amount of power generated by the signal, $\overline{\delta P}$, is given by

$$\overline{\delta P} = K[\overline{\overline{s^2}}\, \sigma_v^2 + \bar{v}\, \overline{\sigma_s^2} + \bar{v}^2\, \overline{\overline{s}}^2] \quad = K[\bar{s}^2 \sigma_v^2 + \bar{v}^2 \sigma_s^2 + \bar{v}^2 \bar{s}^2] \tag{6.12}$$

By the principle of conservation of energy, $\overline{\delta P}$ must be exactly equal to the power supplied to the device in δt which must arise from the signal source. Thus if $(P_s)_i$ is the avege signal input power in time δt and

$$(P_s)_o = K\,\bar{v}^2\,\overline{\bar{s}^2} = K\,\bar{v}^2\,\bar{s}^2 \tag{6.13}$$

the average signal output power in time δt, then from Eq. (6.12)

$$(P_s)_i = K[\bar{v}^2\,\bar{s}^2 + \bar{v}^2\,\sigma_s^2 + \bar{s}^2\,\sigma_v^2]$$

$$\frac{(P_s)_i}{(P_s)_o} = 1 + \frac{\sigma_v^2}{\bar{v}^2} + \frac{\sigma_s^2}{\bar{s}^2} \tag{6.14}$$

To proceed further with the study of this equation it is necessary to make some assumptions about the variances σ_s^2 and σ_v^2.

1. σ_v^2

The assumption is made that the integers have a distribution resembling that of a Poisson distribution so that $\sigma_v^2 \doteqdot \bar{v}$. Thus the term $\frac{\sigma_v^2}{\bar{v}^2} \doteqdot \frac{1}{\bar{v}}$ and since $\bar{v}$ must be a very large number (e.g. for a current of 1mA and $\delta t \doteqdot 10^{-7}$, $v \doteqdot 10^9$) $\frac{1}{\bar{v}}$ is negligible in comparison with unity.

2. σ_s^2

The fluctuations described by σ_s^2 must arise either from fluctuations in the signal source or from fluctuations imposed on the signal by the action of the electronic device, or both. If it is considered that the signal source of supply is under precise control then it is to be anticipated that there would be no fluctuations in the integers s due to the random fluctuations in the signal itself. In other words successive observations of the numbers s occurring in δt at time T, 2T, 3T ... nT, (where T is the period of the repetitive signal) would exhibit a variance of zero. In this case a contribution to σ_s^2 from the signal source is eliminated.

It is therefore postulated that it is the action of the electronic device itself which contributes to σ_s^2, and that the latter is a measure of the irregularity in the response of the device to the signal. For instance if a signal is applied to the grid of a triode valve amplifier, then the characteristic response $\left(\frac{\partial \bar{I}}{\partial V_g}\right)_{V_a}$ or conductance of the device is called into action by the signal. It is supposed that such a characteristic can fluctuate.

Thus if a probability distribution $G_p(x)$ is ascribed to the characteristic for a particular, positive, excursion of signal and the signal is also represented by a probability distribution $E_p(x)$ then the resultant output from the device is obtained by a multiplicative operation represented by the p.g.f.

$$S_p(x) = E_p(G_p(x)) \tag{6.15}$$

from which it follows

$$\bar{s}_p = \bar{e}_p \, \bar{g}_p \tag{6.16a}$$

$$(\sigma_s)_p^2 = \sigma^2_{e_p} \, \bar{g}^2_p + \bar{e}_p \, \sigma^2_{g_p} \tag{6.16b}$$

Since $\sigma^2_{e_p}$ is assumed zero for the reasons previously discussed, this last equation reduces to

$$(\sigma^2_s)_p = \bar{e}_p \sigma^2_{g_p}$$

which on substitution for $\bar{e}_p$ yields

$$(\sigma^2_s)_p = \frac{\bar{s}_p}{\bar{g}_p} \, \sigma^2_{g_p} \tag{6.17}$$

at a given point on its characteristic with a positive signal of fixed size.

Similarly, for negative excursions of signal, by analogy with Eq. (6.16b) it follows that

$$(\sigma^2_s)_n = \sigma^2_{e_n} \, \bar{g}^2_n + \bar{e}_n \, \sigma^2_{g_n}$$

which if $\sigma^2_{e_n}$ is small gives, since $\bar{e}_n$ is negative, a negative value for the variance, a result which is incompatible with the fact that the variance, by definition, is always a positive quantity. Furthermore, by using similar reasoning to that used in developing Eq. (6.15) it follows that the p.g.f. for negative excursions of signals is of the form

$$S_n(x) = E_n((G(x))^{-1})$$

which is anti-physical in that it leads to an infinite series for $S_n(x)$.

It is apparent, therefore, that although Eq. (6.15) may appear to be satisfactory for positive signals it leads to anomalies when applied to negative signals. However, in view of the fact that the system is linear and therefore behaves in the same manner for negative as for positive signals then the relationship

$$\sigma_s^2 = \frac{2}{\nu}\sum_{0}^{\nu} \sigma_{e_p}^2\,\overline{g_p}^2 + 2\bar{e}_p\,\bar{g}_p = \overline{\sigma^2_{e_p}}\,\bar{\bar{g}}_p^{\,2} + 2\bar{\bar{e}}_p\,\overline{\sigma^2_{g_p}} \qquad (6.18)$$

which describes the total variance will be assumed to be representative of the processes occurring.

By using the same reasoning as in developing Eq. (6.17) above then Eq. (6.18) approximates to

$$\sigma_s^2 = 2\bar{\bar{e}}_p\,\sigma^2_{g_p} = 2\bar{\bar{s}}_p\,\frac{\overline{\sigma^2_{g_p}}}{\bar{\bar{g}}_p} = 2A\bar{\bar{s}}_p = 2A_1\sqrt{\overline{\bar{s}_p^2}}$$

Substituting this value for σ_s^2 in Eq. (6.14) gives

$$\frac{(P_s)_i}{(P_s)_o} = 1 + \frac{2A_1\sqrt{\overline{\bar{s}_p^2}}}{\overline{\bar{v}\bar{s}}^2} \qquad (6.19)$$

Assuming that the signal and shot noise are of comparable magnitude so that

$$(\bar{v}\bar{\bar{s}})^2 \doteqdot \bar{v}\,\overline{\sigma_k^2}$$

i.e. $\bar{v}\sqrt{\overline{\bar{s}^2}} \doteqdot \sqrt{\bar{v}}$ since $\overline{\sigma_k^2}$ is equal to 1 (Eq.3.6b) then $\frac{1}{\overline{v}\sqrt{\overline{s}^2}} \gg \frac{1}{\overline{v}}$ and the neglect of the $\frac{\sigma_v^2}{\overline{v}}$ term in developing Eq. (6.19) is still valid. Furthermore, by making the substitutions $\overline{s^2} = \overline{s_p^2} + \overline{s_n^2} = 2\,\overline{s_p^2}$ and $\overline{v}^2\overline{s^2} = \frac{(P_s)_o^{\frac{1}{2}}}{K^{\frac{1}{2}}}$ Eq. (6.19) may be rewritten in the form

$$\frac{(P_s)_i}{(P_s)_o} = 1 + \frac{1}{B(P_s)_o^{\frac{1}{2}}}, \quad B = 1/2^{\frac{1}{2}}AK^{\frac{1}{2}}$$

or
$$\frac{(a_s)_i^2}{(a_s)_o^2} = 1 + \frac{1}{C(a_s)_o} \tag{6.20}$$

[$(a_s)_i$ and $(a_s)_o$ represent the input and output signal amplitudes respectively].

Solving Eq. (6.20) for $\frac{(a_s)_o}{(a_s)_i}$, say x, gives

$$x = \sqrt{\frac{1}{4B^2(a_s)_i^2} + 1} - \frac{1}{2B(a_s)_i} \tag{6.21}$$

It follows, therefore, that since x is a direct measure of the correlation then Eq. (6.21) predicts the manner in which this will vary with the size of the input signal.

A graphical solution of Eq. (6.21) is shown in Fig. 6.5 in which the ordinate represents x and the abscissa log $B(a_s)_i$, i.e. log $(a_s)_i$ + constant. Also shown on these axes is one of Hathaway's experimental curves which has been made to coincide with the theoretical curve at 80%

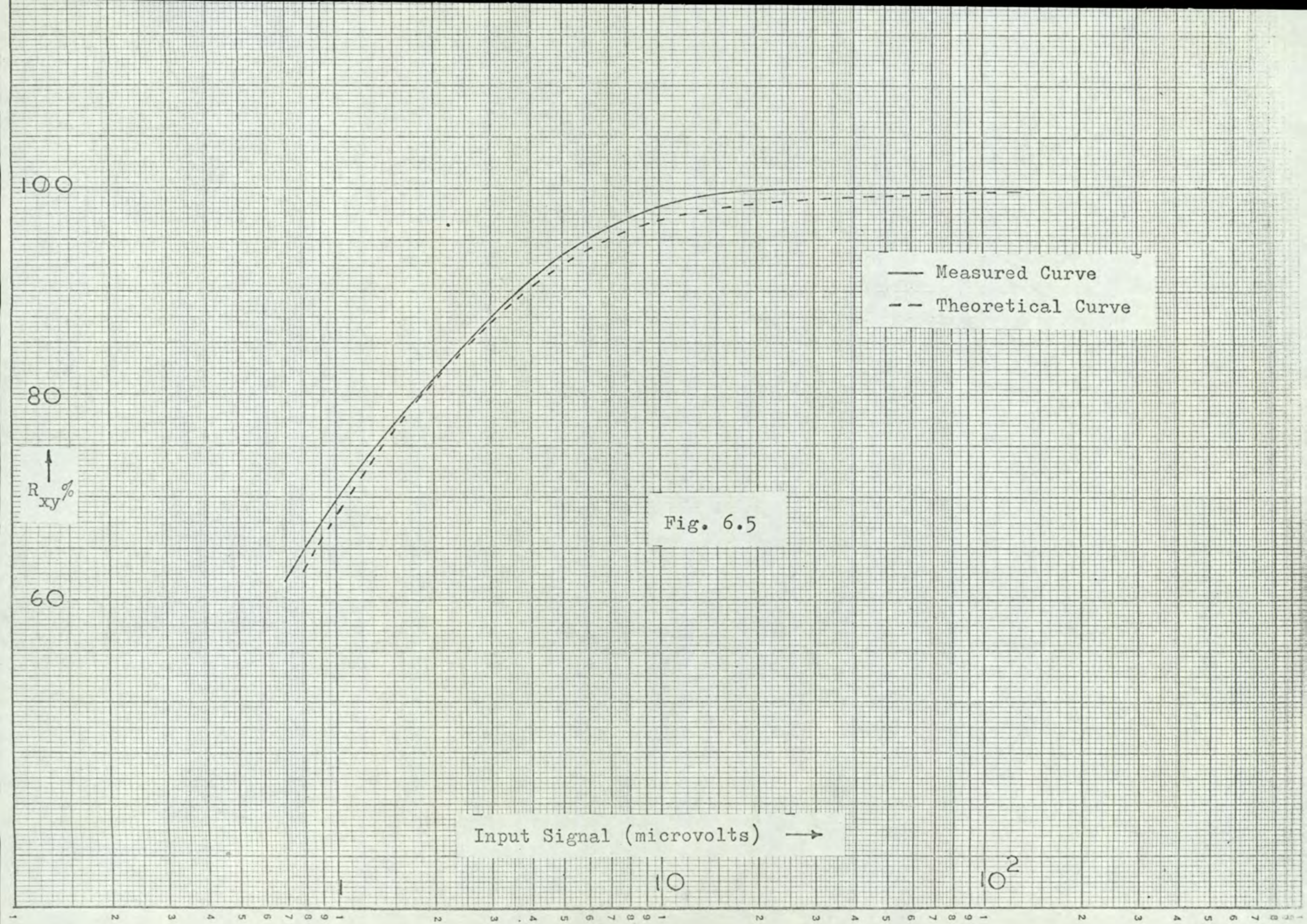

100
80
60
R_{xy}%
Measured Curve
Theoretical Curve
Input Signal (microvolts)
1
10
10^2

Fig. 6.5

diminution in correlation. This procedure has been adopted since the theoretical expression provides only the shape of the correlation - signal amplitude curve and does not predict in an absolute manner, for example, the amplitude of signal at which correlation commences to be less than 100%.

It will be observed that generally quite good agreement between theory and experiment was obtained by Hathaway.

6.5 The Experimental Equipment

A functional diagram of the equipment is shown below (Fig. 6.6). Basically it consisted of three units: a microvolt divider (M.D.), a high gain amplifier (H.G.A.) and a crosscorrelation function analyser (C.F.A.) and these will be discussed in some detail in the three succeeding sections.

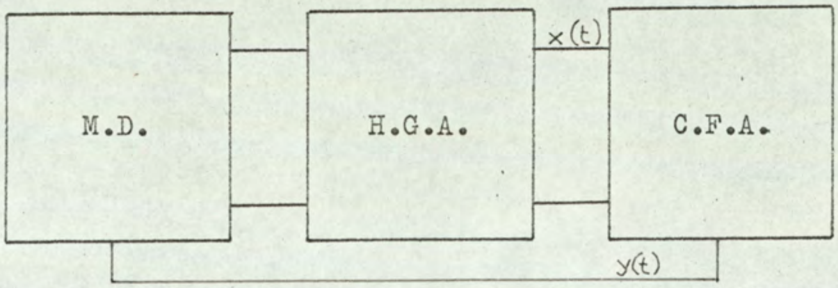

Fig. 6.6

6.6 The Crosscorrelator

6.6.1 Basic Instrument Requirements[5,39]

Given two voltage time history records $x(t)$ and $y(t)$ (corresponding to a noisy and a reference signal) the crosscorrelation is defined by Eq. (2.8), i.e.

$$R_{xy}(\tau) = \lim_{T \to \infty} \frac{1}{T} \int_{-\frac{T}{2}}^{\frac{T}{2}} x(t)y(t + \tau)dt$$

In words the crosscorrelation is estimated by the following operations:

(i) Delaying $x(t)$ relative to the signal $y(t)$ by a time displacement τ secs.

(ii) Multiplying the value of $y(t)$ at any instant by the value of $x(t)$ that had occurred τ secs. before.

(iii) Averaging the instantaneous product over the samplying time T.

In the present work an analogue correlator was used, a functional diagram of which is given in Fig. 6.7, where M.S.V. is a mean square voltmeter of the type described in Chap. 8 (both types of voltmeter were used at different stages in the experiment).

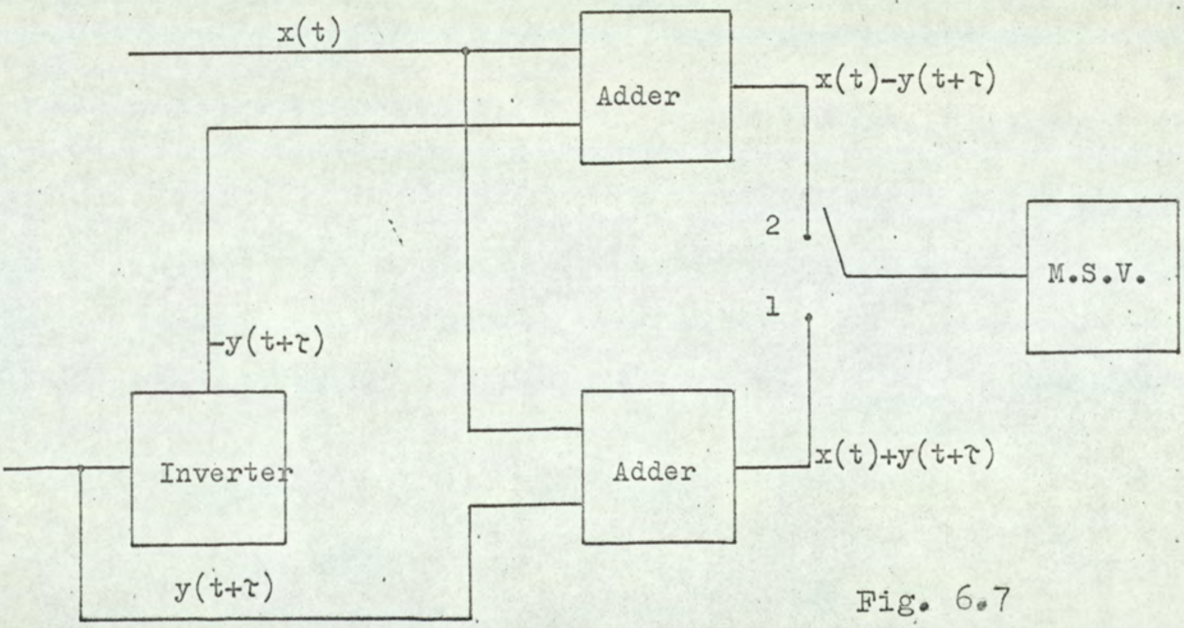

Fig. 6.7

Referring to Fig. 6.7 the crosscorrelation between $x(t)$ and $y(t)$ is obtained by switching from position (1) to position (2) and subtracting the readings obtained. If the m.s.v. deflection in each of these positions is θ_1 and θ_2 respectively then,

$$\theta_1 = \left\langle (x(t)+y(t+\tau))^2 \right\rangle = \left\langle x(t)^2 + y(t+\tau)^2 + 2\,x(t)y(t+\tau) \right\rangle$$

$$\theta_2 = \left\langle (x(t)-y(t+\tau))^2 \right\rangle = \left\langle x(t)^2 + y(t+\tau)^2 - 2\,x(t)y(t+\tau) \right\rangle$$

and

$$\theta_1 - \theta_2 = 4\left\langle x(t)y(t+\tau) \right\rangle = 4\,R_{xy}(\tau) \qquad (6.22)$$

i.e.

$$\frac{\theta_1 - \theta_2}{4} = R_{xy}(\tau)$$ the crosscorrelation.

During the course of the investigation two such correlators were developed. The first, was designed for the processing of frequencies in ranges up to MHz, but this was later replaced by an instrument which was basically the same as that used by Hathaway. In terms of reliability and simplicity of operation this changeover was a retrograde step but it was felt to be necessary to retrace steps on account of the inexplicable disagreement of the results obtained with Hathaway's. This disagreement will be brought out later, and has still not been cleared up nor understood.

6.6.2 Correlator 1

The first correlator is shown in schematic form in Fig. 6.8 where the units A and B represent high gain

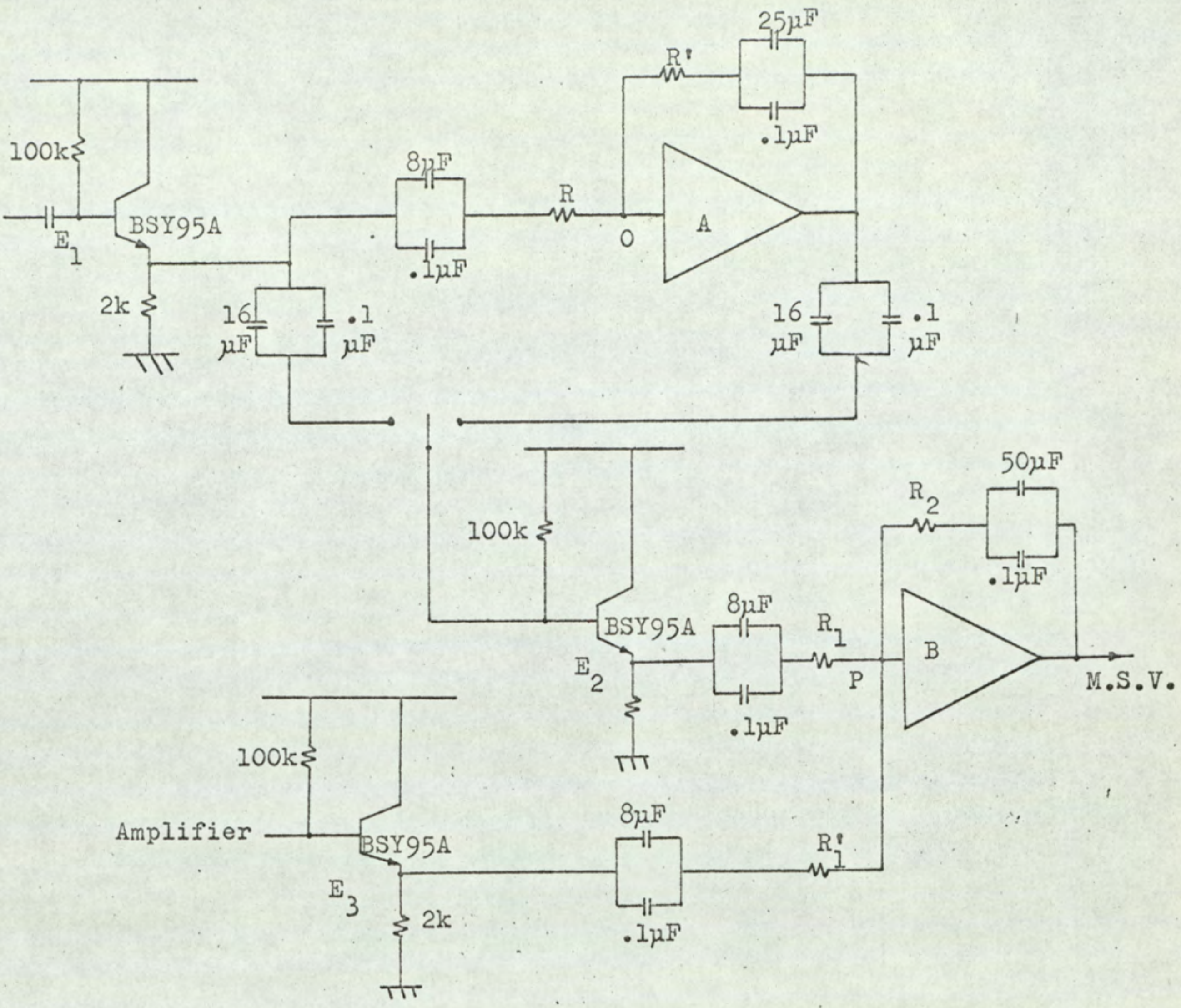

Fig. 6.8 Correlator

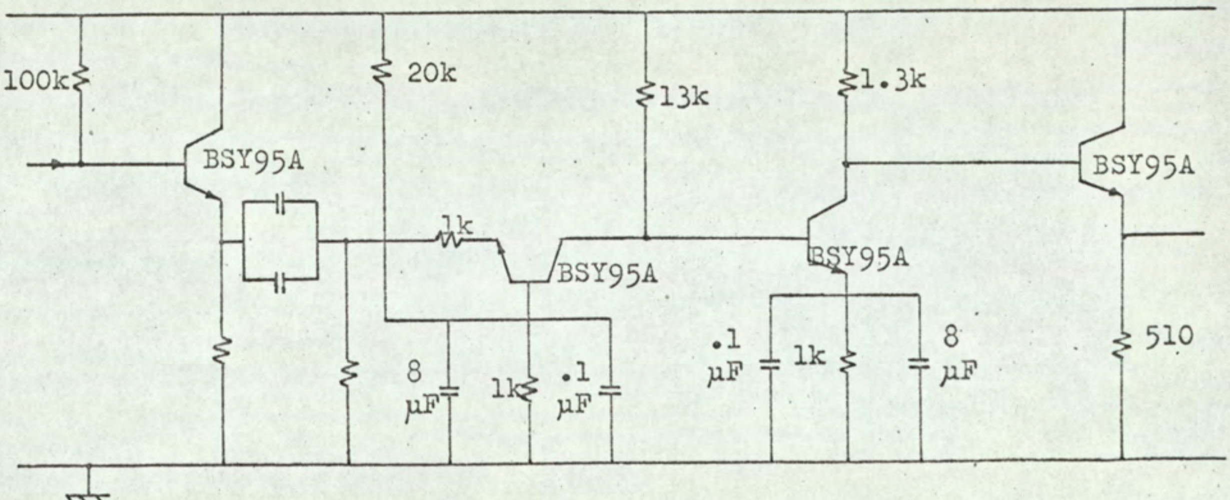

Fig. 6.9 Operational Amplifier

amplifiers having circuits of the type shown in Fig. 6.9. The gain of these amplifiers in the open loop connection is of the order of 50 dBs with an input impedance of 50 kilohms and an output impedance of 10 ohms (which will fall with the application of negative feedback). In actual practice, however, the amplifiers were not used in this manner but were connected in the operational[55] mode (see Appendix 7) so as to perform the mathematical operations of inversion and addition. As an indication of the accuracy with which these could be achieved it was found that the virtual earth points (O, P in Fig. 6.8) were at a potential less than 1/400 of the input.

Of course, although the amplifiers behaved exactly in the manner predicted by the theory this does not mean that the mathematical processing was done without any errors. As can be seen from the theory some inaccuracies were bound to arise due to mismatching of:

(i) the resistors R and R^1 in the inverter unit; and

(ii) the resistors R_1 and R_1^1 in the adder unit.

However, in so far as this was possible these errors were reduced to a very minimum by using carefully selected (within 0.5%) high stability components for R and R^1 and R_1 and R_1^1 and by supplying these resistors from a low impedance source; hence the inclusion of the emitter followers E_1, E_2 and E_2 (Appendix 8). These have an input and output impedance of approximately 50 kilohm and 5 ohm respectively (they also have the additional property that they prevent the transmission of signals from emitter to base and so lessen the chance of any errors due to feedback between the output and input of the correlator).

Because:

(i) the driving voltage of the mean square voltmeter was of the order of 500 mV r.m.s.; and

(ii) the noise peaks could be as high as eight times this value, i.e. up to about 4 V r.m.s.;

it was a useful property of the correlator (and also the noise amplifier) that it should be linear up to voltages of the order of 4 V r.m.s. This was accomplished by carefully selecting the biasing potentials of the supply units.

Hence, as a result of tests with various biasing potentials the adder and inverter circuits described above were produced. These were found to give a linear output of up to 5 V r.m.s. over bandwidths of 200 Hz - 30 MHz (Fig. 6.10a) for the inverter and 20 Hz - 20 MHz (Fig.6.10b) for the adder.

To check the reliability of the correlator it was set up as in the system of Fig. 6.1. With the local signal,

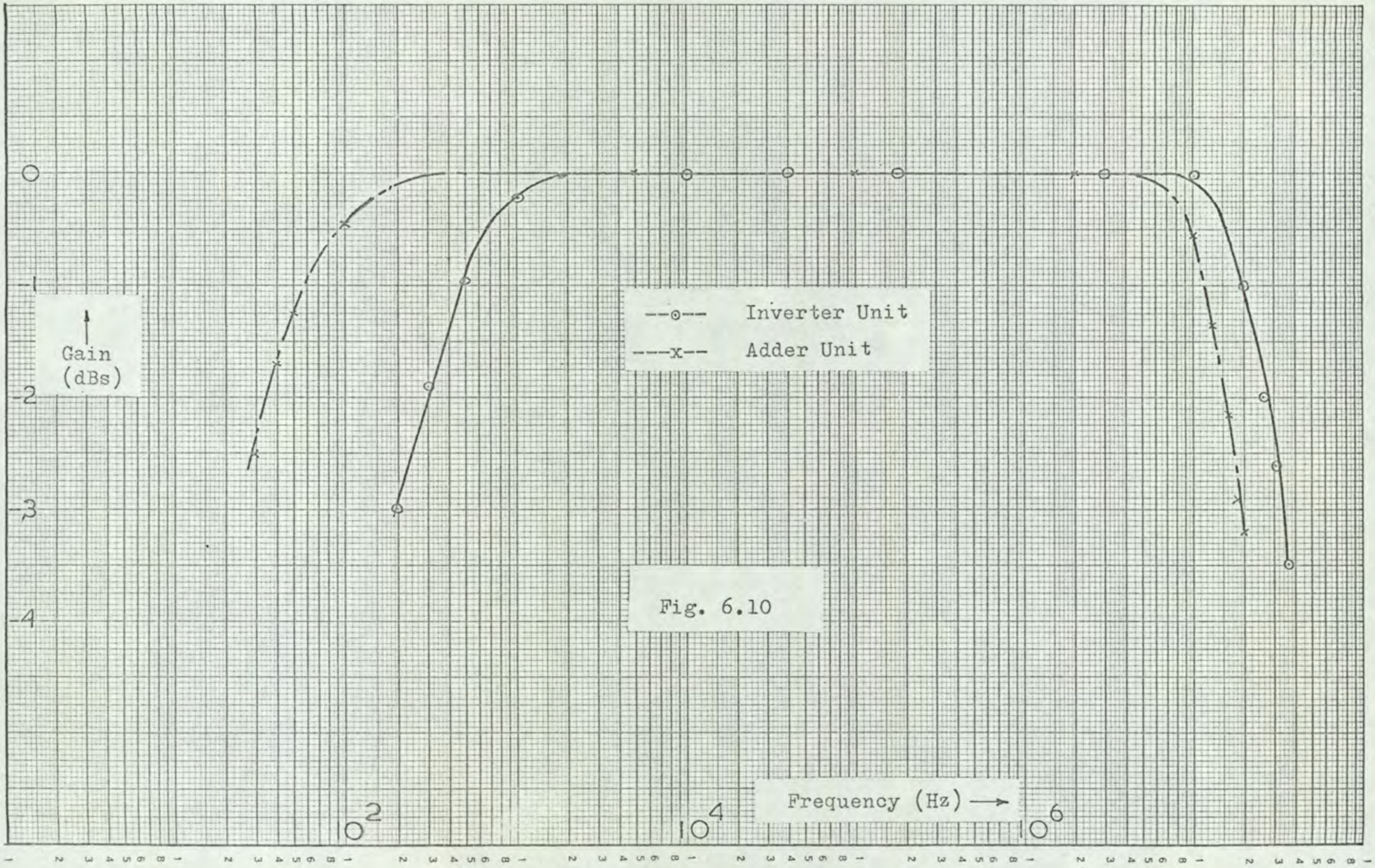
0
-1
-2
-3
-4
Gain
(dBs)
--⊙-- Inverter Unit
---x-- Adder Unit
Frequency (Hz)
10^2
10^4
10^6
Fig. 6.10

say V_y, set to a fixed value, the voltage at the amplifier input - which was set to be much greater than the noise voltage - was varied and for each value of V_x - the amplifier output voltage - the method described above for finding $R_{xy}(\tau)$ was carried out, and the value of V_x (by taking the square root of the mean square voltmeter reading of $\overline{V_x^2}$) was noted. This was repeated for a number of values of V_y, the frequency of the signal remaining constant. This frequency was then changed and the whole procedure repeated.

As can be seen from the graphs - which are a typical sample - of Figs. 6.11 - 6.13 the plots of

(i) $V_x - R_{xy}(\tau)$ for constant values of V_y

and (ii) $V_y - R_{xy}(\tau)$ for constant values of V_x

follow straight line laws; thus confirming that the system carries out the calculations of correlation. It can also be seen from these graphs that when the plot of V_xV_y is drawn then over the mid-frequency band of the amplifier, where τ is zero, the two sets of lines coincide, whereas over the region where the amplifier gain is falling (Fig. 6.26) $V_xV_y > R_{xy}(\tau)$. This is due to the phase shift associated with the fall of gain so that τ, the time delay between the two waves, is no longer zero. However, since the effect of a phase shift is to reduce the instrument sensitivity, the measurements, as has been

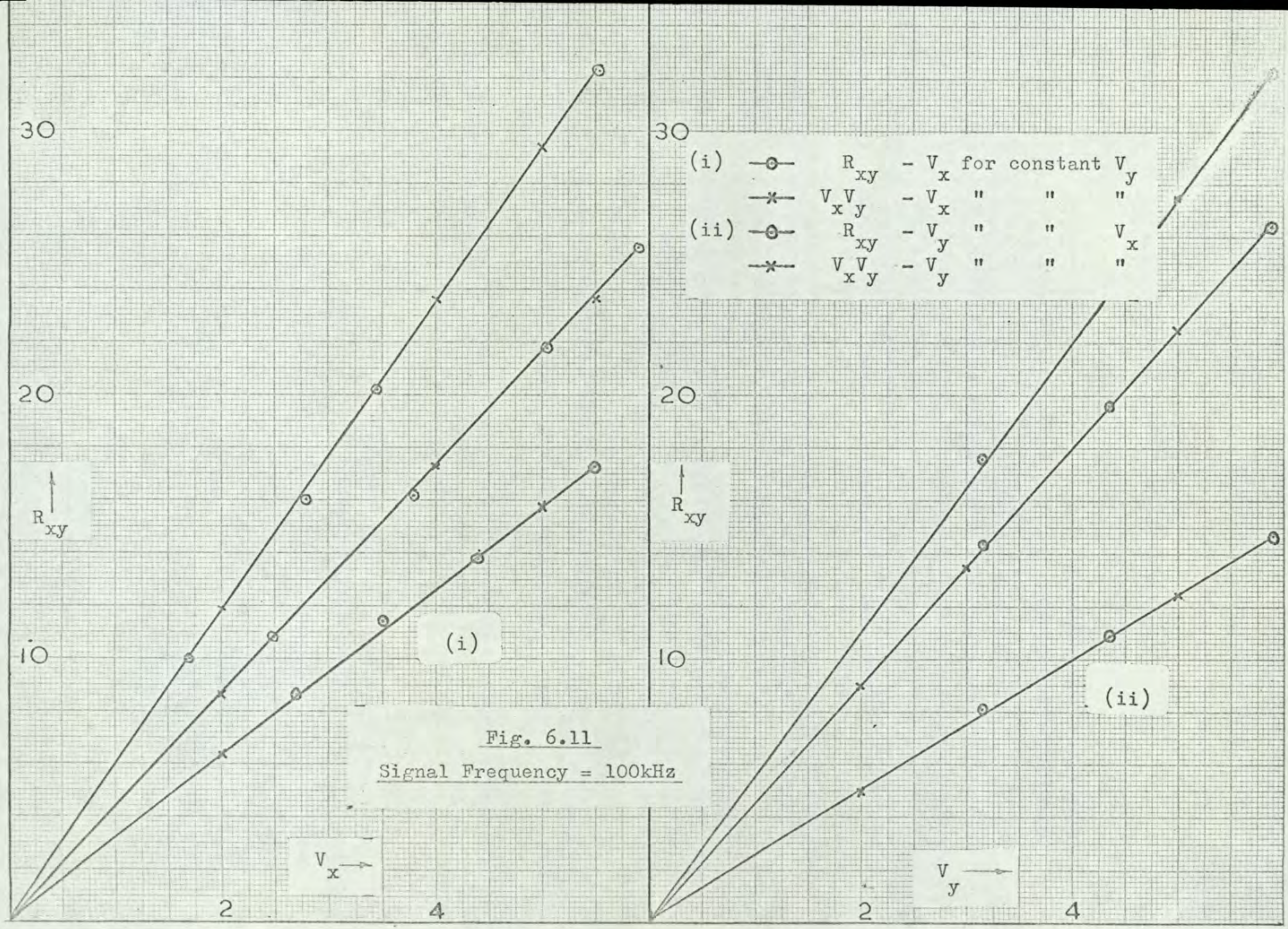

Fig. 6.11

Signal Frequency = 100kHz

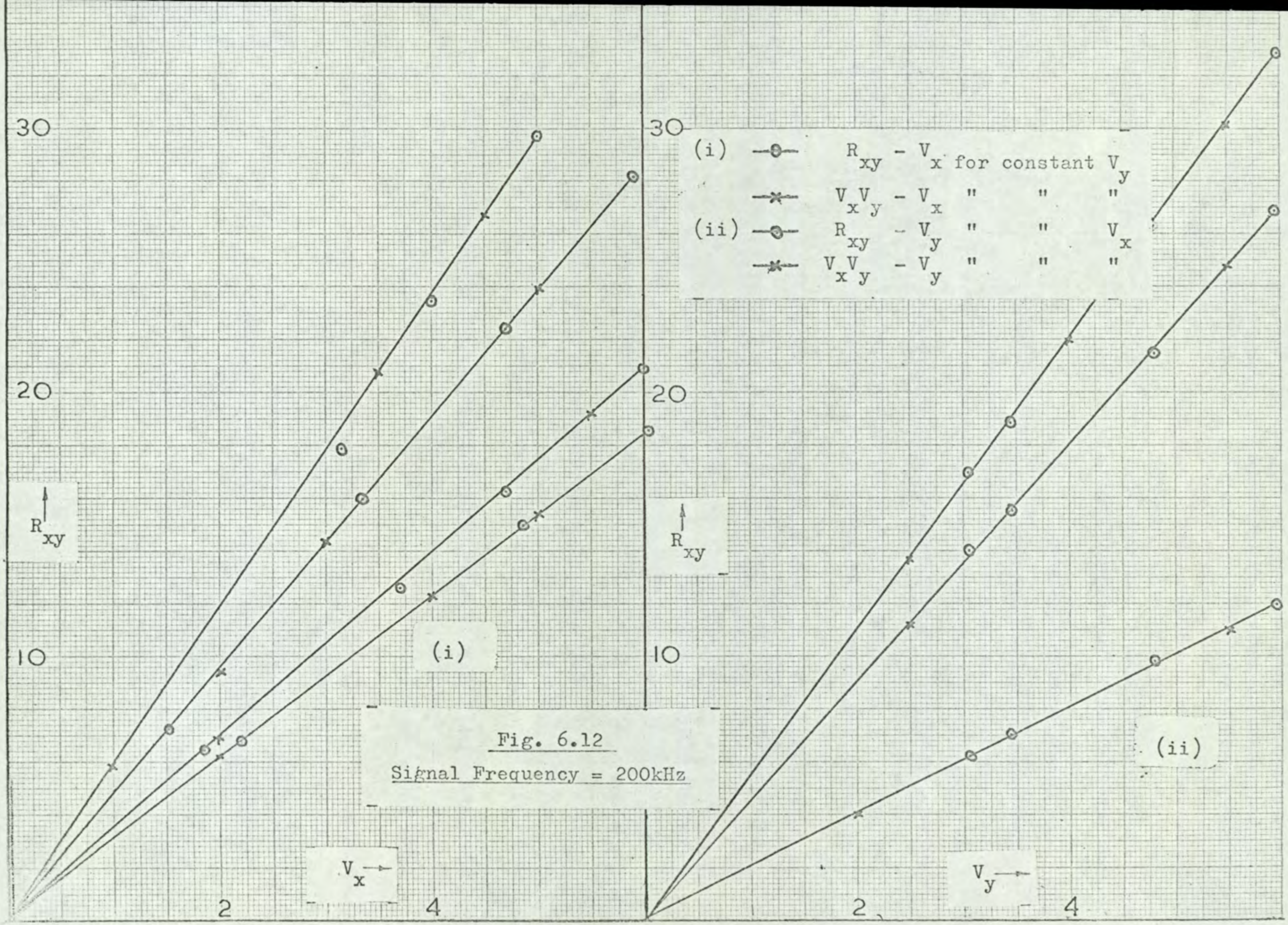

Fig. 6.12
Signal Frequency = 200kHz

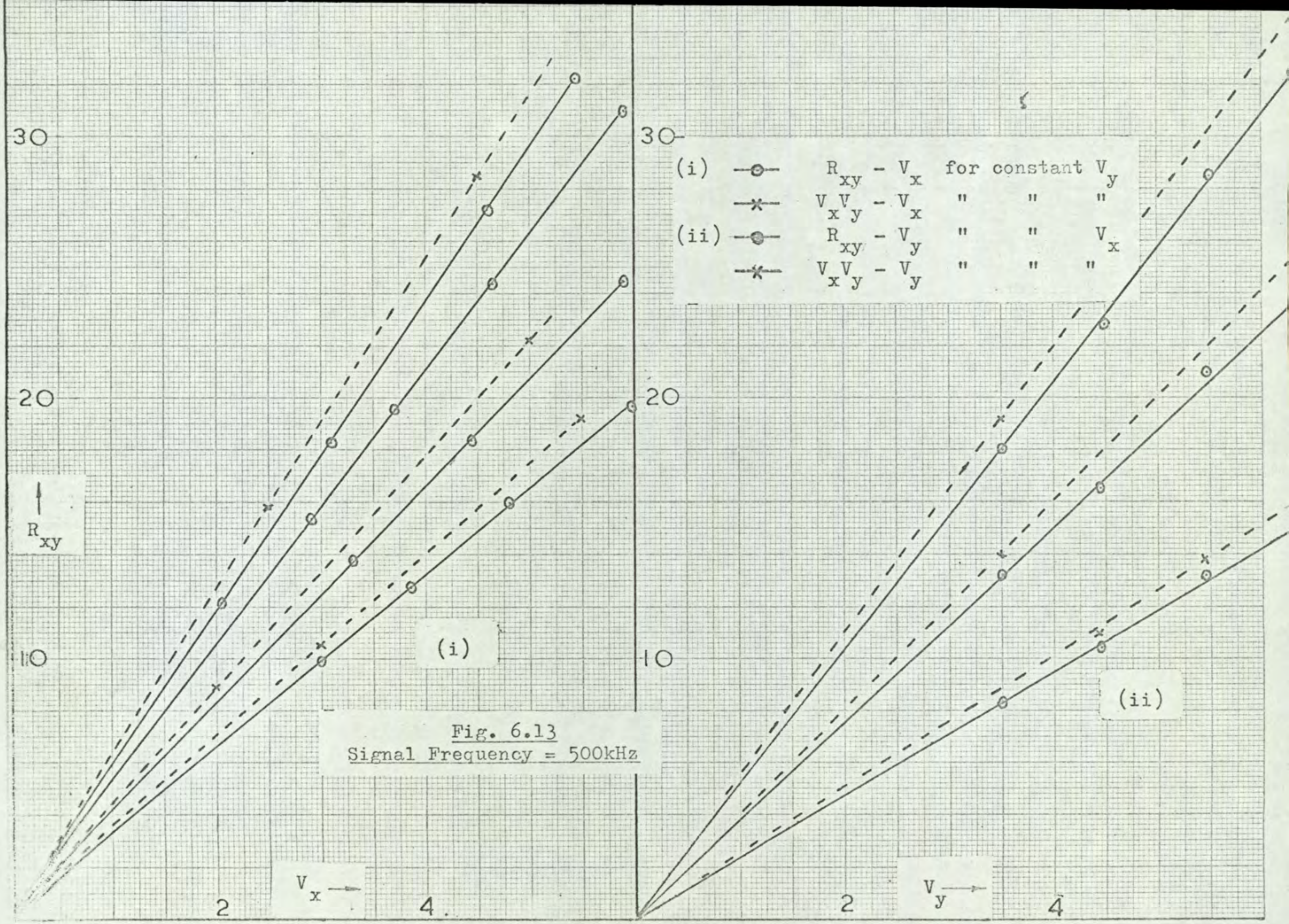

Fig. 6.13
Signal Frequency = 500kHz

mentioned earlier, were made only over the mid-frequency band for which $\tau = 0$.

6.6.3 Correlator 2

For reasons which will become apparent later this correlator was designed to be of the same form as Hathaway's although there were slight differences both in the layout and in the method of obtaining the readings of $\langle(x + y)^2\rangle$ and $\langle(x - y)^2\rangle$.

With regard to this latter point, Hathaway obtained a measure of correlation by using two voltmeters, one at the $(x + y)$ terminal and the other at the $(x - y)$ terminal, and taking the difference between the two voltmeter readings. However, this method suffered from the disadvantages that:

(i) Before any measurement checks had to be made to ensure the meters were of equal sensitivity.

(ii) Great care had to be taken to ensure that at the start of the measurement the meters were simultaneously at zero since the zero shifted erratically with time.

(iii) The inputs to both voltmeters could not be monitored simultaneously and this could lead to errors from unwanted signals.

For this reason it was decided to use the method of Fig. 6.14, i.e. use only one voltmeter, since this facilitated the meter adjustments; e.g. the checks on sensitivity were no longer required in so far as to

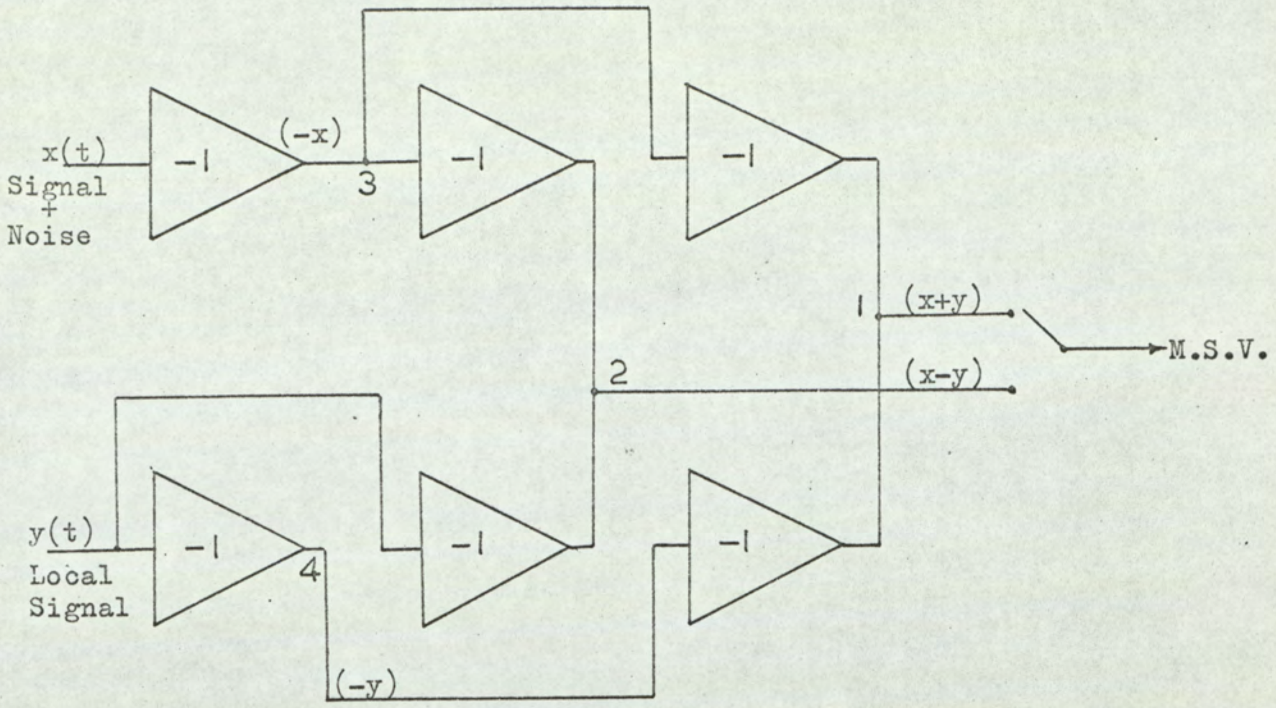

Fig. 6.14 Correlator 2

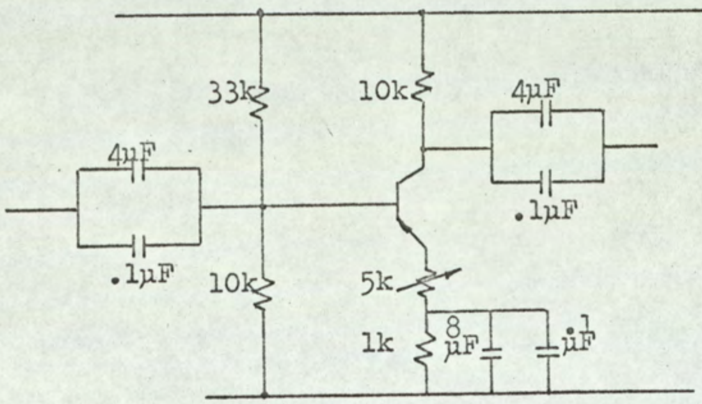

Fig. 6.15 Inverter Unit

ensure that it did not change markedly over the period of a few minutes. The single voltmeter method also had the additional advantage that errors due to unwanted signals - since the voltmeter input was monitored - were eliminated.

Consider now the functional diagram (Fig. 6.14) of the correlator. When the instrument is operating correctly the a.c. voltage distribution at points such as 1, 2, 3, 4 will be of the form shown, the phase reversals being effected with units like that of Fig. 6.15. The latter may be represented by the a.c. equivalent - tee - network[35] of Fig. 6.16. Accordingly, from the results of Appendix 8 it follows that the input and output impedances are approximately 8 kilohm and 10 kilohm respectively.

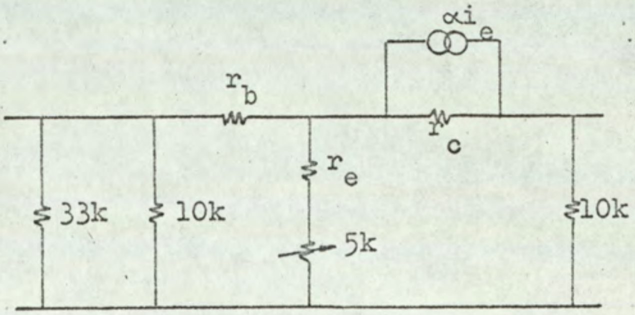

Fig. 6.16

From this last remark it is obvious that if two stages are connected in cascade then for unity voltage gain between successive inputs it is necessary that the first stage has a gain of approximately 2:1 (half its voltage being dropped across its output impedance). Similarly if the first stage is followed by two others in parallel - as is the case in one of the correlator units - then for unity gain between the inputs the first stage gain will have to be approximately 3:1.

The necessary adjustments of gain were effected, in situ, by means of a potentiometer in the emitter lead. Thus, before taking any measurements with the correlator the following procedure was adopted:

(i) With amplified signal x, set to a value X_o say and the local signal, y, at zero the units were adjusted to give voltages $-X_o$ at point 3 and $+X_o$ at points 1 and 2.

(ii) With $x = 0$ and $y = Y_o$ the units were adjusted to give Y_o at point 1 and $-Y_o$ at points 2 and 4.

(iii) With $x = y$ checked to ensure that $x - y = 0$.

This tended to make the measurements a lot more tedious and difficult than with correlator 1 (where $x + y$ and $x - y$ were automatically produced with an accuracy dependent only on the long term stability of the operational resistors). Nonetheless, experimental checks of the type described previously have indicated (Figs. 6.17 and 6.18) that when the instrument is used in the manner of Fig. 6.14 it gives an accurate estimate of the crosscorrelation function $R_{xy}(0)$ for frequencies between 6kHz and 20 kHz. Outside this range, however, because of phase shifts (other than 180^o) within the inverter units (Fig. 6.19) the instrument was no longer reliable.

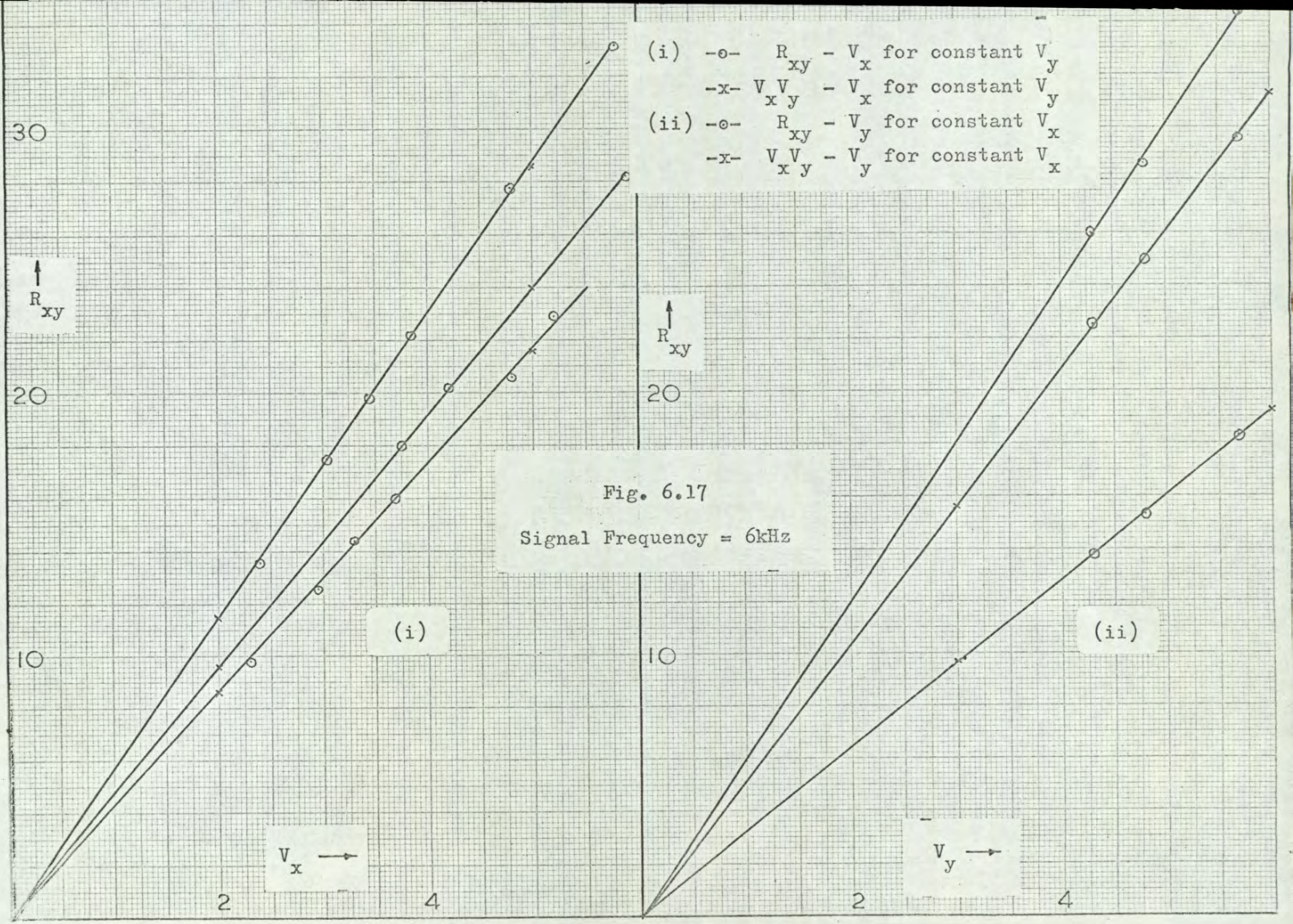

Fig. 6.17
Signal Frequency = 6kHz

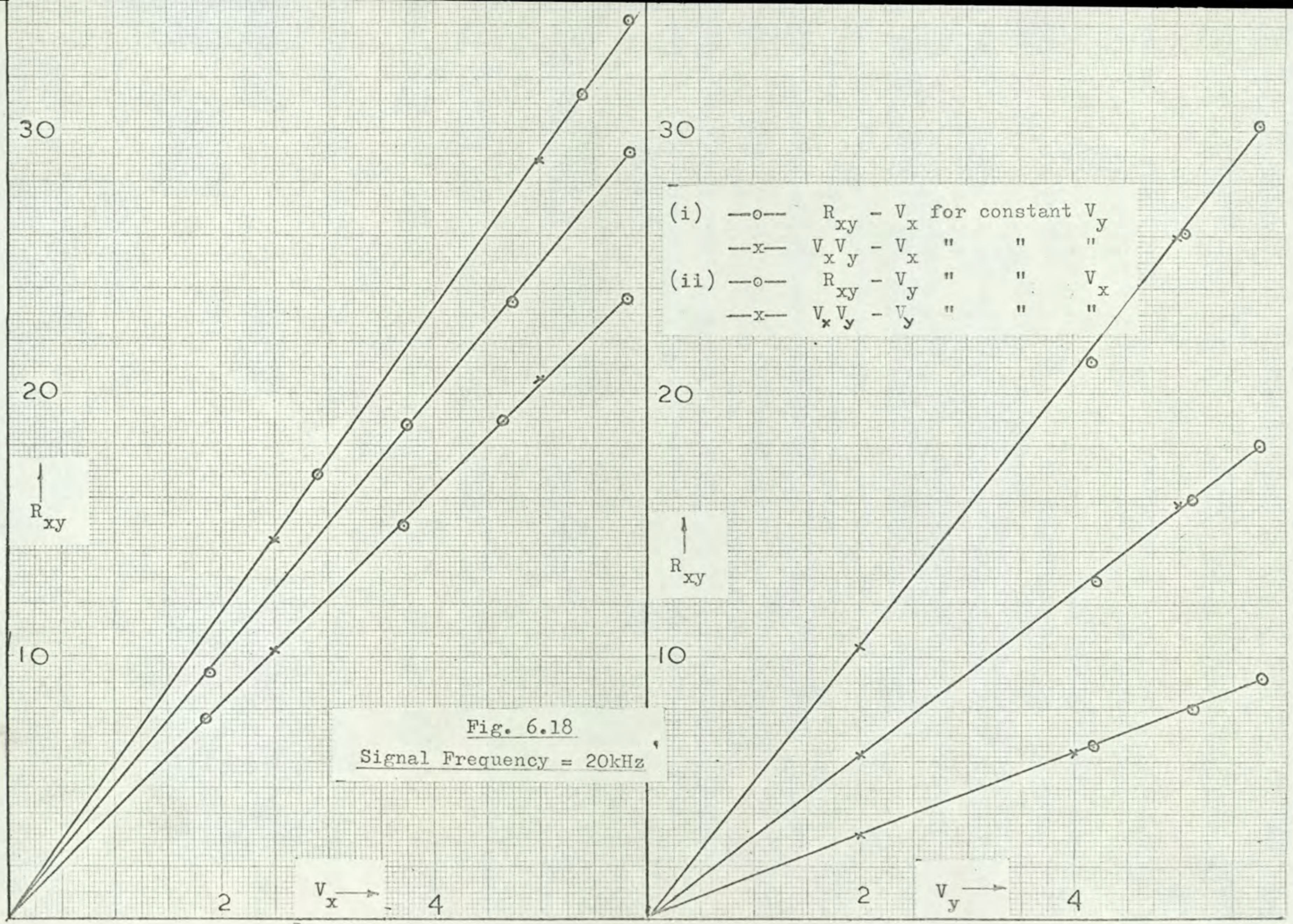

Fig. 6.18

Signal Frequency = 20kHz

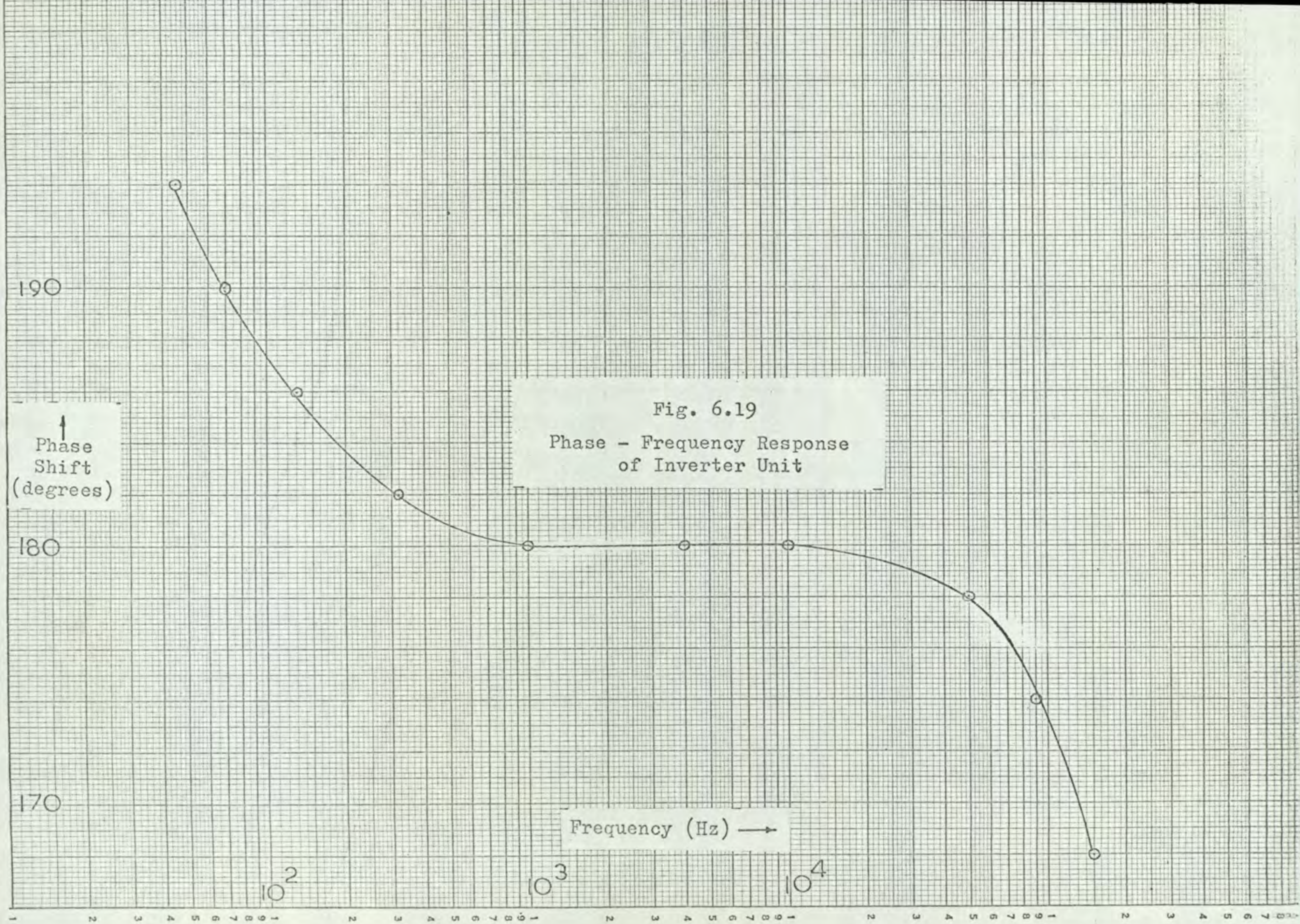

Fig. 6.19
Phase - Frequency Response of Inverter Unit

To illustrate this lack of reliability consider the schematic diagram of Fig. 6.14. Because of the phase shifts in the inverter units the voltage waves at the output terminals 1 and 2 are respectively

$$x(t - 2\tau_p) + y(t - 2\tau_p)$$

and $$x(t - 2\tau_p) - y(t - \tau_p)$$

where τ_p is a time delay representative of the fact that the phase change of the inverter units is not exactly 180°. It follows that the difference between the two voltmeter readings is, therefore,

$$\begin{aligned}\theta_1 - \theta_2 &= 2\langle x(t - 2\tau_p)y(t - 2\tau_p)\rangle + 2\langle x(t - 2\tau_p)y(t - \tau_p)\rangle \\ &\quad + \langle y^2(t - 2\tau_p)\rangle - \langle y^2(t - \tau_p)\rangle \\ &= 2R_{xy}(o) + 2R_{xy}(\tau_p) + R_{yy}(2\tau_p) - R_{yy}(\tau_p)\end{aligned}$$

i.e. it is no longer directly proportional to the cross-correlation of x and y. However, providing the signal frequency is keptwithin the mid-frequency band of the inverter units, as it was in the experiments, the error due to this cause is negligible.

6.7 The Amplifier

The amplifying system used in the experiments had the same basic elements as that described in Chap. 5, i.e. it contained a preamplifier and main amplifier connected in cascade.

The main amplifier was constructed using transistors as the active elements and its circuit remained basically the same throughout the experimental tests. The preamplifier on the other hand was altered several times. In fact three types of preamplifier were used, viz.,

(i) low noise triode amplifier;

(ii) noisy transistor amplifier;

(iii) hybrid amplifier - containing valves and transistors, the first stage being identical to that used by Hathaway;

and in order to distinguish between them they will be referred to as preamplifiers 1, 2 and 3 respectively.

6.7.1 Preamplifier 1

A circuit diagram of the preamplifier is shown in Fig. 6.20a. The amplifying valves were of the Sylvania 6 CW4 type, and are frequently referred to as Nuvistors.[53] They had a mutual conductance of the order of 10mA/V producing a stage gain of approximately 20 dBs and a total gain of 39.5 dBs.

The other relevant information about the amplifier is:

(i) its bandwidth is 600 Hz - 3.5 MHz (Fig. 6.21);

(ii) The input and output impedances are 100 kilohms and approximately 5 ohms respectively; and

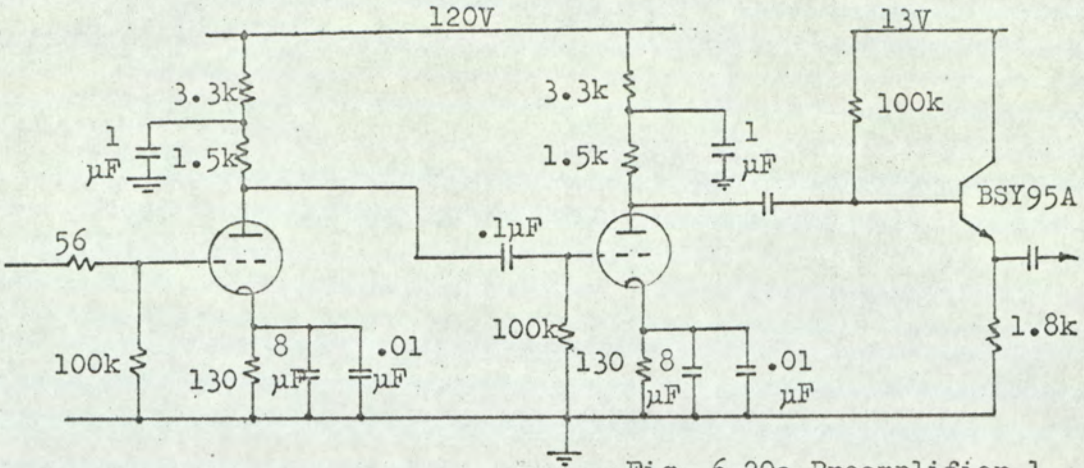

Fig. 6.20a Preamplifier 1

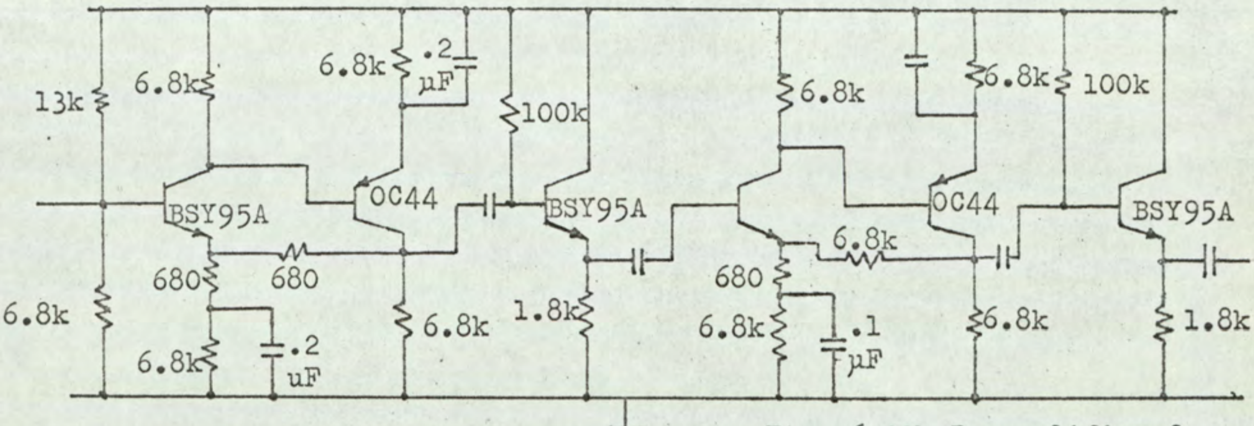

Fig. 6.20b Preamplifier 2

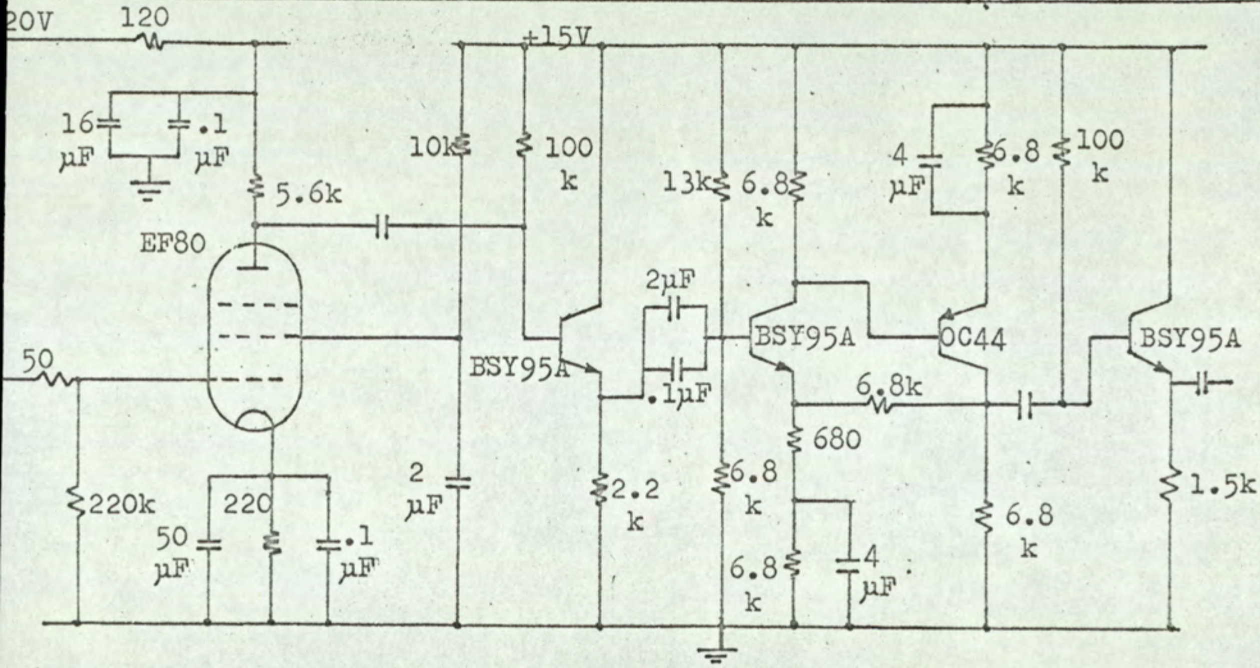

Fig. 6.20c Preamplifier 3

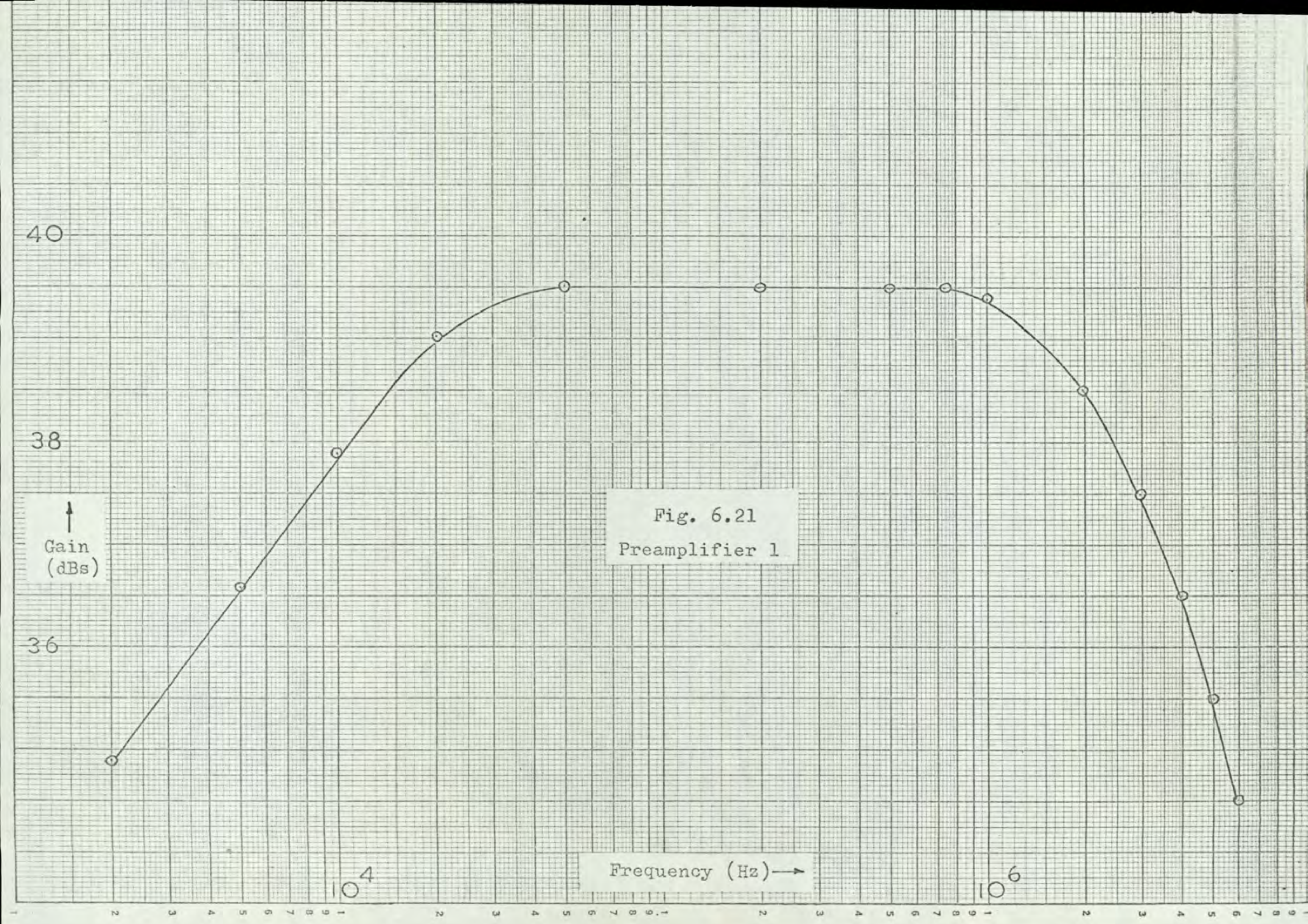
40
38
36
Gain (dBs)
Fig. 6.21
Preamplifier 1
Frequency (Hz)
10^4
10^6

(iii) the equivalent noise resistance (Fig. 6.22a) is of the order of 500 ohms.

6.7.2 Preamplifier 2

A circuit diagram of the amplifier is shown in Fig. 6.20b. The amplifier has a low input impedance (3kΩ), low output impedance and a bandwidth of 3kHz - 4MHz (Fig. 6.23). It was also found to be extremely noisy being approximately four times noisier than preamplifier 1.

6.7.3 Preamplifier 3

As mentioned earlier this amplifier (Fig. 6.20c) is a hybrid of both valve and transistor amplifiers. The input stage consists of a pentode EF80 valve producing a stage gain of approximately 30 dBs which is sufficient to ensure that the noise appearing at the valve anode is much greater than that of succeeding stages (this - as it was for each of the preamplifiers - was checked by removing the first stage).

Just as in the case of the other preamplifiers checks were made on the gain - frequency response, input impedance, output impedance and equivalent noise resistance. The impedance measurements indicated input and output impedances of 100 kilohms and 5 ohms respectively; the results of the other measurements are shown in graphical form in Figs. 6.24 and Fig. 6.22b respectively.

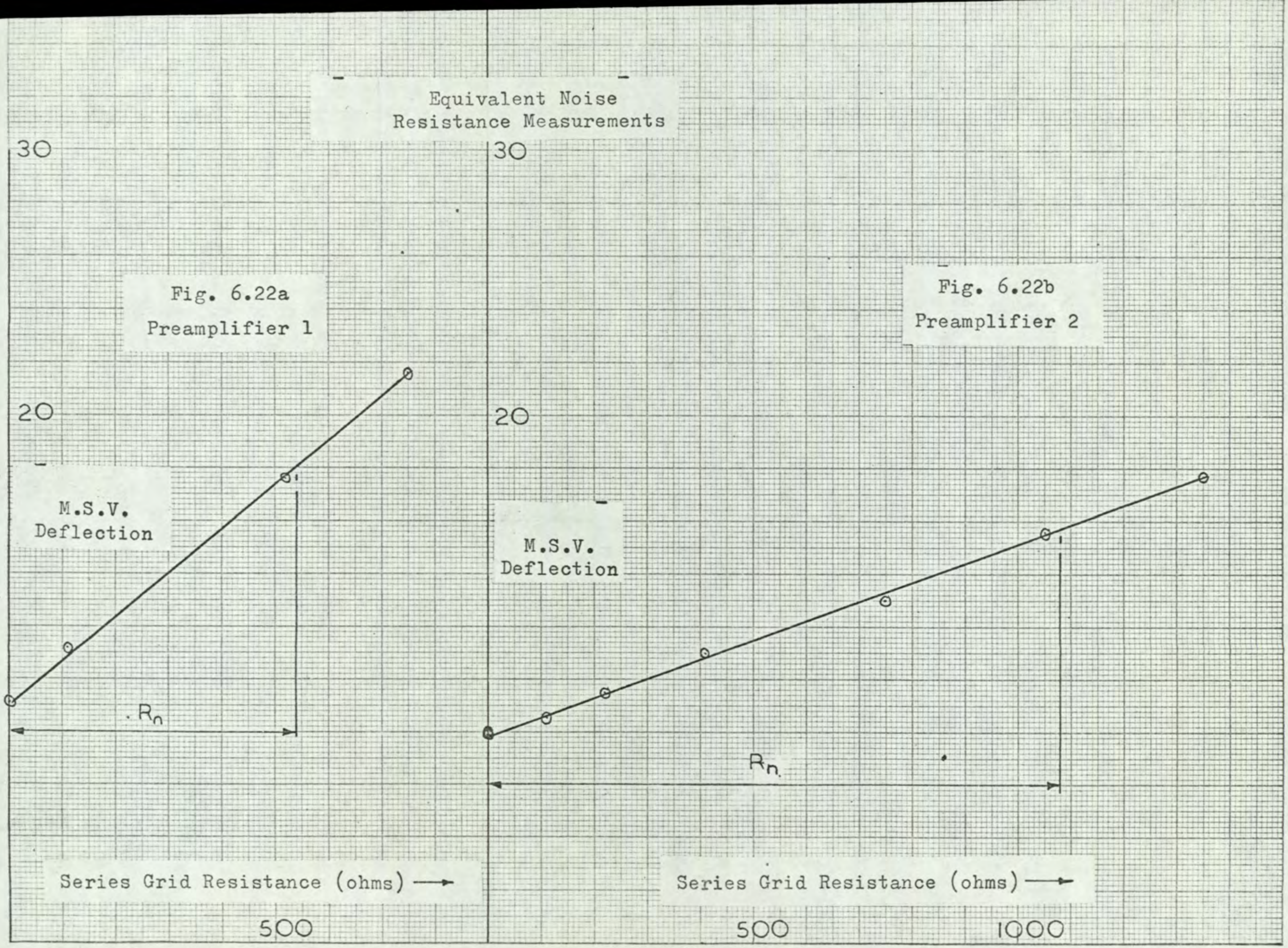
Equivalent Noise
Resistance Measurements
Fig. 6.22a
Preamplifier 1
Fig. 6.22b
Preamplifier 2
30
20
M.S.V.
Deflection
R_n
Series Grid Resistance (ohms)
500
1000

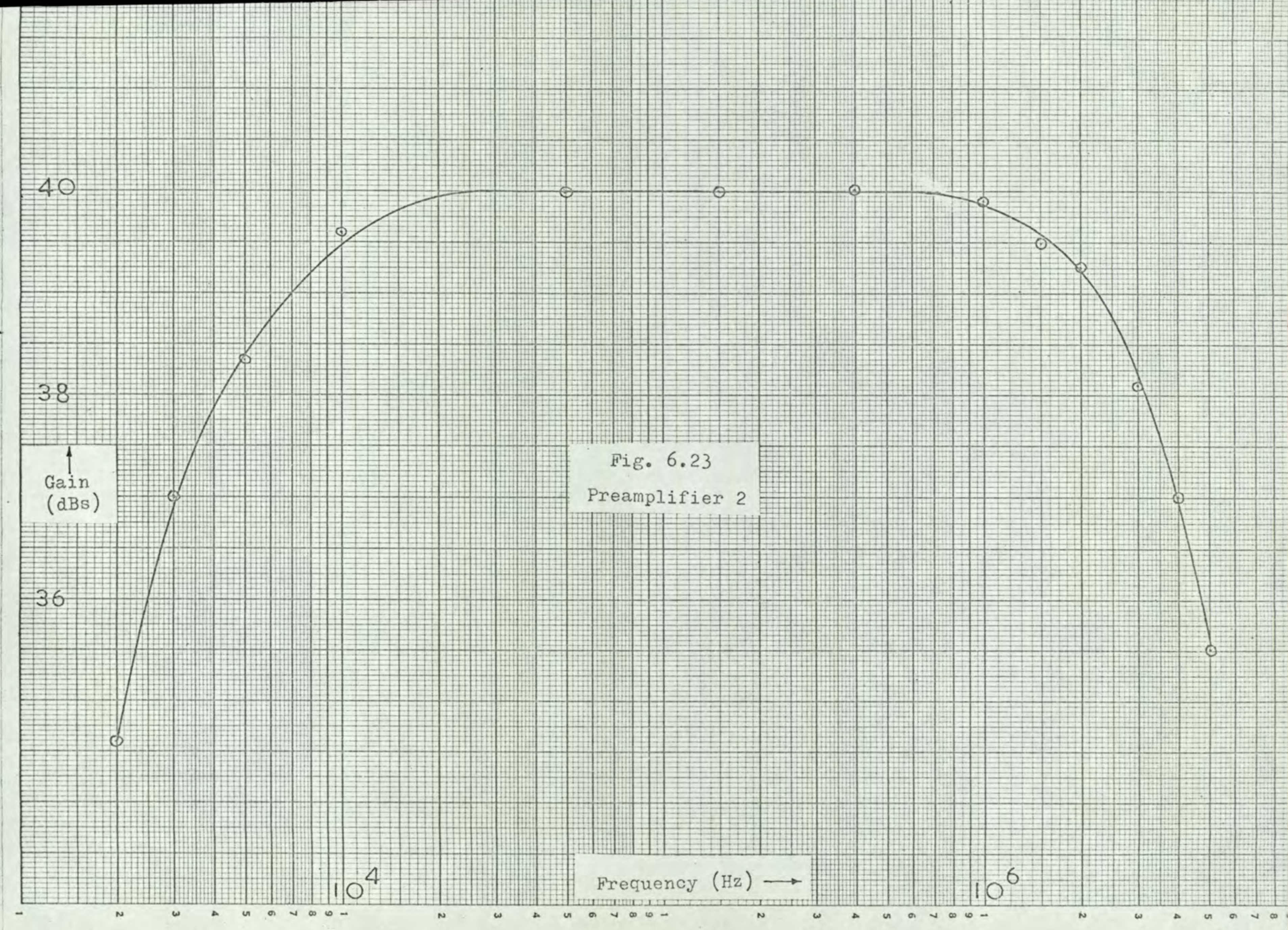

40
38
36
Gain (dBs)
Fig. 6.23
Preamplifier 2
10^4
10^6
Frequency (Hz)

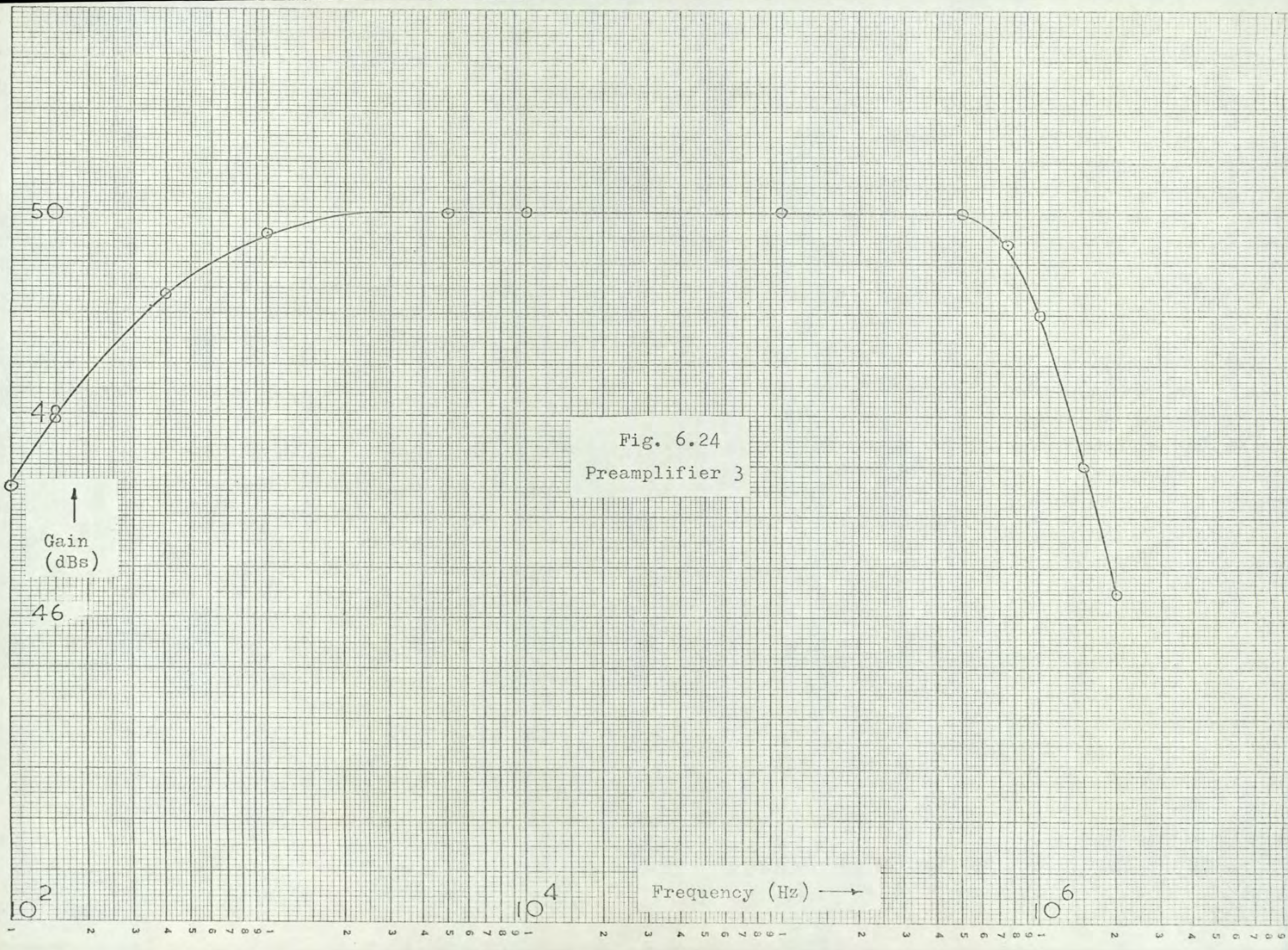
50
48
46
Gain (dBs)
Fig. 6.24
Preamplifier 3
Frequency (Hz)
10^2
10^4
10^6

6.7.4 Main Amplifier

The main amplifier (Fig. 6.25) was a low input impedance (≑ 5 kilohms) low output impedance (< 7 ohms) device and was linear up to approx. 6 V r.m.s. It was constructed using transistors as the active elements and was supplied from batteries so as to eliminate the possibility of introducing hum from mains operated supplies. It consisted of three stages of ampliciation, the first of these being voltage operated and the latter two current driven.

The gain was 67.5 dBs over the bandwidth (Fig. 6.26) 300 Hz - 1.8 MHz although this could be altered - and frequently was - by placing a capacitor in parallel with the 6.8 kilohms feedback resistor of stage 1. This had the effect of increasing the feedback and so decreasing the gain as the frequency increased (the bandwidth could also easily be increased by improving the quality of the transistors in stage 3).

As a means of varying the gain a Wayne Kerr Q251 attenuator was interposed between stages 1 and 2. Care was taken to match this attenuator at both ends and when this was done the overall accuracy of attenuation was of the order of 0.1 dBs in 60.

6.8 The Microvolt Divider

Originally the microvolt divider was designed so that the variations in signal level were made by high accuracy

Fig. 6.25 Main Amplifier

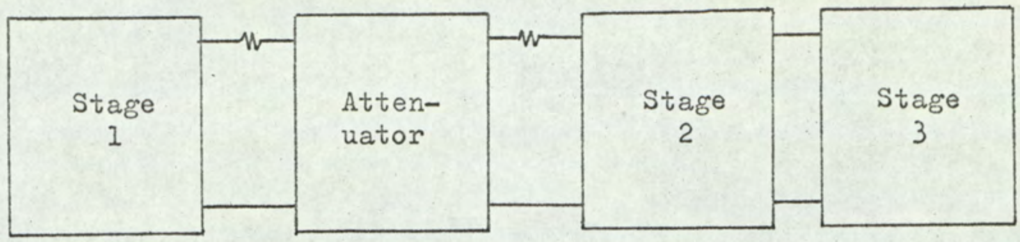

Schematic Diagram

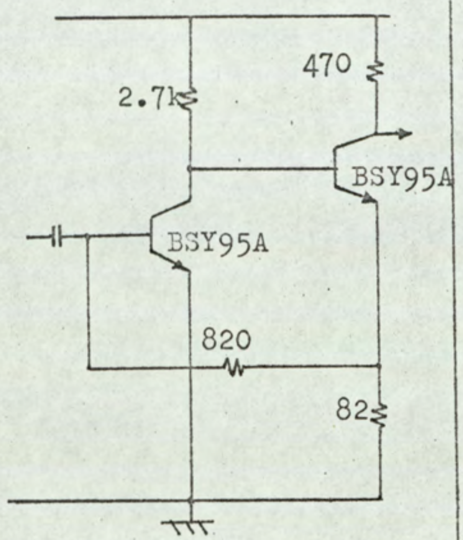

Stage 2

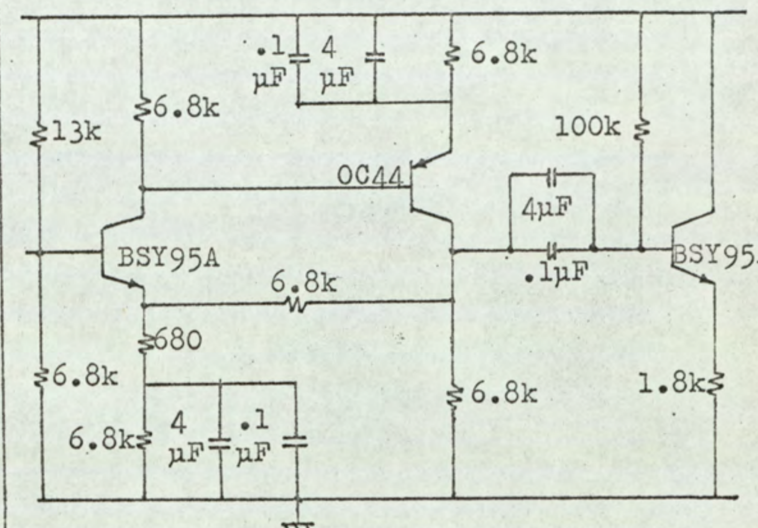

Stage 1

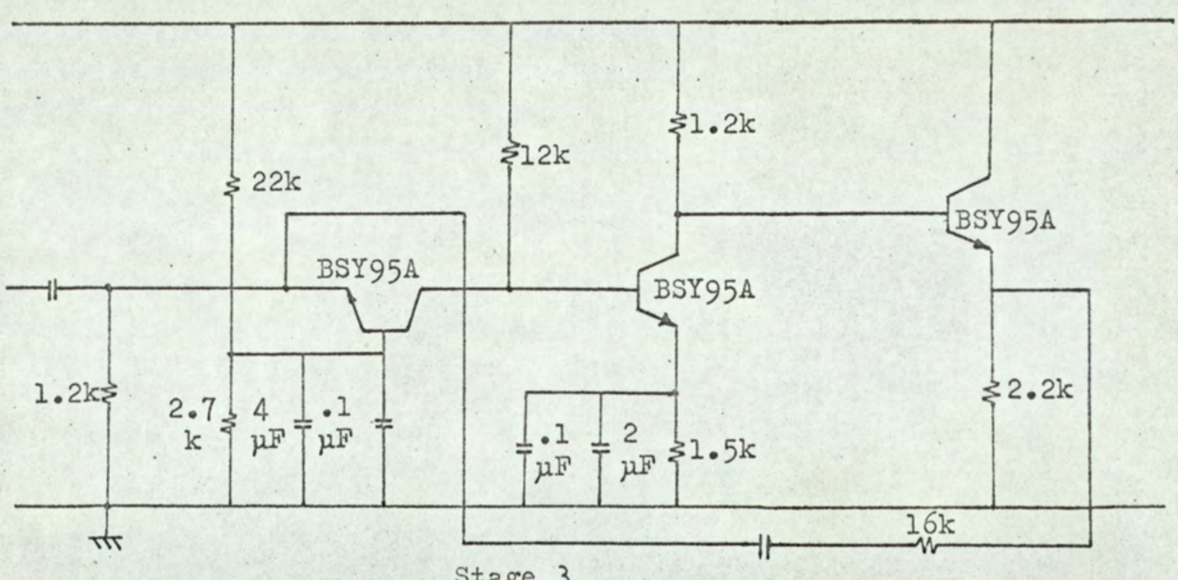

Stage 3

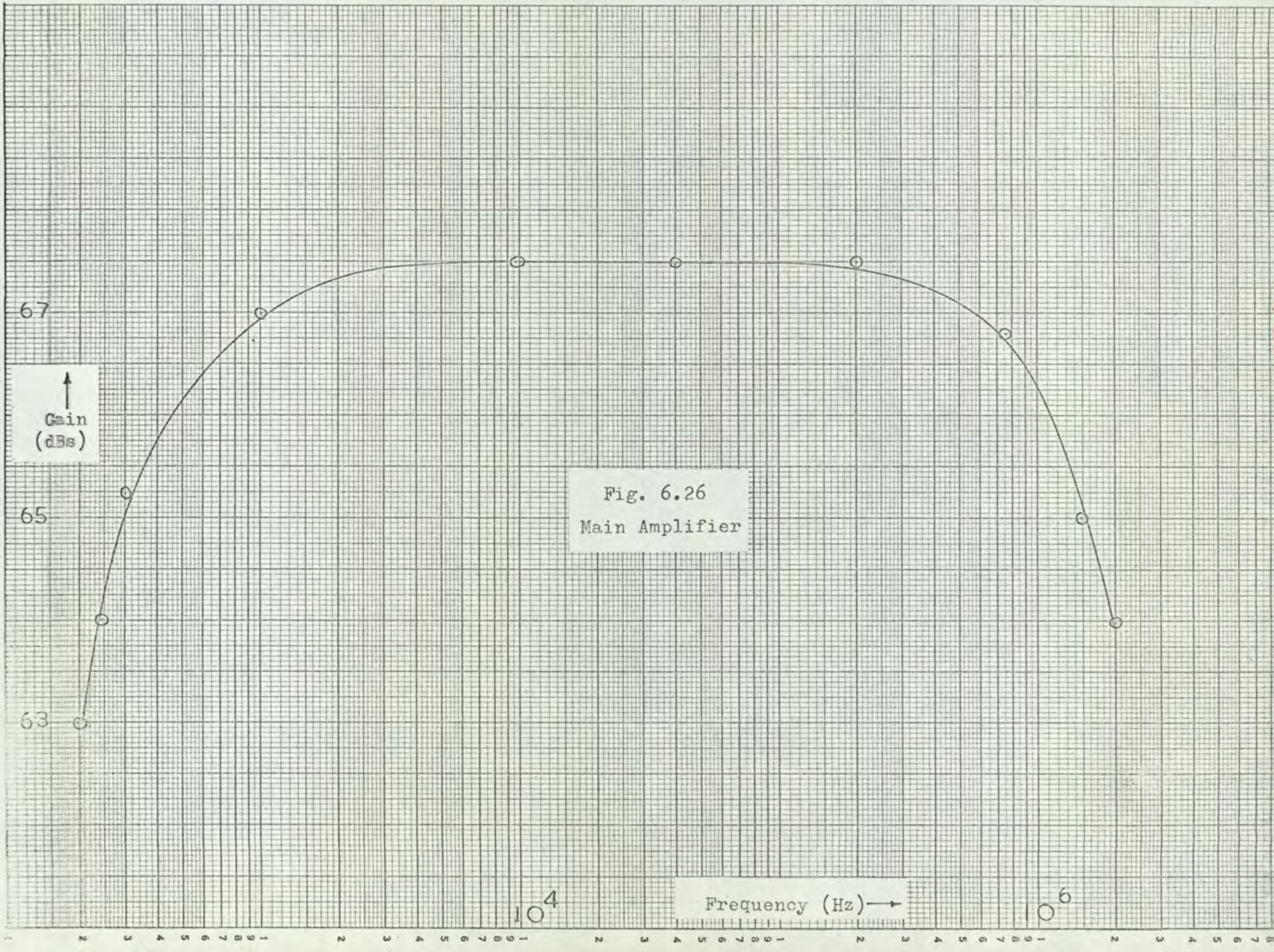

67
65
63
Gain (dBs)
Fig. 6.26
Main Amplifier
10^4
10^6
Frequency (Hz)

attenuators (Appendix 9). However, because it afforded a direct comparison with Hathaway's experiments and was known to be reliable, this was later replaced by the system shown in Fig. 6.27 which is the same as that used by Hathaway with the exception of the emitter follower. The latter served the dual functions of :

(i) Increasing the frequency to which the divider could be used without there being a phase difference between the signals going to the correlator and the amplifier: that is lowering the output impedance of the divider so that the phase change in the 50 ohm line to the correlator was negligible.

(ii) Increasing the degree of isolation between output and input (Appendix 8).

In the main, therefore, the experiments described here will refer to measurements made with the system of Fig. 6.27, although some experiments with the other divider were also carried out.

Basically the system of Fig. 6.27 has three constituent elements, viz:

(i) one ohm divider;

(ii) five dB attenuator;

(iii) signal source.

The one ohm divider was of the type described earlier (Sec. 5.4). The five dB attenuator had the form shown in

Fig. 6.27 Microvolt Divider

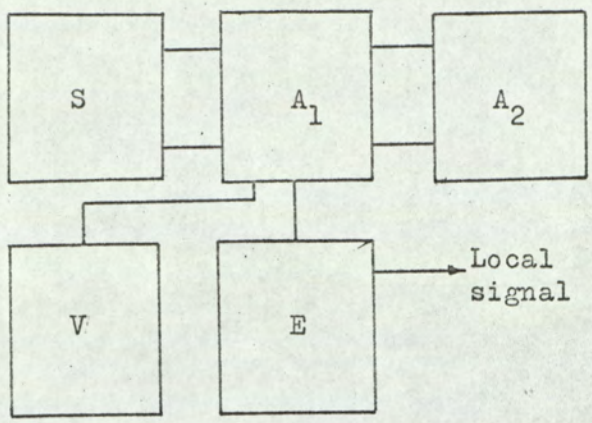

S Source A_1 5dB attenuator
A_2 1 ohm divider V Voltmeter
E Emitter follower

a. Schematic Diagram

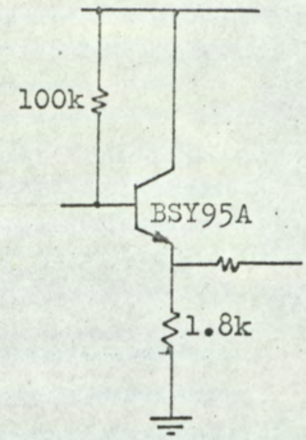

b. Emitter Follower

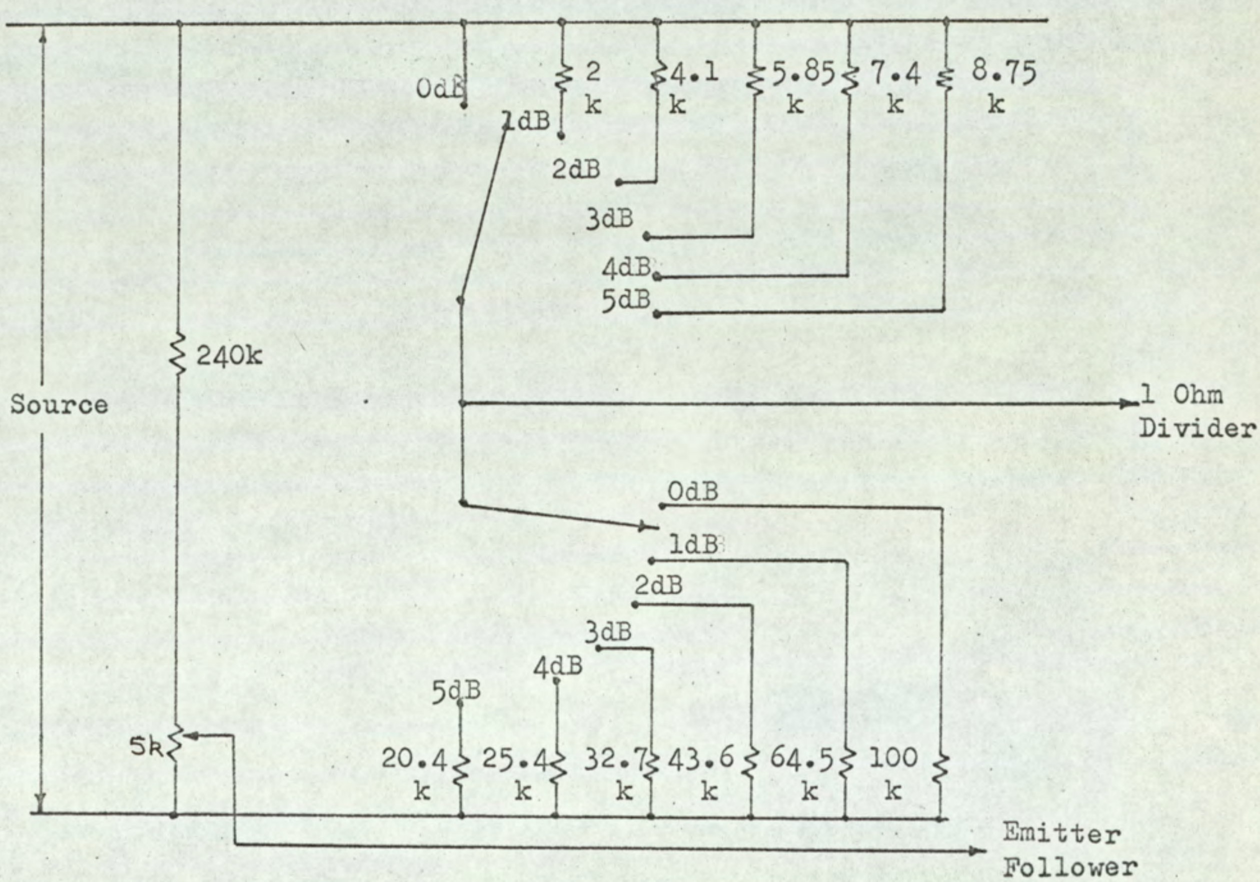

c. Emitter Follower

Fig. 6.27c and by attenuating the input voltage to the one ohm divider, gave 0-5 dBs in 1 dB steps. The signal source was either:

(i) H-1 Advance Signal Generator providing continuously variable 0-26V supply over the frequency range 15 Hz - 50 kHz.

or:

(ii) Airmec Oscillator type 304 which has a 50 ohm output impedance with a continously variable, and calibrated, output voltage of between 50μV and 5V over the frequency range 50 kHz - 100 MHz (although in actual fact practically all the measurements were made at frequencies < 500 kHz).

Depending on which of these sources was used the voltage to the 1 ohm divider, with the 5dB attenuator at zero setting, was set to 25V producing signals at the amplifier of 1μV, 2μV, 4μV etc. - or 3.125V - producing 0.125μV, etc. - the voltage being monitored by means of a Solartron Precision Voltmeter for frequencies < 100 kHz and a calibrated C.R.O. for frequencies above this range.

As a preliminary check on the accuracy of the divider an amplifier of known gain was placed at its output; then with varying voltages down to about 20μVthe amplifier output voltage was measured using a precision voltmeter. This voltmeter when converted into an equivalent amplifier input (divider output) voltage by dividing by the amplifier gain, therefore, provided a check on the divider's accuracy. As a result of these checks it was concluded that the divider could be relied upon to produce signals down to 20μV with an accuracy of the same order as that of the precision voltmeter (which was quoted as 1%).

6.9 Experimental Method Part 1 - Power Measurements

In the preceding section a method of checking the microvolt divider has been found to be very useful for voltages of 20μV and above. Unfortunately, however, when the amplifier input signal was reduced to values much below this level a similar check was impossible because of the presence at the output of noise from the amplifier. However, as was stated in the introduction the intention of the experiments is to test for loss of signal in the amplifier, and Hathaway's work has shown that this is unlikely to occur until the input voltage to the divider is of the order of 2μV. It is apparent, therefore, that before the microvolt divider may be used some indication of its accuracy when supplying these low voltages must be obtained. Furthermore, if the attenuators in the amplifier and the microvolt divider are to be used to maintain the output signal level constant, i.e. in the manner suggested by Hathaway, it is essential that a cross check on their accuracy be made. Accordingly, the power measurements described below were made.

However, before describing these power measurements consider the schematic diagram of Fig. 6.28 where e_s represents the microvolt divider, R_n the equivalent noise resistance of the amplifier A, and M a mean square voltmeter.

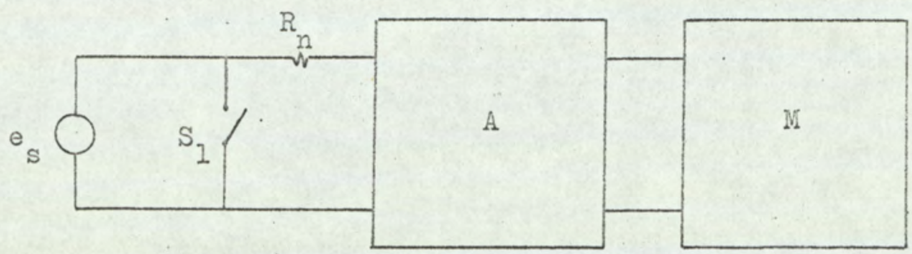

Fig. 6.28

From Chap. 4 the mean square voltmeter readings θ are given by

$$\theta_0 = 4kTR_n \int_0^\infty G_0^2 |F(w)|^2 df \text{ with } S_1 \text{ closed}$$

$$\theta_1 = \theta_0 + G_0^2 \int_0^\infty |F(w)|^2 |e_s^2| \delta(f-f_s)\, df \quad \text{with } S_1 \text{ open}$$

$$= \theta_0 + \theta_s$$

where G_0 is the mid-band gain of the amplifier.

Now suppose that the amplifier gain is linearly increased by a factor N while at the same time the signal level is linearly reduced by the same factor, then

$$\theta_1 = N^2\theta_0 + \theta_s$$

and plots of $N^2\theta_0 - \theta_1$ (noise power - total power) and -

$N^2\theta_0 - N^2\theta_0$ will take the form shown in Fig. 6.29 where the vertical displacement between the curves is a constant representing the signal power $<e_s^2>$. However, if the

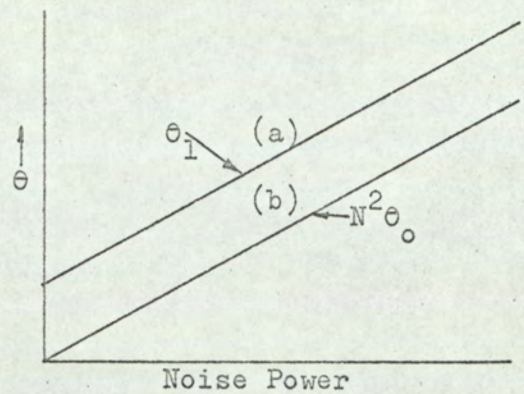

Fig. 6.29

changes in the input signal power do not agree with those of the amplifier or if some signal is lost due to leakage from a connecting lead - or gained via an earth loop - the linear form of Fig. 6.29a will no longer apply nor will it be separated from 6.29b by a constant displacement. Therefore, a useful test of the existence of leakage and other unwanted effects, and of the errors that these could lead to, is to carry out the steps indicated above.

It is obvious, however, that in making a test of this kind that it be made under conditions which are as near as possible the same as those under which the correlation measurements are made, otherwise the apparatus or layout of leads responsible for the loss of, or gain of, signal may be unwittingly removed. Accordingly, the system shown in Fig. 6.30 was set up where the mean square voltmeter was

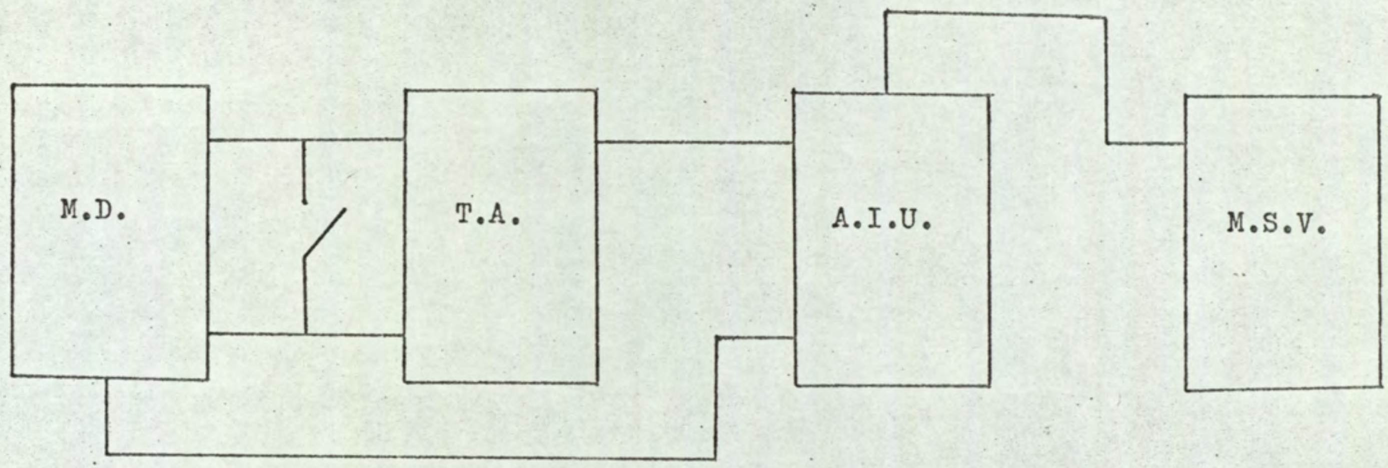

M.D. Microvolt Divider   T.A. Test Amplifier   A.I.U. Adder and Inverter Unit
M.S.V. Mean Square Voltmeter

<u>Fig. 6.30</u>

connected - depending on whether correlator 1 or 2 was being used - so as to give a measure of:

(i) The power from the amplifier to the adder unit of correlator 1.

(ii) The power output of the first inversion stage of correlator 2.

Other tests of a similar nature were also tried in which the local signal was removed and the mean square voltmeter was connected in the manner of Fig. 6.7, i.e. as to give a crosscorrelation. In the main, however, the power measurements were made with the system as described above.

With regard to these power measurements the experimental procedure was as follows:

With an amplifier gain G_o and input signal of $128\mu V$ two mean square voltmeter readings were taken; the first with the amplifier shorting switch closed and the second with it open (corresponding to θ_o and $\theta_o + \theta_s$ respectively). The same two readings were then taken for signal voltages of $64\mu V$, $32\mu V$ etc. with corresponding amplifier gains of $2G_o$, $4G_o$ etc.; i.e. the signal was decreased in 6 dB steps and the amplifier gain increased by a similar amount.

As a result of these measurements graphs of the form shown in Figs. 6.31 - 6.3.4 were obtained. These illustrate measurements made on:

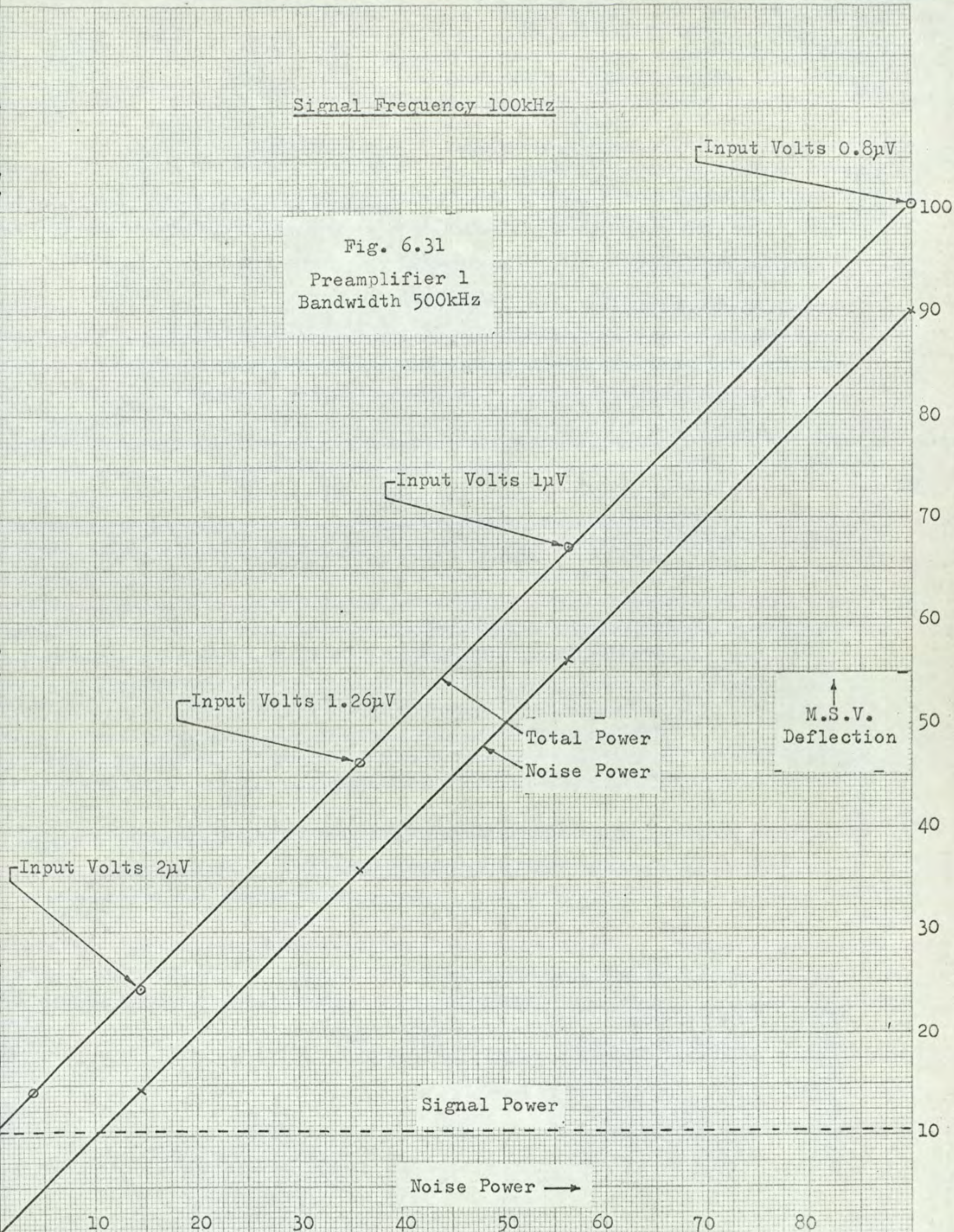
Signal Frequency 100kHz
Fig. 6.31
Preamplifier 1
Bandwidth 500kHz
Input Volts 0.8µV
Input Volts 1µV
Input Volts 1.26µV
Input Volts 2µV
Total Power
Noise Power
M.S.V.
Deflection
Signal Power
Noise Power
10
20
30
40
50
60
70
80
90
100

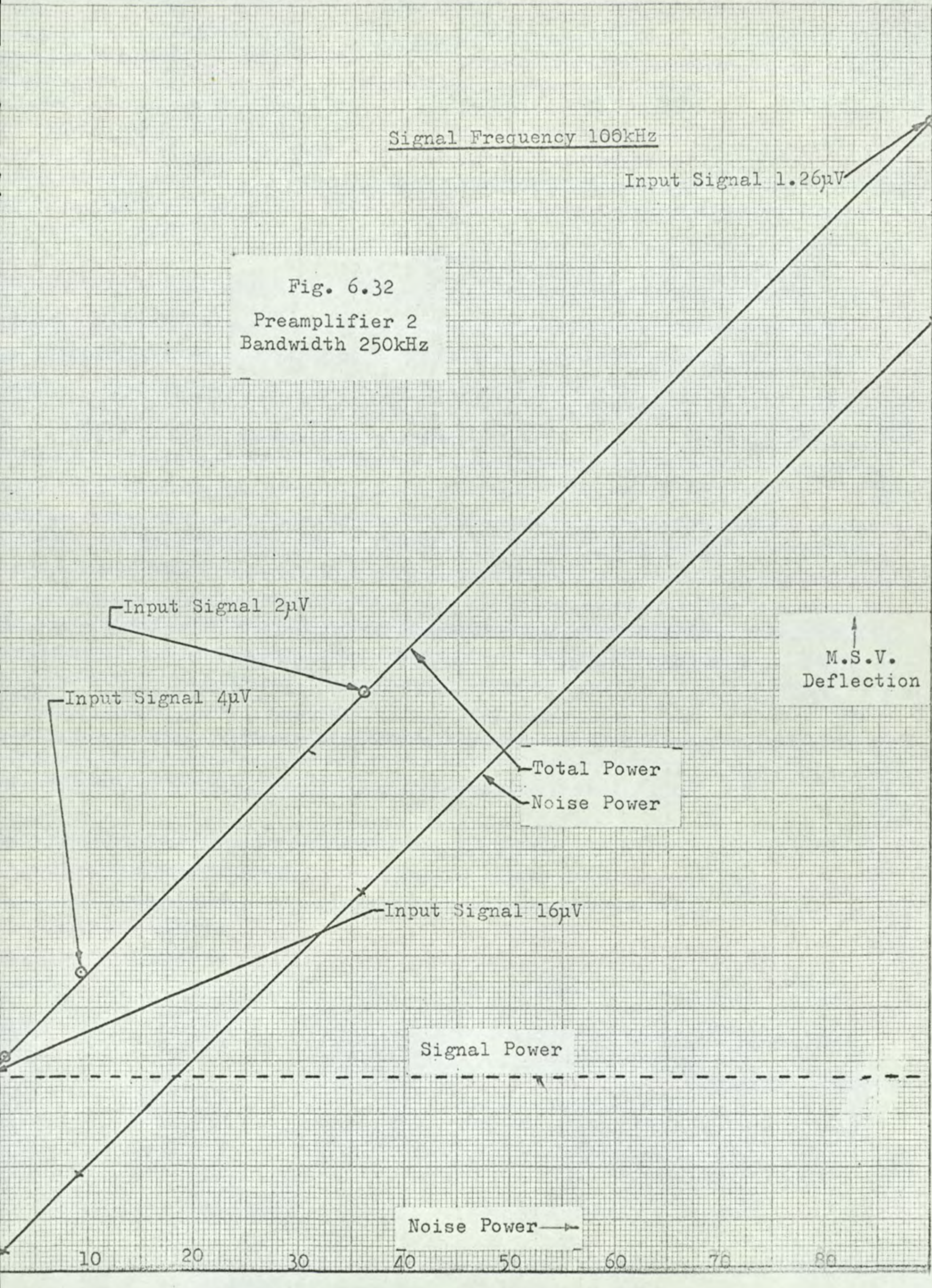
Signal Frequency 106kHz
Input Signal 1.26μV
Fig. 6.32
Preamplifier 2
Bandwidth 250kHz
Input Signal 2μV
Input Signal 4μV
Total Power
Noise Power
Input Signal 16μV
M.S.V.
Deflection
Signal Power
Noise Power
10
20
30
40
50
60
70
80
90
100

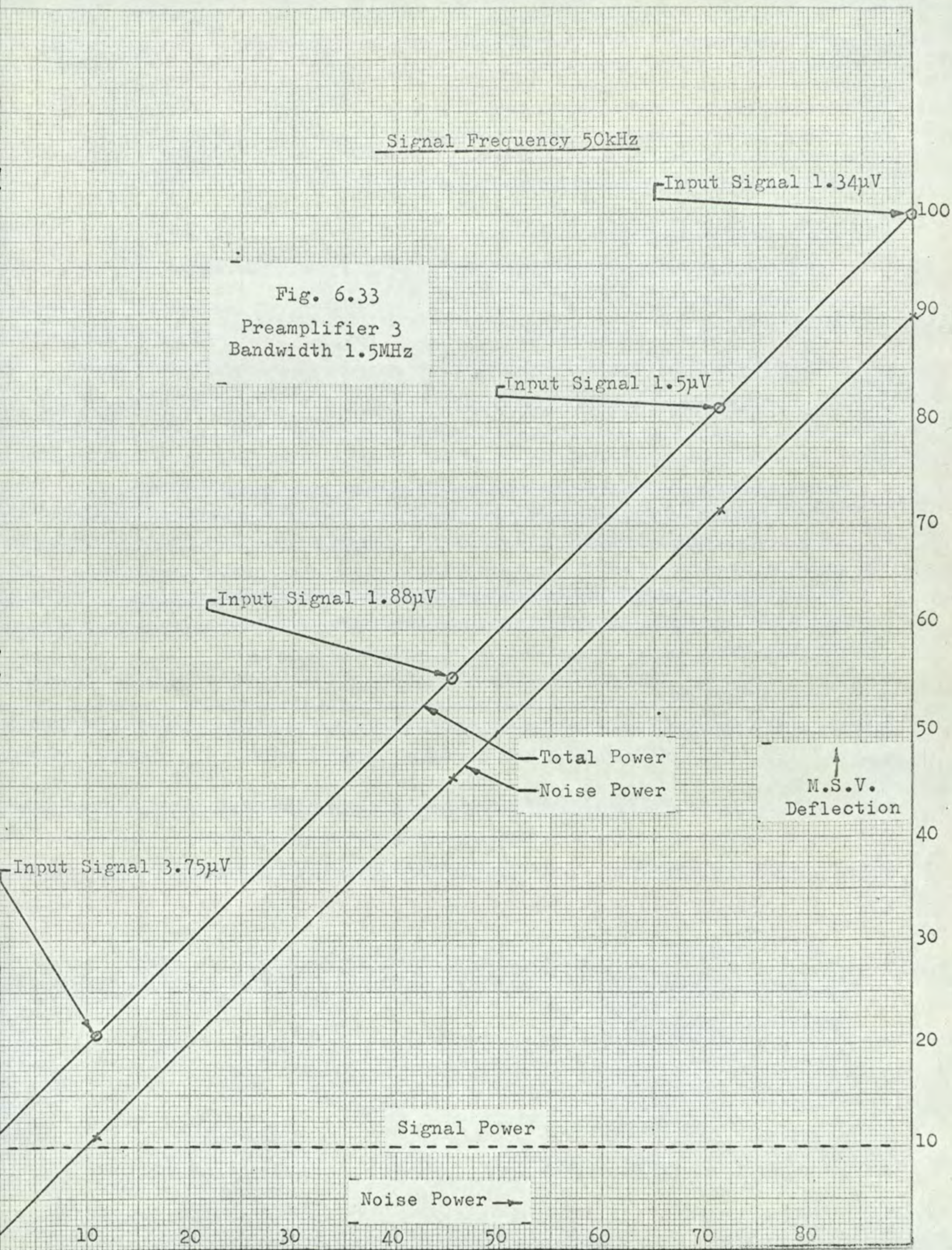
Signal Frequency 50kHz
Fig. 6.33
Preamplifier 3
Bandwidth 1.5MHz
Input Signal 1.34µV
Input Signal 1.5µV
Input Signal 1.88µV
Input Signal 3.75µV
Total Power
Noise Power
M.S.V.
Deflection
Signal Power
Noise Power
10
20
30
40
50
60
70
80
90
100

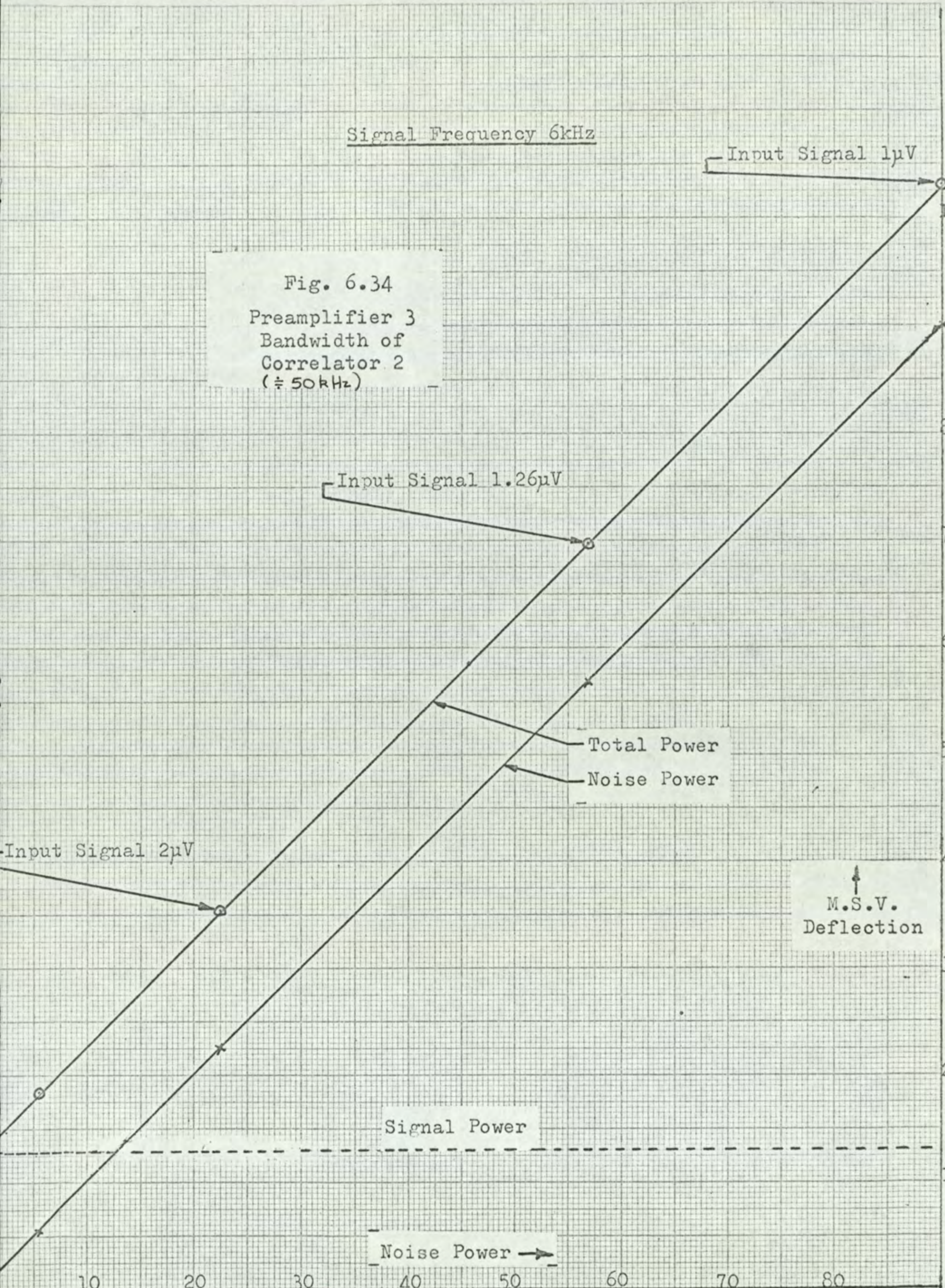

Signal Frequency 6kHz
Input Signal 1µV
Fig. 6.34
Preamplifier 3
Bandwidth of
Correlator 2
(÷ 50kHz)
Input Signal 1.26µV
Total Power
Noise Power
Input Signal 2µV
M.S.V.
Deflection
Signal Power
Noise Power
10
20
30
40
50
60
70
80
90
100

(i) Correlator 1, preamplifier 1, bandwidth $\doteqdot$ 500 kHz (Fig. 6.31).

(ii) Correlator 1, preamplifier 2, bandwidth $\doteqdot$ 250 kHz (Fig. 6.32).

(iii) Correlator 1, preamplifier 3, bandwidth $\doteqdot$ 1.5 MHz (Fig. 6.33).

(iv) Correlator 2, preamplifier 3, bandwidth limited by correlator (Fig. 6.34).

from which it can be seen that they are of the same form as Fig. 6.29, i.e. loss or gain of signal is negligible, even at the smallest levels used.

Although these measurements have been described in such a manner that it may be inferred they were a preliminary to the correlation measurements, in fact, such measurements were never made unless accompanied by a test of the type described above. In this way the influence of leakage effects on the accuracy of the correlation measurements was reduced to a minimum.

6.10 Experimental Measurement Part 2 - Correlation Measurements

The experimental arrangement is as shown in Fig. 6.6. When a correlator 1 was being used measurements were made on each of the three preamplifiers thus enabling a comparison to be made between low, medium and high noise devices. Further checks were then made by altering the amplifier bandwidth so as to discern if altering the signal/noise ratio in this way altered the results obtained. With correlator 2, on the other hand, measurements were made with preamplifier 3 only. Since this amplifier had the same input stage as Hathaway's and the correlator and microvolt divider were approximately the same this last experiment corresponded to a repetition of Hathaway's measurements using, as far as was possible at the time, his original apparatus.

Taking each of the systems in turn the procedure described in Sec. 6.3, i.e. keeping output signal level constant, was followed. The crosscorrelation between a noisy and a "clean" local signal and, as a further check on the equipment, between the local signal and the noise - when it should be zero - was found. The measurements were effected down to input voltages of the order of 1μV for a large variety of values of local signal and a wide range of frequencies (5kHz - 500kHz).

In the case of the tests with correlator 2 some photographs of the output waveforms were obtained. These photographs were taken for both multi and single exposure, corresponding to the C.R.O. being triggered continuously (the exposure being made for several seconds) and being triggered once.

6.11 Results

With correlator 1 a large number of tests were made using a variety of bandwidths and with minor modifications to the system as described. In once such modification the correlator was interposed between the attenuator and stage

2 of the main amplifier (Fig. 6.25), in the hope that the change of position would manifest any earth loops or non-linearities that were present when it was at the amplifier output.

In all these tests, however, the results were the same. Typically they took the form shown in Fig. 6.35, i.e., the value of $R_{xy}(0)$ remained constant irrespective of the signal/noise ratio. It must be added, however, that on a few occasions there was a small reduction (approximately 4%) in the level of $R_{xy}(0)$ as the signal/noise ratio decreased but this could have been due to experimental errors, e.g. drift of voltmeter zero. At no time, however, was the value of $R_{xy}(0)$ observed to increase above the value pertaining to the region where the signal /noise ratio was high, i.e. $R_{xy}(0) = 100\%$.

It was because of the differences between these results and Hathaway's that correlator 2 was developed. However, with this correlator also, the results were the same as in Fig. 6.35, i.e. crosscorrelation remained constant.

Finally, the photographs of the output waveforms are shown inFig.s 6.36(i) - 6.36(xii). Each pair of photographs represents records taken with the same amplifier gain and C.R.O. sensitivity. In the case of the records with odd numbers, these represent the appearance of a small signal which is amplified to

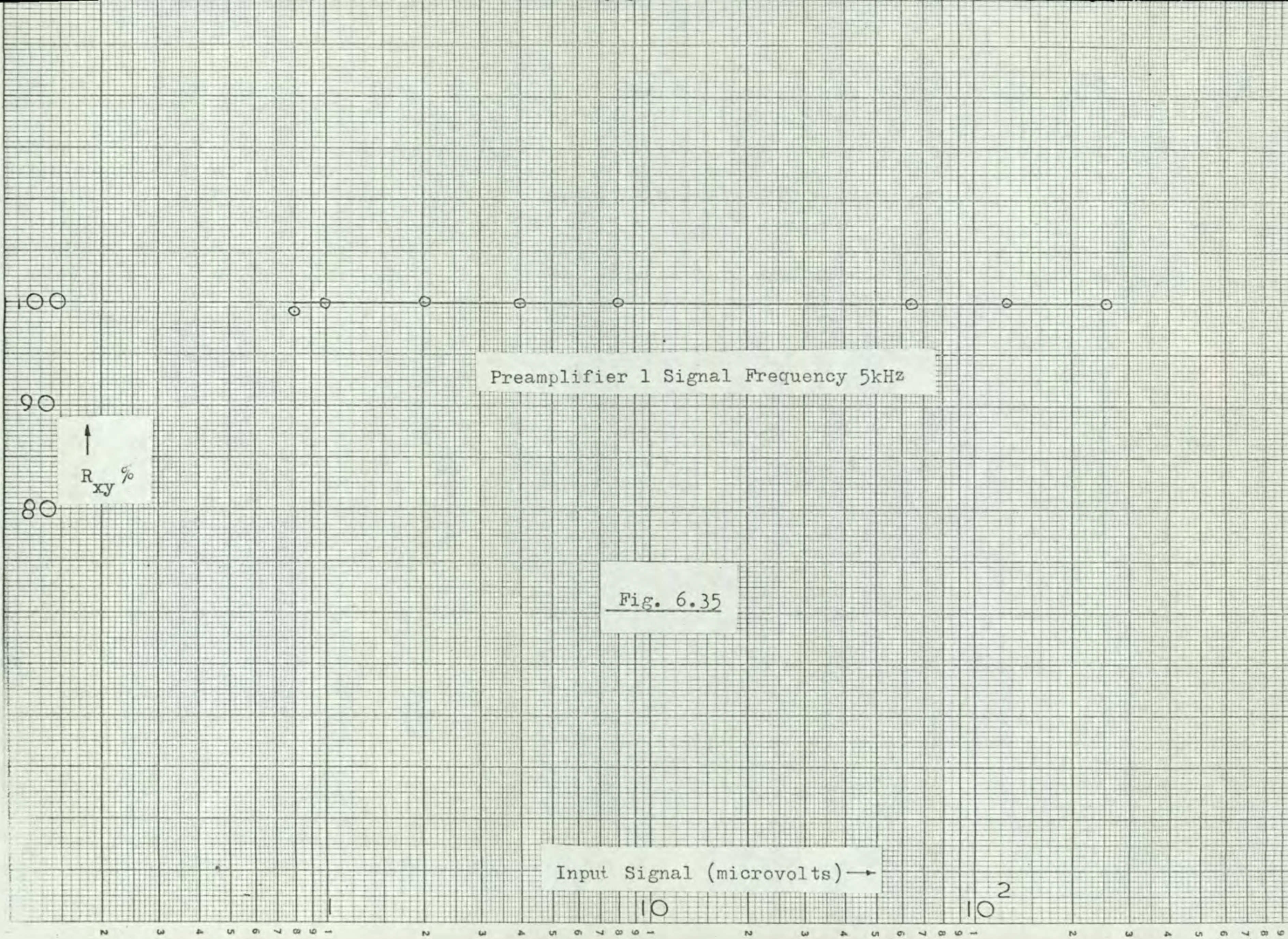
100
90
80
R_{xy} %
Preamplifier 1 Signal Frequency 5kHz
Input Signal (microvolts)
1
10
10^2
Fig. 6.35

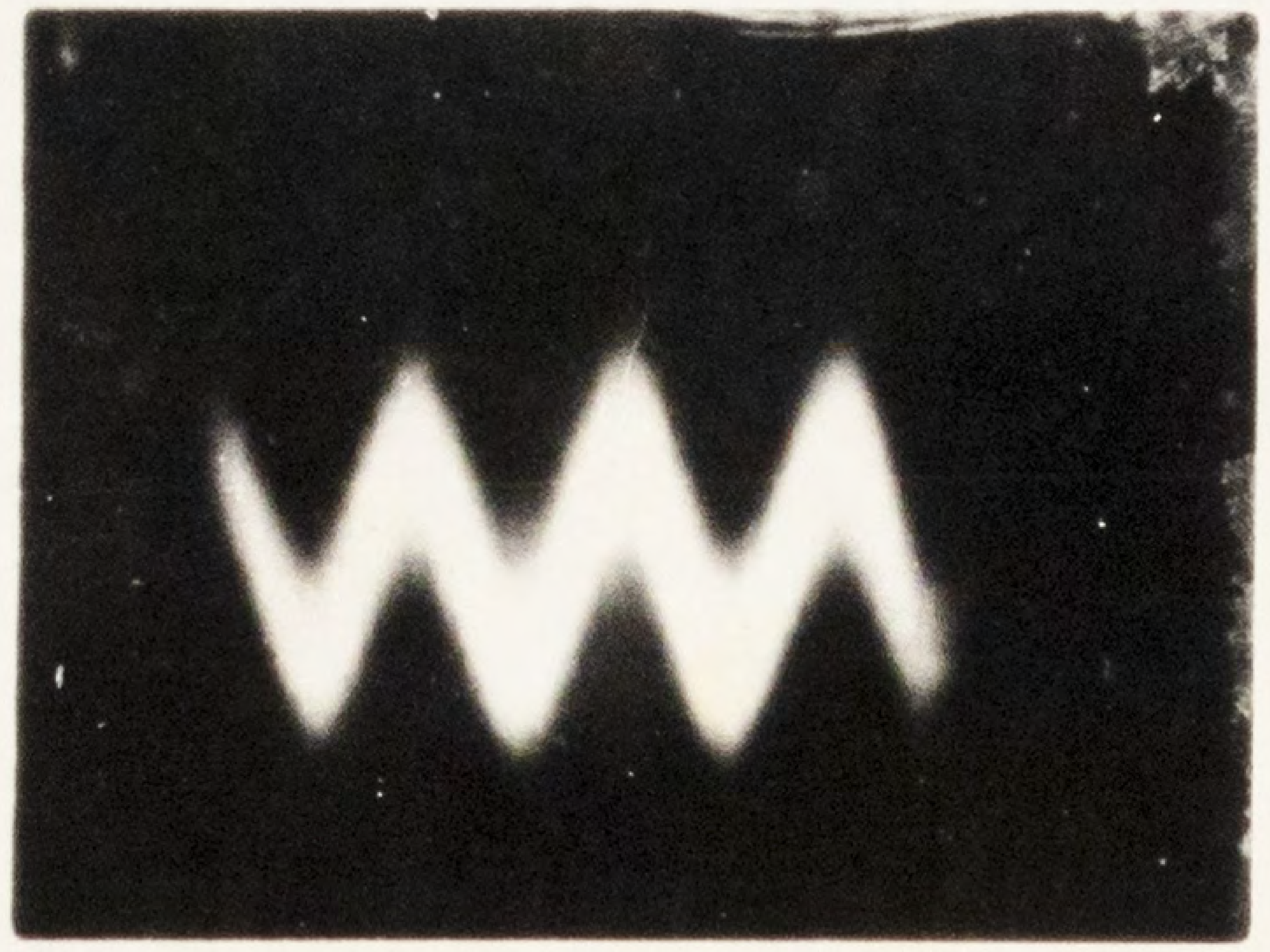

(i) Amplified Signal

Input Signal = 4μV
Output Signal = 53mV

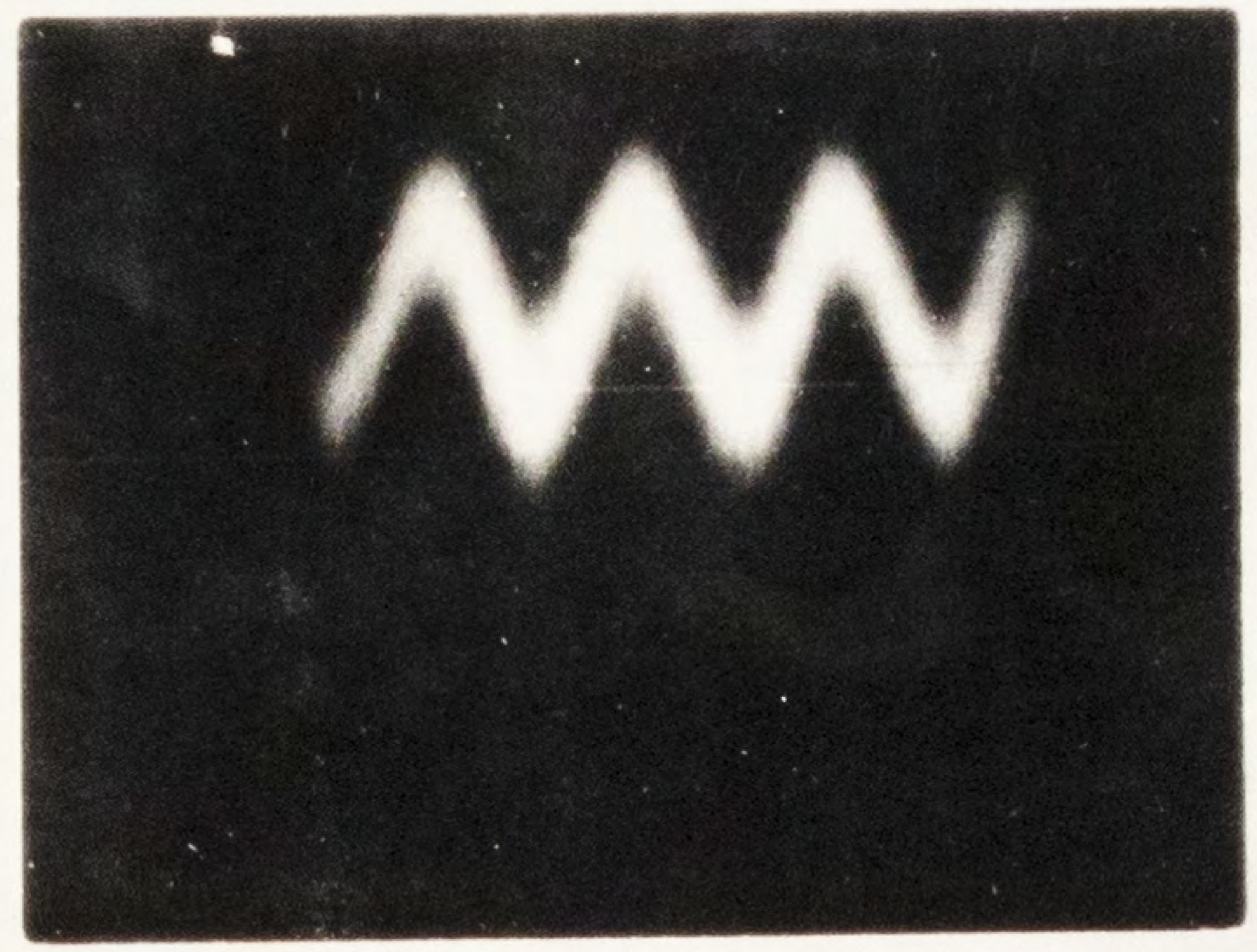

(ii) Signal and Noise Added

Local Signal = 53mV

Fig. 6.36

(iii) Amplified Signal

Input Signal = 2μV
Output Signal = 53mV

(iv) Signal and Noise Added

Local Signal = 53mV

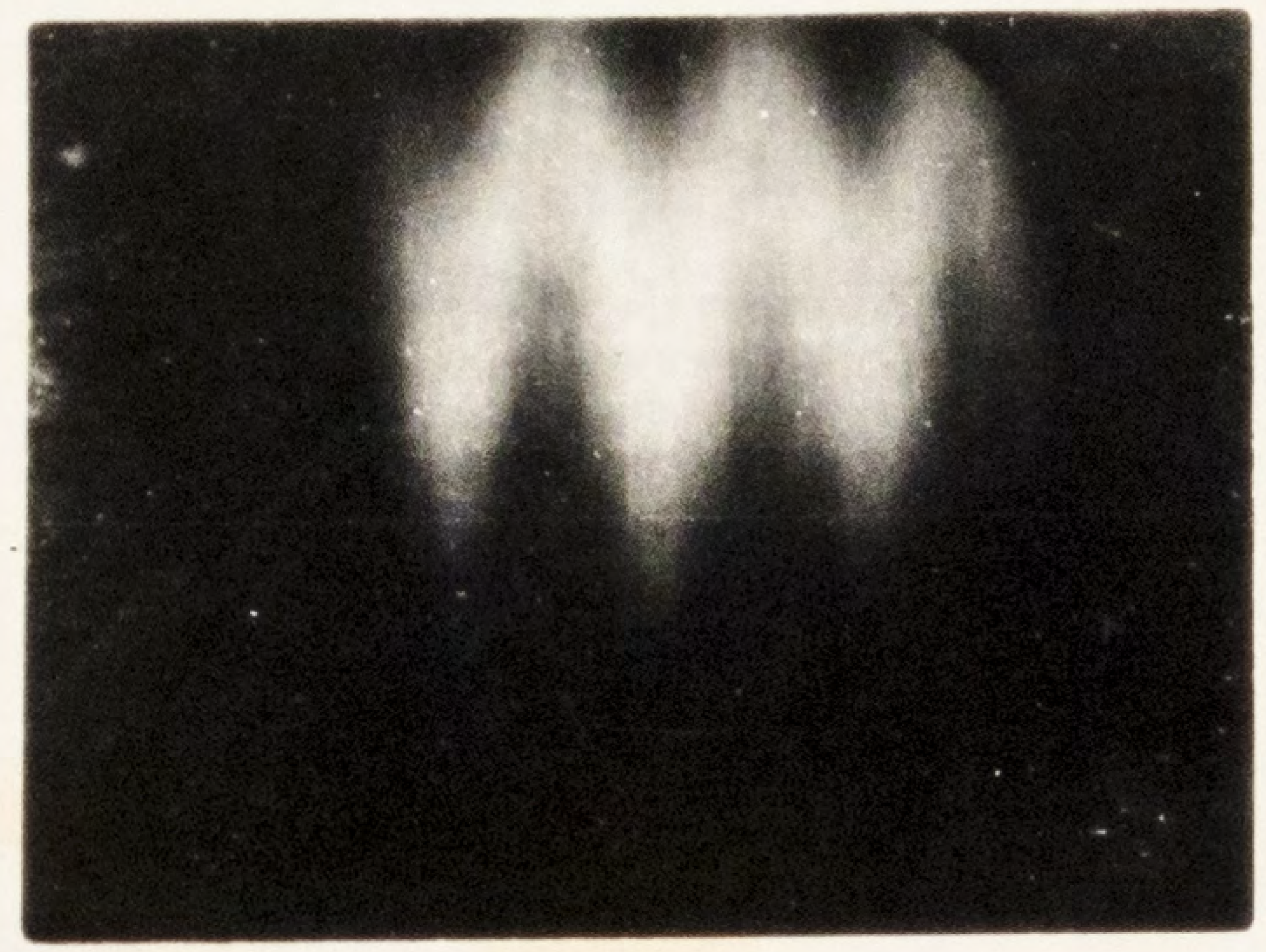

(v) Amplified Signal

Input Signal = 1.26μV
Output Signal = 53mV

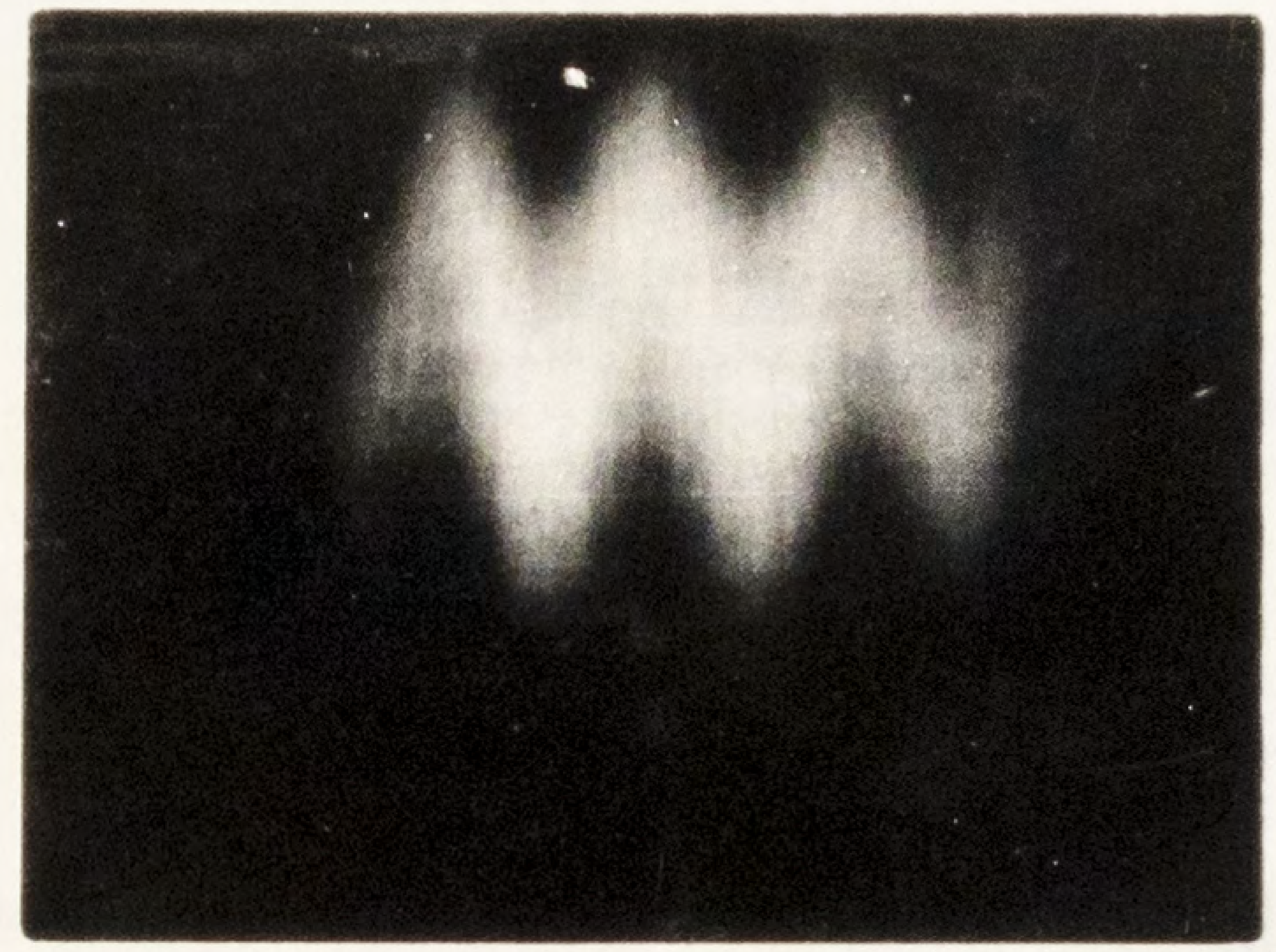

(vi) Signal and Noise Added

Local Signal = 53mV

(vii) Amplified Signal

Input Signal = 1.58μV
Output Signal = 53mV

(viii) Signal and Noise Added

Local Signal = 53mV

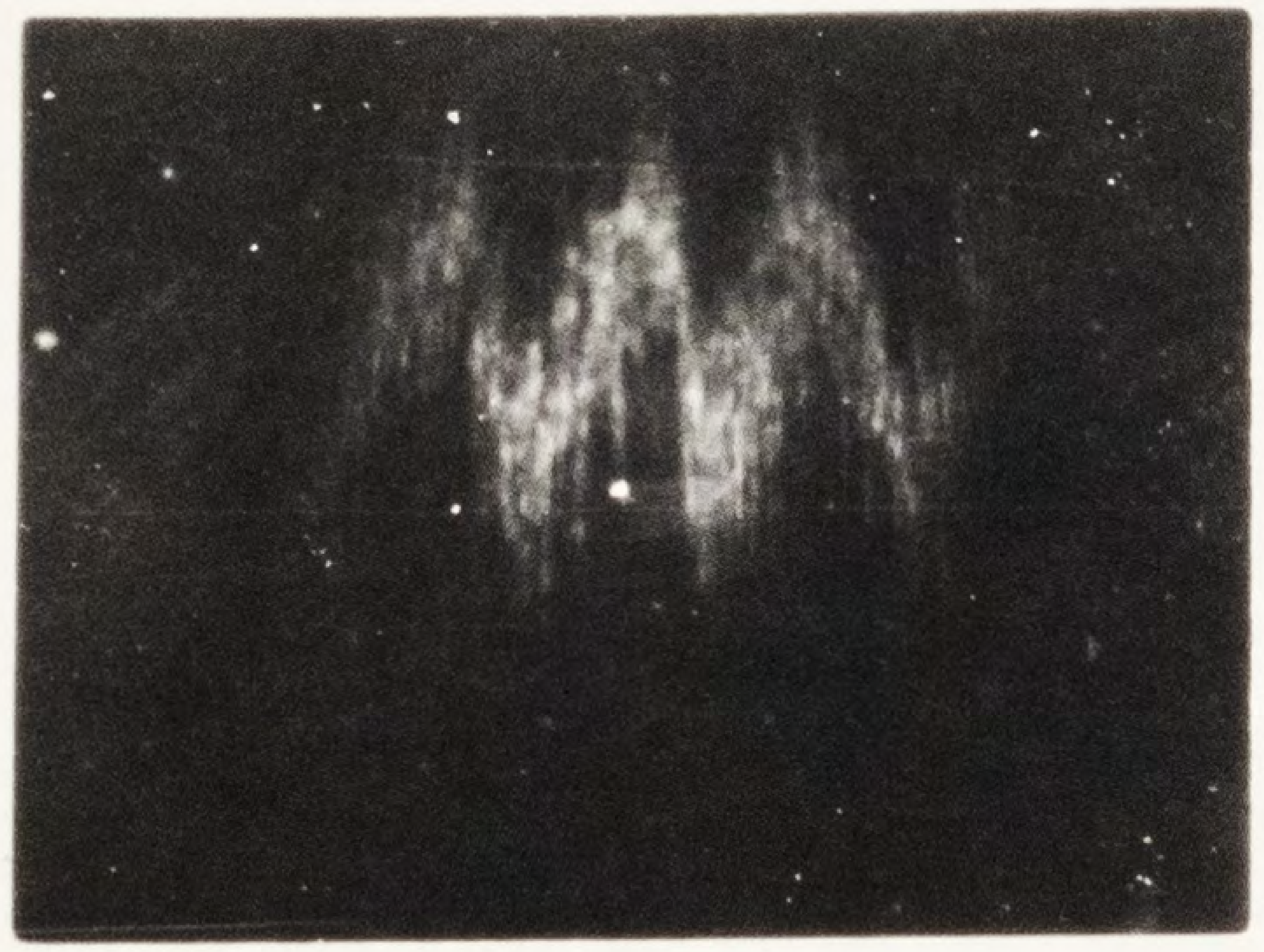

(ix) Amplified Signal

Input Signal = 2μV
Output Signal = 60mV

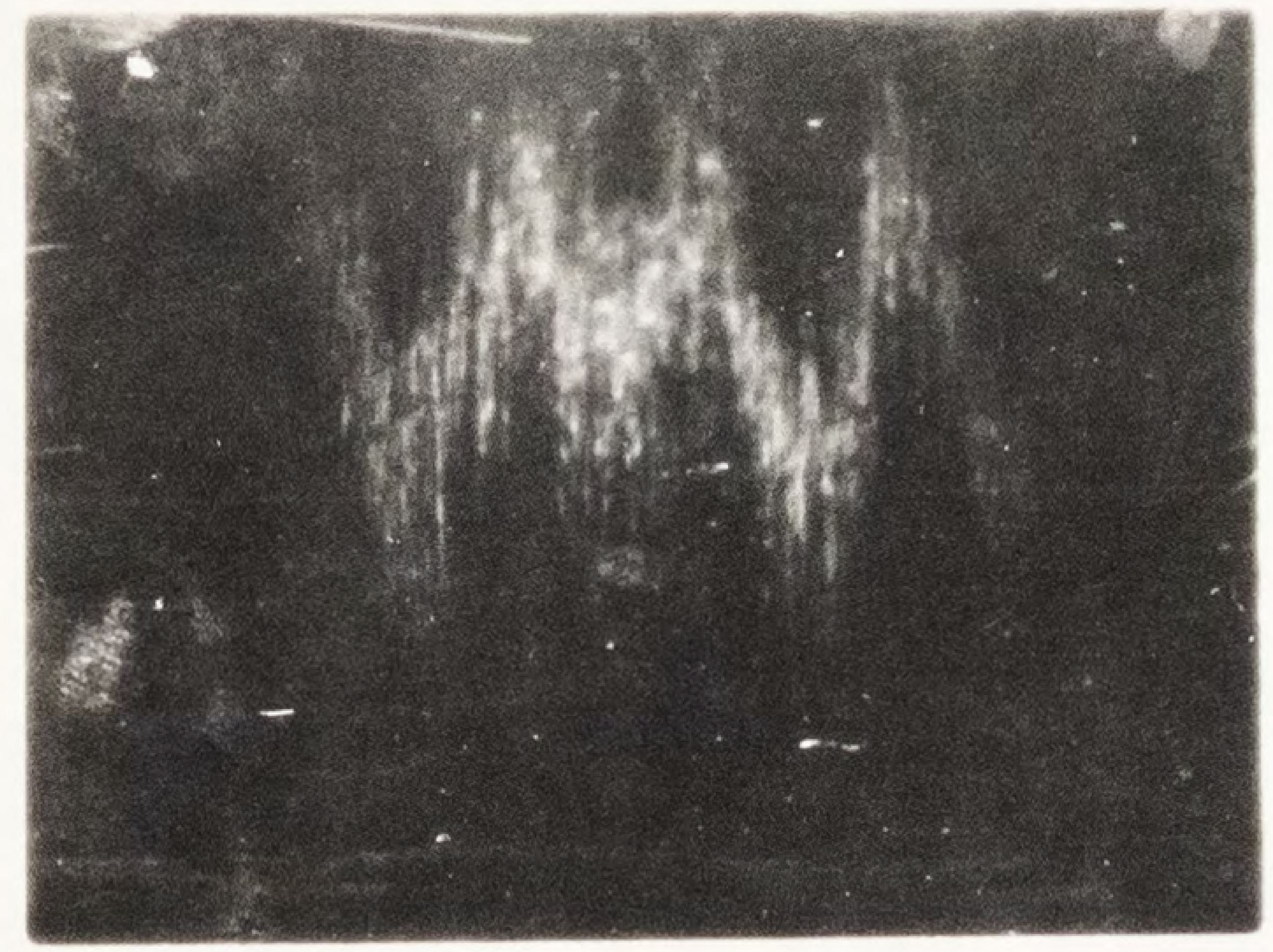

(x) Signal and Noise Added

Local Signal = 60mV

(xi) Amplified Signal

Input Signal = 1.26μV
Output Signal = 60mV

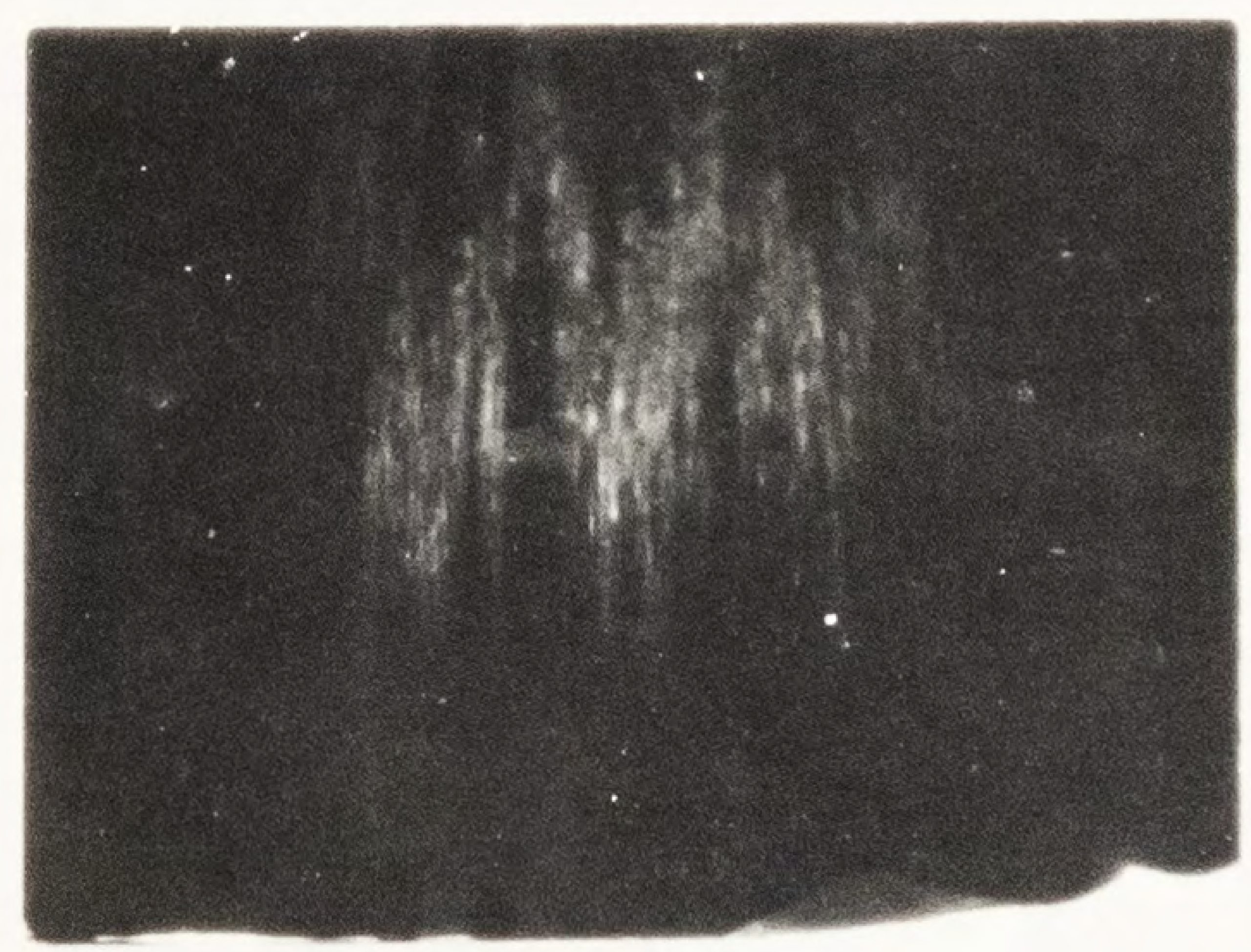

(xii) Signal and Noise Added

Local Signal = 60mV

N mV and photographed at the output of the first inversion stage of the amplifier. The even number records, on the other hand, were photographed at the $(x + y)$ terminal of the correlator when the amplifier was short circuited and the local signal set to N mV, i.e. represent the addition of signal and noise.

In some of these photographic records it will be observed that the traces are distorted. This was a property of the C.R.O. and was in no way due to non-linearities in the measuring equipment.

6.12 Discussion of Results

The correlation measurements indicate that there are large discrepancies between the results reported here and those obtained by Hathaway. From the power measurements it seems unlikely that these differences can be explained in terms of errors due to the pick up of unwanted signal otherwise the signal power would not have remained constant. In addition a comparison of the photographic records, (i) and (ii), (iii) and (iv) etc. - corresponding to the records of amplified signals and the addition of signals and noise - appear the same, which would seem to indicate that there is not a conversion of signal power to noise power in the amnner described by Hathaway.

On the other hand on a few occasions the correlation was observed to fall slightly for small signals. Furthermore, Hathaway's results have been shown, at least possibly, to have some theoretical basis.

In view, therefore, of this disagreement between the two sets of experiments it was decided that further checks were ncessary. However, because the crosscorrelation method had been tried exhaustively without giving a positive indication as to the reasons for the disagreemnt it was further decided to pursue the investigation using a different approach. Consequently, the autocorrelation measurements described in the next chapter were carried out.

7. AUTOCORRELATION MEASUREMENTS

With the intention of checking the validity of the crosscorrelation measurements two experiments using autocorrelation techniques were carried out. The experiments corresponded to :

(i) autocorrelation measurement with long time delay;

(ii) autocorrelation measurement with zero time delay, i.e. power measurement;

and will be described in detail below.

7.1 Long Delay Measurement

7.1.1 Theory of the Method

Consider a process, $x(t)$ consisting of an additive mixture of a deterministic $S(t)$ and random, $N(t)$, component, i.e.

$$x(t) = S(t) + N(t)$$

From Eq. (2.1) the associated autocorrelation function is

$$R_x(\tau) = \langle (S(t) + N(t))(S(t+\tau) + N(t+\tau)) \rangle$$

the brackets $\langle \quad \rangle$ signifying a time average, which simplifies to

$$R_x(\tau) = R_s(\tau) + R_n(\tau) \tag{7.1}$$

when $S(t)$ and $N(t)$ are statistically independent with mean values zero.

With reference to the second of these terms, $R_n(\tau)$, it can be shown that this vanishes when τ is large. To illustrate this consider a system, which approximates to that used in the measurements, with a frequency response given by:

$$W_y(f) = G \quad 0<f<f_o$$
$$W_y(f) = G \frac{f_o}{f} \; f_o<f<\infty \tag{7.2}$$

If a noise waveform having a white noise spectrum, say W_o, is passed through this sytem then the output autocorrelation function $R_n(\tau)$, as defined by Eq. (2.4), is given by

$$R_n(\tau) = W_o \int_0^{f_o} G \cos 2\pi f\tau df + W_o \int_{f_o}^{\infty} G \frac{f_o}{f} \cos 2\pi f\tau df \tag{7.3}$$

Of these two terms the first say $(R_n(\tau))_1$, represents the condition that the measuring system is a perfect low pass filter with infinitely sharp cut off; $(R_n(\tau))_1$ is then given by (Appendix 10)

$$(R_n(\tau))_1 = GW_o f_o \frac{\sin 2\pi f_o\tau}{2\pi f_o\tau} \tag{7.4}$$

The second term, on the other hand, say $(R_n(\tau))_2$, takes into account that the decrease in gain of the system is not infinitely sharp, but gradual, and that this decrease is of the order of 6 dBs/octave.

The values of $(R_n(\tau))_1$ and $(R_n(\tau))_2$ are shown in graphical form in Fig. 7.1 and in tabulated form in Appendices 10 and 11 from which it can be seen that they both decrease

Fig. 7.1 Autocorrelation Function of Noise

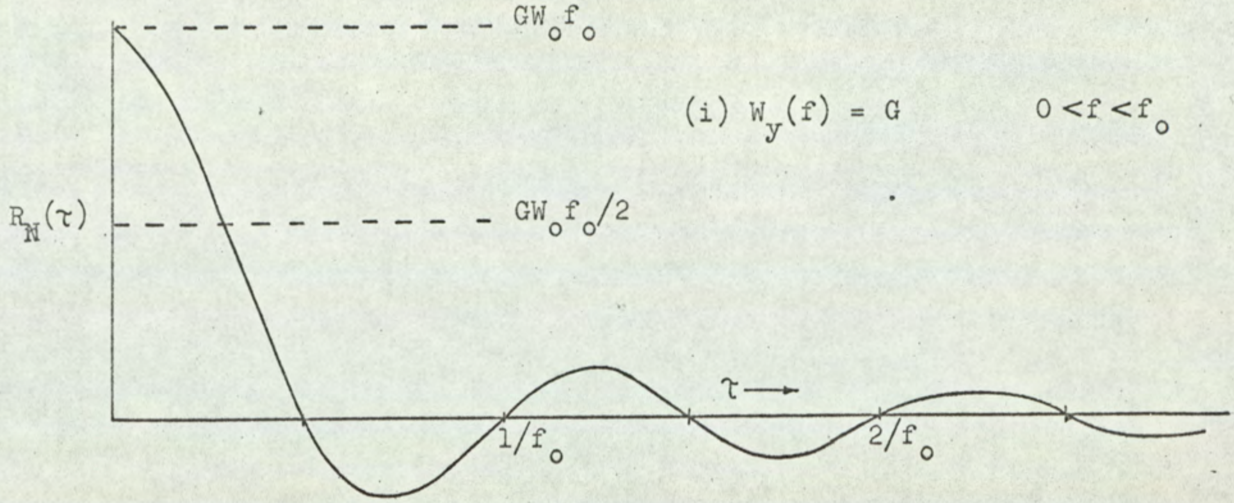

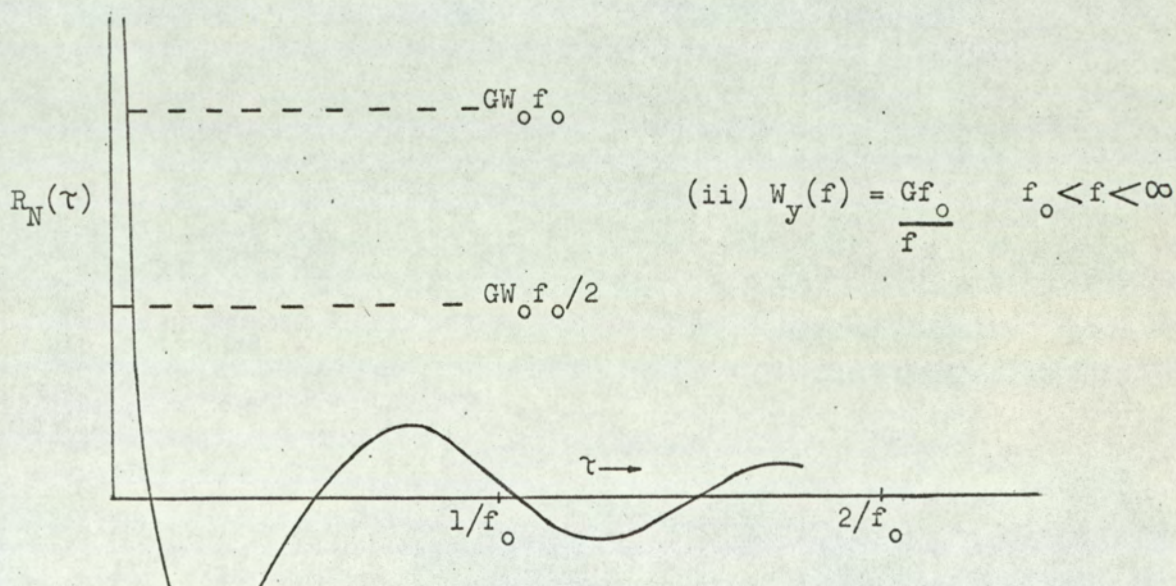

to zero when $f_o\tau$ is large, i.e. for large τ the noise is uncorrelated and $R_n(\tau)$ in Eq. (7.1) is zero (as it is for any system where τ is large).

Thus, since the measuring system used in the experiments had a frequency response of the type described by Eq. (7.2) it would be expected that the output autocorrelation for large τ would be equal to the signal autocorrelation function - $R_s(\tau)$ in Eq. (7.1) - which, in turn, is proportional to the signal power (Appendix 12). It follows, therefore, that if the procedure employed in the crosscorrelation measurements is adopted, i.e. the output signal level for varying input signals is maintained constant, but instead of a crosscorrelation an autocorrelation with a long time delay is made, then depending on whether or not there is a conversion of signal power to noise power the magnitude of the output autocorrelation function $R_x(\tau)$ will fall or remain constant as the noise/signal ratio increases. Hence, the validity of the crosscorrelation measurements may be checked.

7.1.2 Equipment

The experimental arrangement is shown in Fig. 7.2. It comprised:

(i) a low frequency microvolt divider (M.D.) the circuit diagram of which is given in Fig. 6.27;

(ii) a high gain amplifier H.G.A. having the same circuit as amplifier 3 of Sec. 6.7;

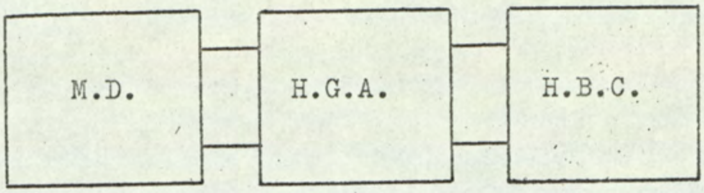

Fig. 7.2 Schematic Diagram

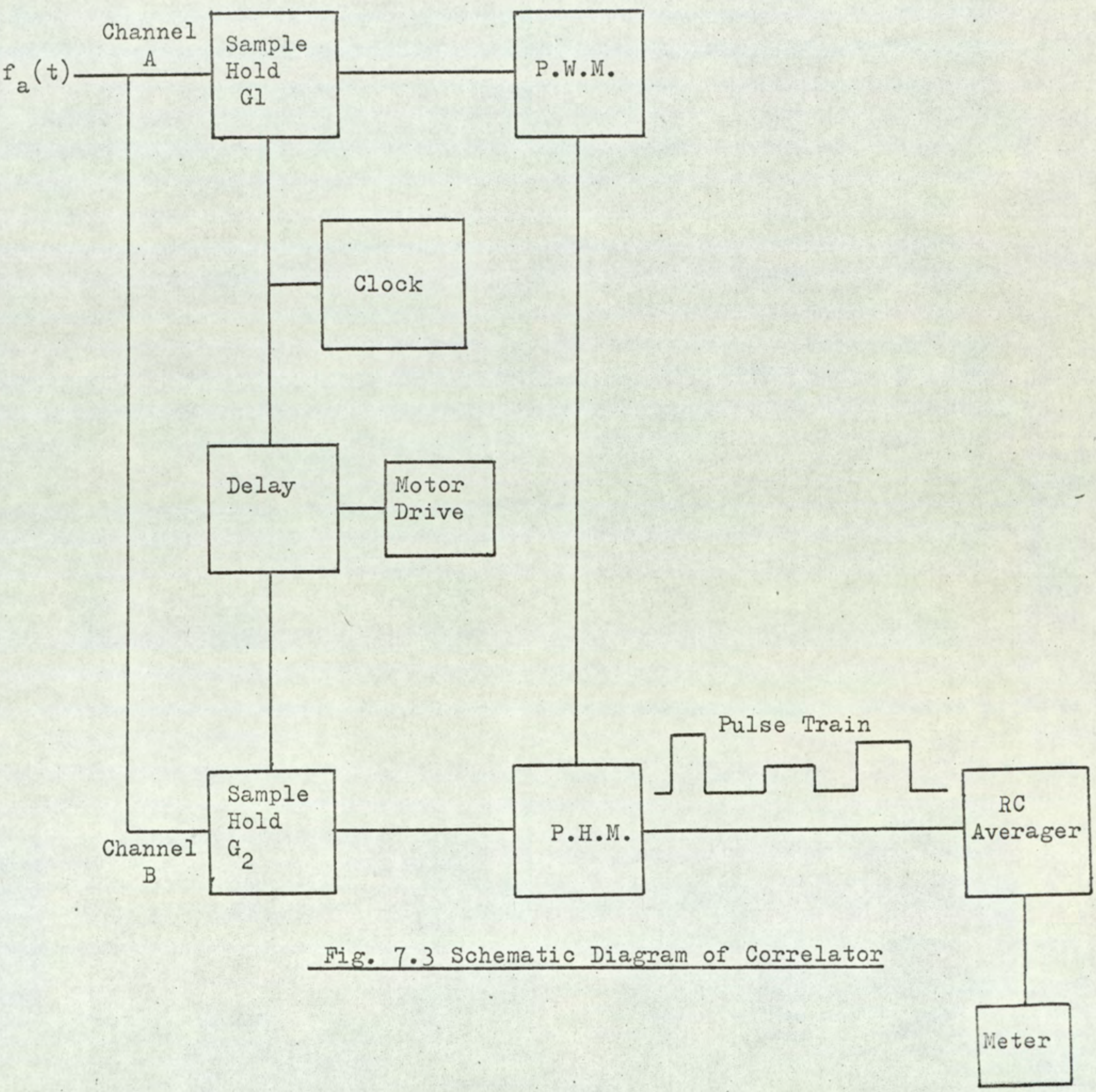

Fig. 7.3 Schematic Diagram of Correlator

(iii) an autocorrelator H.B.C. of the Honeywell Brown 9410 type (Fig.7.3).

Honeywell Brown Correlator

By combining sampling (Appendix 13) with continuous analogue circuits the 9410 correlator provides a means of obtaining correlation functions. The instrument has three bandwidths,

(i) 250 kHz

(ii) 25 kHz

and (iii) 2.5 kHz

Associated with each of these bandwidths is a time delay unit. By adjustment of this unit correlation measurements with time delays of between 0 and τ_m may be made, where τ_m = 0.17 ms, 1.7 ms and 17 ms on the ranges 250 kHz, 25 kHz and 2.5 kHz respectively.

With reference to the simplified block diagram of Fig. 7.3 the basic operation of the 9410 is as follows: Signal $f_a(t)$ is applied to the two channels A and B. At channel A $f_a(t)$ is applied to sample gate G_1 which follows the wave shape until triggered by the first clock pulse at which time sample gate gate G_1 is clamped, retaining the sampled, instantaneous signal value $f_a(t_n)$. Simultaneously, at channel B $f_a(t)$ is similarly acted on by sample gate G_2 except that the sampled value - because of the delay τ - is taken at some later time $(t_n + \tau)$. Hence G_2 retains an instantaneous, sampled voltage $f_a(t_n + \tau)$.

The channel A sample $f_a(t_n)$ is applied to the pulse width modulator (P.W.M.) where the voltage value $f_a(t_n)$ is converted to a pulse of known amplitude but with a width proportional to the sampled voltage value. Correspondingly, the channel B sample, $f_a(t_n + \tau)$ is applied to the pulse height modulator (P.H.M.) to produce a pulse whose height is proportional to the sampled voltage value of $f_a(t_n + \tau)$. The height modulated output of channel B is also gated by the output of the P.W.M., hence the output of the P.H.M. is a pulse whose width is proportional to the sampled voltage $f_a(t_n)$ and whose height is proportional to the sampled voltage $f_a(t_n + \tau)$. Consequently, the generated pulse has an area (W H) which represents the product of $f_a(t_n)$ and $f_a(t_n + \tau)$.

Because the clock operates repetitively and the signals $f_a(t)$, $f_a(t + \tau)$ are continuously applied a train of pulses is generated, each pulse representing the instantaneous product of $f_a(t)$ and $f_a(t + \tau)$ at some instant t_n. The summation of a large number of these pulses is accomplished with the RC averaging circuit the output being proportional to the mean product of $f_a(t)$ and $f_a(t + \tau)$. Thus after a sufficient averaging time an output voltage - displayed on a voltmeter - is available which represents one point on the correlation curve $R_x(\tau) - \tau$.

To determine the rest of the correlation curve necessitates that τ be varied over its entire range. The variation may be made either incrementally, by manual control, or continuously by means of a motor drive.

The accuracy of the correlator, that is of the voltmeter readings, is of the order of $\pm$ 5% of the voltmeter reading when the meter used is that provided with the correlator. However, this accuracy could be improved by using an external voltmeter with a much larger scale so that reading errors would be reduced Accordingly, a Pye Scalamp Galvanometer, with a high series resistance to limit the current, was connected in the correlator circuit and was used as a cross check on the readings obtained with the other voltmeter.

7.1.3 Experiment

Prior to the correlation measurements two checks were made on the correlator. First, using calibrated sine waves at the input and a τ range setting of zero - so that the instrument should be sensitive to power - the meter readings were noted and compared with the input powers, thus giving a check on the instrument reliability. Secondly, with the instrument connected to read the amplifier noise output power the gain of the amplifier was varied in 0.5 dB steps. When the noise power was such that the correlator became overloaded and the dB changes and correlator readings were no longer compatible the amplifier gain was noted. Care was then taken that this gain was never exceeded.

Next with the correlator still connected so as to measure the amplifier noise another autocorrelation measurement was made. This time, however, the measurement was made with the time delay set to continuous sweep and the correlator meter variations were observed so as to find the delay at which the noise became uncorrelated, i.e. meter reading was negligible. This value of τ, say τ_o, was noted.

Having completed these preliminary experiments the equipment was arranged as in Fig. 7.2. Using a delay setting, τ, such that

(i) it was of the order of $3\tau_o$ or more
$(R_n(\tau) = 0)$; and

(ii) it had a value such that the signal correlation was a maximum, i.e.
$2\pi f_s \tau = n\pi$ (Appendix 12);

the amplifier gain and input signal (f_s = 20kHz) were used in a complementary manner so as to maintain the output signal level constant (as in the crosscorrelation measurements). As the input level was varied between 128μV and 1μV the autocorrelation readings were noted.

The frequency range of the correlator was then changed from 25 kHz to 250 kHz and the procedure described above repeated.

Finally, in order to ensure that the results obtained were not peculiar to one valve the measurements were repeated with two other valves of the EF80 type.

7.1.4 Results.

The results (Table 7.1) with the correlator operating on continuous sweep indicated that the noise became uncorrelated at a delay much lower than the maximum setting of the instrument (17×10^{-5} sec. on 250kHz range). Accordingly, by setting the time delay to be of the same order as its maximum value it was possible to arrange for the autocorrelation measurements to be made in a region where the contribution from the noise was negligible ($R_n(\tau) = 0$). The results so obtained are shown in Table 7.2 and although they refer specifically to the 250kHz bandwidth experiments the results with the 25kHz bandwidth were very similar.

Table 7.1

Delay at which readings were a maximum $\times 10^{-5}$ sec.	Correlator readings
0	5
.39	1.2
.675	.6
.955	.3
>3	0

Table 7.2

Input voltage μV	$R_x(\tau)$ with large τ		
	Valve 1	Valve 2	Valve 3
128	5	4.9	5.1
32	5	5.0	5.0
4	5	4.8	5.0
2	5	4.9	5.0
1	4.85	4.8	4.9

7.1.5 Discussion of Results

The results shown in Table 7.2 were obtained in a region where the noise correlation was negligible so that the readings shown are representative of the signal output power.

From Hathaway's work it would be expected that this signal power would decrease as the input signal was reduced - as noise/signal ratio increased - and that this decrease in power would be of the order of 50% as the input voltage was changed from 8μV to 1μV. As can be seen from Table 7.2, however, no such decrease was observed and in fact the autocorrelation (signal power) remained sensibly constant within the limits of accuracy of the instrument, thus confirming the crosscorrelation measurements of the previous chapter (i.e. the amount of signal power converted into noise power is either very small or zero).

7.2 Power Measurements

In the previous chapters frequent reference has been made to the results of two experimentors Bozic[8] and Hathaway. It will now be shown that their results may be interpreted in a manner which leads to the design of a new experiment for checking the author's crosscorrelation measurements.

First of all consider the theoretical section of the previous chapter. Here, it was shown that the excess noise power, N_{ex}, due to signals is given by

$$N_{ex} = K[\bar{v}\,\sigma_s^2 + \bar{s}^2\,\sigma_v^2] \tag{7.5}$$

and it was argued that the term $\bar{s}^2 \sigma_v^2$ could be neglected and that under this condition the equation approximates to (p.80)

$$N_{ex} = \text{const.}\ \bar{v}\,\bar{s} \tag{7.6}$$

$$\text{i.e.}\quad N_{ex} \propto \sqrt{\text{signal power}}$$

A comparison was then made between Eq. (7.6) and Hathaway's results and it was concluded the two were in broad agreement.

If now reference is made to Bozic's work it will be found that he carried out a series of experiments on semiconductor devices. He found that the application to these devices of sinusoidal signals in the range 10 - 50 mV generated excess noise which was one of two kinds. The first kind has, like shot noise, a more or less uniformly distributed spectrum and is directly proportional to the signal power, i.e.,

$$W_{ex}(f) = K_1 V_s^{\alpha} \tag{7.7}$$

where $\alpha \doteq 2$, K_1 = constant, V_s = r.m.s. signal voltage and $W_{ex}(f)$ the frequency spectrum of the excess noise. The second kind of noise increases as the frequency f_c, the centre band frequency of the amplifier, approaches the signal frequency. For this second kind of noise, if Δf is the modulus of the difference between the signal and measuring frequency, the noise power varies according to

$$W_{ex}(f_c) = K_2 V_s^{\beta} (\Delta f)^{-\gamma} \tag{7.8}$$

in which $\beta \doteqdot 2$, $\gamma \doteqdot 1$ and K_2 is a constant.

Thus, if a comparison is made between the excess noise as described by Eq. (7.6) - which agrees with Hathaway's results - and its behaviour as observed by Bozic there are obvious differences. These may possibly be accounted for by extending the theory on which Eq. (7.6) was based.

Such an extension was made by Bull[15] in which he postulated that the processes taking place were not, as was assumed in developing Eq. (7.6), independent of the events occurring in the previous time intervals. As a result he obtained an expression for the excess noise which may be written

$$N_{ex} = \text{const.}[\bar{v}\,\sigma_s^2 + \bar{v}^2\,\sigma_t^2] \tag{7.9}$$

where:

(i) $\bar{v}\sigma_s^2$ is identically equal to the excess noise of Eq. (7.6); and

(ii) $\bar{v}^2\sigma_t^2$ represents an additional term which appears because the processes taking place in the time interval immediately preceding the one under consideration were taken into account.

It is this second term which may possibly be used to account for the differences in behaviour between Bozic's and Hathaway's results.

Returning now to the experimental results it would seem that a useful method of checking the validity of the crosscorrelation measurements is to apply signals to the noise amplifier and test for an increase in noise level

Now from Eqs. (6.13) and (6.14)

$$(P_s)_i = N_{ex} + (P_s)_o$$

therefore

$$N_{ex} = (P_s)_i\left(1 - \frac{(P_s)_o}{(P_s)_i}\right) = (P_s)_i(1 - x^2) \quad (7.10)$$

where x is the ratio of the output $(a_s)_o$ and input $(a_s)_i$ signal amplitudes (i.e. % correlation). Hathaway's results indicate that x when plotted against log $(a_s)_i$ takes the form shown in Fig. (6.5) from which it can be seen that when $(a_s)_i = 1\mu V$ then $x^2 = 0.49$ so that (from Eq. (7.10))

$$N_{ex} = 10^{-12}(0.51)\ (\text{volts})^2$$

Assuming that this noise is distributed uniformly over the bandwidth of the preamplifier, approximately 2MHz, the associated noise power spectrum $W_{ex}(f)$ is given by:

$$W_{ex}(f) = \frac{0.51 \times 10^{-12}}{2 \times 10^6} = 0.25.\ 10^{-18}(\text{volts})^2/\text{Hz} \quad (7.11)$$

Comparing this power spectrum with that of the amplifier shot noise, $W_a(f)$, gives

$$\frac{W_{ex}(f)}{W_a(f)} = \frac{0.25.10^{-18}}{4kT_c R_n} \tag{7.12}$$

which for an amplifier with an equivalent noise resistance, R_n, of 1 kilohm (approximate noise resistance of Hathaway's amplifier) gives

$$\frac{W_{ex}(f)}{W_a(f)} = \frac{0.25.10^{-18}}{4.1\cdot38.10^{-23}.3\ 10^5} \doteqdot 1.5.10^{-2} \tag{7.13}$$

Now, if, as Eq. (7.6) predicts, N_{ex} is proportional to the signal r.m.s. voltage then by increasing the signal from 1μV to 100μV should increase the ratio of $W_{ex}(f)/W_a(f)$ from 1.5×10^{-2} to 1.5, i.e. with an input signal of 100μV then Hathaway's results would seem to indicate that the excess noise power will be approximately 1.5 times the shot noise power.

Of course the above calculations are based on the assumption of a uniform power spectrum over the amplifier bandwidth. However, in view of the fact that they are based on information obtained from Hathaway's experiments in which he found that the rate at which signal is lost and converted into noise is independent of frequency, the assumption of a uniform spectrum seems reasonable. Certainly, if some of the signal was converted into noise with a non-uniform spectrum of the type described by Bozic, then it would be expected that as the signal frequency moved away from the mid-band frequency of the amplifier (the measuring frequency f_c) the noise power and hence the rate of loss of signal would decrease.

On the other hand, if it is assumed that the excess noise has a white noise spectrum with large bandwidth then $W_{ex}(f)/W_a(f)$ over a narrow band would be negligibly small, a result which is contradictory to Bozic's work.

7.2.1 Equipment

A schematic diagram of the experimental arrangement is shown in Fig. 7.4 and consists of:

(i) A signal generator (S.G.) which depending on whether the signal was greater or less than 50 kHz was an Airmexc type 304 or an Advance type H-1.

(ii) A buffer unit B.U. (Fig. 7.5) to prevent feedback between the adder unit (see below) and the preamplifier and provide matching for the two Wayne Kerr attenuators ATT.1 and ATT.2.

(iii) A Solartron Precision Millivoltmeter (S.P.M.).

(iv) A preamplifier (P.A.) of the same form as preamplifier 3 of Sec. 6.7.3.

(v) An adder unit A.U. (see below).

(vi) A main amplifier M.A. (see below).

(vii) A double beam oscilloscope (D.B.O.) which could be locked on either the signal generator voltage (via an emitter follower) for signal balancing purposes (see Sec. 7.2.2) or on an internal 50 Hz signal to monitor for unwanted

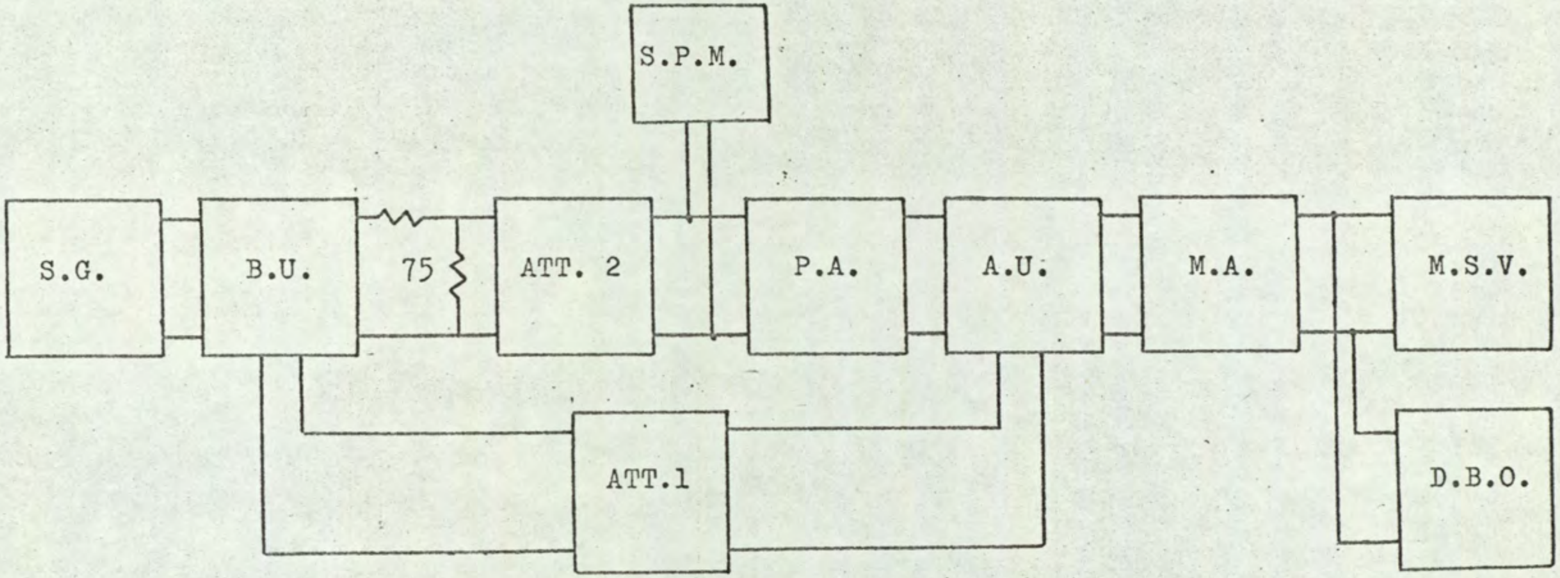

Fig. 7.4 Schematic Diagram of Equipment for Power Measurements

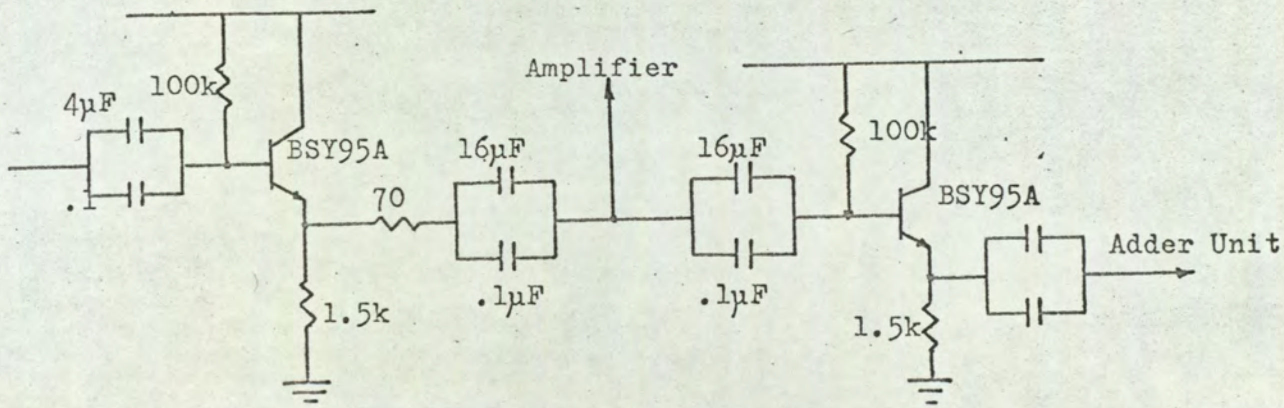

Fig. 7.5 Buffer Unit

mains pick up.

(viii) A mean square voltmeter (M.S.V.) of the type designed by Bozic (Sec. 8.2).

Adder Unit.

This unit (Fig. 7.6) was used to cancel the periodic part, say S_p, of the preamplifier output voltage. To do this a signal proportional to the signal generator voltage was added to S_p. Because there was a phase reversal in the preamplifier then it was only necessary to make adjustments of magnitude, with ATT.1 and the 1 kilohm potentiometer, and slight adjustments of phase (using C_1 and C_2) to ensure that the two waveforms when applied to the operational amplifier unit cancelled.

With regard to the latter it was a commercially available integrated circuit of the Fairchild μA709C type. This circuit was used in preference to those designed earlier because of the fact that its open loop gain was much higher (of the order of 40,000:1) so that its virtual earth point was much nearer to the true earth potential and therefore gave a more exact addition.

The adder unit when connected as shown in Fig. 7.6 was found to have a frequency response which was flat over the range 20 Hz - 400 kHz and to be 3 dBs down at approximately 700 kHz.

Main Amplifier

Originally the main amplifier took the form of that

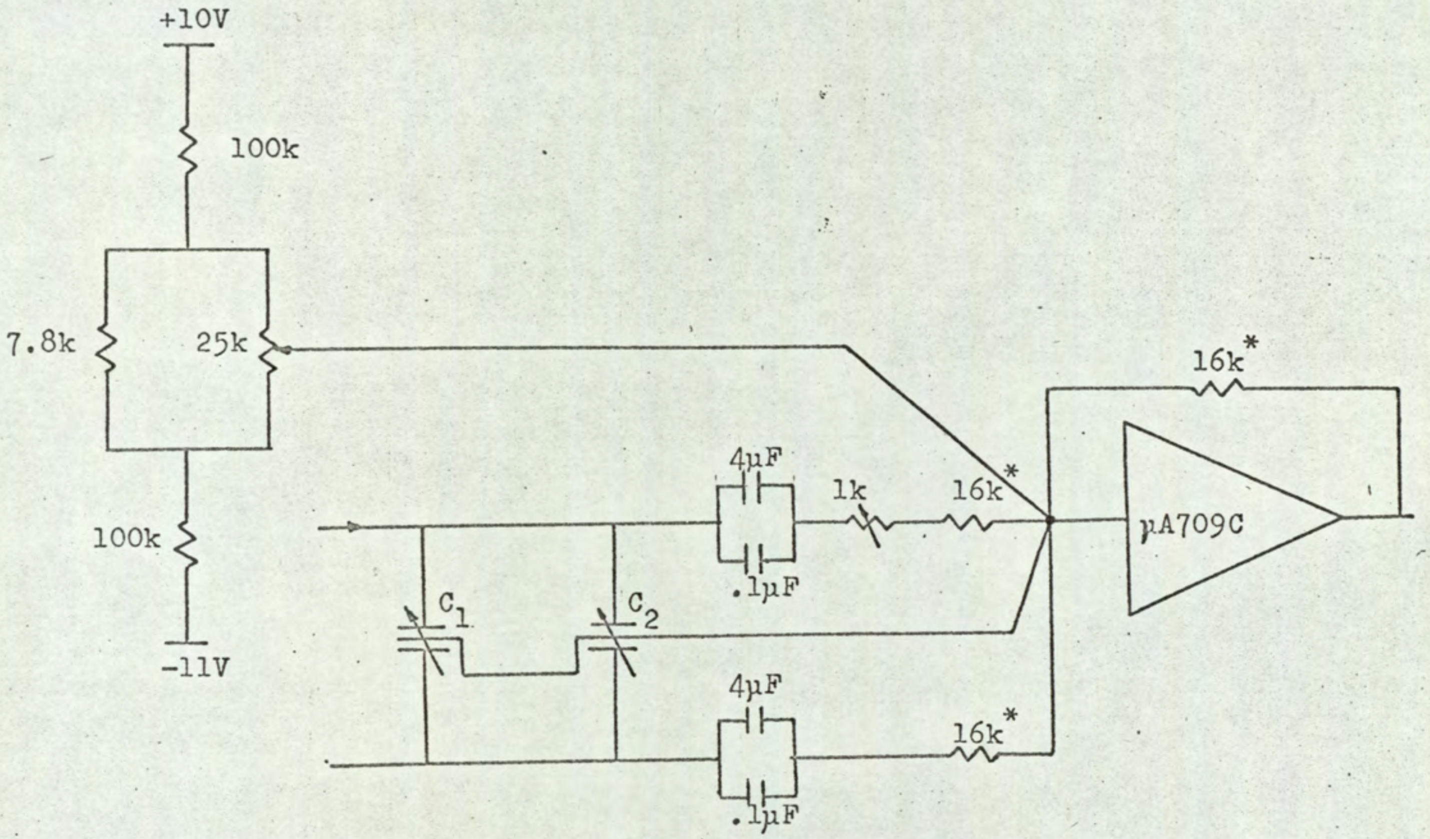

* High stability resistors C_1, C_2 Differential capacitors C_1=30pFs C_2=10pFs

Fig. 7.6 Schematic Diagram of Adder Unit used in the crosscorrelation measurements in which a low pass filter (Appendix 14) was placed at the output - immediately preceding the mean square voltmeter - to limit its bandwidth to approximately 350 kHz (the bandwidth of Hathaway's main amplifier). Later this was replaced by an Airmec type 853 Wave Analyser.

The latter, is a bandpass filter in which the frequency of the centre band may be varied. It operates (Fig. 7.7) on the principle of a heterodyne system in which the frequencies of the original wave are converted into a fixed frequency range of 4 kHz (Fig. 7.8).

By varying the centre band frequency of the analyser it was possible to make measurements over the entire bandwidth of the preamplifier. Hence it was possible to ascertain whether or not there was over a small part of the spectrum an excess noise such that it was large compared to valve shot noise over a narrow band, yet was negligible compared with the same noise measured over a wide band.

7.2.2 Experiment

With the wide-band amplifier the oscilloscope trigger was locked on the oscillator signal and the adder unit adjusted until the noise voltage on the oscilloscope screen was seen to be free of signal. With the narrow band amplifier on the other hand there was a frequency conversion within the amplifier (i.e. wave analyser) so

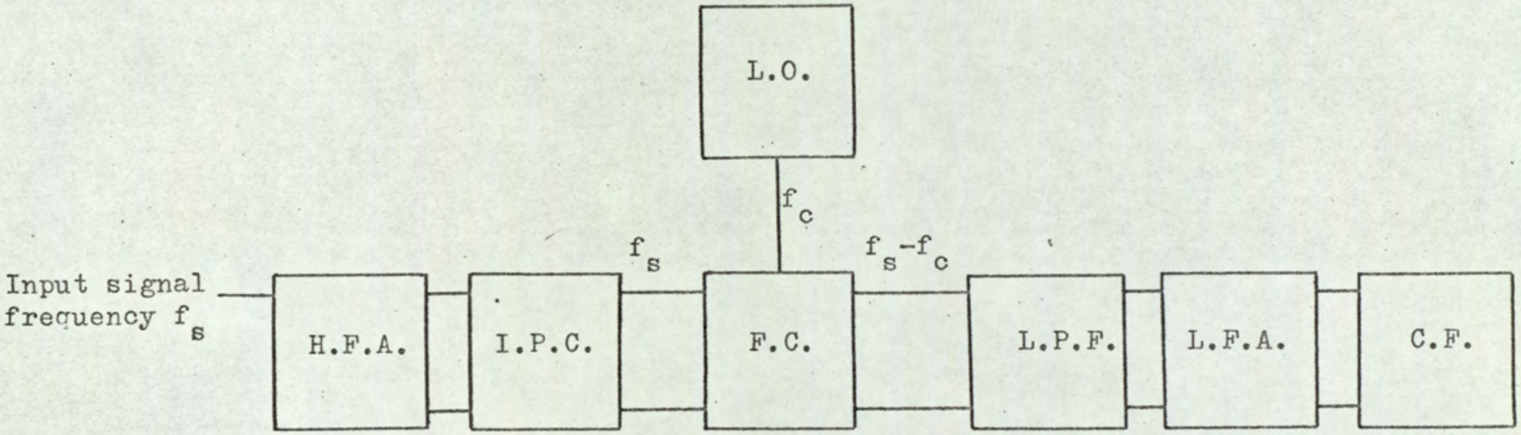

H.F.A. High frequency attenuator   I.P.C. Input tuned circuit tuned to signal frequency

L.O. Local oscillator frequency f_c F.C. Frequency changer   L.P.F. Low pass filter

L.F.A. Low frequency amplifier   C.F Cathode follower

Fig. 7.7 Block Schematic of Wave Analyser

--- Obtained from manufacturer's data

-⊙- Measured

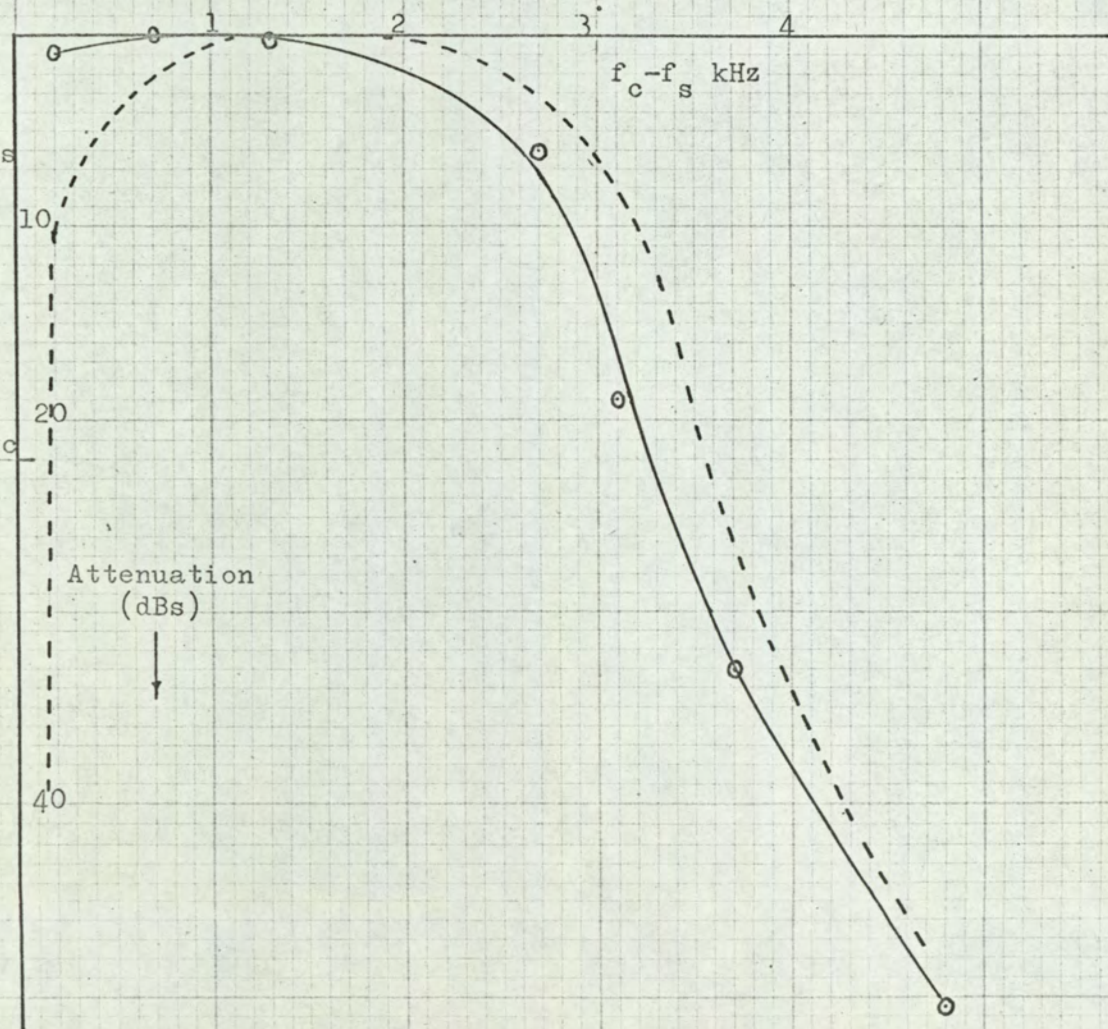

Fig. 7.8 Frequency Characteristic of Wave Analyser

that the original signal frequency was no longer observable at the output. Accordingly, when using the analyser the cancellation of signal was effected by tuning to the signal frequency and adjusting the adder unit until the mean square voltmeter reading was a minimum.

The noise measurements were effected with a variety of input signals the maximum voltage used being 1.33 mV. Above this value of input voltage the signal became distorted and it was impossible to cancel the signal harmonics thus produced.

At the start of the measurements the signal input voltage was set to approximately 1.3 mV, this voltage being read by means of the precision millivoltmeter. The excess noise measurements were then carried out as follows:

(i) The adder unit was balanced, the a.c. signal removed and the noise level measured.

(ii) The a.c. signal was then applied again the new noise reading obtained.

(iii) The procedure of step (i) was repeated.

The measurements were then repeated with input signals of 0.65 mV, 0.32 mV, 0.16 mV and .08 mV, i.e. reduced in 6 dB steps, and with three different EF80 in the input stage.

When the wide-band amplifier was being used signals of frequency 10 kHz and 20 kHz were employed. With the narrow band amplifier on the other hand several frequencies extending over the range 50 kHz - 200 kHz were tried and at each of these frequencies, Δf, the difference between the measuring and signal frequency was varied between 3 and 10 kHz.

7.2.3 Results

Results typical of those obtained are shown in Tables 7.3 and 7.4. The first of these tables refer to measurements made with the wide band amplifier when the signal frequency was 10 kHz and the input signal was varied over the range 0.325 mV - 1.3 mV.

The second table refers to measurements made with the narrow band amplifier. Input signals of between 0.08 and 1.28 mV at a frequency of 50 kHz were used and the centre band frequency of the amplifier was set to 47,45 and 40 kHz, i.e. Δf = 3, 5 and 10 kHz.

Table 7.3

Input signal mV	Noise power with signal	Noise power with signal removed.
.325	40	39.5
.65	40.5	39.5
1.3	39.5	39.5

Table 7.4

Input signal mV	Noise power with signal			Noise power with signal removed
	Δf=3khz	Δf=5kHz	Δf=10kHz	
.08	34	34	33.5	33.5
.32	34.5	34	34	34
.64	35	34.5	34.5	34
1.28	35	34	35.5	34

7.3 Discussion of Results

A comparison of the results of the autocorrelation experiments with the crosscorrelation experiments of the previous chapter shows there is broad agreement between them. Both types of experiment indicate that when a signal is transmitted through an amplifier the proportion of signal converted into noise power is either zero or is very small. This result is obviously a contradiction of Hathaway's work.

A further contradiction arises if the results of Bozic's experiments, as given earlier, are compared with the power measurements of the preceding section since these power measurements have indicated that there is a negligible increase of noise with signal; a result which seems to conflict with Bozic's work. However, closer investigation of Bozic's experiments shows that these were conducted with signals of the order of tens of millivolts, and that although the ratio of the excess and shot (or thermal) noise power spectra will be of the order of unity with these large signals, it would be expected to fall to negligible proportions for signals of 1 mV (i.e. of the order used in the present experiments). From this point of view, therefore, the power measurements do not contradict Bozic's results; but neither do they support them.

If, however, a similar comparison is made between Bozic's and Hathaway's experiments it can be shown that there is a marked difference between the magnitude of the excess noise as found by Bozic and its value as observed by Hathaway. To illustrate this point consider Eq. (7.13) which was derived from Hathaway's work. This equation predicts that the power spectra ratio $W_{ex}(f)/W_a(f)$ will be of the order of 150:1 with input signal of 10 mV. This is a different order of magnitude to the value observed by Bozic; a difference which seems rather large to explain purely in terms of differences between various devices in the degree of the fluctuations.

From this latter point it could be inferred, therefore, that Hathaway's results are wrong. However, in obtaining these results the equipment was checked and rechecked. Furthermore, the results have been shown to behave in a manner similar to that predicted by the theory of Sec. 6.4, although as can be seen by the curves of Figs. 7.9a and 7.9b the degree to which the theoretical and experimental curves agree depends on the point of matching. Thus, in Fig. 7.9a the theoretical and

experimental

curves are matched at 80% correlation and it can be seen that the discrepancies between them are much smaller than inFig. 7.9b where the curves are matched at 90% correlation.

Of course the fact that Hathaway's results may be shown to give good agreement with theory does not necessarily mean that the author's results will invalidate this theory. As can be see by referring to the relative section (Sec.6.4) this theory does not predict exactly at what voltage the signal starts to be converted into noise power but only predicts the rate, relative to the startingvoltage, at which conversion takes place. Thus, if the amount of signal power converted into noise power is very small, as the present experiments tend to show, then it would be quite possible - although because of limitations in the sensitivity of the equipment it couldn't be checked - that the theoretical curve showing the rate of loss of signals will still apply but at much smaller signal levels than those used by Hathaway.

From this latter point of view, therefore, there is no theoretical reason for supposing that Hathaway's results are more likely to be representative of the rate of loss of signal than the author's; and this is supported by the fact that the degree of agreement between Hathaway's theoretical and experimental curves is, to a large extent, dependent on the selection of an arbitrary matching point. Furthermore,

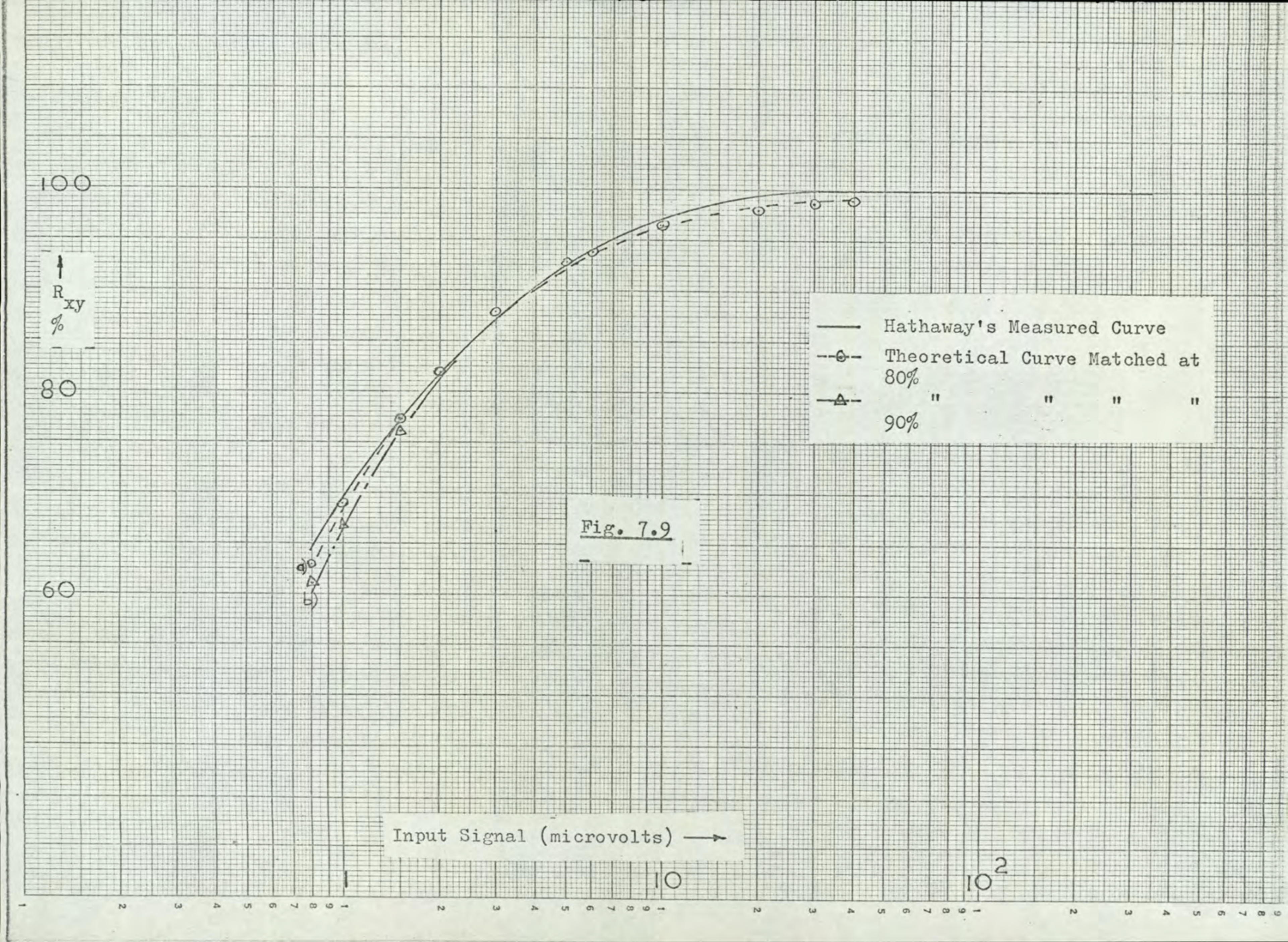
100
80
60
R_{xy} %
Hathaway's Measured Curve
Theoretical Curve Matched at 80%
" " " " 90%
a)
b)
Input Signal (microvolts)
1
10
10^2

Fig. 7.9

in view of :

(i) the results of the present experiments - both autocorrelation and crosscorrelation - all of which indicate that the amount of signal power converted into noise power is small; and

(ii) the quantitative conflict between Hathaway's and Bozic's work;

it seems to the author that Hathaway's results are open to doubt and that the amount of signal power converted into noise power is more likely in agreement with Bozic's than with Hathaway's results.

Finally with regard to the excess noise theory of Sec. 6.4 and to the validity of its application, it has already been pointed out in the text that this theory has deficiencies. However, in order to generate any type of noise a source of power is required and if the view is taken - as in the theory of Sec. 64 - that the source of power for the excess noise is the signal source it follows that some signal power will be converted into noise power and, hence, that a theory, at least resembling that discussed in Sec. 6.4 will apply.

7.4 Conclusions

It has been shown that the loss of signal power in an amplifier is more likely in agreement with Bozic's than with Hathaway's results. It has been further pointed out that the theoretical expression for the amount of signal power converted into noise power, i.e. for the excess noise, does not predict exactly at what level of signal power this occurs and that it is possible that it starts at signal levels lower than those observed by Hathaway. Finally, attention has been drawn to the fact that the theoretical expression for the excess noise as derived in Sec. 6.4 contains deficiencies in its manner of derivation but that if it is accepted that the power source for the excess noise is the signal then a theory, at least resembling that of Sec. 6.4, must apply.

8. MEAN SQUARE VOLTMETER

Probably the simplest measure of a random process is its mean square value or, as it is known statistically, its variance; and this has been frequently used in the previous chapters for the description of noise processes.

In equation form the mean square value of a random process is given, in the time domain, by

$$R_x(0) = \lim_{T \to \infty} \frac{1}{T} \int_0^T x^2(t)\, dt \tag{8.1}$$

and the purpose of a mean square voltmeter is to perform the operations described by this equation.

One method of obtaining the mean square value of a wave is to apply the signal to the heater element of a thermocouple and measure the d.c. output. This output is a measure of the mean heater power and hence of the mean square value of the input voltage. Thermocouple instruments however, suffer from two disadvantages, viz.:

(i) they are sluggish; and

(ii) they are delicate - due to the fact that they operate near their burnout point.

Other instruments[10,50] involving non-linear devices, especially diodes, amy also be used but in general they suffer from the disadvantages that they are slow and tedious to use and involve some form of calibration technique.

One instrument which overcomes many of these difficulties

(Bozic 1962) employs the filament of a thermionic diode as the sensing element and was used by the author in the shot noise measurements (Chap. 5). This instrument was found, for these measurements, to be very satisfactory, although on overload it sometimes occurred that the filament burnt out. More often, however, for a 0.75-1 full scale meter reading the zero drifted 1 - 2% which although not important in the shot noise measurements could lead to errors when used in a correlator instrument of the type described in Chap. 6.

To illustrate this latter point consider the equation

$$R_{xy}(0) = \theta_1 - \theta_2$$

which represents the readings of the correlator, θ_1 and θ_2 being mean square voltmeter deflections (Eq. 6.22). Then

$$\delta R = \delta\theta_1 - \delta\theta_2$$

and $$\frac{\delta R}{R} = \frac{1}{(1 - \frac{\theta_2}{\theta_1})} \quad \frac{\delta\theta_1}{\theta_1} + \frac{\delta\theta_2}{\theta_2} \tag{8.2}$$

which for typical values of $\theta_2/\theta_1 = 0.7$, $\delta\theta_1/\theta_1 = \delta\theta_2/\theta_2 = 0.02$ gives $\delta R/R = 0.12$, i.e. an error of 12%. By careful checking and rechecking it was possible to reduce this error to negligible proportions but it was time consuming. In addition the instrument's susceptibility to overload created further problems since the overload either burnt out the filament, which then had to be replaced, or caused such a large shift of the zero setting that this needed readjustment. Accordingly, it was decided to modify the circuit of the diode voltmeter to give a more stable robust instrument.

The new voltmeter utilised a light sensitive system as the sensing element but basically it had the same form as the older, diode, instrument. For this reason it is proposed to begin by considering the basic system then continue by describing each of the voltmeters in turn.

8.1 Description of Circuit

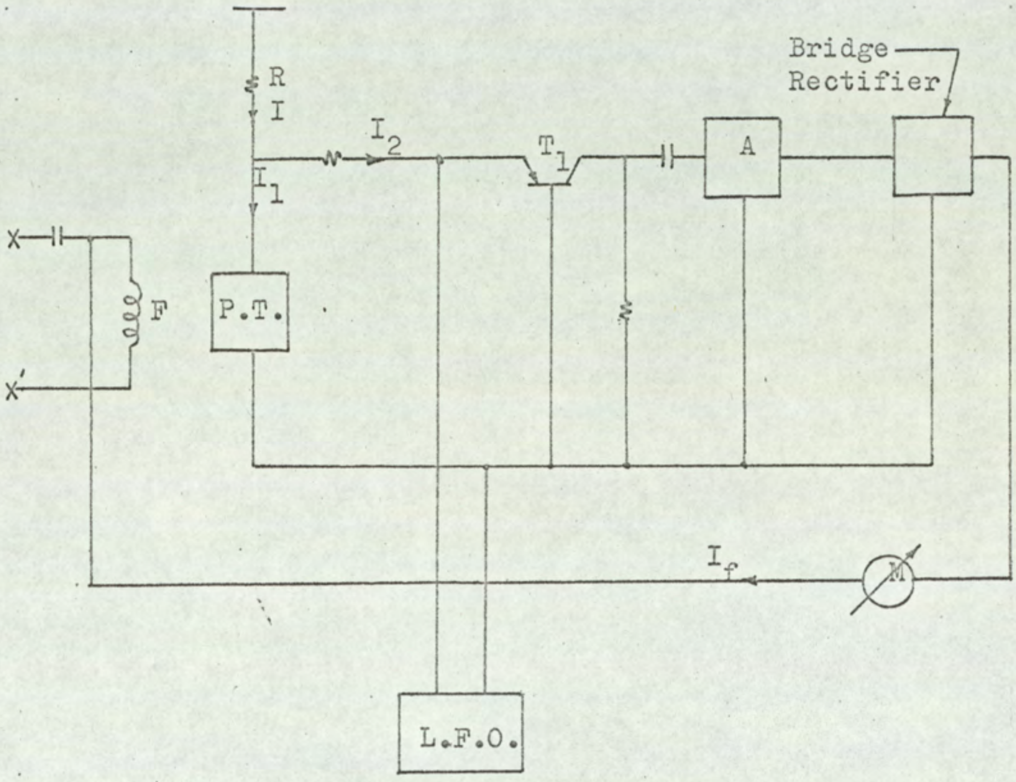

Fig. 8.1

A block schematic of the system is shown in Fig. 8.1 The circuit is arranged so that the potential drop across the resistor R is much larger than that across the transducer P.T. and the current I is maintained sensibly constant by the supply system. The transducer is coupled to the sensing filament F in such a manner that an increase in filament power produces a corresponding increase in I_1 and hence a decrease in I_2. The effect of this change in I_2 is to decrease the gain of the stage T_1^{17} by an amount which is proportional to the change in I_2, and to reduce the amount of a.c. signal from the low frequency oscillator L.F.O., transmitted through the a.c. amplifier A. Hence the d.c. current I_f which represents the mean, rectified, output current of the a.c. amplifier will be reduced also. Thus when an a.c. waveform is applied to the voltmeter input terminals xx^1 it disturbs the existing equilibrium condition by increasing the current I_1 which, in turn, causes the current I_f to be reduced.

For small signal changes, therefore, the circuit of Fig. 8.1 may be represented by that shown below (Fig.8.2) where ΔP_i represents the change in a.c. input power to

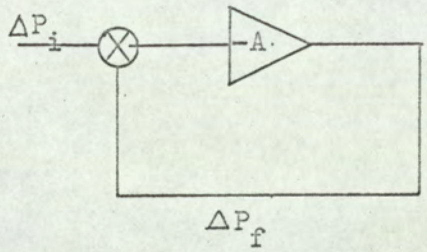

Fig. 8.2

the sensing filament, ΔP_f is the resulting change in power fed back and -A the power gain of the system when the feedback loop is open. From this figure, p, ΔP_i and ΔP_f are related by

$$p = \Delta P_i + \Delta P_f$$

$$\Delta P_f = - A_p$$

so that

$$\Delta P_f = - A(\Delta P_i + \Delta P_f)$$

that is

$$\Delta P_f = \frac{- A}{(1 + A)} \Delta P_i \qquad (8.3)$$

Hence, if the gain is large $\Delta P_f = -\Delta P_i$ and the change in filament power p due to a change in a.c. power ΔP_i will be very small.

It follows, therefore, that for the circuit of Fig. 8.1 in which the power gain is large, the filament power will remain sensibly constant. Hence, providing the filament is fine enough so that skin effect[57] is negligible and the filament resistance is constant it follows that a.c. and d.c. currents are related by

$$I_f^2 + \overline{i^2} = I_{fo}^2$$

where I_{fo} is the initial feedback current and $\overline{i^2}$ is the mean square noise current. Rewriting this equation in the form

$$I_f = (I_{fo}^2 - \overline{i^2})^{\frac{1}{2}}$$

and expanding the term on the r.h.s. gives

$$I_f = I_{fo}\left(1 - \frac{\overline{i^2}}{2I_{fo}^2} + \ldots\ldots\right)$$

and

$$\Delta I_f = \frac{\overline{i^2}}{2I_{fo}}$$ (providing $\overline{i^2}/I_{fo}^2$ is of the same order or less than 0.2). Thus the change in feedback current may be used as a measure of a mean square noise current.

8.2 Diode Voltmeter

A detailed diagram of the voltmeter is given in Fig. 8.3. The sensing element is the filament of a Hivac XFY43 thermionic diode, the filament temperature being such that the valve operates in the saturated region. Since the anode current of this diode is a function of its filament temperature any variations in its filament power and hence its temperature will manifest itself as a change in the anode current. It is upon this property that the action of the voltmeter is based.

The d.c. power for the sensing filament is derived, as mentioned in the previous section, from an oscillator. This oscillator is shown in Fig. 8.3 and has an operating frequency of 9 kHz the frequency of operation being determined by a tee network in the negative feedback loop - the oscillation occuring at the frequency at which the feedback is a minimum. Also incorporated in the

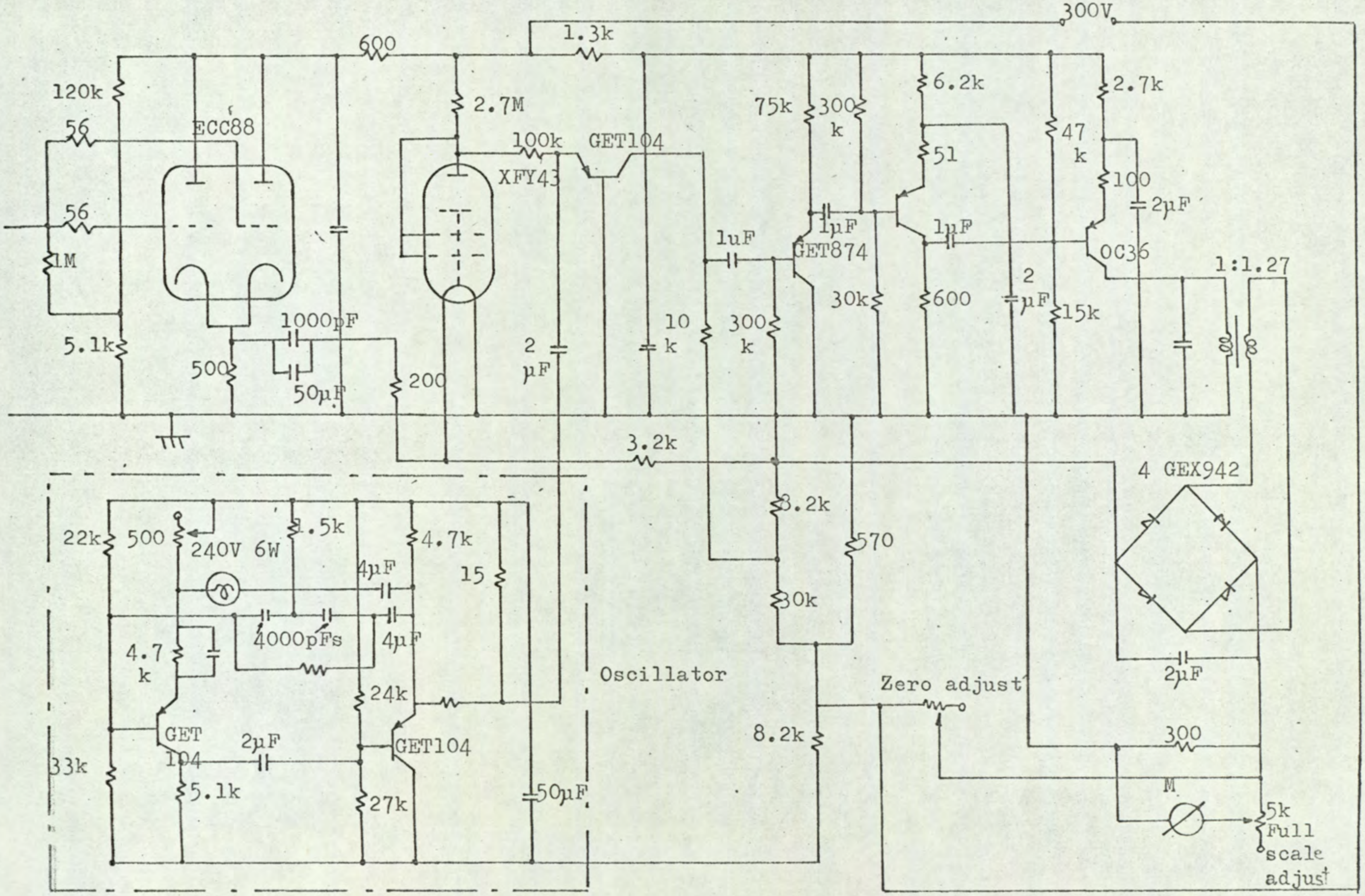

Fig. 8.3 Diode Mean Square Voltmeter

oscillator circuit is a lamp for stabilising the oscillations since any variations in this amplitude will cause variations in I_f and so alter the zero setting of the meter M.

Some of the more important operating features of the instrument are:

(i) cathode follower, and hence high impedance, input;

(ii) frequency response flat to within $\pm$ 1dB from 30 Hz 10 MHz;

(iii) response time of approximately 3 secs.;

(iv) full scale deflection of approximately 0.8 V r.m.s.;

(v) linear operation for peak to mean square values of the order of 10 thus preventing clipping of noise peaks;

(vi) sufficient sensitivity to ensure that the input amplitude demanded is not very large, i.e. the last stage of the noise amplifier should be able to give $\pm$ 8V amplitude with good linearity.

8.3 Light Sensitive Voltmeter

The second type of voltmeter has a circuit very similar to that of the diode voltmeter the only difference being in the sensing device. The circuit arrangement is shown in Fig. 8.4 in which the a.c. amplifier (A.C.A.), cathode follower (C.F.) oscillator (L.F.O.) and bridge rectifier (B.R.) take the same form as for the diode instrument.

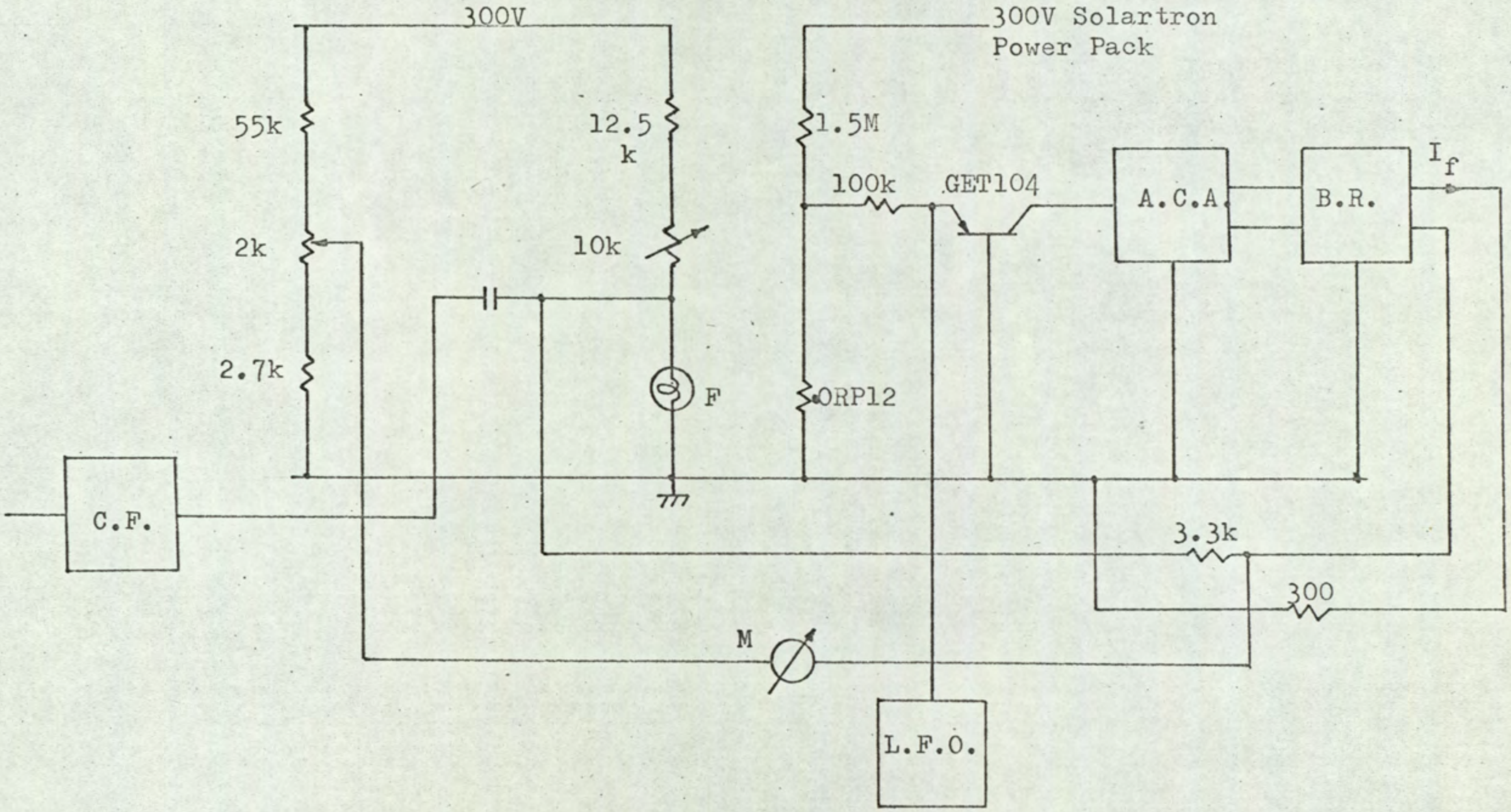

A.C.A. A.C. Amplifier   B.R. Bridge Rectifier   C.F. Cathode Follower

L.F.O. Low Frequency Oscillator

Fig. 8.4 Light Sensitive Voltmeter

Referring now to the circuit of Fig. 8.4 the tungsten lamp F, which acts as the sensing element, has a nominal rating of 6V and 60 mA. Any increase in power to the lamp increases its luminous flux power which produces a change in the resistance of the ORP12 photoconductive cell (Appendix 15). This, in turn, produces, as described previously, a change in d.c. filament current.

From tests on the voltmeter it was found that the drift of the zero setting was much smaller than the diode instrument and that other features include:

(i) The property that the instrument could be overloaded for a few seconds, after shorting the indicating meter, with 30 times full scale input voltage, i.e. 1000 times full scale overload in terms of power input, and almost immediately return to the initial zero setting. Furthermore, if whilst this test was being made the lamp was observed, by opening the box enclosing it in a darkened room, it could be seen to vary in brightness only very slightly; thus showing the feedback was very effective.

(ii) Insensitivity of the sensing elements, ORP12 and tungsten lamp F, to temperature variations (the metal box containing the elements was heated to about 100°C when the change in zero setting was observed to be only of the order of 2% of full

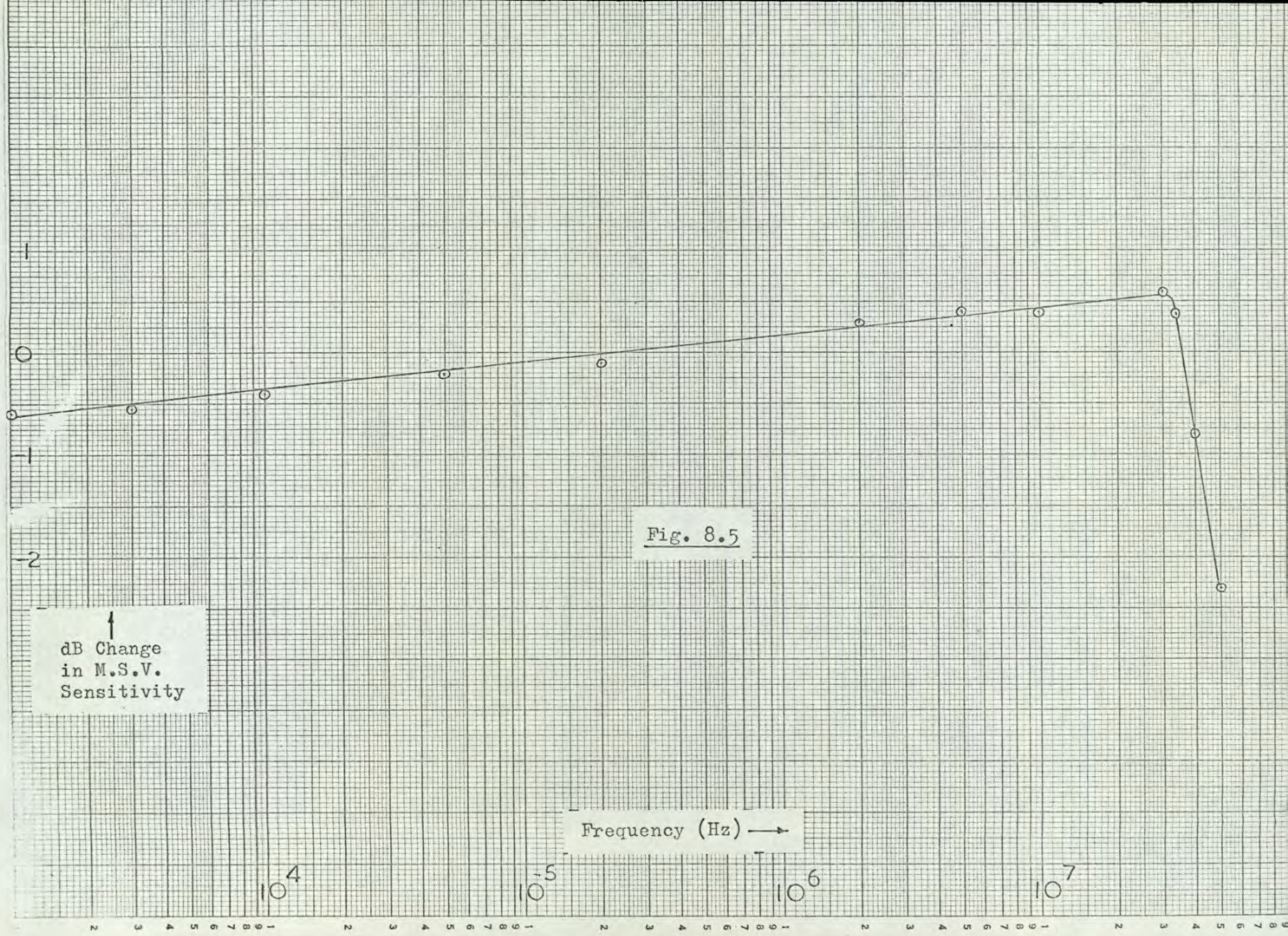

1
0
-1
-2
dB Change
in M.S.V.
Sensitivity
Frequency (Hz)
10^4
10^5
10^6
10^7

Fig. 8.5

scale deflection).

(iii) A frequency response flat (Fig. 8.5) to $\pm$ 1 dB over the range 1 kHz - 35 MHz.

(iv) A response time of approximately 1 second.

(v) Linear operation, even for noise voltages, up to twice full scale deflection.

(vi) A more stable oscillator than in the diode instrument this being effected by encasing the lamp for controlling the oscillator amplitude in a black araldite block which prevented sudden changes in temperature affecting the lamp resistance and hence amplitude. Such changes could be obtained by changes in ambient illumination due to sunshine and proved troublesome in the diode voltmeter.

REFERENCES

1. Beck, A.H.W., "Thermionic Valves," Cambridge University Press, 1953.
2. Bell, D.A., "Electrical Noise," Chap.1, Van Nostrand, London, 1960.
3. Bell, D.A., Ibid., Chap. 8.
4. Bendat, J.S., and Piersol, A.G., "Measurement and Analysis of Random Data," Chap.1, Wiley, London 1966.
5. Bendat, J.S., and Piersol, A.G., Ibid., Chap.7.
6. Bennett, W.R., Proc. I.R.E., 44, 609 (1956).
7. Bozic, S.M., J. Sc. Inst., 39, 210 (1962).
8. Bozic, S.m., "Fluctuations in the Characteristics of Semiconductors," Thesis for Ph.D., University of Aston in Birmingham 1965.
9. Breeze, P., "Fluctuations in Thermionic Diodes," Thesis for M.Sc., University of Wales, 1963.
10. Bull, C.S., J. Sc. Inst., 24, 254 (1947).
11. Bull, C.S., Proc. I. E. E., Part III, 97, 159 (1950)
12. Bull, C.S., Proc. I. E. E., Part III, 98, (1951).
13. Bull, C.S., Proc. I. E. E. Part IV, 99, Monograph. No. 41 (1952).
14. Bull, C.S., Proc. I. E. E., Part IV, Monograph No. 61 (1953).
15. Bull, C.S., "Fluctuations of Stationary and Non-Stationary Electron Currents, " Butterworth, London, 1966.

16. Campbell, N., Proc. Camb. Phil. Soc., 15, 117 (1909).

17. Chaplin, G.B.B., and Owens, A.R., Proc. I. E. E., 105B, 249 (1958).

18. Chemical Rubber Company, "C.R.C. Handbook of Tables for Mathematics," 3rd ed., Chemical Rubber Company, Cleveland, 1967.

19. Davenport, W.B., and Root, W.L., "An Introduction to the Theory of Random Signals and Noise," London,1958.

20. Dekker, A.J. "Solid State Physics," Macmillan, London 1962.

21. Dirac, P.M., Scientific American, May 1963.

22. Everitt, W.L., and Anner, G.E., "Communication Engineering," 3rd ed., McGraw-Hill, New York, 1956.

23. Farnsworth, H.E. Phys. Rev., 31, 405 (1928).

24. Feller, W., "An Introduction to Probability Theory and its Applications," Chap. XI, Vol. 1, 2nd ed., Wiley, London, 1957.

25. Fitch, R.K., and Bull, C.S., Br. J. App. Phys., 12, 566 (1961).

26. Freeman, J. J., "Principles of Noise," Chap. 1, Wiley, New York, 1958.

27. Furth, R., Proc. Royal Soc. A., 192, 593 (1947).

28. Hathaway, D.E.G., "The Masking of Continuous and Discontinuous Signals," Thesis to be submitted for Ph.D., University of London.

29. Hull, A.W., and Williams, N.H., Phys.Rev.,25, 147, 1925.

30. Hyde, F.J., "Physical Basis of Noise," from "Noise in Electron Devices" published on behalf of the Inst. of Physics by Chapman and Hall, London, 1961.

31. Ince, J., "Noise Measurements with a Square Law Voltmeter," Diploma in Technology Project Report, College of Advanced Technology, Birmingham, 1963.

32. Johnson, J.B., Phys. Rev., 26, 71 (1925).

33. Johnson, J.B., Phys. Rev., 32, 97 (1928).

34. Jorgensen, T., Am. J. Phys., 16, 285 (1948).

35. Joyce, M.V., and Clarke, K.K., "Transistor Circuit Analysis," Addison-Wesley, London, 1964.

36. Ledley, R.S., "Digital Computer and Control Engineering," Chap. 22, McGraw-Hill, New York, 1960.

37. Le,, Y.W., and Wiesner, J.B., Electronics, June 1950,86.

38. Lee, Y.W., Cheatham, T.P., and Wiesner, J.B., Proc. I. R. E., 38, 1165 (1950).

39. Lee, Y.W., "Statistical Theory of Communication," Wiley, New York, 1964.

40. Llewellyn, F.B., Proc. I. R. E., 18, 243 (1930).

41. Llewellyn, F.B., Bell System Technical Journal, 14, 659 (1935).

42. Middleton, D., "Introduction to Statistical Communication Theory," Chap. 3, McGraw÷Hill, London, 1960.

43. North, D.O., R. C. A. Rev., 4, 441 (1940).

44. North, D.O., R. C. A. Rev., 5, 106 (1941).

45. Nyquist, H. Phys. Rev. 32, 110 (1928).

46. Panter, P.F., "Modulation, Noise and Spectral Analysis," Chap. 17, McGraw-Hill, London 1965.

47. Pearson, G.L., Physics, 5, 233 (1934).

48. Pearson, G.L., Physics, 6, 6 (1935).

49. Reich, H. J., Skalnik, J.G., and Krauss, H.L., "Theory and Application of Active Devices," Van Nostrand, London, 1966.

50. Richards, C.B., "The Equivalent Noise Resistance of a Thermonic Valve," M.Sc. Thesis, University of Wales, 1955.

51. Rogers, F.E., "Theory of Networks in Electrical Communication and other Fields," Macdonald, London,1957.

52. Rowland, E.N., Proc. Camb. Phil. Soc., 32, 580 (1936).

53. Ryder, J.D., "Electronic Fundamentals and Applications," Pitman, London, 1964.

54. Shaw, B.M., "The Measurement of Noise in Thermionic Valves," M.Sc. Project Report, 1966.

55. Shea, R.F., "Amplifier Handbook," McGraw-Hill, London, 1966.

56. Schottky, W., Ann. d. Phys., 57, 541 (1918).

57. Terman, F.E., "Radio Engineers' Handbook,", Sec. 2, McGraw-Hill, London,1943.

58. Van der Ziel, A., "Noise," Prentice-Hall, New York, 1954.

59. Williams, F.C. J. I. E. E., 78, 332 (1936).

APPENDICES

Appendix 1

The unit impulse, or delta (δ) function, is defined by the equation

$$\delta(f - f_o) = \int_{-\infty}^{\infty} e^{-2\pi i(f - f_o)t}\,dt$$

and has the properties

$$\delta(f - f_o) = 0 \text{ for } f \neq f_o \quad ,$$

$$\delta(f_o) = \infty \ , \ \delta(-f) = \delta(f) \ ,$$

$$\int_{f_o-\epsilon}^{f_o+\epsilon} \delta(f - f_o)\,df = 1 \quad \text{for any } \epsilon > 0$$

$$\int_{f_o-\epsilon}^{f_o+\epsilon} F(f)\delta(f - f_o)\,df \equiv F(f_o) \text{ for any function } F(f).$$

Appendix 2

Using Eqs. (2.12) and (2.17) the variance of the numbers nm is found as follows:

$$(NM)'(x) = \frac{d}{dx} N(M(x))$$

$$= \frac{d(N(M(x)))}{d(M(x))} \quad \frac{d(M(x))}{dx}$$

$$\therefore \quad \overline{nm} = (NM)'(1) = N'(1)\, M'(1) = \bar{n}.\, \bar{m}.$$

Also

$$NM''(1) = \frac{d^2(N(M(x)))}{d(M(x))^2} \left\{ \frac{d(M(x))}{dx} \right\}^2 + \frac{d(N(M(x)))}{d(M(x))} \; \frac{d^2(M(x))}{dx^2}$$

$$\therefore \quad (NM)''(1) = N''(1)\, M'(1)^2 + N'(1)\, M''(1)$$

Hence substituting from the above in the expression for the variance (Eq. 2.12) gives

$$\sigma^2_{nm} = (NM)''(1) - [(NM)'(1)]^2 + (NM)'(1)$$

$$= [\overline{n^2} - \bar{n}]\bar{m}^2 + \bar{n}[\overline{m^2} - \bar{m}] - \bar{n}^2.\bar{m}^2 + \bar{n}.\bar{m}$$

$$= \sigma^2_n\, \bar{m}^2 + \bar{n}\, \sigma^2_m$$

Appendix 3

Campbell's Theorem

Suppose that the arrival of an electron at time $t = 0$ produces a response $F(t)$ in the output circuit. If the circuit is such that the effects of the various electrons add linearly the total effect at time t due to all the electrons is

$$I(t) = \sum_{k=-\infty}^{\infty} F(t - t_k) \quad .$$

where the k^{th} electron arrives at t_k.

Campbell's theorem states that the average value of $I(t)$ is

$$\overline{I(t)} = \lambda \int_{-\infty}^{\infty} F(t)\, dt$$

and the mean square value

$$\overline{[I(t) - \bar{I}(t)]^2} = \lambda \int_{-\infty}^{\infty} F^2(t)\, dt$$

where λ is the average number of electrons arriving per second.

Appendix 4

Eq. (3.10) gives

$$\Delta V(x) = U(F(W(x))).\ U(F(W(x^{-1})))$$

from which it follows that

$$\Delta V'(x) = U'(F(W(x))).\ F'(W(x)).\ W'(x).U(F(W(x^{-1}))) - \frac{1}{x^2}\ U'(F(W(x^{-1}))).\ F'(W(x^{-1})).\ W'(x^{-1}).\ U(F(W(x)))$$

and

$$\begin{aligned}\Delta V''(x) = {} & U''(F(W(x))).[F'(W(x))\ W'(x)]^2.\ U(F(W(x^{-1}))) \\ & + U'(F(W(x))).\ F''(W(x))).\{W'(x)\}^2.\ U(F(W(x^{-1}))) \\ & + U'(F(W(x))).\ F'(W(x)).\ (W''(x)).\ U(F(W(x^{-1}))) \\ & - \frac{1}{x^2}\ U'(F(W(x))).\ F'(W(x)).\ W'(x).\ U'(F(W(x^{-1}))). \\ & \qquad F'(W(x^{-1})).\ W'(x^{-1}) \\ & + \frac{1}{x^4}\ U''(F(W(x^{-1}))).\{F'(W(x^{-1})).\ W'(x^{-1})\}^2\ U(F(W(x))). \\ & + \frac{1}{x^4}\ U'(F(W(x^{-1}))).\ F''(W(x^{-1})).\{W'(x^{-1})\}^2\ U(F(W(x))). \\ & - \frac{1}{x^2}\ U'(F(W(x^{-1}))).\ F'(W(x^{-1})).\ W'(x^{-1}).\ U'(F(W(x))). \\ & \qquad F'(W(x))\ W'(x). \\ & + \frac{2}{x^3}\ U'(F(W(x^{-1}))).\ F'(W(x^{-1})).\ W'(x^{-1}).\ U(F(W(x))). \\ & + \frac{1}{x^4}\ U'(F(W(x^{-1}))).\ F'(W(x)).\ W''(x^{-1}).\ U(F(W(x))).\end{aligned}$$

Using the relationships between $\Delta V'(1)$ and $\overline{\delta v}$ and $\Delta V''(1)$ and $\sigma^2_{\delta v}$ (Sec. 2.5) then these give

$$\overline{\delta v} = \Delta V'(1) = \bar{u}\ \bar{f}\ \bar{w} - \bar{u}\ \bar{f}\ \bar{w} = 0$$

and $\sigma^2_{\delta v} = \Delta V''(1) + \Delta V'(1) - \{\Delta V'(1)\}^2$

$$= U^{11}(1)[\bar{f}\,\bar{w}]^2 + \bar{u}\,\bar{w}^2\,F^{11}(1) - (\bar{u}\,\bar{f}\,\bar{w})^2 + (\bar{f}\,\bar{w})^2\,U^{11}(1)$$

$$+ \bar{u}\,\bar{f}\,W^{11}(1) + \bar{u}\,\bar{w}^2 F^{11}(1) - (\bar{u}\,\bar{f}\,\bar{w})^2 + 2\,\bar{u}\,\bar{f}\,\bar{w}$$

$$+ \bar{u}\,\bar{f}\,W^{11}(1)$$

$$= 2[(\bar{f}\,\bar{w})^2\,U^{11}(1) + \bar{u}\,\bar{w}^2 F^{11}(1) + \bar{u}\,\bar{f}\,W^{11}(1) + \bar{u}\,\bar{f}\,\bar{w}$$

$$- (\bar{u}\,\bar{f}\,\bar{w})^2]$$

Hence, making the further substitutions

$$U^{11}(1) = \sigma_u^2 + \bar{u}^2 - \bar{u}$$

$$F^{11}(1) = \sigma_f^2 + \bar{f}^2 - \bar{f}$$

$$W^{11}(1) = \sigma_w^2 + \bar{w}^2 - \bar{w}$$

then this last equation simplifies to

$$\sigma_{\delta v}^2 = 2\,[\bar{f}^2\,w\;\sigma_u^2 + \bar{u}\,\bar{f}\,\sigma_w^2 + \bar{u}\,\bar{w}^2\;\sigma_f^2]$$

Appendix 5

Consider a diode of plane parallel structure. In the temperature limited region the anode current is given by

$$I_t = I_o \text{ exp.const. } (V_a + \phi_c - \phi_a)$$

and in the retarding region by

$$I_r = I_o \text{ exp. } \frac{-e}{kT_c} (V_a + \phi_c - \phi_a)$$

where I_o = emission current from cathode

ϕ_c = cathode work function

ϕ_a = anode work function

It follows from these equations that the plots of $\ln I_t - V_a$ and $\ln I_r - V_a$ will be straight lines and if these lines are extrapolated they will meet at a point such that the current and voltage at this point will represent I_o and the negative of the contact potential difference respectively (since $V_a + \phi_c - \phi_a = 0$).

In a series of experiments with EB91 valves and low cathode temperatures Fitch used the above method to determine the variation of contact potential with temperature. The contact potentials so determined were then used in conjunction with the characteristic curves for higher, and normal, temperatures to determine the total emission. A typical set of results is shown in Fig. A.5.1 and illustrates that the assumption of complete space charge limitation in the application of the space charge smoothing factor theories is valid.

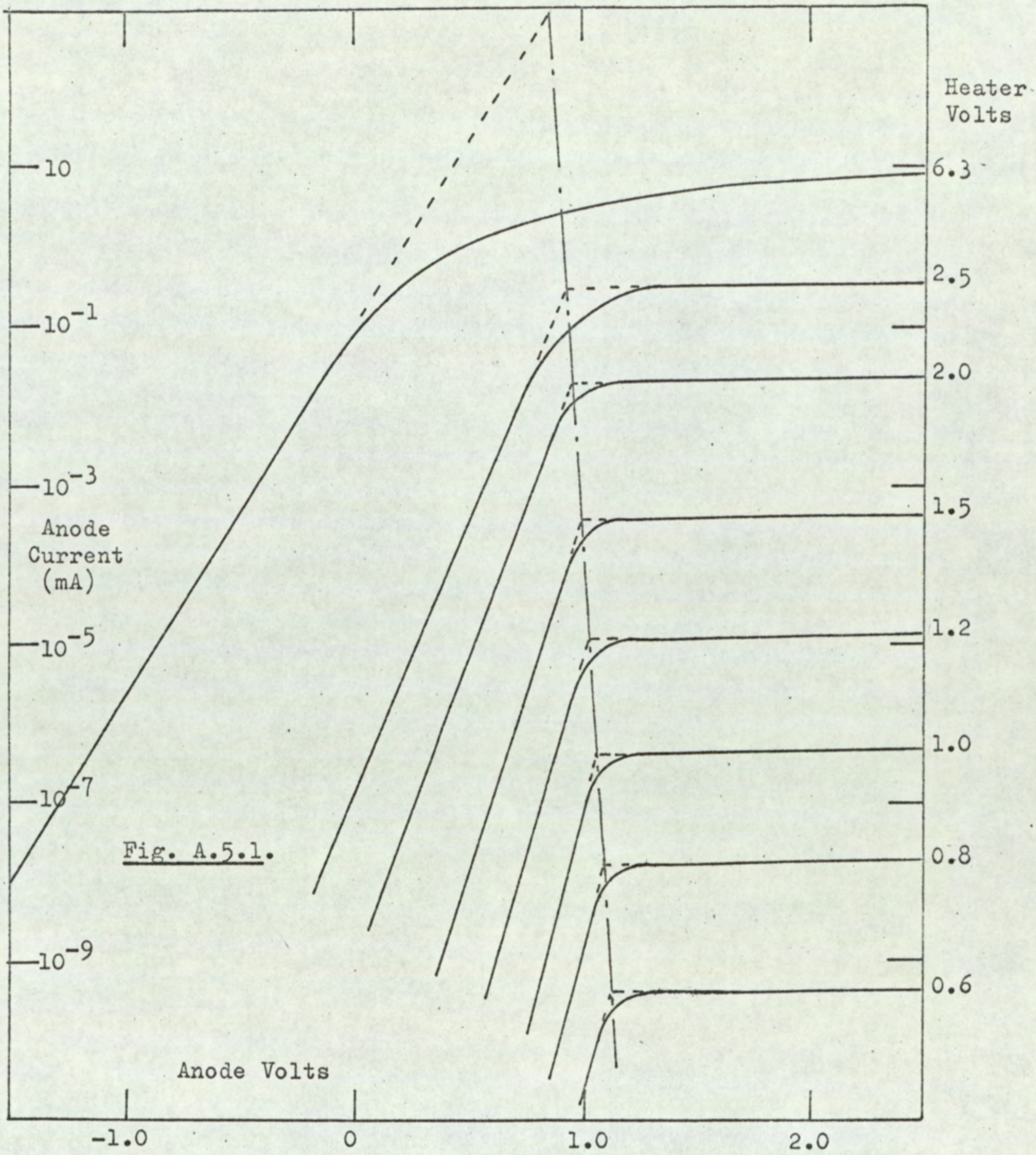
Heater Volts
10
10^{-1}
10^{-3}
Anode Current (mA)
10^{-5}
10^{-7}
10^{-9}
6.3
2.5
2.0
1.5
1.2
1.0
0.8
0.6
Anode Volts
-1.0
0
1.0
2.0

Fig. A.5.1.

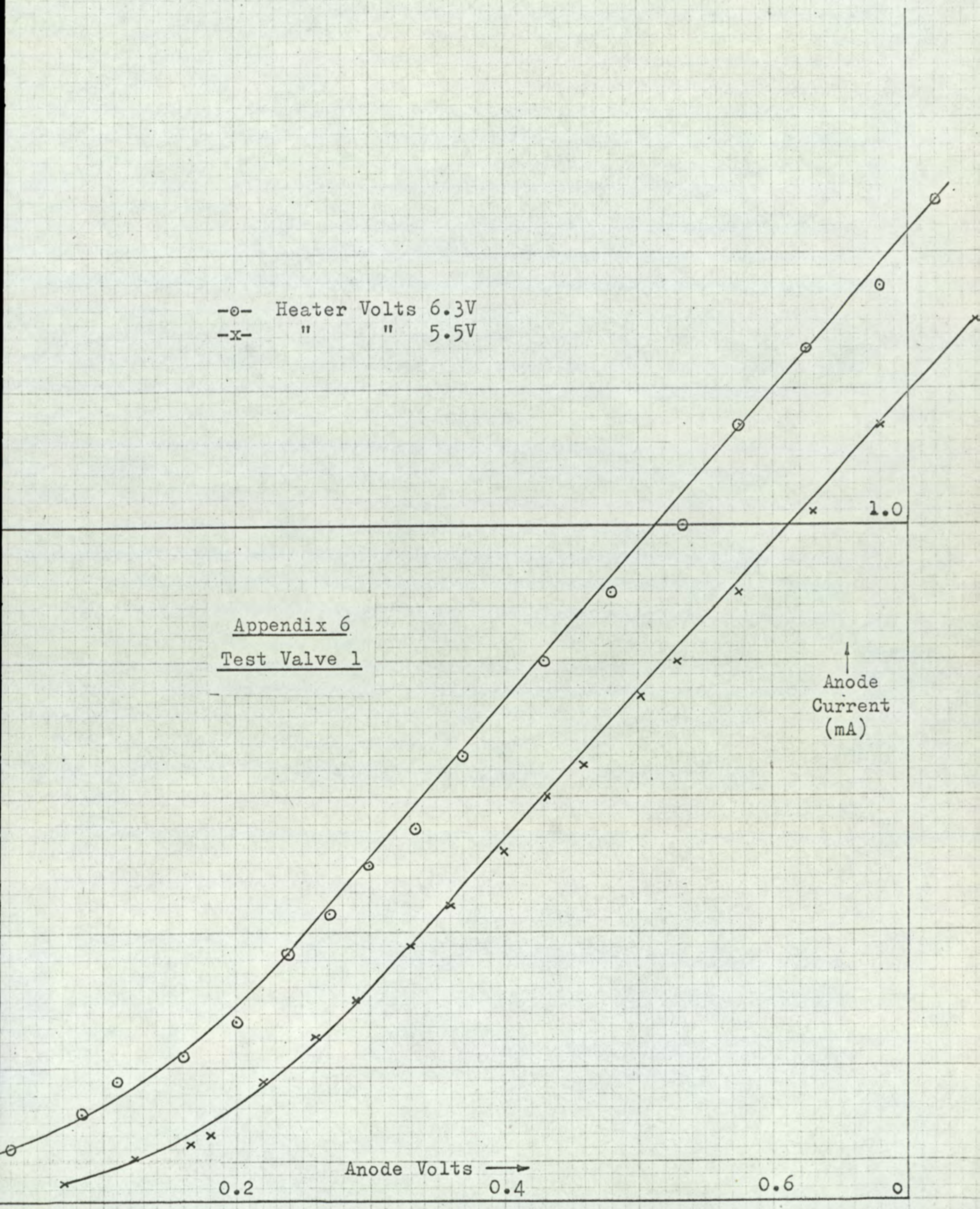
-⊙- Heater Volts 6.3V
-x- " " 5.5V
Appendix 6
Test Valve 1
Anode Current (mA)
1.0
Anode Volts
0.2
0.4
0.6
0

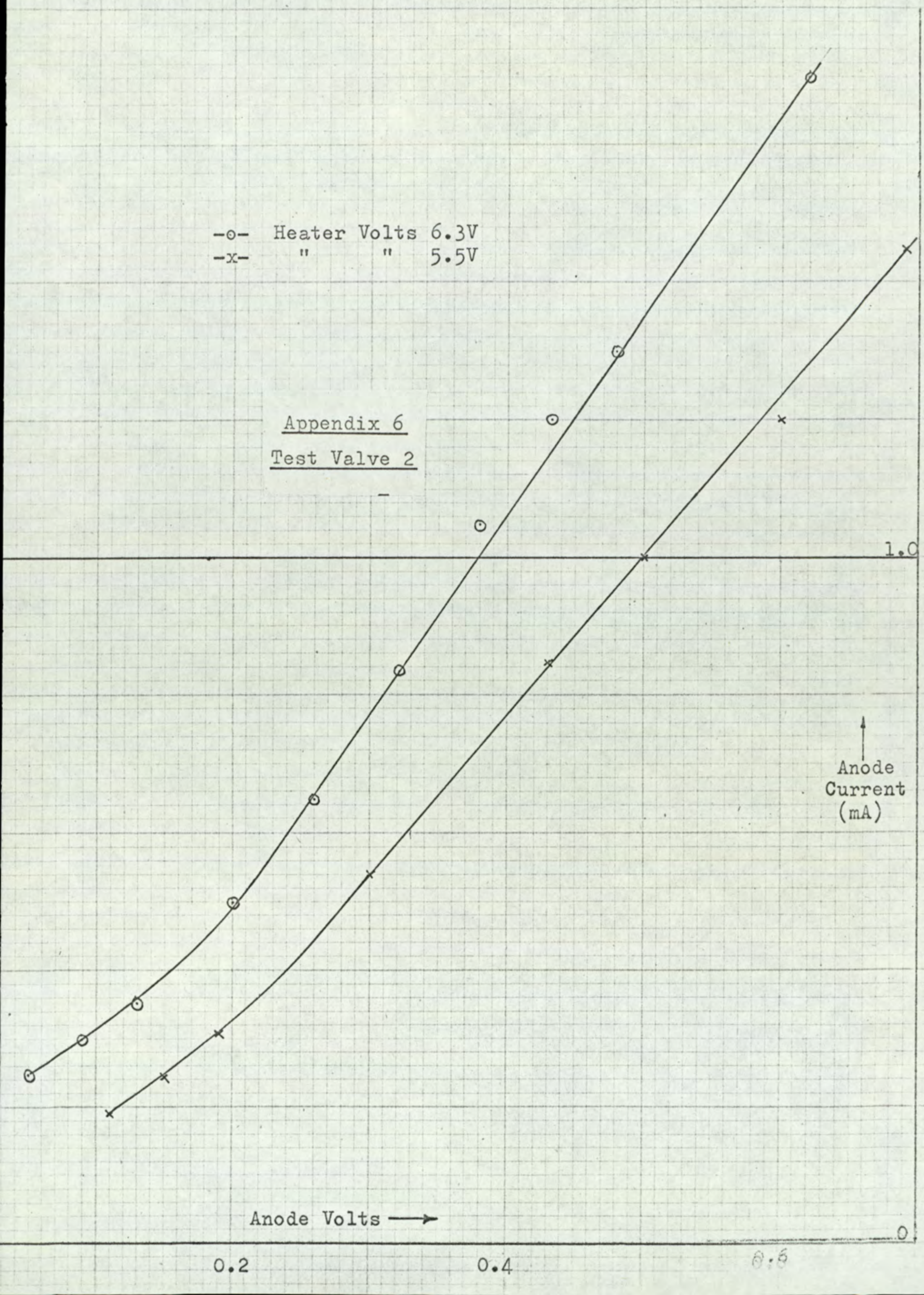
-o- Heater Volts 6.3V
-x- " " 5.5V
Appendix 6
Test Valve 2
1.0
Anode Current (mA)
Anode Volts
0
0.2
0.4
0.6

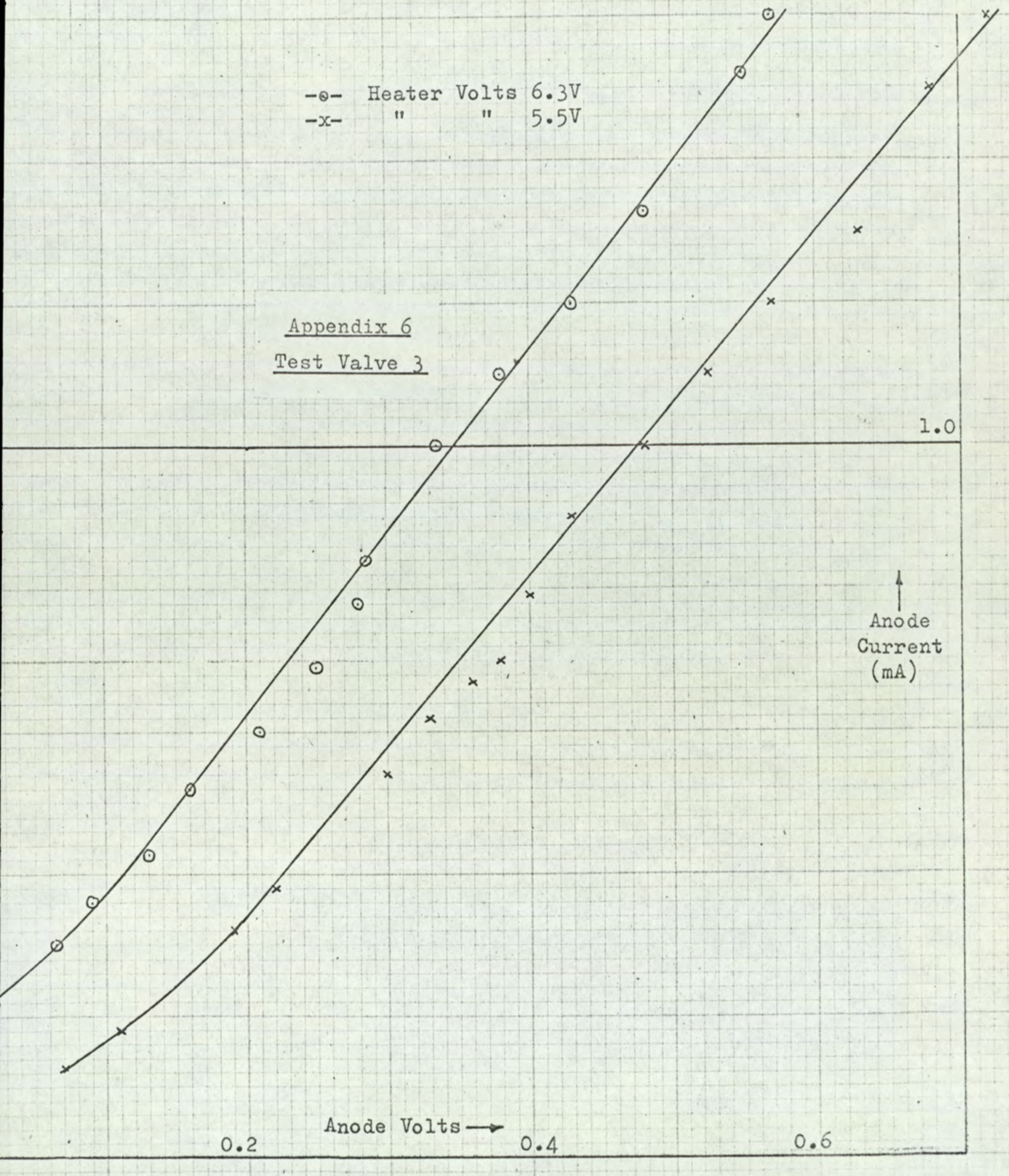
-⊙- Heater Volts 6.3V
-x- " " 5.5V
Appendix 6
Test Valve 3
1.0
Anode Current (mA)
Anode Volts
0.2
0.4
0.6

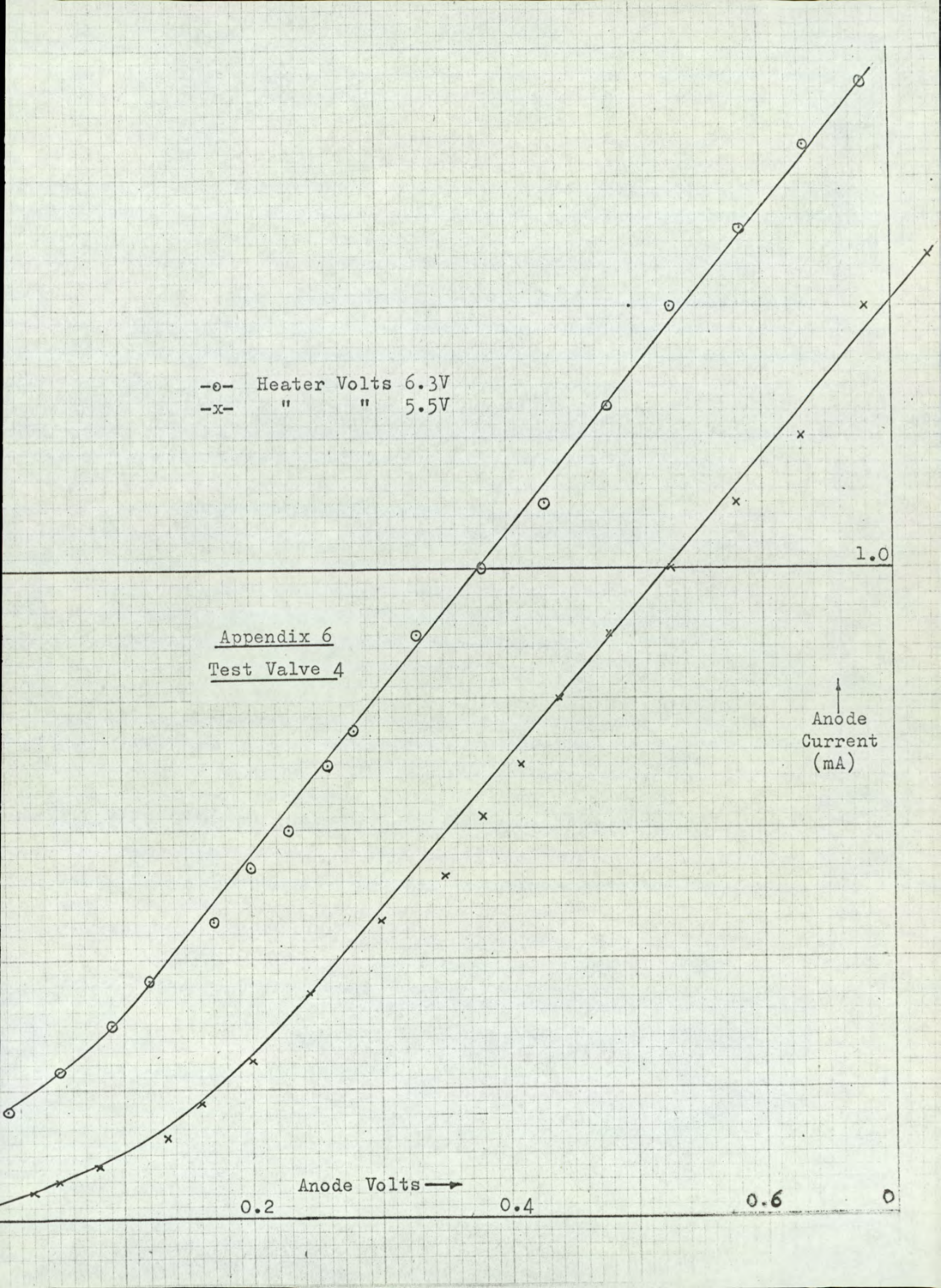
-⊙- Heater Volts 6.3V
-x- " " 5.5V
Appendix 6
Test Valve 4
1.0
Anode
Current
(mA)
Anode Volts
0.2
0.4
0.6
0

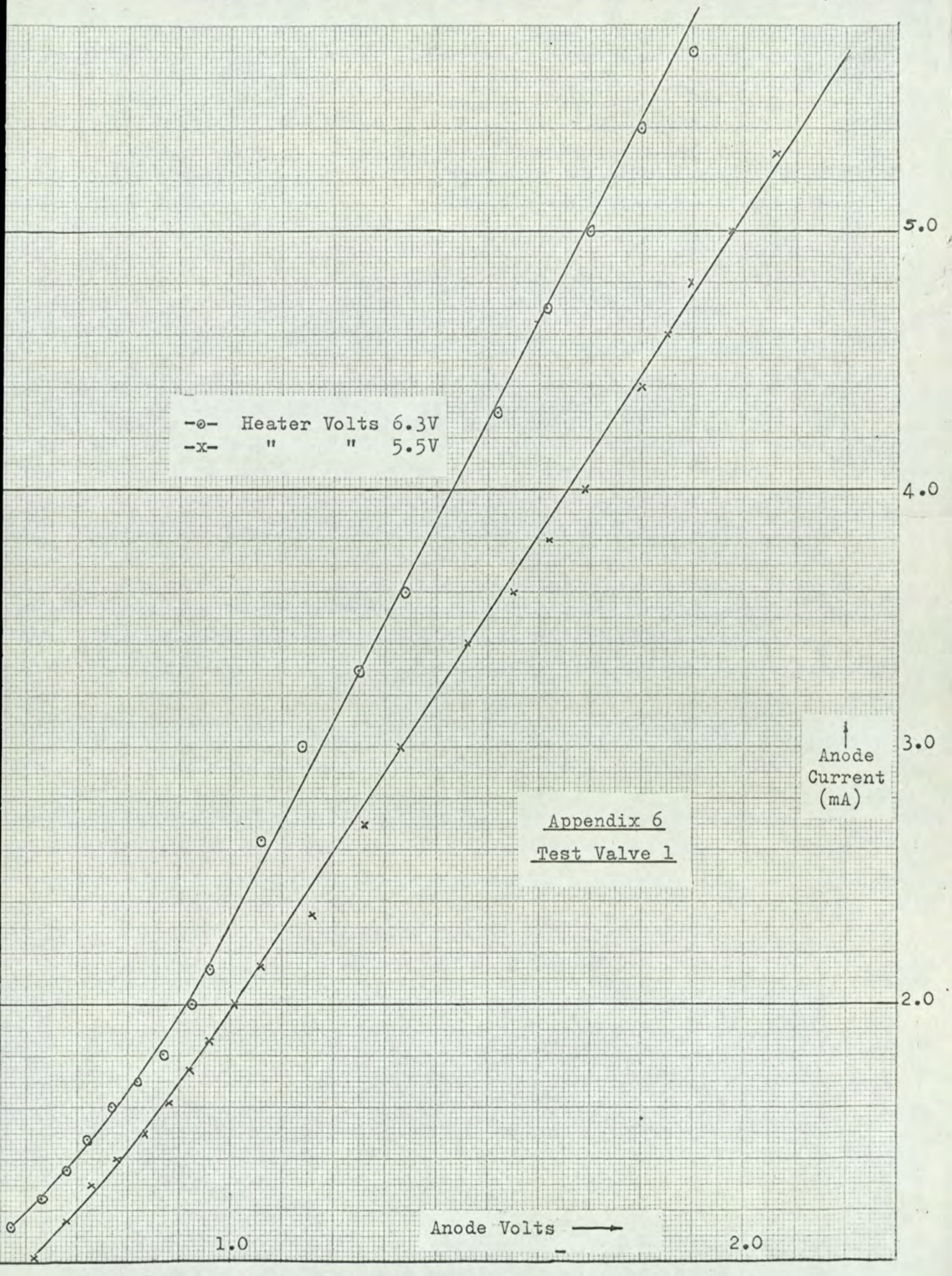

-⊙- Heater Volts 6.3V
-x- " " 5.5V
Appendix 6
Test Valve 1
Anode Current (mA)
Anode Volts
1.0
2.0
2.0
3.0
4.0
5.0

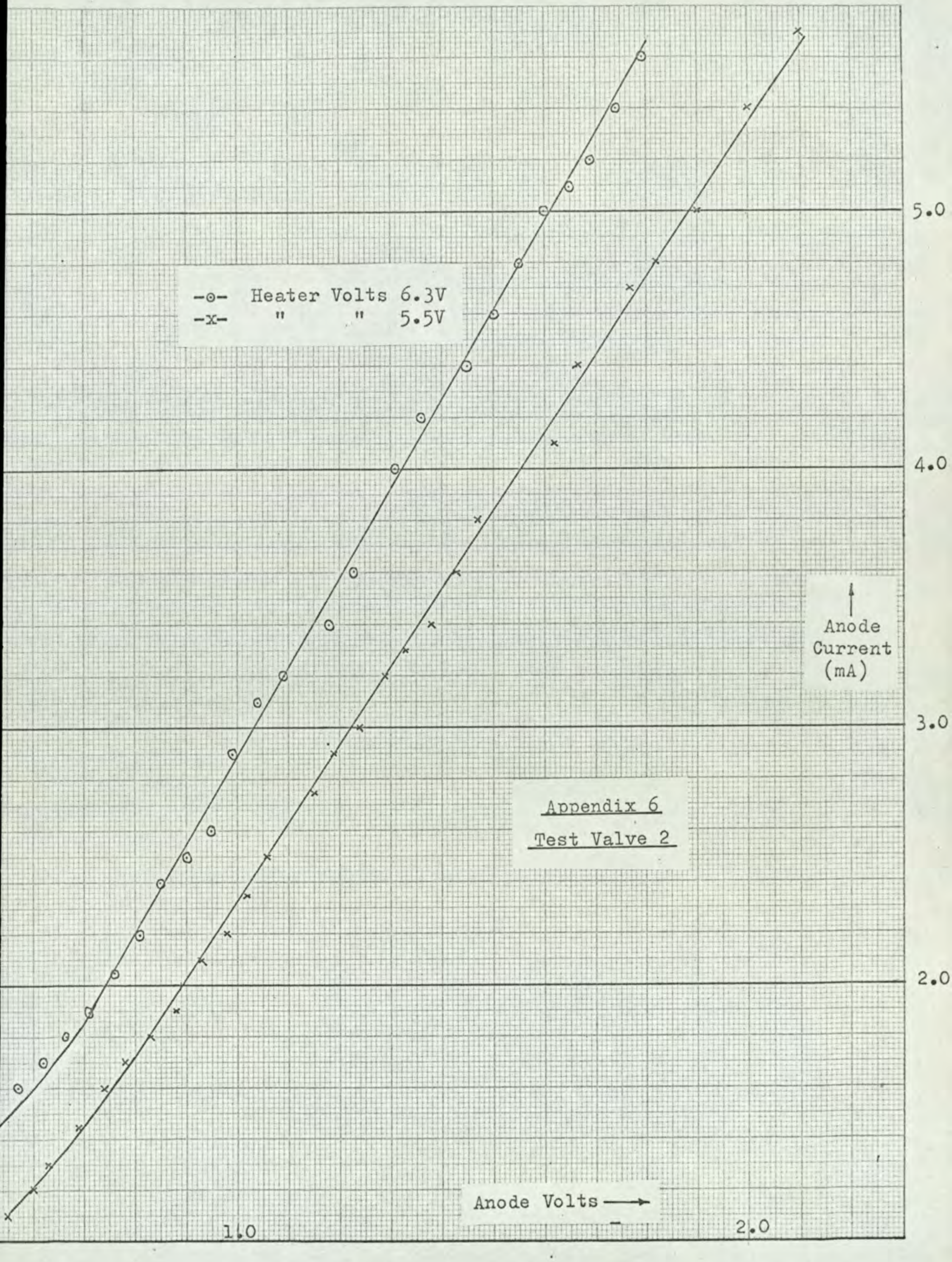

-⊙- Heater Volts 6.3V
-x- " " 5.5V
Appendix 6
Test Valve 2
Anode Current (mA)
Anode Volts
5.0
4.0
3.0
2.0
1.0
2.0

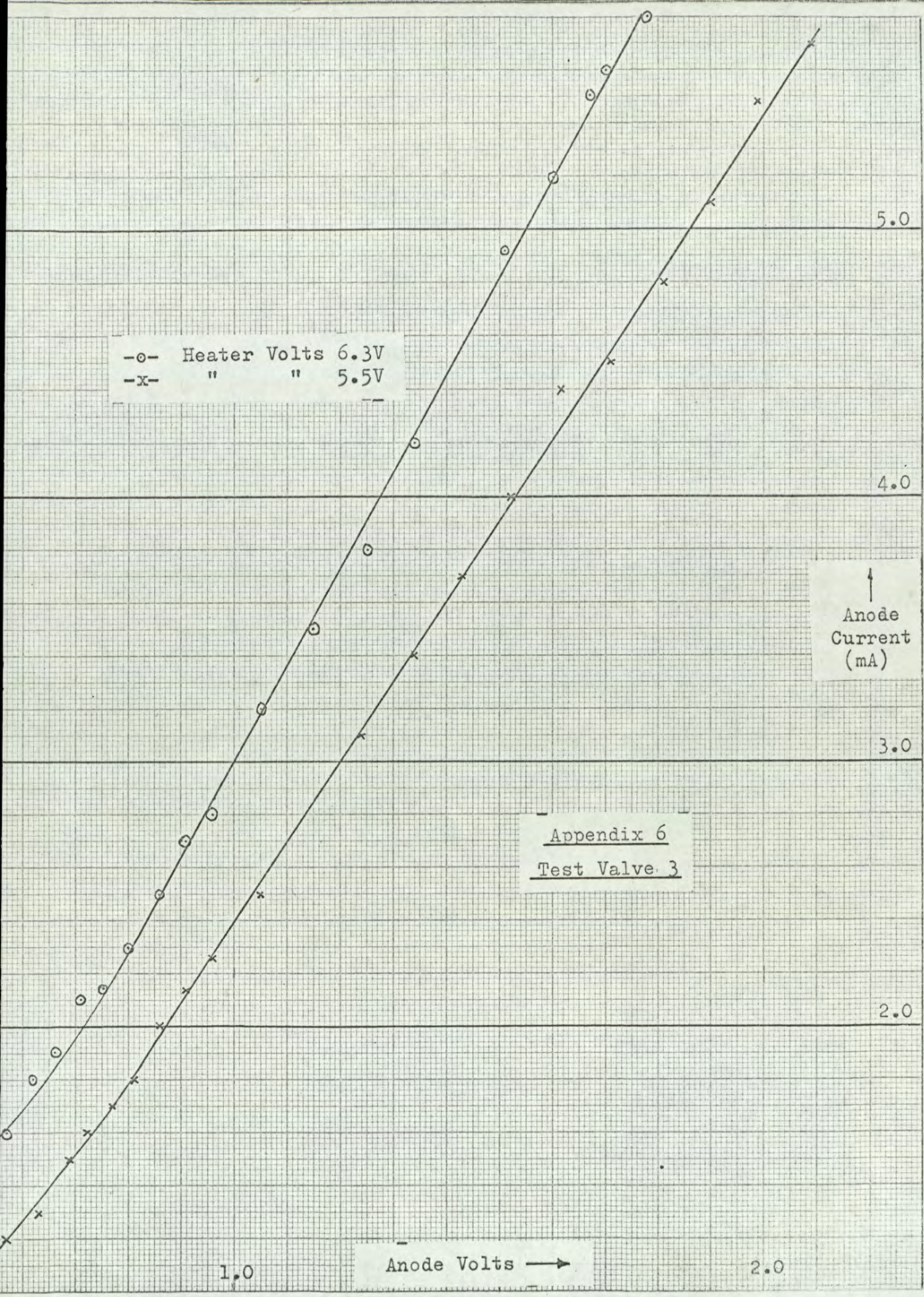

-⊙- Heater Volts 6.3V
-x- " " 5.5V
5.0
4.0
3.0
2.0
Anode Current (mA)
Appendix 6
Test Valve 3
1.0
Anode Volts
2.0

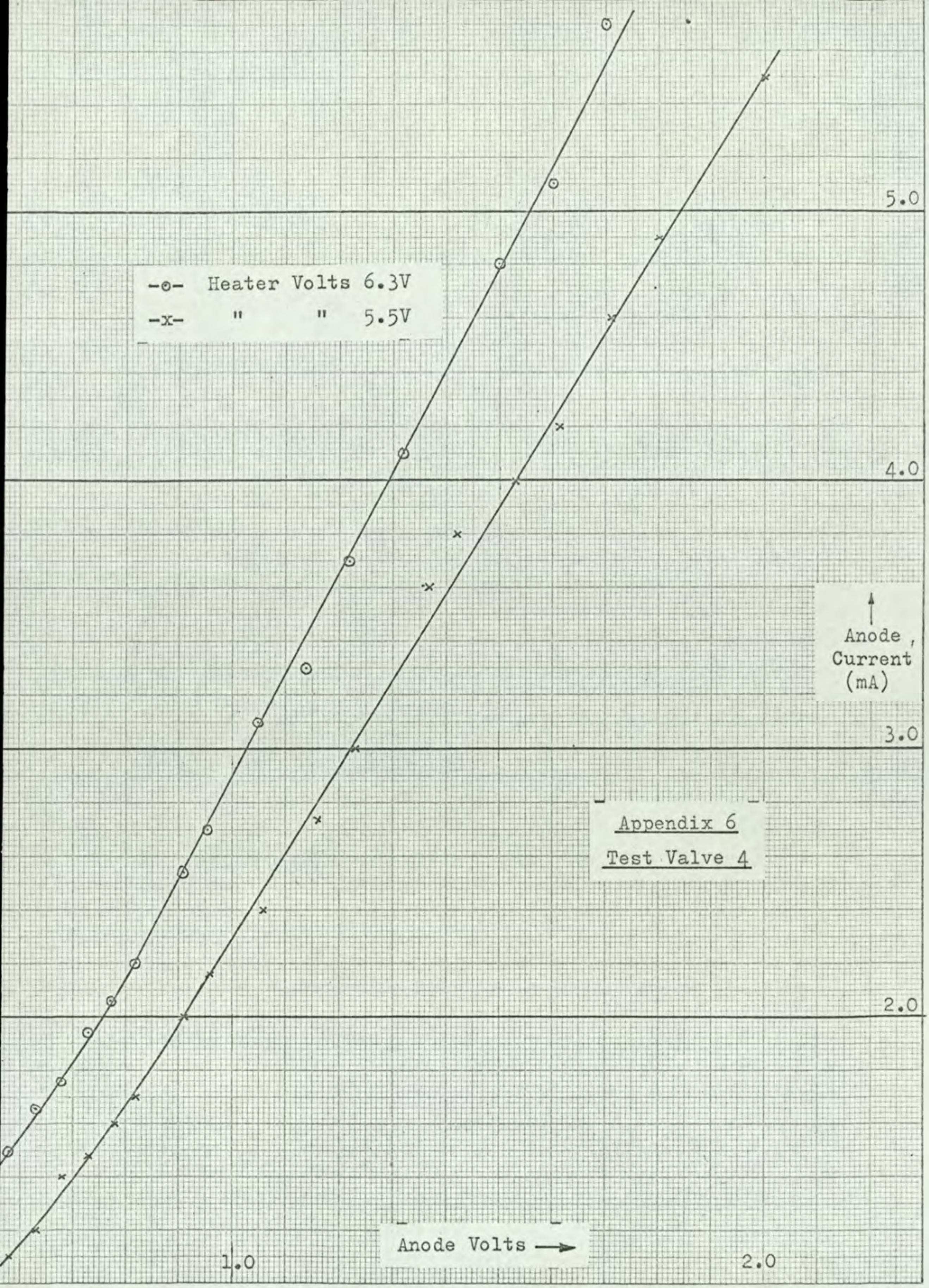

-⊙- Heater Volts 6.3V
-x- " " 5.5V
5.0
4.0
3.0
2.0
Anode Current (mA)
Appendix 6
Test Valve 4
Anode Volts
1.0
2.0

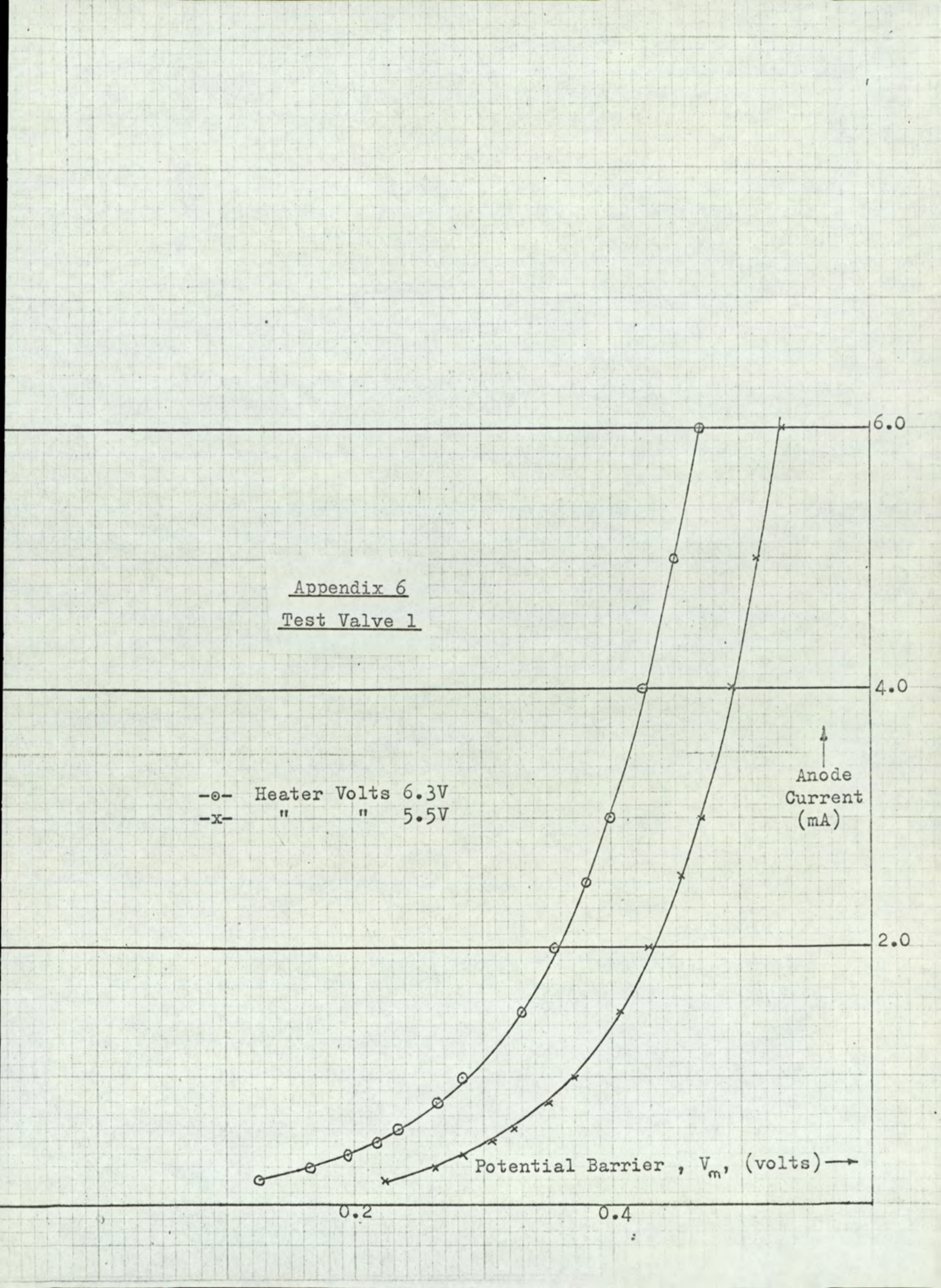

Appendix 6
Test Valve 1
-⊙- Heater Volts 6.3V
-x- " " 5.5V
Anode Current (mA)
6.0
4.0
2.0
Potential Barrier , V_m, (volts)
0.2
0.4

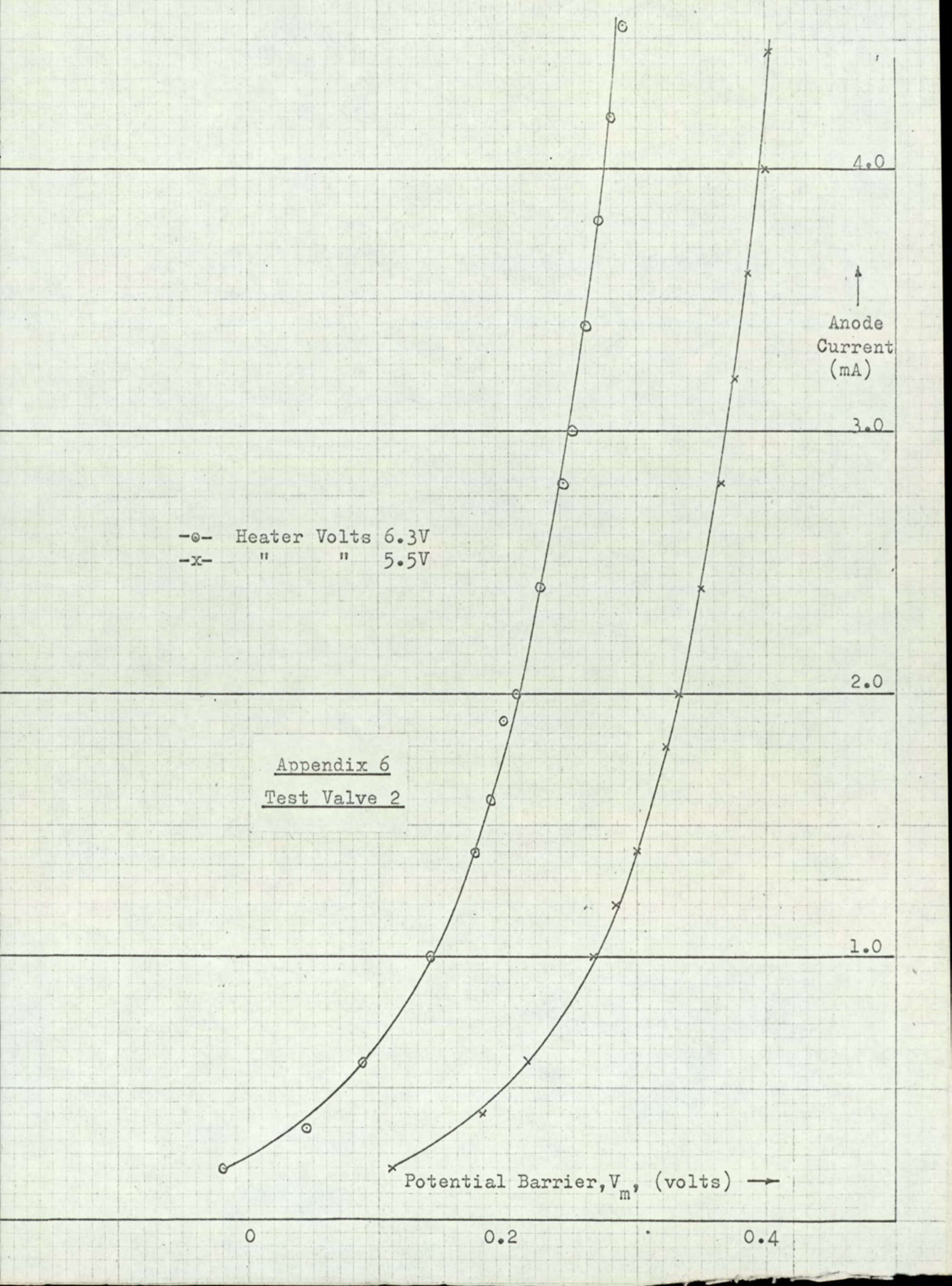

-⊙- Heater Volts 6.3V
-x- " " 5.5V
Appendix 6
Test Valve 2
Anode Current (mA)
4.0
3.0
2.0
1.0
0
0.2
0.4
Potential Barrier, V_m, (volts)

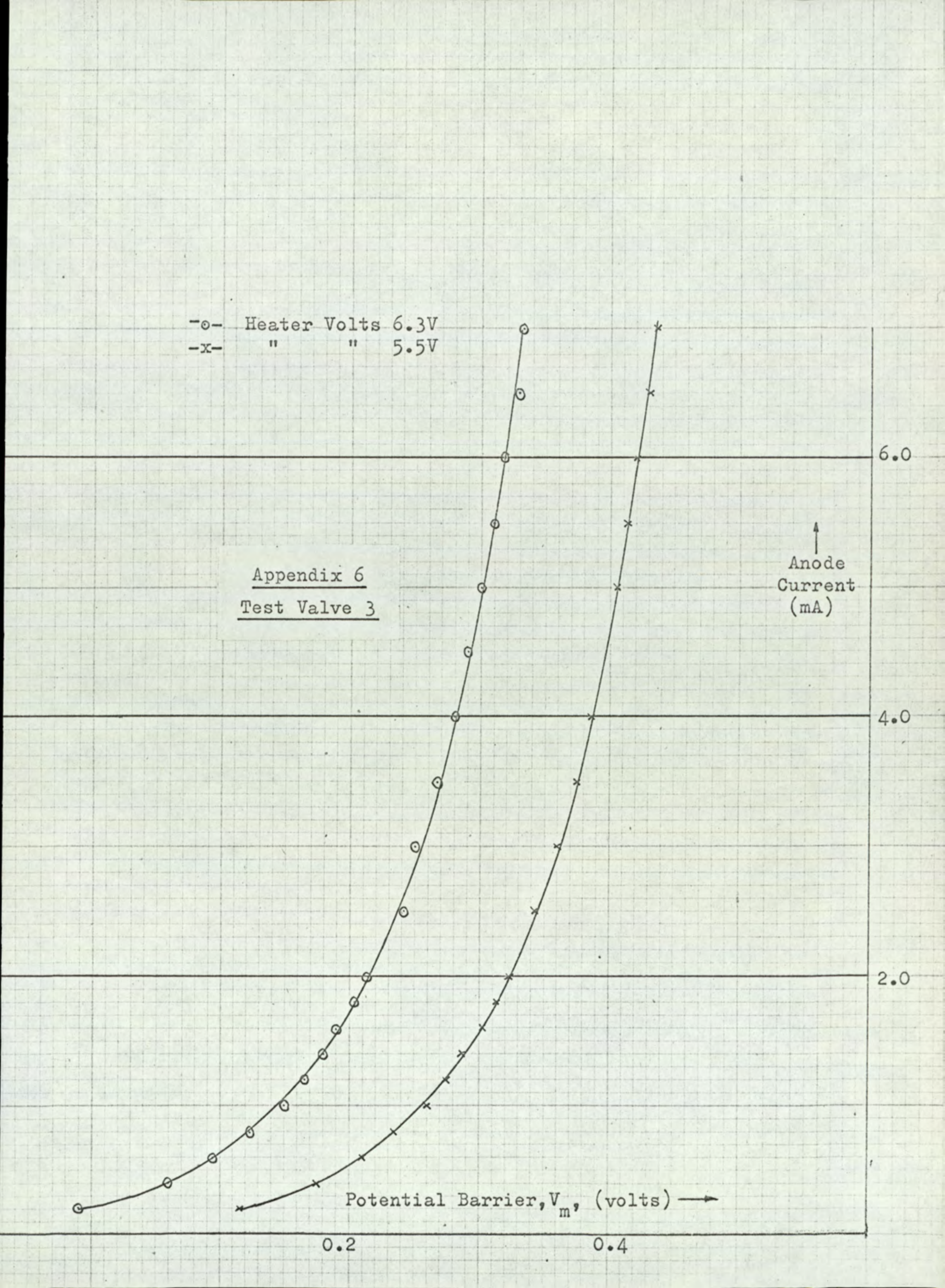

-o- Heater Volts 6.3V
-x- " " 5.5V
Appendix 6
Test Valve 3
Anode Current (mA)
6.0
4.0
2.0
Potential Barrier, V_m, (volts)
0.2
0.4

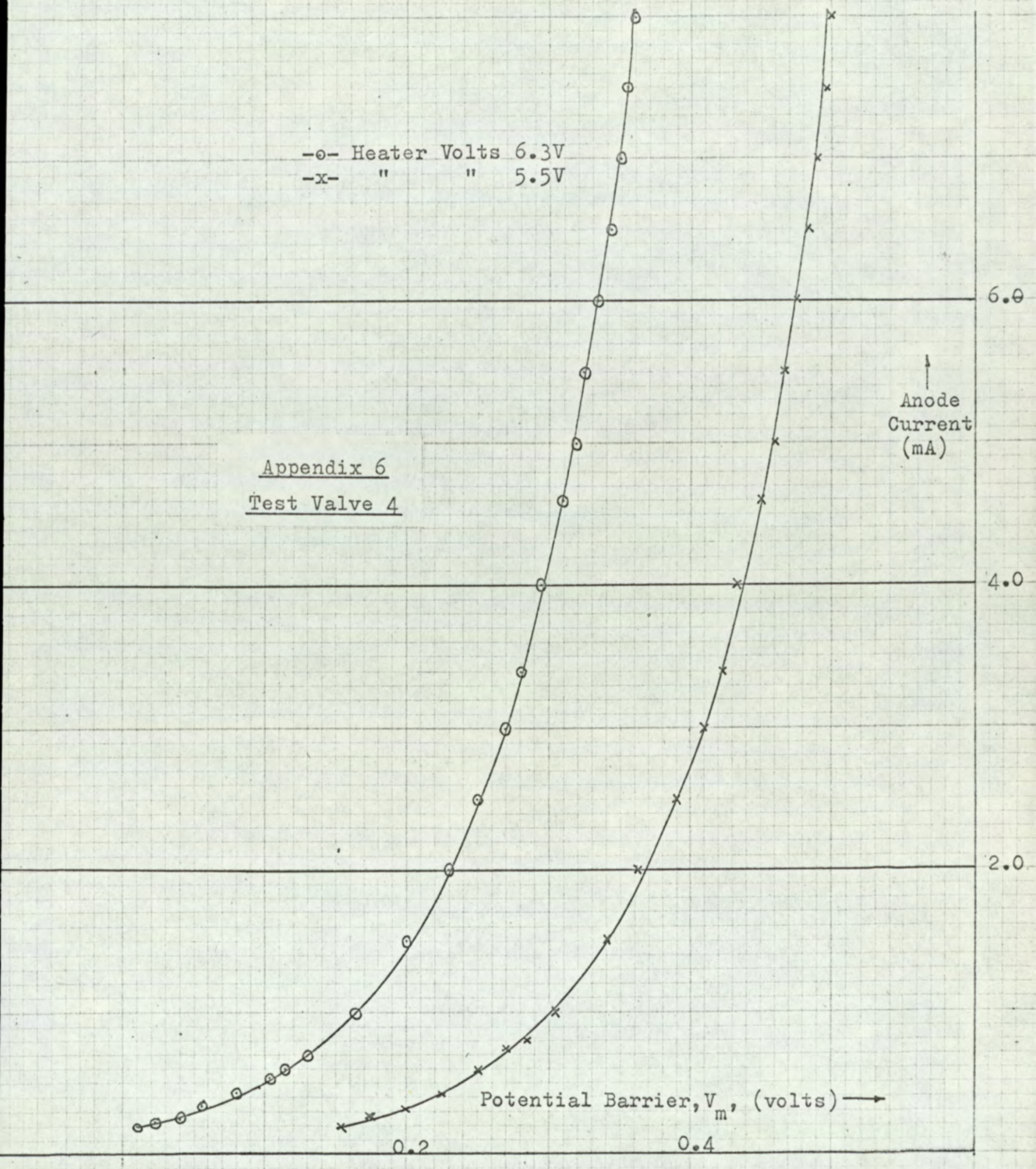
-o- Heater Volts 6.3V
-x- " " 5.5V
Appendix 6
Test Valve 4
6.0
4.0
2.0
Anode Current (mA)
Potential Barrier, V_m, (volts)
0.2
0.4

Appendix 7

Operational Amplifiers

By the use of feedback elements certain amplifiers may be made to produce an output which is proportional to the algebraic sum, the time derivative, or simply a multiple of the input signal. Such designs are widely used as building blocks for analogue computers and, because of their versatility, are termed operational amplifiers.

When operational amplifiers are used the system may be represented as in Fig. A.7.1 where Z_i is the input impedance of the amplifier, Z_o the output impedance, $-A_v$ is the open loop (without feedback) voltage amplification and Z_1 and Z_f are the gain - determining operational impedances.

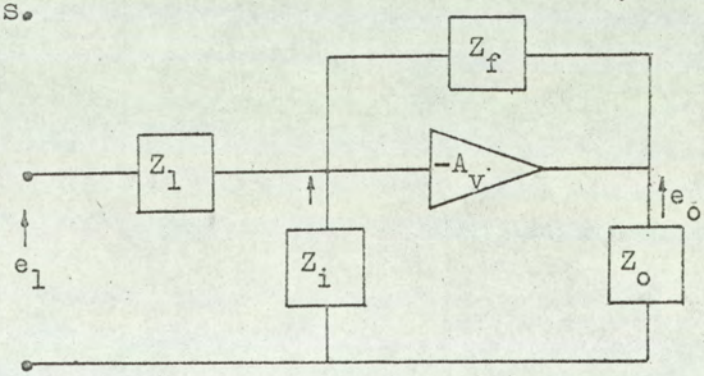

Fig. A.7.1

Defining β_v, the feedback fraction, as $\frac{e}{e_o}$ with $e_1 = 0$ if follows that

$$\beta_v = \frac{Z_1 Z_i}{(Z_f + Z_o)\, Z_1 + (Z_f + Z_o) Z_i + Z_1 Z_i}$$

Furthermore since $e_o = -A_v e$ then from the principle of superposition

$$e = \frac{e_1 Z_i (Z_f + Z_o)}{Z_1 Z_i + Z_1(Z_f + Z_o) + Z_i(Z_f + Z_o)(1 + \beta_V A_V)}$$

$$= e_1 \frac{(Z_f + Z_o)\beta_V}{Z_1(1 + \beta_V A_V)} \qquad \text{(A.7.1)}$$

$$\text{and } G_V = \frac{e_o}{e_1} = \frac{-A_V\beta_V}{1+A_V\beta_V} \quad \frac{Z_f + Z_o}{Z_1} \qquad \text{(A.7.2)}$$

It follows from Eq. (A.7.1) that providing $A_V\beta_V >> 1$ and $A_V >> \frac{Z_f + Z_o}{Z_1}$ then the voltage e will be very small; because of this point O is called a virtual earth point. Furthermore, if in addition to $A_V\beta_V$ being large Z_o is small in comparison with Z_f - as it is in the operational amplifier of Sec. 6.6.2 - then

$$G_V = - \frac{Z_f}{Z_1}$$

i.e. the gain is determined by the ratio of the operating impedances. For the particular case of $Z_f = Z_o$, $G_V = -1$ - corresponding to an inversion - and this is the method employed in correlator 1 for inverting the reference signal.

Now consider the system shown in Fig. A.7.2 in which there are two inputs to the amplifier.

By analogy with the equations above and the application of circuit theory, then

$$\beta_V = \frac{Z_{12}Z_i}{(Z_f + Z_o)Z_{12} + (Z_f + Z_o)Z_i + Z_{12}\, Z_i}\ , \quad Z_{12} = \frac{Z_1 Z_2}{Z_1 + Z_2}$$

$$e_o = - e_1 \left(\frac{Z_f + Z_o}{Z_1}\right) \frac{A_V\beta_V}{(1 + \beta_V A_V)} \quad - e_2 \frac{(Z_f + Z_o)}{Z_2} \frac{(A_V \beta_V)}{(1 + \beta_V A_V)}$$

so that if $A_V\beta_V >> 1$, $Z_f >> Z_o$ then

$$e_o = - e_1 \frac{Z_f}{Z_1} - e_2 \frac{Z_f}{Z_2} \tag{A.7.3}$$

$$= -\frac{Z_f}{Z} (e_1 + e_2) \text{ for } Z_1 = Z_2 = Z \tag{A.7.4}$$

Hence by operating the amplifier in the manner described by Eq. (A.7.4) it is possible to obtain an output voltage proportional to the sum of the input voltages.

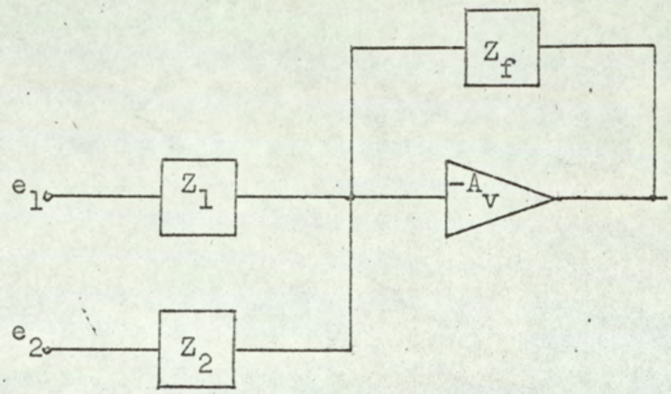

Fig. A.7.2

Appendix 8

The Junction Transistor

Simple-Tee-Model Equivalent Circuit

A low frequency equivalent circuit[49,55] of the transistor, applicable to all frequencies below the cut off frequency, is shown in Fig. A.8.1 where e, b and c are the emitter, base and collector respectively and b' represents the active base region of the transistor. The elements α, r_e, r_c and r_b represent respectively:

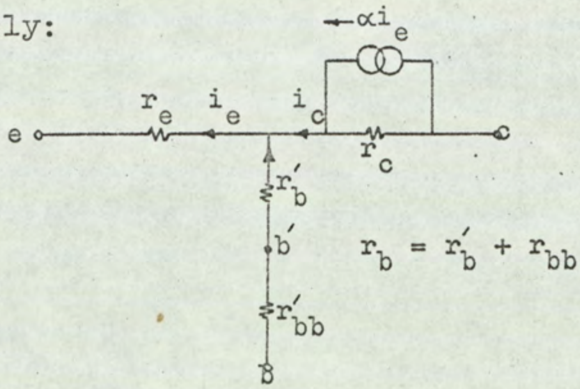

Fig. A.8.1

α = short circuit current gain between emitter and collector. Typically α is of the order of 0.98 although this decreases with frequency (value of frequency at which α falls to 3 dBs below its low frequency value is termed the cut off frequency).

r_e = forward resistance of the base emitter diode. The magnitude of r_e may be calculated from $r_e = \frac{25}{I_e}$ ohms, where I_e is the mean emitter current in milliamps.

r_c = a resistor which accounts for collector current changes due to changes in the voltage $V_{cb'}$. Typically, r_c lies in the range 1 - 3 megohms.

r_b = the sum of two resistors $r_{bb'}$ and r_b' where $r_{bb'}$ represents the resistance between the active base region and the connection to the external base lead and r_b' accounts for the fact that changes in the voltage V_{cb}' produce changes in the base current. For most transistors r_b will lie in the range 200 - 400 ohms.

With the model of Fig. A.8.1 it is now proposed to show how the transistor may be used to give:

(i) A low output impedance, high input impedance source which has the additional property that it severely attenuates the reverse transmission of signals (i.e. from output to input). In this mode of operation the transistor will be used in the grounded collector (emitter follower) configuration.

(ii) A phase inversion.

(a) The Emitter Follower

Fig. A.8.2 shows the transistor connected in the emitter follower mode where the voltage source is represented as a zero impedance generator in series with its source resistance R_s.

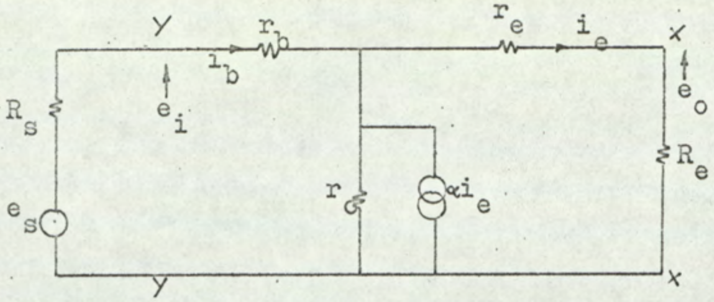

Fig. A.8.2

From network theory it can shown:

(i)

$$Z_{in} = \frac{e_i}{i_b} = r_b + \frac{r_c(r_e + R_e)}{r_d + r_e + R_e} \quad , r_d = r_c(1 - \alpha)$$

$$\doteq R_e(1 + \beta),\ \beta = \frac{\alpha}{1-\alpha} \ , \text{ when } r_d >> R_e >> r_e$$

(ii) The impedance seen to the left of xx, with e_s short circuited, i.e. the output impedance Z_o, is given by

$$Z_o = r_e + \frac{r_c(r_b + R_s)(1 - \alpha)}{(r_c + r_b + R_s)}$$

$$\doteq r_e + (1 - \alpha)r_b \text{ when } R_s \to 0$$

(iii)

$$\text{Voltage gain } A_v = \frac{e_o}{e_i} = \frac{1}{1 + \frac{r_e}{R_e} + \frac{r_b[r_e + R_e + r_c(1 - \alpha)]}{r_c R_e}}$$

i.e. $A_v \doteq 1$ for $r_c >> R_e >> r_e$

(iv)

Reverse transmission factor F_v, i.e. the voltage appearing across YY due to the application of a voltage across XX is

$$F_v = \frac{R_s}{R_e}\ \frac{r_c(1-\alpha)}{r_b + R_s + r_c} = \frac{R_s}{R_e}(1-\alpha) \text{ for } r_c >> r_b + R_s$$

To sum up the emitter follower has the following properties:

(i) high input impedance,

(ii) low output impedance,

(iii) unity voltage gain,

(iv) a high reverse transmission factor.

(b) Transistor Inverter

Consider now the transistor connected in the manner shown in Fig. A.8.3, i.e. as in correlator 2. From network theory it can be shown:

(i)

$$\text{Input impedance } Z_{in} = \frac{e_i}{i_b} = r_b + \frac{(r_e + R_e)(R_c + r_c)}{r_e + R_e + r_d + R_c}$$

$$\doteqdot r_b + R_e(1+\beta) \text{ for } r_d >> R_e + R_c$$

(ii)

$$\text{Output impedance } Z_o = r_d + (r_b + R_s + \beta r_d)\frac{(r_e + R_e)}{r_e + R_e + r_b + R_s}$$

which for $R_e >> r_b + R_s + r_e$ gives

$$Z_o \doteqdot r_d(1+\beta) + r_b + R_s \doteqdot r_c$$

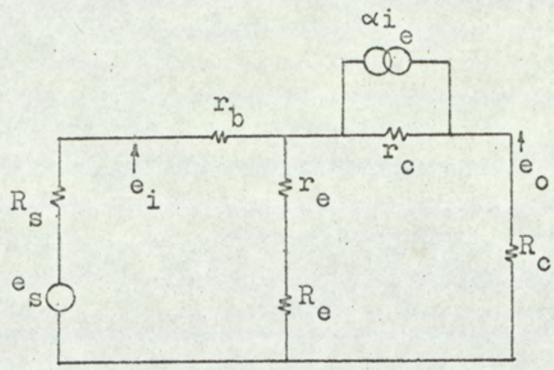

Fig. A.8.3

(iii)

$$\text{Voltage gain, } A_v = \frac{e_o}{e_i} = \frac{-R_c[\beta r_d - (r_e + R_e)]}{r_b(r_e + R_e + r_d + R_c) + (r_c + R_c)(r_e + R_e)}$$

which approximates to

$$A_v = \frac{-R_c}{R_e} \text{ for } r_c >> R_e, r_c >> R_c, R_e >> r_e$$

(iv)

$$\text{Reverse transmission factor } F_v = \frac{R_s.(R_c + r_d)}{R_c(r_b + R_s + \beta r_d}$$

$$F_v = \frac{R_s}{\beta R_c} \text{ for } r_d >> R_c, \beta r_d >> R_s.$$

Thus the arrangement of Fig. A.8.3 has the properties:

(i) a high input impedance,

(ii) a high output impedance,

(iii) voltage gain dependent only on the resitors R_c and R_e (although there is a phase reversal).

(iv) high reverse transmission factor.

Appendix 9

Consider Fig. A.9.1 which represents a high frequency microvolt divider in which S.G. is an Airmec type 304 signal generator. From this generator the signal is fed, via a 50 ohm line, to a tee junction. The latter is included so as to provide matching for the line to the genrator, the 50 ohm line to the inverter and the 75 ohm Wayne Kerr Attenuator (W.K.A.). Thus if R_1, R_2 and R_3 represent respectively the impedances seen at points A, B and C then:

$$R_1 = 50 \text{ ohm}, \; R_2 = 75 \text{ ohm and } R_3 = 50 \text{ ohm}$$

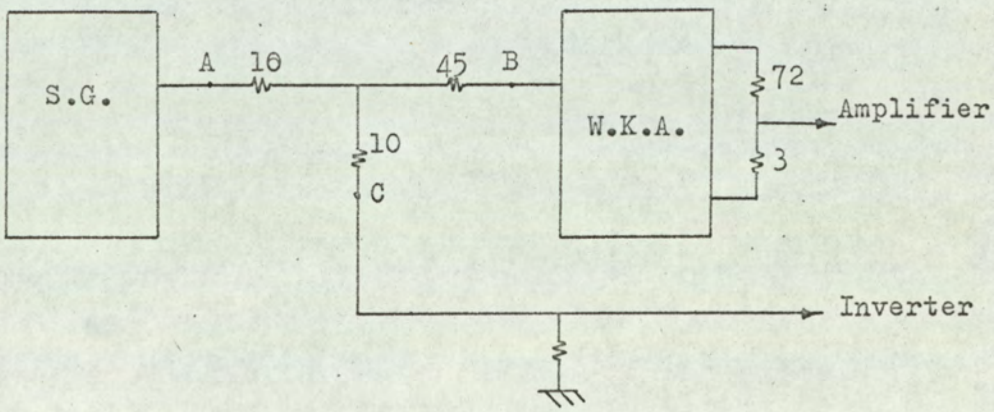

Fig. A.9.1

At the output of the attenuator the matching 75 ohm resistor was made of a 72 ohm and 3 ohm resistor in series. The signal to the amplifier was taken from across the 3 ohm resistor so that the addition of noise from this source was small.

The magnitude of the voltage to the amplifier was determined from a knowledge of the source voltage, the attenuation of the tee network, the ratio of the 3 ohm and 72 ohm resistors and the attenuator dB settings. When using this method of obtaining small voltages power measurements of the type described in Sec. 6.9 were made and were compared with similar measurements - using the same amplifier gain and bandwidth - with the system of Fig. 6.2.7. The results so obtained are shown in Fig. A.9.2 from which it can be seen that difference between the two dividers are only slight.

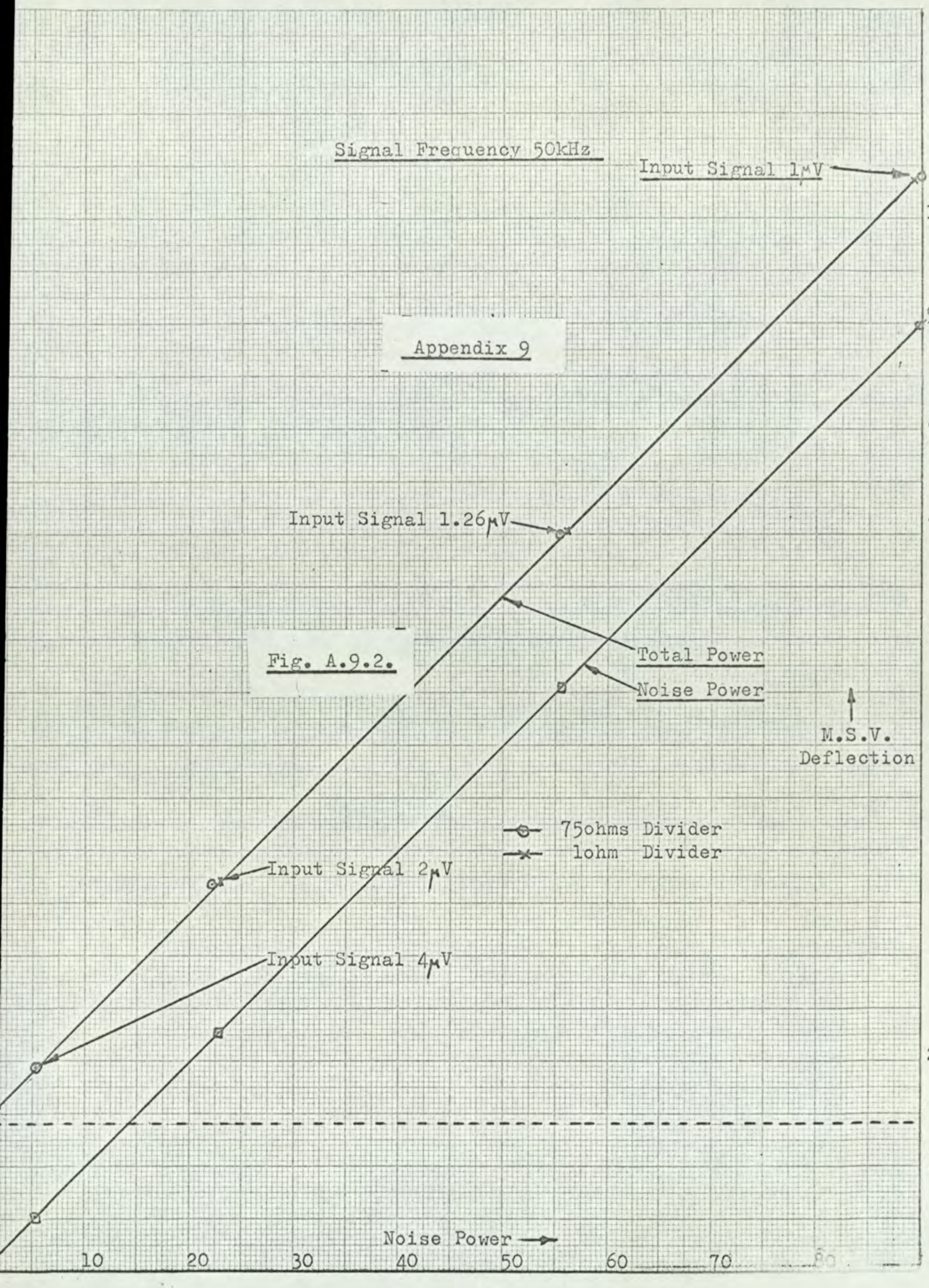
Signal Frequency 50kHz
Appendix 9
Input Signal 1μV
Input Signal 1.26μV
Fig. A.9.2.
Total Power
Noise Power
M.S.V.
Deflection
75ohms Divider
1ohm Divider
Input Signal 2μV
Input Signal 4μV
Noise Power
10
20
30
40
50
60
70
80
90
100

Appendix 10

The integral

$$(R_n(\tau))_1 = G\int_0^{f_o} \cos 2\pi f\tau df$$

$$= Gf_o \frac{\sin 2\pi f_o\tau}{2\pi f_o\tau}$$

where the term $\sin 2\pi f_o\tau/2\pi f_o\tau$ takes the values shown in Table A.10.

Table A.10

$\theta=2\pi f_o$ radians	$\frac{\sin\theta}{\theta}$	$\theta=2\pi f_o$ radians	$\frac{\sin\theta}{\theta}$	$\theta=2\pi f_o$ radians	$\frac{\sin\theta}{\theta}$
0	1	$7\pi/4$	-.129	$13\pi/4$	-.069
$\pi/4$	.9	2π	0	$7\pi/2$	-.091
$\pi/2$	.637	$9\pi/4$	.1	$15\pi/4$	-.06
$3\pi/4$	.3	$5\pi/2$	.127	4π	0
π	0	$11\pi/4$	.0818	$9\pi/2$	.0705
$5\pi/4$	-.18	3π	0	$17\pi/2$	.037
$3\pi/2$	-.212				

Appendix 11

The integral

$$(R_n(\tau))_2 = G\, f_o \int_{f_o}^{\infty} \frac{\cos 2\pi f\tau}{f}\, df$$

can be shown to have a series solution - obtained by writing $\cos 2\pi f\tau$ in terms of a power series - of the form

$$(R_n(\tau))_2 = G\, f_o \left[\sum_{n=1}^{\infty} \frac{(-1)^{n-1}(2\pi f\tau)^{2n-2}}{(2n-2)!\,(2n-2)}\right]_{f_o}^{\infty}$$

where the term in brackets $C_i(f_o)$ has been tabulated[18] and takes the values shown in Table A.11 (turning points of the function being marked thus *).

Table A.11

$2\pi f_o\tau$	$C_i(f_o)$	$2\pi f_o\tau$	$C_i(f_o)$
0	∞	4	0.14
0.5	0.18	5 *	0.19
0.6	0.02	5.5	0.14
1.0	-0.33	6	0.068
1.5 *	-0.47	8 *	-0.12
2.0	-0.42	9	-0.05
3.0	-0.11	11 *	0.09
3.4	0.004	21 *	-0.041
		26.5 *	-0.036

Appendix 12

Periodic waves can be expressed in terms of the Fourier series

$$S(t) = \sum_{n=o}^{\infty} (a_n \cos nw_s t + b_n \sin nw_s t)$$

$$= \sum_{n=o}^{\infty} C_n \cos (nw_s t + \phi_n)$$

where

$$a_n = \frac{1}{T_s} \int_o^{T_s} S(t) \cos nw_s t \, dt \; ; \quad T_s = \frac{2\pi}{w_s}$$

$$b_n = \frac{1}{T_s} \int_o^{T_s} S(t) \sin nw_s t \, dt$$

$$C_n = \sqrt{a_n^2 + b_n^2}$$

$$\phi_n = -\tan^{-1} \left(\frac{b_n}{a_n}\right)$$

Hence

$$R_s(\tau) = \frac{1}{nT_s} \int_o^{nT_s} \sum_{n,m}^{\infty} C_n \cos (nw_s t + \phi_n) C_m \cos(mw_s(t+\tau) + \phi_m)$$

$$= \frac{1}{2} \sum_{n \neq o}^{\infty} C_n^2 \cos nw_s \tau$$

from which it can be seen that $R_s(\tau)$ has the properties:

(i) same period as the original wave

(ii) amplitude equal to the signal power; and

(iii) all phase information is suppressed.

It follows, therefore, that the sinusoidal signal of the autocorrelation measurements will have an autocorrelation function of the form shown in Fig. (A.12.1), i.e. a sinusoid having the same frequency as the signal frequency f_s.

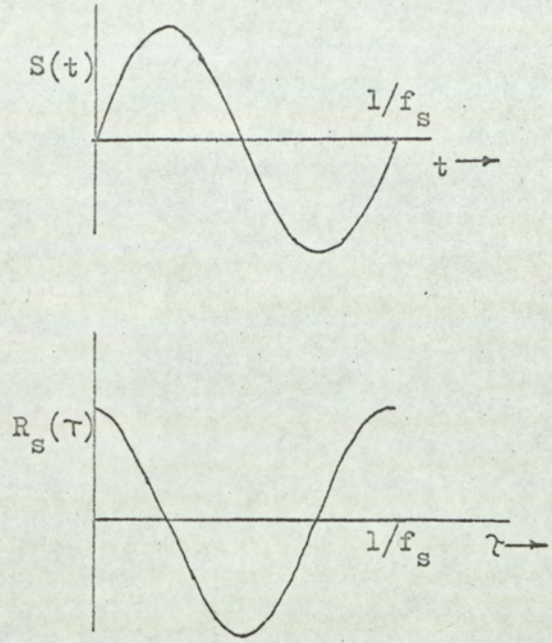

Fig. A.12.1

Appendix 13

Sampling of Waveforms

The process of sampling[36,46] consists of converting continuous data into discrete numbers. The problem now arises as to how close the samples should be chosen, i.e. at what increments of time the data should be sampled (Fig. A.13.1).

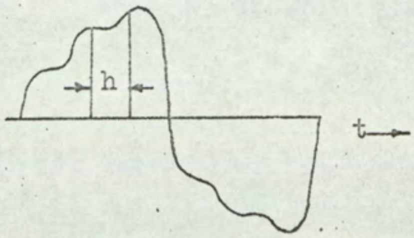

Fig. A.13.1

Consider a signal that is sampled at frequency f_m, i.e. at times $\ldots \frac{-2}{f_m}, \frac{-1}{f_m}, 0, \frac{1}{f_m}, \frac{2}{f_m} \ldots \frac{k}{f_m}$ for integral k. Then for $0<\epsilon<\frac{f_m}{2}$ and odd integers of n, it is easily seen that

$$\cos\left[(n\pi f_m + 2\pi\epsilon)t\right] = \cos(\pi f_m - 2\pi\epsilon)t \qquad A.13.1$$

$$\cos(n\pi f_m - 2\pi\epsilon)t = \cos(\pi f_m - 2\pi\epsilon)t \qquad A.13.2$$

whenever $t = k/f_m$, i.e. whenever t is a sampling time.

Thus at time k/f_m each frequency greater than πf_m rads./sec., i.e. $f_m/2$ Hz, is indistinguishable from some frequency in the range 0 to $f_m/2$. In other words the frequency scale may be divided into intervals of length $f_m/2$ (Fig. A.13.2a) such that any frequency will fall in an interval $nf_m/2 + \epsilon$ or $nf_m/2 - \epsilon$ (for $0 < \epsilon < f_m/2$ and odd $n > o$) and hence at $t = k/f_m$ will correspond to some frequency $f_m - \epsilon$ in the interval 0 to $f_m/2$. The correspondence is shown in Fig. A.13.2b where the lines indicate the correspondence on the frequency scale, and in Fig. A.13.2c where the correspondence can be visualised as a folding of the frequency scale all the frequencies on the same horizontal line being indistinguishable when $t = k/f_m$.

The effect of the folding is illustrated in Fig. A.13.3 Here, the $\cos(\pi f_m - 2\pi\epsilon)t$ wave is identical to the $\cos(\pi f_m + 2\pi\epsilon)t$ wave where $t = k/f_m$. The result is an effective doubling of the $\cos(\pi f_m - 2\pi\epsilon)t$ wave in so far as the information contained in the samples is concerned (vertical lines in Fig. A.13.3) since by Eq. (A.13.1)

$$\cos(\pi f_m + 2\pi\epsilon)\frac{k}{f_m} = \cos(\pi f_m - 2\pi\epsilon)\frac{k}{f_m}$$

Now suppose that a signal has negligible amplitudes for frequencies higher than f^* then in order to sample the signal unambiguously it must be sampled at a frequency f_m such that $f_m/2 \geqslant f^*$ whence the sampling frequency $f_m \geqslant 2f^*$.

Providing the sampling frequency is chosen so that it fulfils this requirement the autocorrelation function may be estimated from the continuous data by a sampling

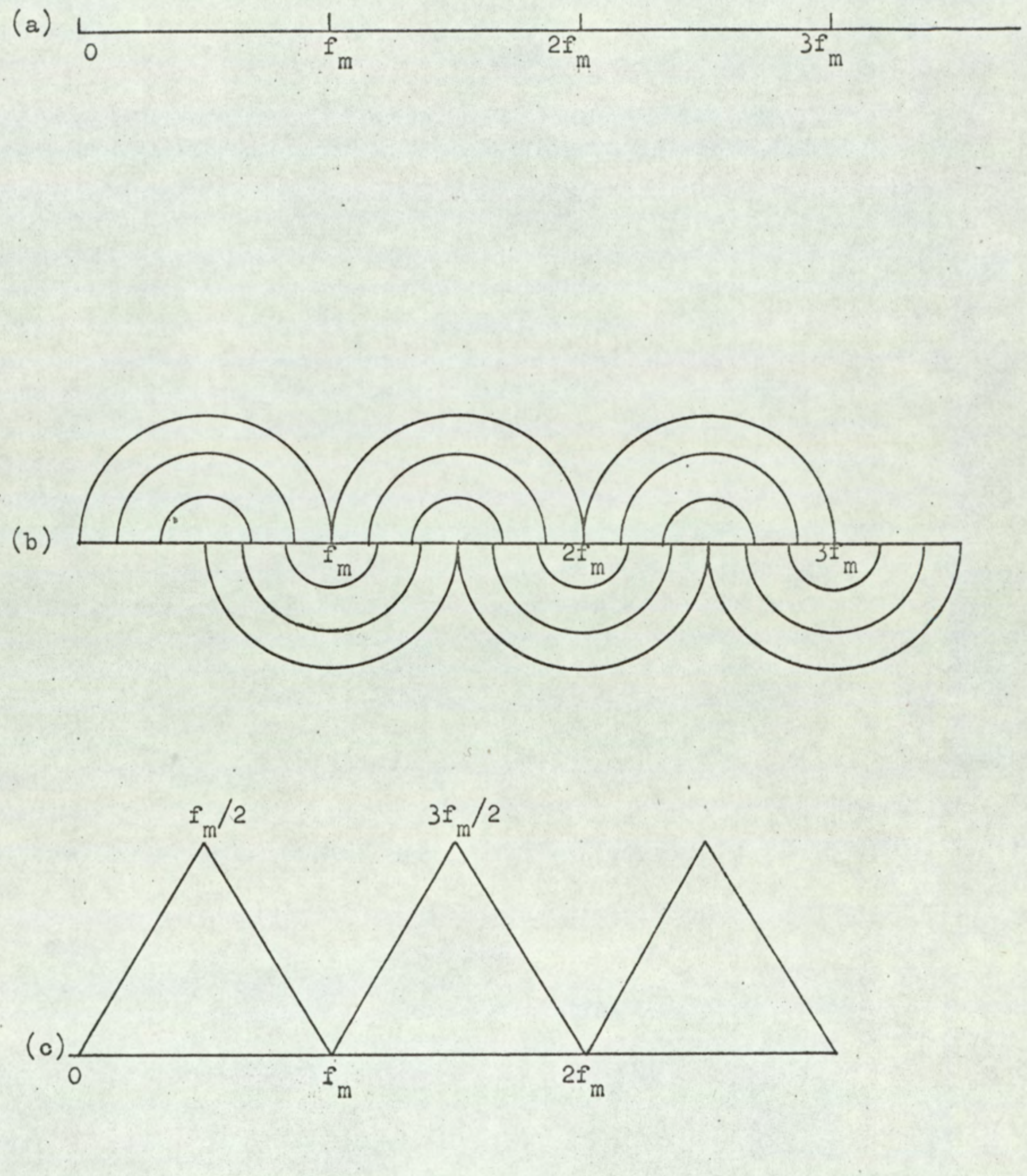

Fig. A.13.2

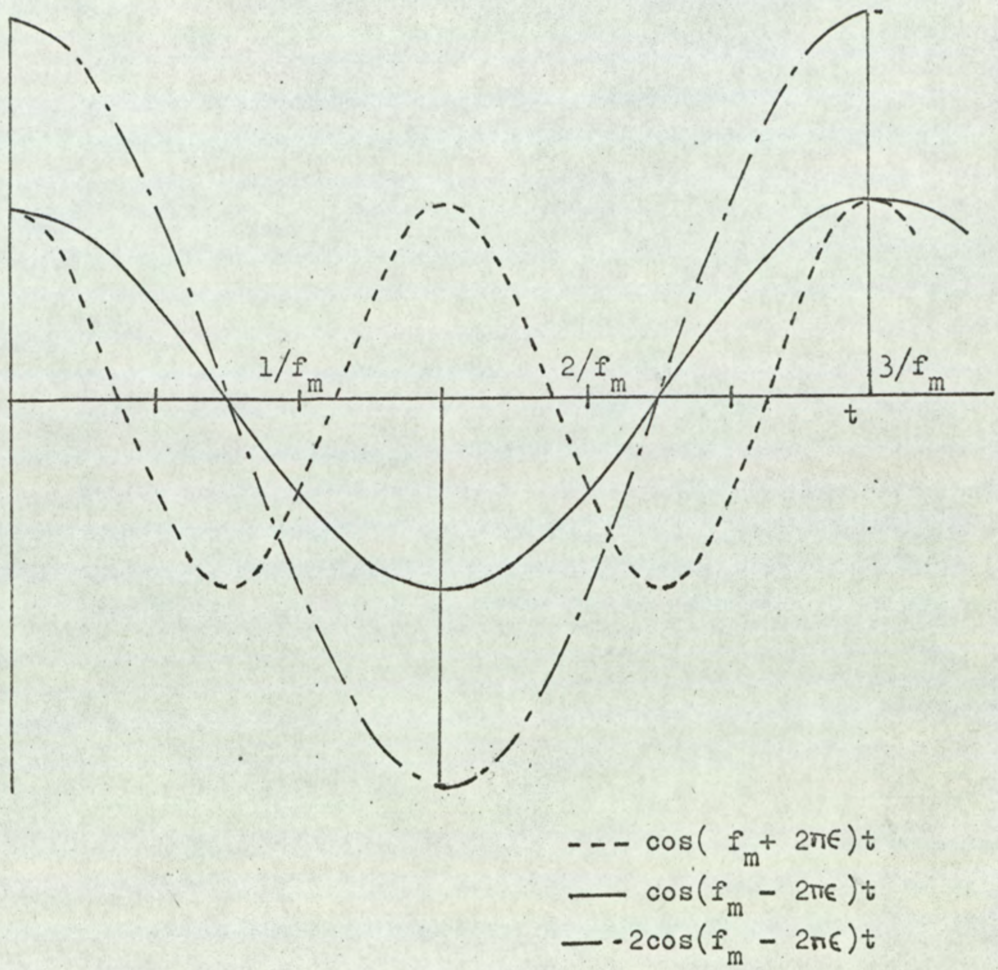

Fig. A.13.3

method.

From N data values (x_n), n = 1, 2, ... N, from a record which is stationary with $\bar{x} = 0$, the estimated autocorrelation function at the displacement $\tau = rh$, h being the time between successive samples, is defined by the formula

$$R_x(rh) = \frac{1}{N-r} \sum_{n=1}^{N-r} x_n x_{n+r}$$

As the number of samples increases the average shown here tends to the value of the autocorrelation function for $\tau = rh$. This interpretation of the autocorrelation function is in agreement with the meaning of the ensemble average (Eq. 2.2).

Appendix 14

Low Pass Filter

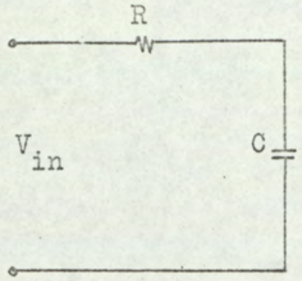

Fig. A.14.1

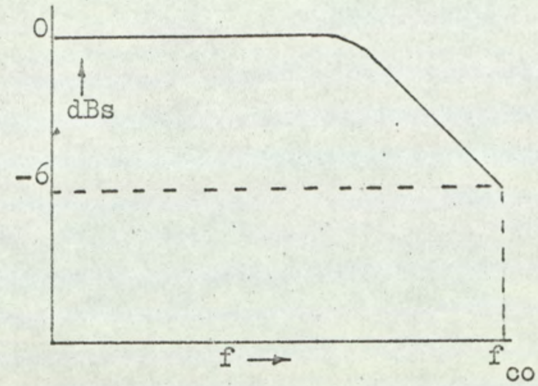

Fig. A.14.2

Consider the circuit shown which is supplied from a voltage source (e.g. amplifier with low output impedance). From circuit theory

$$V_o = \frac{V_{in}}{jwCR+1}$$

therefore

$$\frac{V_o}{V_{in}} = \frac{1}{\sqrt{1 + w^2 \; C^2 R^2}} \quad -\tan^{-1} wCR$$

Thus $|V_o/V_{in}|$ takes the form shown in Fig. A.14.2, i.e. high frequencies are attenuated at 6 dBs/octave and the gain falls to half its low frequency value when $f = f_{co} = \sqrt{3}/2\pi RC$. Hence, the circuit of Fig. A.14.1 may be used as a low pass filter.

Appendix 15

Mullard ORP12 Photoconductive Cell

Photoconductive cells are two terminal variable resistances enclosed in a protective envelope of glass or plastic. In the particular case of the ORP12 the cell is made by sintering photoconductive cadmium sulphide powder into ceramic-like disc-shaped tables. The cadmium sulphide used is an insulator in the dark but becomes conductive when light falls upon it due to the release of electrons within the material. The resistance varies almost in inverse proportion to the light falling on to the cell a typical graph of cell resistance - light intensity being shown in Fig. A.15.1 where the source was a tungsten filament.

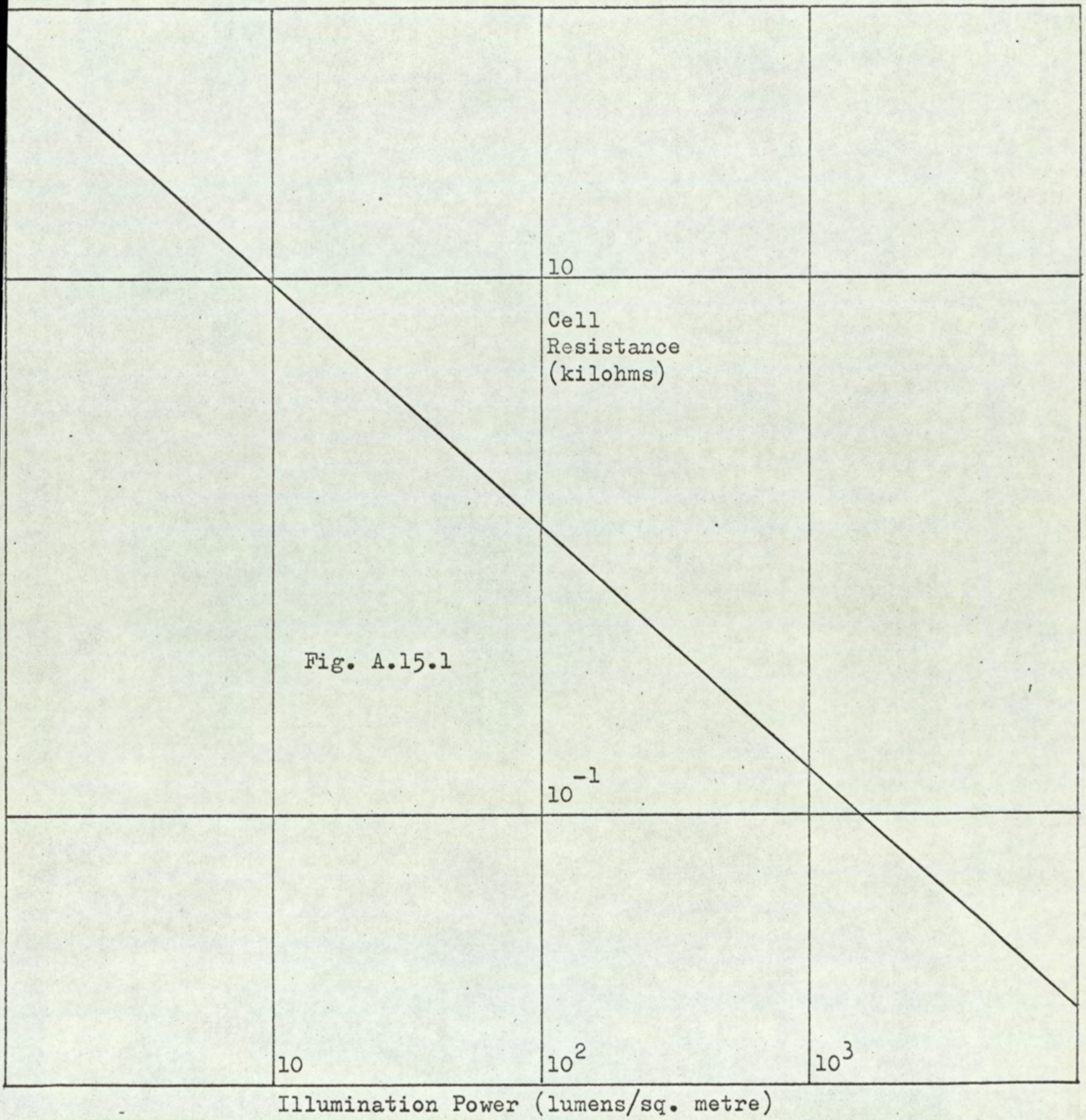
10
Cell
Resistance
(kilohms)
10^{-1}
10
10^2
10^3
Illumination Power (lumens/sq. metre)
Fig. A.15.1

ACKNOWLEDGEMENTS

The author would like to express his gratitude to Dr. C. S. Bull for introducing him to the subject and to both him and Mr. D. E. G. Hathaway for their many helpful discussions. He would also like to thank the other members of the Physics Department, both past and present, for their help and co-operation with the research programme. Finally, he would like to thank his wife for her patience and encouragement during the more frustrating periods of the work.

- 0 - 0 - 0 - 0 -